UNIVERSIDAD POLITÉCNICA DE MADRID
Escuela Técnica Superior de Ingenieros Industriales

USER-CENTERED BIO-INSPIRED METHODOLOGIES FOR UPPER LIMB REHABILITATION EXOSKELETONS: DESIGN, SIMULATION AND CLINICAL VALIDATION

D O C T O R A L T H E S I S

Submitted for the degree of Doctor by:

DEIRA SOSA MENDEZ
Master in Robotics

Madrid, 2024

UNIVERSIDAD POLITÉCNICA DE MADRID
Escuela Técnica Superior de Ingenieros Industriales

Doctoral Degree in Automatic Control and Robotics

USER-CENTERED BIO-INSPIRED METHODOLOGIES FOR UPPER LIMB REHABILITATION EXOSKELETONS: DESIGN, SIMULATION AND CLINICAL VALIDATION

DOCTORAL THESIS

Submitted for the degree of Doctor by:

DEIRA SOSA MENDEZ
Master in Robotics

Under the supervision of:
Dr. Cecilia Elisabet García Cena.

Madrid, 2024

Title: USER-CENTERED BIO-INSPIRED METHODOLOGIES FOR UPPER LIMB REHABILITATION EXOSKELETONS: DESIGN, SIMULATION AND CLINICAL VALIDATION

Author: DEIRA SOSA MENDEZ

Doctoral Programme: Automatic Control and Robotics

Thesis Supervision:

Dr. Cecilia Elisabet García Cena, Titular Professor, Escuela Técnica Superior de Ingeniería y Diseño Industrial (Supervisor)

External Reviewers:

Thesis Defense Committee:

Thesis Defense Date:

To my parents and siblings, who have been my pillar and constant source of inspiration and unconditional support

Acknowledgement

To God, for giving me the strength, health, and wisdom to achieve my goals.

To my family, especially my parents, for being a great example in life and for their unconditional support. To my mother and sister, for always listening to me and motivating me to keep moving forward

To my thesis advisor Prof. Cecilia E. García Cena for accepting to take on that role, in addition to providing me with her support, dedication, and patience throughout my doctoral project.

To all the students who have worked on this project under my supervision (José and Felipe).

To the staff of the Electronics (Pablo and Javier) and Mechanics (Raúl) department at ETSIDI, UPM, for their constant support and collaboration.

To Dr. Saad, for his dedication and generosity in sharing his knowledge during my international intership. And to the members of the Research Group in Power Electronics and Industrial Control and Robotics at the École de Technologie Supérieure (ETS), for their hospitality. Especially, to my friend David, for his friendship and unconditional support (we are a great team).

To my friends Ramón, Verónica, Hipatia, Diego, Viviana, Belén, Eva, and others, for being my emotional support and source of joy.

To Antonio Martín González, in charge of the Advanced Technologies Unit in Design and 3D Printing at Hospital 12 de Octubre, for his accessibility, availability, and unconditional support during the manufacturing stage of my device.

To the patients and personnel of the rehabilitation service at Hospital 12 de Octubre who agreed to be part of the testing group to validate my device. In particular, to the physiotherapists Juan Ignacio, Elías, Eliecer, María Eugenia, Eva, and Laura, for sharing their time, experiences, and advice to improve the evaluated device.

To CONAHCYT (Mexican National Council of Humanities, Science and Technology) for the support under grant 795353. CONAHCYT was previously named CONACYT (Mexican National Council of Science and Technology)

Abstract

Currently, exoskeletons are emerging as effective tools in medical rehabilitation. However, they face challenges related to movement compatibility, automatic control, cost, and human-robot interaction, among others.

This thesis aims to develop a rehabilitation exoskeleton for individuals with limited mobility in the upper limbs. It will address challenges such as optimizing the mechanical design, ensuring compatibility and ergonomics with upper limb movements, and implementing control strategies to manage disturbances and uncertain modeling in the exoskeleton's performance. Additionally, the thesis will develop the human-robot interface and conduct a comprehensive evaluation to assess the device's usability and efficiency in real-world settings.

To achieve this, a user-centered, task-focused bioinspired methodology was employed, consisting of 12 activities grouped into three phases: design, simulation, and physical prototyping. This methodology features two optimization stages: the first aims to enhance the mechanical design of the device using a weighted objective function, while the second focuses on optimal control through a sliding mode controller with an exponential reach surface. Both stages utilize metaheuristic algorithms. The methodology also includes mathematical modeling (kinematic and dynamic), virtual environment use, technological integration, and a comprehensive clinical evaluation.

The results achieved include the development of a bioinspired device with a weight reduction of approximately 49% compared to the initial design, thanks to mechanical design optimization. Additionally, digital twins of the device were created: 1) The digital twin prototype validated safety and performance factors through trajectory tracking control strategies via software, and 2) The digital twin instance enabled a thorough clinical evaluation under real conditions.

A human-robot interface was designed to facilitate communication between medical personnel and the exoskeleton, incorporating both simulation and movement execution phases. An industrial PD controller was used for the 5 DOF exoskeleton, while a sliding mode controller with an exponential reach surface, optimized using the particle swarm optimization algorithm, was employed for the 7 DOF ETS-MARSE exoskeleton. Both controllers proved efficient in passive rehabilitation exoskeletons, with RMSE values of less than 0.88 rad and 0.05 rad, respectively.

The evaluation results include assessments of the human-robot interface usability, workload index, exoskeleton usability, therapy satisfaction, and the exoskeleton's performance in both simple and complex therapeutic routines. It is worth noting that the clinical evaluation of the robotic rehabilitation therapy is beyond the scope of this thesis. However, the results presented in this PhD thesis provide a solid foundation for future clinical validation from a therapeutic perspective.

At the conclusion of this work, a viable robotic exoskeleton was developed for passive rehabilitation therapies for individuals with limited mobility in the upper limbs. The device is lightweight, features an interface that meets usability standards, and has a physical prototype evaluated in a clinical setting.

Resumen

Actualmente, los exoesqueletos se perfilan como herramientas eficaces en la rehabilitación médica. No obstante, enfrentan desafíos relacionados con la compatibilidad del movimiento, el control automático, el costo y la interacción humano-robot, entre otros.

El objetivo de esta tesis es desarrollar un exoesqueleto de rehabilitación para personas con movilidad limitada en los miembros superiores. Se abordarán desafíos relacionados con la optimización del diseño mecánico, la compatibilidad y ergonomía del exoesqueleto con los movimientos del miembro superior, y las estrategias de control para enfrentar perturbaciones y modelado incierto en el desempeño del exoesqueleto. Además, se desarrollará la interfaz humano-robot y se evaluará el dispositivo de manera integral para cuantificar su usabilidad y eficiencia en entornos reales.

Para lograr este objetivo, se empleó una metodología bioinspirada centrada en el usuario y enfocada en la tarea, compuesta por 12 actividades agrupadas en tres fases: diseño, simulación y prototipo físico. Esta metodología incluye dos etapas de optimización: la primera se enfoca en mejorar el diseño mecánico del dispositivo mediante una función objetivo ponderada, y la segunda se centra en el control óptimo, utilizando un controlador por modos deslizantes con superficie de alcance exponencial. Ambas etapas implementan algoritmos metaheurísticos para alcanzar sus objetivos. Además, se consideran etapas de modelado matemático (cinemático y dinámico), uso de entornos virtuales, integración tecnológica y evaluación integral en un entorno clínico.

Los resultados obtenidos tras aplicar la metodología fueron: la creación de un dispositivo bioinspirado con una reducción de peso de aproximadamente el 49% respecto al diseño inicial gracias a la fase de optimización del diseño mecánico. Además, se desarrollaron gemelos digitales del dispositivo: 1) el prototipo de gemelo digital permitió validar el factor de seguridad y el desempeño mediante estrategias de control para el seguimiento de trayectorias a través de softwares. Y 2) la instancia del gemelo digital permitió realizar una evaluación integral en un entorno clínico bajo condiciones reales.

Se diseñó una interfaz humano-robot que permite la comunicación entre el personal médico y el exoesqueleto, incluyendo una etapa de simulación y otra de ejecución de movimientos en el dispositivo. Se utilizó un controlador industrial (PD) para el exoesqueleto de 5 DOF diseñado en esta tesis, y un controlador por modos deslizantes con superficie de alcance exponencial, optimizado mediante el algoritmo de enjambre de partículas, para el exoesqueleto ETS-MARSE de 7 DOF. Ambos controladores demostraron su eficiencia en el uso de exoesqueletos enfocados en rehabilitación pasiva, presentando RMSE menores a 0.88 rad y 0.05 rad, respectivamente.

Los resultados de la evaluación incluyen valoraciones de la usabilidad de la interfaz humano-robot, el índice de carga de trabajo, la usabilidad del exoesqueleto, la satisfacción con la terapia y el rendimiento del exoesqueleto tanto en rutinas terapéuticas simples como complejas. Cabe destacar que la evaluación clínica de la terapia de rehabilitación robótica está fuera del alcance de esta tesis. Sin embargo, los resultados presentados en esta tesis doctoral proporcionan una base sólida para futuras validaciones clínicas desde una perspectiva terapéutica.

Al concluir este trabajo, se desarrolló un exoesqueleto robótico viable para terapias de rehabilitación pasiva para individuos con movilidad limitada en los miembros superiores. El dispositivo es ligero, cuenta con una interfaz que cumple con los estándares de usabilidad y tiene un prototipo físico evaluado en un entorno clínico.

Table of Contents

List of Figures

List of Tables

Abbreviations and acronyms

Ab-m Ability to move

Accep Acceptability

Acc Accuracy

ACT Active-assistive robotic intervention

ADLs Activities of daily living

AIS American Spinal Injury Association Impairment Scale

APP Application

BMD Becker MD

CG Control group

Cm Comfort

CMD Congenital MD

CP Cerebral Palsy

CS Controller software

DMD Duchenne MD

DOF Degree of freedom

Ec Encephalitis

EEG Electroencephalography

Eff Effectiveness

EG Experimental group

ELM Electromyographic

EOG Electrooculography

ETP Existing training program

Exo Exoskeleton

E-FE Elbow flexion-extension

Fea Feasibility

FMA Fugl-Meyer Assessment

FMA-UE FMA Shoulder, elbow, forearm, wrist, and hand; 33 items, 0–66

FMA-prox FMA Shoulder, elbow, and forearm; 18 items, 0–36

FS Frozen shoulder

IEC International Electrotechnical Commission

IG Intervention group

ISO International Organization for Standardization

LGMD2 Limb Girdle type 2 MD

LikS Likert-Scale

LL Lower limb

MD Muscular Dystrophy

MDS Mechanical design software

MS Multiple Sclerosis

NGOs Non-Governmental Organization

NM Not mentioned

Ov Overall

PID Proportional-integral-derivative controller

P&P Pick& Place

Phys Physiotherapists

PSV Passive robotic intervention

QUEST 2.0 Quebec User Evaluation of Satisfaction with Assistive Technology

Qs Questionnaire

Rb Reliability

RCT Rotator cuff tendinosis

Reh Rehabilitation

RMS Root Mean Square

RTLX Raw NASA-Task Load Index

Sat Satisfaction

SCI Spinal Cord Injury

Secu Security

Sf Safety

SIS Stroke Impact Scale

SMC Sliding mode controller

SPT Supraspinatus partial tear

SS Shoulder surgery

ST Supraspinatus tear

STen Supraespinatus tendinosis

Stro Stroke

SUS System Usability Scale

S-AA Shoulder abduction-aduction

S-d Self-direction

S-FE Shoulder flexion-extension

S-IER Shoulder internal-external rotation

TBI Traumatic Brain Injury

TF Troquiter Fracture

Tr Trust

TS Tendinosis supraspinatus

TT Trajectory tracking

UE User experience

UL Upper limb

ULE Upper limb exoskeleton

UPM Universidad Politécnica de Madrid

U-fr User-friendliness

Usab Usability

WMFT Wolf Motor Function Test

W-AA Wrist abduction-aduction

Chapter 1

Introduction

"Never give up on what you really want to do. The person with big dreams is always way ahead of those who have none".

Amelia Earhart.

1.1 Overview and Motivation

According to the World Health Report by the WHO and the World Bank, around 1 billion people worldwide will experience a temporary or permanent disability at some point in their lives, representing approximately 15% of the global population. Of this total, between 110 and 190 million face severe difficulties in their daily lives, and the vast majority encounter constant obstacles. These figures underscore the need to address the physical, social, and economic barriers that hinder the full integration of these individuals into society (Bank, 2011).

The term "disability" encompasses all impairments, limitations, and restrictions in participation. It also refers to the negative aspects that arise from the interaction between a person with a health condition and their contextual factors, whether environmental or personal. This interaction, along with attitudinal and environmental barriers, prevents individuals with different abilities from fully and effectively participating in society on an equal basis with others.

One way to reduce the level of mobility disability is through rehabilitation programs, where a physiotherapist commonly attends to a patient for a set period of time. However, these programs face several issues, such as long waiting times in medical institutions, which prolong the recovery period and increase costs. Additionally, due to the continuous increase in the number of people with disabilities, the demand for specialized personnel is essential.

An alternative that has proven to be efficient is the use of robotic devices during rehabilitation therapies. In this context, medical and rehabilitation robotics has emerged, aiming to apply advanced technologies (mechanical engineering, electrical engineering, artificial intelligence, sensor and actuator technology, control, etc.) for the rehabilitation and assistance of

people with disabilities, seeking to restore their independence. This is how wearable robots have emerged through interaction with humans. These portable devices are used by people to complement, replace, or enhance the function of the limb they are used on (Pons, 2008, Desplenter et al., 2020, Morone et al., 2020).

In recent decades, the development of wearable robotic devices has been particularly focused on robotic exoskeletons, which offer innovative solutions for a variety of issues in the fields of rehabilitation and human assistance. These devices are designed to provide mechanical support, increasing both the strength and endurance of the user, thus aiding in the rehabilitation of patients with reduced mobility and enhancing the quality of life for those with physical disabilitie (Choutri et al., 2023; Clark et al., 2019; Gandolla et al., 2021).

However, the mechanical design of exoskeletons presents several challenges. One of the main issues is the need to create structures that are both robust and lightweight, to avoid adding excessive weight that could cause fatigue to the user. Additionally, they must be ergonomic and adjustable to accommodate different body types and allow natural movements without causing discomfort or injury. The materials used must be durable and resistant to wear, while the movement mechanisms must be precise and fluid to effectively replicate human movements (Asad et al., 2023; Coorey et al., 2022; Elayan et al., 2021; P.-h. Huang et al., 2022; Y. Liu et al., 2019).

The control of these devices demands advanced systems capable of interpreting and responding to user signals in real-time. This entails integrating sensors and control algorithms capable of swiftly processing information to coordinate the exoskeleton's actuators. Latency and response precision are critical to ensure safe and efficient operation, particularly in medical and rehabilitation applications. Furthermore, considerations like adaptability to varying user needs, intuitive interfaces, and incorporation of machine learning techniques for predictive control could further enhance device functionality and user experience (Aichaoui and Ikhlef, 2022; Aole et al., 2022; Fei et al., 2017; Fellag et al., 2017; Palazzi et al., 2022; Qureshi and Mudassir, 2021; Yu et al., 2023)

Finally, the evaluation of robotic exoskeletons is crucial to ensure their effectiveness and safety. This involves conducting comprehensive tests both in controlled environments and in real-life situations, involving end-users, to validate their performance. Additionally, it is essential to identify potential areas for improvement and ensure that the devices meet users' expectations and needs. Evaluation criteria should not be limited to technical performance but should also encompass aspects such as comfort, ease of use, and overall impact on users' quality of life. These factors contribute to the continuous evolution of these devices (Catalán et al., 2023; Costanzi et al., 2023; H. K. Kim et al., 2021; La Bara et al., 2021; Moulaei et al., 2024; Pérez et al., 2022; Vélez-Guerrero et al., 2021; Yurkewich et al., 2019).

The use of exoskeletons in rehabilitation holds great promise for enhancing therapies for patients with functional diversity. These devices emerge as tools that will not only benefit patients but also streamline the work of physiotherapists by enabling precise, repetitive, and intensive therapies. Therefore, current development efforts are focused on creating exoskeletons that are lightweight, precise, and easy to handle, ensuring the safety of both patients and the medical staff operating them.

To achieve this goal, it is essential to leverage cutting-edge technologies such as computational tools, innovative materials, and advanced manufacturing processes. Furthermore, integrating artificial intelligence and machine learning systems could enhance the exoskeleton's adaptability to the specific needs of each patient, thereby optimizing therapy outcomes, among other possibilities.

Moreover, interdisciplinary collaboration among engineers, physicians, therapists, and end-users is crucial for developing exoskeletons that meet the highest standards of quality and effectiveness. This holistic approach not only ensures the safety and efficacy of the device but also fosters continuous innovation in the field of technology-assisted rehabilitation.

1.2 Thesis objectives

Design and develop a bio-inspired 5-degree-of-freedom exoskeleton to provide passive rehabilitation therapy for the upper limbs of individuals with physical disabilities (with limited range of motion). This device is designed to be used on the lateral aspect of the upper limb, facilitating natural movements of the shoulder (internal-external rotation, abduction-adduction, flexion-extension), elbow (flexion-extension) and wrist ((abduction-adduction).

- Use a user-centered and task-oriented design methodology to establish the development process of the exoskeleton, based on the premise that the robot has two users: the patient and the physiotherapist.
- Design the exoskeleton for upper limb rehabilitation using CAD and CAE software, and create its virtual digital twin.
- Design and implement a methodology to optimize the mechanical design of the exoskeleton using a multi-objective metaheuristic approach.
- Perform the mechanical analysis of the designed exoskeleton using finite element analysis with specialized software to determine its safety factor.
- Obtain and validate the kinematic (forward, inverse, and differential) and dynamic model of the designed device.
- Design and implement control strategies by incorporating therapeutic routines for the upper limb, using simulation environments.
- Design and implement robust control strategies to optimize gains in controllers applied to rehabilitation exoskeletons.
- Design a human-robot interface that serves as a channel of interaction between the physiotherapist and the exoskeleton.
- Manufacture a physical prototype of the designed device using 3D printing technologies and lightweight materials.
- Design and implement a validation methodology for the designed device in clinical settings, assessing the performance of the exoskeleton as well as the usability, satisfaction level, and perceived workload by users and physiotherapists.

- Analyze the obtained results and draw relevant conclusions.

1.3 Outline

This document is structured into the following chapters:

1. In Chapter 2, the state of the art addressed in this thesis is examined, focusing on areas such as methodologies for mechanical design of exoskeletons, controllers applied to exoskeletons, and the evaluation of exoskeletons in rehabilitation.
2. In Chapter 3, the mathematical fundamentals underpinning this thesis are detailed, addressing aspects related to human anatomy and physiology, mathematical modeling, biomechanical models, automatic control strategies, among others.
3. In Chapter 4, the implemented development methodology is addressed, along with its application in the mechanical design phase to obtain the virtual digital twin and create the physical digital twin.
4. In Chapter 5, the detailed results obtained from the application of the methodology are presented, including mathematical modeling, control strategies, validation in simulation environments, and the development of the human-robot interface.
5. In Chapter 6, a comprehensive evaluation of the designed exoskeleton is conducted in a clinical environment, showcasing the results of usability, satisfaction level, workload index, and robot performance.
6. In Chapter 7, the robust control strategy applied to a 7 DOF rehabilitation exoskeleton is presented, which includes the use of a sliding mode controller with an exponential reaching law, along with its experimental implementation.
7. In Chapter 8, the relevant aspects deserving attention in this work are discussed.
8. In Chapter 9, the conclusions regarding the main contributions of this thesis are presented and future work is discussed.

1.4 Related publications

The following are the publications related to the thesis that have been produced.

Articles

Table 1.1: Article 1.

Title	Innovative Metaheuristic Optimization Approach with a Bi-Triad for Rehabilitation Exoskeletons
Details	• AUTHORS: Sosa Méndez, Deira and García Cena, Cecilia E. and Bedolla-Martínez, David and Martín González, Antonio. • JOURNAL: Sensors. • Volume: 24. • Year: 2024. • Number: 7. • URL: https://www.mdpi.com/1424-8220/24/7/2231 • PubMedID: 38610443. • ISSN: 1424-8220. • DOI = 10.3390/s24072231.

Table 1.2: Article 2.

Title	Robotic digital twin as a training platform for rehabilitation health personnel
Details	• AUTHORS: Sosa Méndez, Deira and García Cena, Cecilia E. • JOURNAL: Enfoque UTE. • Volume: 14. • Year: 2023. • Number: 3. • URL: https://ingenieria.ute.edu.ec/enfoqueute/index.php/revista/article/view/971 • DOI = 10.29019/enfoqueute.971

Conference Proceedings

Table 1.3: Conference proceeding 1

Title	Rehabilitation Upper Limb Exoskeleton: Human-Robot Simulation Framework.
Details	• AUTHORS: Sosa Méndez, Deira, and García Cena, Cecilia E., and Saltarén Pazmiño, Roque • Booktitle: Advances in Automation and Robotics Research. • Year: 2024. • Publisher: Springer Nature Switzerland. • Online ISBN: 978-3-031-54763-8. • Print ISBN: 978-3-031-54762-1.

Table 1.4: Conference proceeding 2.

Title	Bioinspiración: Requisitos para robots con aplicaciones médicas.
Details	• AUTHOR: Sosa-Méndez, Deira. • Conference: IV SIMPOSIO INTERNACIONAL SOBRE BIOMIMÉSIS. • Place and date: Barcelona, Spain. 22-24 de Noviembre de 2023. • Role: Author and speaker.

Table 1.5: Conference proceeding 3.

Title	Robótica de Rehabilitación 4.0: Diseño y desarrollo del gemelo digital
Details	• AUTHORS: Sosa-Méndez,D., García-Cena,C.E., Martín-Gonzaléz, A., Saltarén-Pazmiño, R. • Conference: Jornadas Nacionales de Robótica y Bioingeniería 2023. • Place and date: Madrid, Spain. 14 al 16 de Junio de 2023. • DOI: https://doi.org/10.20868/UPM.book.74896 • Role: Author and speaker.

Table 1.6: Conference proceeding 4.

Title	Metodología para la optimización en el diseño de robot bioinspirado para aplicaciones médicas.
Details	• AUTHOR: Sosa-Méndez,D. • Conference: I Jornada de Investigación de la ETSIDI • Place and date: Madrid, Spain. 21 de Noviembre de 2022. • Role: Author and speaker.

Chapter 2

State of the art

"The universe doesn't just have one history, but every possible history".

Stephen Hawking.

Rehabilitation exoskeletons constitute a dynamic and multidisciplinary field that has experienced significant growth in recent years. In this context, this chapter provides a comprehensive overview of the latest advances related to their mechanical design, motion control, and clinical evaluations conducted. The aim is to explore current trends, pending challenges, and emerging opportunities in this constantly evolving field.

2.1 Introduction

According to the World Health Organization in 2019 (Cieza et al., 2020), 2.4 billions people experienced conditions that could benefit from rehabilitation services (1 in 3 impaired people globally). Between 1990 and 2019, there was a 69.4% rise in the population living with disabilities. Among the disability leading causes worldwide are: musculoskeletal disorders and strokes (Organization., 2022), which lead to limited functional capacities, especially in aspects related to mobility. For example, annually worldwide, a stroke occurs every 3 s according to data from the World Stroke Organization (2022), and the average is 12.2 million new cases (Zhao et al., 2023).

Promoting well-being in the population is one of the sustainable development goals, and rehabilitation plays a crucial role in this regard. This health service is gaining increasing relevance as it applies to people with various conditions throughout different stages of life and across various levels of care. Its primary objective is to improve individuals' functioning and mitigate their disabilities, keeping them as independent and active as possible (Organization., 2024). The rehabilitation services objectives are patient-centered and aimed at gaining independence, where physical rehabilitation is a fundamental treatment in functional recovery.

Current rehabilitation treatments are usually expensive and the lack of medical personnel

weakens their efficiency. Within these treatments, robotic-assisted rehabilitation has proven to be efficient, because it allows personalized treatments (repetitive and precise movements) to be performed and their intensity to be increased (Moulaei et al., 2023, Choutri et al., 2023). Examples of these devices are exoskeletons, which are serial robotic systems based on bio-inspired models (similar in shape and functions to the human body) that are externally attached to the user (Rocon and Pons, 2011, Pons, 2008).

Some of the main benefits of these devices include increased repeatability and precision in rehabilitation treatments, assistance to medical specialists, the ability to treat multiple patients with a single therapist as supervisor, timely use can reduce rehabilitation times, and the possibility of offering personalized therapies, among other (Asad et al., 2023; Buccelli et al., 2022; Clark et al., 2019; Coorey et al., 2022; Dalla Gasperina et al., 2022; Elayan et al., 2021; Gandolla et al., 2021; P.-h. Huang et al., 2022; Y. Liu et al., 2019; Palazzi et al., 2022; Postol et al., 2021; K. Zhang et al., 2018). However, their presence and use in medical environments is still limited. The main causes are that they are not compact enough, they do not comply with safety standards and/or regulations and they do not have feedback for the patient or the therapist.

To address these issues and achieve greater acceptance in clinical environments, exoskeletons must use multidisciplinary methodologies for their development (Struijk et al., 2022). These methodologies must be immersed in "know-how" (user-centric and task-focused) throughout the development process of these devices, which includes mechanical design, mathematical modeling (biomechanical models), bio-inspired simulation, human–machine interface and experimental testing. Its goal is to provide devices that are able to adapt to different patients, allow repetitive movements to be generated and also present a good interaction with the user (Aole et al., 2022).

According to Moulaei et al in (Moulaei et al., 2023), the robots in physical rehabilitation are used to rehabilitate diseases such as stroke, multiple sclerosis and cerebral palsy, among others. The same study highlights eight areas of disability in order of frequency, where the first three that can also receive rehabilitation through robots are the upper limb, wrist and fingers. Their main goal is to improve musculoskeletal functions (strength, sensation, perception, vibration, muscle coordination, spasticity, flexibility and range of motion).

According to the English national quality standard, patients who have suffered a stroke must receive therapies for a minimum of 45 min 5 days a week, and there are three phases where the robots are used according to their modes of operation (Zhao et al., 2023):

- Assistive mode (active rehabilitation, 1–7 days). The robot provides all limb movements through passive control (passive trajectory following, passive reflex and passive stretch), passive activated control and partially assisted control (impedance, admittance control, attractive force field, model-based assistance and online adaptive control). Generally, controllers with high gains are used (adjusting these gains should not harm the patient, avoiding muscle strains).
- Corrective mode (passive rehabilitation, 1 week to 6 months). The robot accompanies the movements of the limb through tunneling and coordination control.

- Resistive mode (passive rehabilitation, 6 months and on). It opposes the movement of the limbs, using spring and damper methods.

Due to the nature of the application (physical rehabilitation) for exoskeletons, comprehensive multidisciplinary methodologies must be used (considering the knowledge of their developers, patients and medical specialists). The main challenges and ideal solutions when developing this type of robot are the following (Gull et al., 2020; Palazzi et al., 2022; Zhao et al., 2023):

- Motion compatibility: design kinematic compatibility with the human body.
- Discomfort: design joint alignment between the exoskeleton and the joints of the wearer.
- Singularity problem of the mechanical system: design powerful control approaches or mechanical designs with constraints.
- Control: technical complexity (which entails high costs both in development and implementation) requires constant calibrations and adjustments to ensure optimal performance (which can be demanding for both therapists and patients). Some algorithms may require a significant amount of time to be learned and adapted, among other aspects.
- Cost: design using instrumentation for cost-effectiveness (computational resources, sensors, actuators).
- Human–robot interaction: measure the interactions between the human and the exoskeleton (visual, tactile and auditory).
- Sensing and estimation: (1) At the lower level, proprioceptive sensors are used in feedback control to estimate the physical state/properties of the exoskeleton (joint position, speed, acceleration and engine torque). (2) At a higher level, exteroceptive sensors are used to define task-oriented interpretation of sensor data and enable integration of sensor information across space and time to facilitate planning.

Due to the challenges mentioned above, most of the proposed design methodologies only consider a design point of view as well as a mode of operation in the interface, which limits usability for users. In addition, very few exoskeletons comply with ranges greater than 50% of the ranges of motion of the healthy human and above all do not consider biomechanically viable solutions for them, which limits the therapeutic routines they can perform.

Other challenges encompass the creation of control algorithms adaptable to the individual needs of patients, and, above all, the assessment of exoskeletons in real-world environments. So, the challenges related to mechanical designs, control systems, and the evaluation of rehabilitation exoskeletons will be addressed in the following sections.

2.2 Design Methodologies for Robotic Exoskeletons

During physical rehabilitation treatments, practical and biomechanically effective devices are required to enable manual activities. Therefore, to increase their adoptability, usability and safety, various methodologies have been implemented to develop exoskeletons, highlighting

those based on bio-inspired models and real scenarios (Buccelli et al., 2022; Cruz Martínez and Z.-Avilés, 2020; Tröster et al., 2020). For these reasons, developing an exoskeleton is a multidisciplinary challenge that requires the collaboration of patients, medical specialists and exoskeleton developers.

Due to the physical nature of the application, certain robotic challenges are presented. One way to address them is through designs based on evolutionary robotics, which according to Alattas et al. in (Alattas et al., 2019), aims to design automatically adaptive autonomous robots that can evolve to perform a specific task while adapting to environmental changes. One method for designing and implementing evolutionary robots is through modular robotics, whose main characteristics are versatility, robustness, low cost, self-assembly, self-reconfiguration, self-repair and self-reproduction.

In addition to the methods to design robots, other aspects that are strongly related the performance of exoskeletons are the following: the selection of the manufacturing material (strong, rigid and light), the manufacturing method (conventional or additive) and the performance method (power capacity, torque–weight ratio and precision) (Hussain et al., 2021).

In the field of rehabilitation robotics, it is highly desirable to have exoskeletons that are as light as possible, to reduce loads and benefit the movements to be performed by patients, thus generating a design optimization problem. Responding to this type of problem is challenging, because you must choose the most effective process capable of providing an optimal result. However, today, no theoretical method has been found that helps in the selection of such a process; therefore, designers depend on their knowledge and experiences.

The typical methods for solving such problems are classified into heuristics and metaheuristics. According to Peres et al. in (Peres and Castelli, 2021), the latter can solve optimization problems efficiently and flexibly because they do not have "strong" links to any specific problem. Also, optimal solutions to given optimization problems will be found if a balance is found between the following two aspects:

1. **Exploration:** This aims to identify promising areas in the search space with high-quality solutions.
2. **Exploitation:** This intensifies the search in a good region (solutions with excellent quality) of the search space to find a better solution.

In the same previous study, optimization problems are divided into two categories: Continuous decision variables can generate an infinite number of valid solutions. Combinatorial or discrete decision variables have a finite number of solutions and this number depends on the requirements of the problem and its solution representation).

It is essential to consider the time it takes for an algorithm to provide the final solution, since in most combinatorial problems the computational complexity for the search space is usually exponential with respect to the size of the input. However, the success of metaheuristic algorithms is due to the fact that they are usually inspired by some characteristics found in nature. Although there is no evidence that there is a standardization for the design and implementation of these algorithms, in general a metaheuristic experiment considers the

following steps (Peres and Castelli, 2021):

1. **Objectives definition:** Aims to define the experiments' drivers, goals and research questions.
2. **Design:** Aims to specify, plan and prepare the experiment; it includes defining the measures and terminology, determining the metaheuristics, defining the parametrization tuning strategy and determining the report format.
3. **Execution:** Aims to experiment, running each configuration and collecting its data.
4. **Conclusion:** Aims to analyze the results of the experiment.

Optimization can be performed throughout the different stages of the product life cycle through simulations using their digital twins (DTs), and in most cases the proposed methods seek to satisfy multiple objectives. This process is computationally demanding and one way to approach it is through sequential optimization, since it allows for finding optimal solutions in the different application stages. The constraints of the target functions for optimization must be precise and well defined, because the performance of the final optimal design depends on them (Dinh et al., 2021). Neglecting them can produce economically optimal but structurally unacceptable designs or vice versa (Papavasileiou and Charmpis, 2016).

In engineering, this aspect must be taken into account during the mechanical design stage and is known as topology optimization (TO); its objective is to obtain an optimal design (minimize or maximize one or several specific characteristics of the design). TO is a multidisciplinary field in which disciplines such as mathematics, mechanics and computer science play a key role in the design (Meza et al., 2015). While TO is capable of producing high-performance designs, one of its challenges is the physical production of the generated models because the manufacturing method must be able to produce them, or constrain the complexity of the geometry itself and establish a compromise between complexity and performance (T. Wang et al., 2023).

Some of the main requirements of rehabilitation devices are (1) light weight (this benefits the movements made by patients, reduces loads and allows for the selection of compact sensors and actuators), (2) ergonomic design (the robot must be compatible with human kinematics) and (3) automatic control strategies compatible with their application. The first requirement can be achieved through topological optimization by mechanical design: Table 2.1 shows some examples of assistance and rehabilitation robots to which some type of optimization was applied to meet the assigned task.

Table 2.1: Optimization of bio-inspired designs

Reference	Device	Design Requirements	Studies and Tools Used	Results
Greco et al. in (Greco et al., 2023)	Exo for wrist reh.	Design: prototype for an adult. Movement: wrist FE and ulnar/radial deviation. Requirements: lightweight, ungrounded and soft.	Optimization: design and selection of materials and components (3D manufacturing).	Applicability in performing passive and active reh. The device weighs 0.13kg and the exercises were performed with an average error= 0.98°.
Vélez et al. in (Vélez-Guerrero et al., 2021)	Exo to support autonomous neuromotor reh.	Wearable robotic exo (E-FE) with autonomous artificial intelligence-based control. Requirements: lightweight, compact, modular and replicable.	The prototype was tested in controlled environments anthropometrically and with trajectory tracking.	Features device: weight= 988g, motion range= 0-135° and also can regulate the angular velocity. It attaches via external sensors and its average response time is 366 s.
Delgado et al. in (Delgado et al., 2021)	Bio-exo for elbow reh.	The task-based synthesis method is proposed to generate the 3D movements of E-FE.	The elbow joint is analyzed through a motion capture system to develop the bio-exo.	The exo does not need to align with the corresponding limb joint to generate the desired anatomical movement. The error is X = 0.0574, Y = 0.01132 and Z = 0.0804 inches.
Ning et al. in (Ning et al., 2022)	8 DOF reh exo (shoulder, elbow and wrist).	The structural parameters of the shoulder joint are optimized to maximize the range of motion of the UL (anatomical and physiological).	Kinematic analysis is used to track the position of the glenohumeral shoulder joint and reduce the human-machine force interaction.	The exo can satisfy the patient's shoulder, elbow and wrist range of motion.
Heidari et al. in (Heidari et al., 2018)	Thumb exo design.	The design process is a task-based methodology adapted to the body.	The design methodology has three stages: (1) motion capture, (2) dimensional kinematic synthesis and (3) link optimization. which satisfies a set of performance requirements.	A prototype of the Bricard mechanism was obtained, whose translation error varies from 1 to 3 mm.

Reference	Device	Design Requirements	Studies and Tools Used	Results
Zeiaee et al. in (Zeiaee et al., 2019)	CLEVERarm: 8 DOF UL reh exo (shoulder, elbow and wrist).	Optimization consists of achieving minimum volume and maximum dexterity in the workspace. Focused on shoulder design, maximizes usability and improves portability.	The formulated multi-objective optimization problem is solved in two stages, using a genetic algorithm and the weighted sum approach.	A model of the spherical series link in the shoulder and A new index for the effective characterization of the kinematic dexterity of wearable robots.
Sanjuan et al. in (Sanjuan De Caro et al., 2022)	Assistive robot mounted on a wheelchair (6 DOF serial manipulator).	Optimal link length selection of the robot to minimize the torque demands of each joint while increasing the workspace coverage.	The proposed algorithm acts as an objective function, which is optimized using a genetic algorithm for each torque measurement.	The mean square pair (QAT) optimization produces the least workspace with the minimum overall torques of all the joints.
Zhou et al. in (X. Zhou and Zheng, 2021)	Occupational UL exo for aerial lifting activities.	A commercial exo was used and a musculoskeletal model of the upper extremities (5 DOF) was integrated for virtual human evaluation of the exo design and control.	Different assistance methods were evaluated to examine their biomechanical effects on musculoskeletal loading, including interaction forces and moments, muscle activations and joint reaction moments and forces.	Results suggest the effectiveness in reducing biomechanical loadings; exo could reduce maximum loading on the shoulder joint by up to 46%. Active assistance goes beyond the passive assistance approach.
Li Gao et al. in (L. Gao et al., 2022)	UL exo cam mechanism for reh.	The global optimization was performed with adaptive non-dominated sorting genetic algorithm-II (NSGA-II).	A mathematical model for a cam mechanism was established to accurately restore the physical model of the exo motion trajectory, and then optimization was applied. The cam mechanism was tested under dry friction.	The Pareto optimal solution sets of dynamic characteristic parameters of the cam mechanism were obtained, which improves the performance of the exo

Based on the information presented in the previous tables and considering requirements 1 (lightweight) and 2 (ergonomic design), a comprehensive multidisciplinary methodology is proposed for the development of an exoskeleton intended for upper limb rehabilitation. The contributions of this methodology are as follows:

- A design methodology that integrates the points of view of clients, designers and the community, to perform the process of topological optimization and design validation.
- The medical robot achieved is lightweight, highly modular and features safety levels ensuring its proper functionality during passive therapies. Moreover, it covers at least 80% of the upper extremity workspace for a healthy individual in most movements. As a result, it facilitates the execution of a broad spectrum of therapeutic routines without compromising patient mobility.
- The exoskeleton offers three operational modes, and the mathematical model implemented for therapeutic routines ensures feasible and comfortable solutions for patients and medical specialists alike.
- A human-robot interface based on "know-how" was developed, incorporating the use of virtual and physical digital twins.
- The device validation involved movements with patients. It was approached from a teaching and replication perspective, utilizing typical therapeutic routines employed at the initiation and conclusion of a physical rehabilitation treatment for individuals with limited upper limb mobility.

Therefore, mechanical design focuses on creating robust and ergonomic structures that adapt to human anatomy, ensuring comfort and functionality. Additionally, a rehabilitation device must include control systems that manage the interaction between users and the exoskeleton, ensuring that it is effective and safe. The synergy between design and control allows for the development of exoskeletons that not only support and amplify the user's movements but also dynamically adapt to specific therapeutic needs, thus improving rehabilitation outcomes. The following section provides a brief description of the landscape of control approaches implemented in rehabilitation that ensure these points.

2.3 Control Systems in Rehabilitation Exoskeletons

Control systems in rehabilitation exoskeletons present both advantages and disadvantages. Among the advantages, their ability to provide personalized motor assistance stands out, adapting to the individual needs of each patient, typically through trajectory tracking (Ali and Tokhi, 2018; Aole et al., 2022; Fei et al., 2017; Fellag et al., 2017; Mahmoud and Saidi, 2022; Palazzi et al., 2022; Qureshi and Mudassir, 2021). This customization enhances the effectiveness of rehabilitation and accelerates recovery. However, achieving these benefits requires precise and secure interaction between the user and the exoskeleton, thereby reducing the risk of injuries and improving patient comfort during therapy sessions. Table 2.2 provides examples of control approaches implemented in rehabilitation.

Table 2.2: Features exoskeletons

Reference	Modeling	Controller	Trajectories
Mahmoud et al in (Mahmoud and Saidi, 2022). ULE for children. APP: REH.	2 active DOF (ULE of 7 DOF)-Dynamic and strongly nonlinear (considers modeling errors).	Sliding mode (PI). Control: robust model-based and adaptive.	Tracking: yes. Type: Smooth sinusoidal $\theta(t) = A\sin(\omega t + \phi) + \beta$
Fei et al. in (Fei et al., 2017). ULE for Chinese male adults. APP: REH.	D-H model kinematics of 6 DOF. Model-free Control method	PID and robust time delay estimation based intelligent PID controllers. CS: Matlab/Simscape.	Tracking: yes. Type: NM
Ali et al in (Ali and Tokhi, 2018). ULE	2 active DOF (Exoskeleton of 5 DOF))	A fuzzy-based PD controller and PID.	Tracking: yes. Type: NM.
Fellag et al (Fellag et al., 2017) 5 DOF ULE. APP: REH.	Characterization of an approximated model based on experimental knowledge using MATLAB Toolbox.	SMC vs PID. PID gains are tuned using MATLAB Control System Designer SISO tool	TT (instructed by a therapist)
Palazzi et al in (Palazzi et al., 2022). APP: REH or P&P	2 DOF shoulder and elbow flex/ext.	Impedance control	Dynamic movement primitive to record, play back and customize trajectories in the task space
Qureshi et al in (Qureshi and Mudassir, 2021) ULE of 3 DOF (shoulder, elbow, wrist)	Kinematic model (D-H convention) for flexion and extension. Nonlinear equations of motion for the exoskeleton (Euler-Lagrange)	SMC and a high gain observer (HGO) is incorporated to estimate the states of the system	Tracking the trajectories in the presence of parametric variation and constant undesired disturbance.
Aole et al in (Aole et al., 2022) ULE of 2 DOF (shoulder and elbow)	2 DOF model in the sagittal plane (Euler-Lagrange method).	PID vs Active disturbance rejection control (ADRC) requires the nominal information of the plant.	The trajectory amplitude was 0.7855 rad/s with an external parameter variation perturbation of +20%.
Gonzalez et al in (González-Mendoza et al., 2022). ULE APP: REH	3 DOF	Passive therapy: PD controller with gravity compensation. Active therapy: admittance control	Passive therapy: Tracking (type: NM).

Considering the application of exoskeletons in rehabilitation, the main challenges can be divided into two groups: a) those that come from their physical characteristics and b) those that come from their application. The former address aspects of the engineering design for the physical components, workspace and kinematic/kinetic models of the robot. The latter contemplate aspects related to the nature of rehabilitation treatments, such as: precision (personalized treatments), physical assistance by the physiotherapist (resistive or assisted therapy), coupling between the robot and the patient (generates highly nonlinear systems with changing dynamic models), among others (Gull et al., 2020, J. Wang et al., 2021).

These latter aspects are challenging for developers, as they require automatic control strategies that ensure compliance while also providing security to users. Traditionally, the controller gain tuning has been done heuristically or based on the biomechanical properties of a given patient group. However, the following drawbacks are present: a) they limit the applications of the exoskeleton to small user groups and b) they are time-consuming and tedious (J. Wang et al., 2021). Therefore, there is a need to devise approaches for the automatic determination of controller parameters, taking into account the intricacies of the systems along with their model uncertainties and external disturbances, such as human-exoskeleton interaction.

To solve this issue, some authors have developed control strategies based on: previous measurements and/or experimentation (neural networks and/or fuzzy logic). Nevertheless, they are susceptible to variations and the characteristics of the tasks to be performed (Belov et al., 2022, Habiba et al., 2022, Al-Waeli et al., 2021, de Medeiros and Muñoz, 2022). Robust control algorithms have been implemented where the parameters are not straightforward to adjust heuristically (Aichaoui and Ikhlef, 2022, Yu et al., 2023, Safira et al., 2023, Bembli et al., 2021, Broad et al., 2020, Ratiba et al., 2022). Therefore, it is necessary to implement control approaches based on metaheuristic optimization that can be adapted in real time to different users. These algorithms allow to find more efficient configurations for the controller than traditional methods, so that the tuning of these robust controllers maintains the stability of the system.

This type of approach can overcome the drawbacks of the approaches mentioned above, so the key steps for this approach are outlined below:

1. Establish an objective function.
2. Optimizer Selection.

The optimization procedure entails identifying the most favorable values for a predefined set of parameters within a particular system. This aims to meet specified criteria while taking into account the minimal or maximal associated cost. Therefore, the first step can be defined through one or more objective functions, or through a weighted objective function, which must be conveniently selected according to the optimization objective (minimization or maximization).

In the second step, direct methods (response surface method, gradient descent, etc.) or swarm-based methods (evolutionary algorithms, EAs) can be used. Direct methods are sensitive to noise which reduces their performance, and they also have the following limitations:

solutions based on a single criterion, converging to local optimal and issues related to an unidentified search space. Meanwhile, the swarm-based methods have shown an excellent performance concerning the former (J. Wang et al., 2021, Samala, 2023, Silawatchananai and Parnichkun, 2019, Amiri et al., 2019).

Lately, the particle swarm (PS) algorithm has emerged as one of the EAs utilized for optimizing controller parameters in exoskeletons, due to the following characteristics (J. Liu et al., 2021, Soleimani Amiri et al., 2020, Sreejeth et al., 2023):

- Its simplicity and high convergence speed.
- It does not need any assumptions about the problem to be optimized.
- It can explore extensive solution spaces.
- It possesses the capability to handle intricate complex nonlinear systems with a high number of dimensions and challenges in dynamic optimization across diverse domains.
- It doesn't demand a precise dynamic model or accurate system parameters beforehand.
- A limited number of parameters that require adjustment.
- It exhibits a high likelihood and efficiency in discovering global optima.

Despite the qualities that the PS algorithm presents, it also has some disadvantages (Belkadi et al., 2017, J. Liu et al., 2021, Soleimani Amiri et al., 2020, Han et al., 2022):

- The time required for convergence might be extended, potentially leading to undesirable chattering phenomena in a control context.
- The potential problem of early convergence could hinder the ability to adapt to sudden changes in the system and the environment.
- There is a risk of early convergence, leading to entrapment in local optima.

Therefore, it is imperative to choose a robust controller capable of meeting these challenges. Such a controller should meet the following fundamental characteristics (Ratiba et al., 2022, Wu et al., 2014, Fitzsimons et al., 2020, Saveriano et al., 2023, Dehio et al., 2022): robustness to external disturbances and model uncertainties, noise in the measurements, and set-point stability. The earlier is since exoskeletons are systems coupled to different users while performing different tasks, the second is because of the dynamic model approximations and/or simplification of the real system, and the latter is due to the physical characteristics of the exoskeletons.

SMC is a well-recognized robust control approach designed to handle uncertain dynamics (Narayan et al., 2022, G. Zhang et al., 2022, Silawatchananai and Howimanporn, 2020, Mahmoud and Saidi, 2022). This controller offers several advantages, including rapid response to changes over time, resilience to changes in parameters, and ease of implementation. Nonetheless, it has as its main disadvantage the presence of chattering. An alternative that has been used to simultaneously reduce chattering and the reaching time is the inclusion of an exponential function as reaching law (Komurcugil et al., 2022, Brahmi et al., 2020). Employing this exponential scope law does not compromise the robustness of the SMC.

To tackle the mentioned aspects, along with addressing the issues of chattering and trajectory tracking in the control scenario, the robust SMC with an ERL controller was chosen in this study (Fallaha et al., 2010). Whose design process is described below:

1. Select the sliding surface S based on the tracking error.
2. Select the reaching law that facilitates the convergence of the error vector to the sliding surface.

This controller involves two control gains to suppress chattering and address response speed. Typically, gains are selected through trial and error regarding the chattering amplitude versus reaching time. To tackle the aspect associated with gain selection, this work suggests the following contributions:

- Propose online tuning of gains using ERL and the metaheuristic algorithm PSO in an exoskeleton (highly nonlinear system).
- Implement the robust control algorithm PSO-ERL in a 7-DOF exoskeleton for online gain tuning for trajectory tracking (allowing the exoskeleton controller to adapt online to changes in users' morphology and motor skills).
- Conduct experimental validation of the proposed control algorithm on healthy subjects exhibiting diverse physiological characteristics.

Considering that the effective performance of rehabilitation exoskeletons is inherently linked to their mechanical design and control system, it is essential to conduct a thorough evaluation of these elements. This assessment should extend beyond mere measurements of the device's mechanical efficiency and accuracy, also encompassing its impact on the interaction dynamics between the user and the exoskeleton, as well as its ease of use. Therefore, a brief literature review focusing on the evaluation of rehabilitation exoskeletons is presented below.

2.4 Evaluation of Robotic Exoskeletons in Rehabilitation

Currently, the use of exoskeletons in the field of rehabilitation shows great potential, offering new opportunities to improve the mobility and quality of life for people with physical limitations. Their effectiveness lies in the ability to provide personalized and adaptable biomechanical support, allowing users to perform controlled and functional movements (Gandolla et al., 2021, Longatelli et al., 2021, Semprini et al., 2022, La Bara et al., 2021). This capability not only immediately enhances mobility but also accelerates the recovery process, especially in patients with neurological or musculoskeletal injuries.

Therefore, assistive or rehabilitation devices are typically evaluated by measuring their performance. The most commonly used metrics include ranges of motion (Yurkewich et al., 2019, the level of assistance Yurkewich et al., 2019, Z. Zhou et al., 2021), and the application of different controllers (Costanzi et al., 2023, Morishita and Murakami, 2023, McDonald et al., 2020, Vélez-Guerrero et al., 2021, Z.-J. Chen et al., 2021).

To achieve this, it is crucial that robotic technology is easy and appealing to use Lambelet et al., 2020. One way to accomplish these aspects is by considering feedback from end users during both the design and evaluation stages (Khan et al., 2022). However, evaluation remains a challenge, primarily when measuring ease of use, due to the diversity of user actions and perspectives involved. Among the main obstacles to acceptance are the complexity of the controls (which generally require specialized knowledge or training for use and functionality), and the cognitive workload (Moulaei et al., 2024, La Bara et al., 2021).

When devices have low usability, it is common for users to experience frustration during use. This can result in limitations in functionality and cause errors, inefficiencies, and a reduction in productivity, thus negating the intended benefits of these technologies. To overcome these obstacles and fully leverage these devices (ensuring effective use and optimizing user satisfaction), it is essential to integrate end-user evaluations at various stages of development (La Bara et al., 2021, Barrera-Gálvez et al., 2017, Villarejo et al., 2018, Moulaei et al., 2024, Meyer et al., 2019, Halim et al., 2022, Struijk et al., 2022, Khan et al., 2022). This approach can significantly impact the quality of life by improving usability, increasing satisfaction, comfort, and user experience (Meyer et al., 2019, Halim et al., 2022). Implementing this approach can help bridge the gap between laboratory prototypes and clinical applications. A notable example of this integration is the CYBATHLON event, where teams consisting of technology developers from universities, companies, or NGOs, along with individuals with disabilities, tackle various everyday tasks using their latest assistive technologies.

Although some evaluations focus on physical interaction variables, most use protocols with subjective aspects, such as questionnaires, to assess user perception during the execution of a training task. This practice is appropriate since these devices are based on user-centered designs, meaning their evaluation is directly related to user experience (Meyer et al., 2019, Moulaei et al., 2024). For instance, in surgical fields (Cha et al., 2020) and industrial settings (Franco et al., 2023, Moreno Franco et al., 2023, Franco et al., 2024, Ostuni et al., 2023), the main evaluations conducted include usability, functionality, user experience, workload index, satisfaction, among others. In the field of rehabilitation, the evaluations are generally similar; however, the application conditions and users have special characteristics. Nonetheless, in all cases, the data collected in these evaluations are essential for understanding user feedback, identifying areas for device improvement, and ultimately enhancing user experience. All of this aims to increase the acceptance and adoption of such robots in the long term.

Evaluation of Exoskeletons in Rehabilitation Contexts: A Systematic Review

Given the complexity of assistive devices, it is crucial to evaluate them from a multidimensional perspective that encompasses key aspects such as performance, usability, satisfaction level, and workload. These evaluations should be conducted under real-use conditions, taking into account the experience and feedback of the users involved. To improve the consistency of measurements, it is essential to use questionnaires based on international standards.

In the realm of usability and human-computer interaction ergonomics, the ISO/IEC 9241 standard stands out, developed by ISO (International Organization for Standardization) and

IEC (International Electrotechnical Commission). This standard aims to enhance the user experience when using digital products or services, ensuring they are intuitive, efficient, and satisfying. Its implementation ensures usability, efficiency, and user satisfaction, positively impacting the quality and competitiveness of the products and services offered.

Part II of the ISO 9241 standard defines usability as the effectiveness, efficiency, and satisfaction with which specific users achieve specific goals in a particular environment. This implies that products and services designed according to this standard should facilitate the achievement of goals effectively and efficiently, providing a satisfactory experience for users where:

- Effectiveness: refers to the accuracy and completeness with which a user achieves a specific goal in a particular context. This means that users perform a defined set of tasks, and the success or failure rate in their execution is measured.
- Efficiency: is described as the relationship between the resources used and the accuracy and complexity of the goals achieved. This involves measuring the time participants invest in completing tasks.
- Satisfaction: refers to the comfort and acceptance of the system by users and other individuals impacted by its use. It serves to evaluate usability in a broad sense.

Some studies reporting the evaluation of different assistive devices are shown in Table 2.3. According to the Table 2.3, usability is generally evaluated through subjective assessments that qualitatively analyze assistive technologies. The System Usability Scale (SUS) is one of the most common methodological tools in user experience for this purpose. However, customized metrics and questionnaires designed specifically for the characteristics of the evaluated devices are also employed.

Table 2.3: Evaluation Metrics and Evaluating Subjects

Ref.	Description	Evaluations and Metrics		Evaluators				Location
				Medical personnel		Patients		
		Device	Others	Number and type	Details	Number and type	Details	
Catalán et al. in (Catalán et al., 2023)	Compare an UL Exo (NESM-β, which includes a pronation-supination module and a hand exoskeleton) with an external manipulator (Jaco® robot produced by Kinova, Boisbriand, Canada).	Unspec	Workload: NASA-TLX Qs. Hybrid interface EEG/EOG to evaluate ADLs. UE: Cm, Sf and Rb (LikS Qs). Custom Qs based in 5-point LikS (8 items).	Unspec	Unspec.	10 Impaired participants (5 females and 5 males): Neurological condition (Ec, Stro, TBI, SCI, CP, MS, MD).	Age: 52±16 years. ADLs (Drinking and pouring task).	Northern Ireland
Verdel et al. in (Verdel et al., 2022)	Quantify the influence of 3 different physical interfaces applied to the ABLE active UL Exo: a strap with no DOF, a thermoformed orthosis with 1 DOF (translation), and one with 3 DOF (translation and rotations).	Interaction efforts (forces and torques). Kinematic parameters (10 infrared cameras).	ELM measurements (muscular activity, RMS) y subjective feelings (semi-directed Qs with 6 items based in a LikS (Cm, Ab-m, Acc))	Unspec.	Unspec.	18 healthy right-handed subjects (11 females and 7 males).	Age: 25±6 years old, height: 171.9 ±7.9 cm, weight: 64.8 ±11 kg, arm length 28.6±2.8 cm, forearm length: 25.3 ±1.8 cm and hand length: 19.2±1.3 cm. Blocks of 15 flexion and 15 extension elbow movements with an amplitude of 60 degrees.	Unspec.
Kim et al in (H. K. Kim et al., 2021)	Develop an assessment tool (usab and user value) for the Exowalk® (HR-02, HMH Co. Ltd, South Korea) LL Exo and gait rehab training.	Usab (Qs: Reh Eff, Tr, Ov-Sat) and User value (Qs: S-d and Secu).	Unspec.	38 Therapists	Who assisted in the use of the Exo	102 Reh patients (64 males and 34 females): 51 using Exo and 51 under the ETP without robots	Age: 56 ±22.53 years. Each subject: 20 sessions, 5 times a week within a 4-week span (30-minute walking practice session).	Dongguk University Ilsan Hospital, Chungnam National University Hospital, and Seoul National University Bundang Hospital in South Korea.

Ref.	Description	Evaluations and Metrics		Evaluators				Location
				Medical personnel		Patients		
		Device	Others	Number and type	Details	Number and type	Details	
Ferrero et al in (Ferrero et al., 2022)	Evaluate the acceptance of an EEG and EOG brain-machine interface used by the LL Exo H3 (Technain, Spain).	Sat (QUEST 2.0)	Workload (NASA-TLX (by patients)), perceived effort at different times during each session (Borg Rating of Perceived Exertion Scale.)	Unspec.	Unspec.	2 patients who had suffered an incomplete SCI (from National Hospital of paraplegics of Toledo.)	Males, Age: 37 and 59 years old, Height: 1.73m and 1.74m, weight: 79 kg and 74 kgs. EEG and EOG equipment were used. Patients completed 14 trials across various sessions (mean session duration $\approx$ 2.5 hours.	Spain.
Alguacil et al in (Alguacil-Diego et al., 2021)	Detail the usab, accep, and ov-accep of a hybrid exo designed for passive UL Reh (ExoFlex).	Usab (SUS Qs)	Sat (custom clinician Qs (5 items are rated on a 5-point LikS)).	Unspec.	Unspec.	7 patients (6 females and 1 male). Patients' Injuries: SS, TF, TS, SPT, FS, ST, RCT and STen.	Age: 50-79 years old. The test consisted of a series of passive mobilizations of the affected UL (shoulder flexion, shoulder abduction and shoulder elevation with an intermediate aperture angle).	Clinic Center of Getafe (Madrid, Spain)
Dalla et al in (Dalla Gasperina et al., 2022)	Evaluate the usab and efficacy of the AGREE reh platform for improving arm deterioration after stro.	Usab of the AGREE system (SUS Qs)	Therapist: Usab of the AGREE system (SUS Qs)	2 phys (from clinical center).	The phys were trained to use the AGREE platform. Halfway through the reh intervention with the first patient, the SUS Qs was administered.	2 groups of 16 subjects each: CG (performing conventional physiotherapy) and EG (performing AGREE-assisted reh). 15 sessions of 45 minutes of arm training 3 times a week.	Unspec.	Casa di Cura del Policlinico, Milan, Italy.

Ref.	Description	Evaluations and Metrics		Evaluators				Location
				Medical personnel		Patients		
		Device	Others	Number and type	Details	Number and type	Details	
Perez et al in (Pérez et al., 2022)	The design and development process of Exogames (virtual reality exercise game) is reported, as well as the evaluation of its potential for physical and emotional reh. Exogames works with Nukawa, a LL reh robot. Together, they constitute the general Kina system.	Unspec.	Initial stage (survey designed ad-hoc, 13 health professionals). Second evaluation (standardized surveys (SUS Qs, Physical Activity Enjoyment Scale (PACES- 18 items evaluated on a 7-point LikS), and the Game Experience Qs (GEQ, 6 items evaluated on a 5-point LikS)	Initial stage: 13 health professionals. Second assessment round: 5 phys	Initial stage: 11 of them were phys and 2 were speech therapists. All had a specialization or Master's degree, over 4 years of professional experience, and ages between 25 and 44 years old. Second assessment round (evaluated the Kina system): 3 females and 2 males, all of them with a postgraduate, over 9 years of professional experience, and ages between 30 and 37 years old, with an average height of 1.68m and an average weight of 73 kg. None of them participated in the 1st assessment round	1 male with a lower limb amputee.	Subject had completed his reh and prosthesis adaptation processes, whose academic level is Baccalaureate. Features: 51 years old, 1.62m and 75 kg. He didn't participate in the 1st assessment round	Medellín, Colombia.

Ref.	Description	Evaluations and Metrics		Evaluators				Location
				Medical personnel		Patients		
		Device	Others	Number and type	Details	Number and type	Details	
Gandolla et al in (Gandolla et al., 2021)	Evaluate an assistive UL Exo controlled by multimodal interfaces for severely impaired patients.	Externally-assessed functional benefit (performance of ULs module), self-perceived functional benefit assessed (ABILHAND Qs) and system usab (SUS Qs)	Unspec.	Unspec.	Unspec.	Participants were recruited from inpatients and outpatients services: 14 patients (1 female and 13 males)	Age: mean 21 years (range 15-53 years). Participants had a high degree of disability, with a median Muscular Rating Council index at the Deltoid level equal to 1.00 (IQR 1.00), and at the Biceps Brachii equal to 1.00 (IQR 0.50). These values indicated that patients could not move their arms even in the absence of gravity.	Scientific Institute IRCCS E. Medea and Rehabilitation Institute Villa Beretta.
Park et al in (Park et al., 2020)	Evaluate the differences in clinical and kinematic outcomes between active (Armeo® Power, Hocoma Inc, Zurich, Switzerland) and passive (Armeo® Spring robot, Hocoma Inc, Zurich, Switzerland) robotic reh among stro survivors.	Usab of the robots through interviews with patients, therapists, and physiatrists.	The primary WMFT-score and -time: measures activity, and secondary FMA and SIS scores: measure impairment and participation, respectively; kinematic outcomes. Evaluate the benefits of two types of therapies administered through different types of exos.	Unspec.	Unspec.	First group: 10 patients (ACT). Second group: 9 patients (PSV). Both group are stro survivors with UL dysfunction	First group: age (54.9 ± 10.7), time after stro onset (11.8 ± 11.0 month), hemiplegic side (right=6 subjects and left=4 subjects), sex (2 females and 8 males). Second group: age (53.9 ± 16.7), time after stro onset (9.6 ± 4.5 month), hemiplegic side (right=5 and left=4), sex (1 females and 8 males). Groups in a 1:1 ratio and administered 20 sessions of 30-min robotic intervention (5 days/week, 4 weeks).	National Rehabilitation Center in South Korea.

Ref.	Description	Evaluations and Metrics		Evaluators				Location
				Medical personnel		Patients		
		Device	Others	Number and type	Details	Number and type	Details	
Longatelli et al in (Longatelli et al., 2021)	Evaluate functional improvement in patients with MD using 2 commercial arms: a passive device (Jaeco's Wrex) and a semi-active device (Armon Ayura).	Eff with an externally-assessed scale (performance of the UL-PUL-module), a self-perceived scale (Abilhand Qs), and a usab scale (SUS). Significant functional gain for PUL module (Friedman's test and Abilhand Qs). Moreover, PUL changes were compared by means of the Friedman's test.	Unspec.	Unspec.	Unspec.	36 patients (4 females and 32 males). Participants from in-patients and outpatients services at IRCCS E. Pathology: DMD (16 patients), BMD (8 patients), LGMD2 (10 patients) and CMD (2 patients)	Age (years): 30 [19.5-54], DMD: 19 [15.5-21.5], BMD: 52 [38.5-58.5], LGMD2: 54 [31-57], CMD: 56 [51-61]. Dominant arm: right (31) and left(5). MRC deltoid: 2.00 [0.5-3]. MRC biceps brachii: 2.00[1.5-2.75]	IRCCS E. Medea and Villa Beretta Rehabilitation Center.
Nann et al in (Nann et al., 2020)	Examined the fea, sf, and u-fr of EEG/EOG-based brain/neural robotic control in stro survivors using NESM-β.	Fea (descriptive statistics). U-fr and Sf (Custom Qs (7 items are rated on a 5-point LikeS))	Unspec.	Unspec.	Unspec.	5 patients (1 female and 4 males): Post-stroke patients with severe hemiparesis.	Age: 39-69 years. Impaired limb: 1 right and 4 left. Time since injury 6.2 $\pm$ 5.8 years. They performed a drinking task (including reaching, grasping, manipulating, and drinking).	Campus Bio-Medico University of Rome, Italy.
Van et al in (van Dijsseldonk et al., 2020)	Aassess the amount, purpose, and location of exo use in the home and community environment, without any restrictions (ReWalk Personal 6.0, a wearable robotic exo from ReWalk Robotics).	Participants kept a daily logbook, and completed two UE Qs (D-QUEST and SUS).	Unspec.	Unspec.	Unspec.	Patients with complete SCI. 14 patients (7 females and 7 males)	Age (mean [min, max] years): 29 [24-49], time post injury (mean [min, max]): 6.25 [0.75-27], neurological level of SCI (thoracic, median [min–max]): Th9 [Th4–L1], classification of SCI level (low (Th7–12)/high (Th1–6)): 8/6, AIS* (A/B): 13/1.	Unspec.

Ref.	Description	Evaluations and Metrics		Evaluators				Location
				Medical personnel		Patients		
		Device	Others	Number and type	Details	Number and type	Details	
Lambelet et al in (Lambelet et al., 2020)	It presents the development, characterization, and portability evaluation of a fully portable exo for active wrist extension/flexion support in stro reh (the exo is composed of 2 modules placed on the forearm/hand and the upper arm.)	wearability, usab (SUS), device evaluation (SUS customized with 32 items that includes aspects as learnability, efficiency, memorability, errors and sat.)	Workload experienced during a task (RTLX)	Unspec.	Unspec.	Healthy (15 subjects: 7 females and 8 males) and stro survivors subjects (2 males)	Healthy subjects: Age (mean age: 26±3.4, ranging: [22, 33] years), Handedness: 8 right-handed, 5 left-handed and 4 ambidextrous. Stro survivors: Age (68 and 52 years), both left-arm impaired and both suffered a haemorrhagic stro 167 and 113 months ago, respectively, handedness: both right-handed.	Zurich
Semprini et al in (Semprini et al., 2022)	It identifies the end-users needs and to develop a user-centered-based control system for the TWIN LL exo to provide post-stro reh.	Usab, accep and barriers to usage. Before and after all testing (wearing the exo) and observation (observing another person testing the TWINActa) custom Qs consisting of semi-structured interviews and the SUS with a 5-point LikS	Unspec.	T2 group: 5 internal clinical experts. A panel of 4 external health professional experts.	T2 group: 3 physical therapist, 1 expert neurologist and 1 bioengineer. The panel of external health professional experts observed the T2 session and provided a further feasibility evaluation of the system.	5 post-stro patients (5 males)	age (years): 53.4 ± 9.0, body mass (kg): 77.4± 11.0, body height (cm): 173.6 ± 4.2, thigh length 35.5–47.5 cm, shank length: 40.5–48.5 cm, pelvis width 69–99 cm, shoe size 36–45.	Milan, Italy.
Meyer et al in (Meyer et al., 2019)	Evaluate a novel fixation system designed with a focus on paraplegic users, which is used in the LL Exo: VariLeg.	Usab (SUS Qs with a 5-point LikS)	UE (custom Qs focusing on the long-term use of the Varileg (7-point LikS)). Local discomfort heat map (to assess the wearing comfort during the execution, it was designed on the basis of simple pain rating scales and it was rated on a 7-point LikS)	Unspec.	Unspec.	Native German speakers: Paraplegic (2 subjects) and healthy (5 subjects)	Paraplegic: males, ages: 57 and 40 years old, height: 1.77m and 1.83m, weight: 85 kg and 77 kg. Healthy: males, ages: 25 ± 2.3 years, height: 1.82 ± 0.003, weight: 76.6 ± 5.2 kg). Session duration≈ 60 min	Unspec.

Ref.	Description	Evaluations and Metrics		Evaluators				Location
				Medical personnel		Patients		
		Device	Others	Number and type	Details	Number and type	Details	
Perez et al in (Pérez-Rodríguez et al., 2019)	It evaluates the usab, accep and UE of the FriWalk robotic walker from the patients and clinical professionals' perspectives.	Usab (SUS Qs, patients and clinical profesional)	UE (UE Qs, only clinical professional), accep (Technology Acceptance Model with 12 items, patients and clinical professional) and a customized short qualitative interview for the clinical proffesionals and patients respectively (3 items).	1 clinical professional.	The clinical professional responsible for the administration of the functional decline prevention treatment based on the FriWalk completed the SUS Qs monthly.	2 groups: CG and IG. CG: 20 subjects (13 females and 7 males), IG: 22 subjects (14 females and 8 males). Only IG group did the evaluation	13 patients participated in the evaluation of the system in terms of usability, UE and acceptance since CG participants did not have the opportunity to use the FriWalk during the clinical pilot. CG: age (75-85 years=6 subjects, +85 years=14), setting: Acute care unit-ACU (18 subjects) and Orthogeriatric Unit-OU (2 subjects). IG: age (75-85 years=7 subjects, +85 years=15 subjects), setting: Acute care unit-ACU (19 subjects) and Orthogeriatric Unit-OU (3 subjects)	Getafe University Hospital, located in the South of the Autonomous Community of Madrid.

SUS consists of a 10-question questionnaire with reliable and valid results, where each question is scored from 1 to 5, with 1 being "Strongly Disagree" and 5 being "Strongly Agree". Scores range from 0 to 100, with usability considered high if scores exceed 80 points, while scores below 70 are classified as low usability. To measure usability, Lewis and Sauro in (Lewis and Sauro, 2009) recommend a minimum of 12 participants. This same number is supported by Julious in (Julious, 2005), arguing that 12 participants are adequate for the sample size per group when designing a clinical trial, based on feasibility, precision around the mean and variance, as well as regulatory considerations..

Another variable highlighted in the evaluations is workload, which uses the NASA TLX protocol as a technique to reduce variability in subjective ratings. This multidimensional technique allows organizations to measure workload, understood as the effort required by a human operator to achieve a certain level of performance. In this context, workload is defined based on the interaction between task requirements, the circumstances in which it is carried out, and the skills, behaviors, and perceptions of the operator (Barrera-Gálvez et al., 2017). This index utilizes indicators such as effort, frustration, mental load, temporal load, and stress to assess the relationship between usability and utility in human-robot interaction systems (HRpI).

A prominent standard in interface evaluation is ISO/IEC 25010:2011, which provides guidance for evaluating various quality aspects in software products and systems. This standard is essential for ensuring that these products and systems meet the requirements and expectations of the end user. Among the quality characteristics defined in this standard are functionality, reliability, usability, efficiency, maintainability, portability, and security.

When it comes to assessing device performance, the most common methodology involves analyzing its accuracy, repeatability, and reproducibility. For this reason, in this study, we will focus on measuring these aspects using the Root Mean Square Error (RMSE). This error is calculated by applying therapeutic movements, both simple and complex, to a variety of patients with different motion specifications.

Therefore, the main contribution of this work lies in the comprehensive evaluation of the usability of an exoskeleton designed for upper limb rehabilitation, conducted in a clinical environment (real application conditions). This analysis covers two fundamental aspects: 1) the application of standardized and customized questionnaires, based on quality standards, directed at both users and physiotherapists, which involves subjective and quantitative evaluations; and 2) the assessment of the device through the performance of simple and complex movements, both in simulation and real conditions. All these evaluations were carried out during rehabilitation sessions under real conditions.

In the following sections, the methodology for developing a robotic rehabilitation exoskeleton as a mechatronic product will be detailed, covering from identifying the need to obtaining the physical prototype and evaluating it in clinical settings. Its mathematical foundation will be explored, along with its implementation in both software and hardware, and finally, evaluation will be conducted in real-world environments.

Chapter 3

Mathematical foundations

"Knowledge is power".

Francis Bacon.

In this section, the theoretical foundations supporting the proposed methodology for the development of an upper limb rehabilitation exoskeleton are presented. Fundamental aspects are explored, encompassing mechanical design and its topological optimization, along with innovative manufacturing methods. Additionally, mathematical/biomechanical models describing the system's behavior are analyzed, as well as optimal control systems applied in physical rehabilitation, with a focus on the physical interaction of the exoskeleton with the human body. Human-robot interfaces and usability evaluation methods are also considered.

3.1 Design Fundamentals

Mechanical Design

Mechanical design plays a vital role in crafting machinery, devices, or systems by applying engineering and design principles to tailor solutions meeting specific requirements, from conception through to production. Emphasizing interdisciplinary collaboration and leveraging advanced technologies like simulation and computer-aided manufacturing are pivotal for generating innovative and efficient mechanical solutions (Norton, 2016; Shigley et al., 2019; Juvinall et al., 2013).

Typically, the design process adheres to an iterative cycle, with its primary stages outlined as (Norton, 2016):

- Precisely define the problem to be addressed.
- Set clear and attainable objectives from a functional standpoint.
- Ideation and invention encompass the analysis of machinery kinematics and dynamics to devise mechanisms that fulfill specific functions and yield novel devices. This process

entails defining performance specifications, delineating what the system must achieve, and design specifications, outlining how it should be executed.

- Select a design that is potentially viable and feasible.
- Develop a prototype based on the chosen design.
- Perform validation tests on the developed prototype, spanning from basic operation and observation of its functionality to the precise measurement of specific variables.
- Production of the final version of the device.

To assess the device's reliability through stress analysis, various types of stresses are identified (Mott et al., 2006).

- Static stress: arises when a consistent load is steadily applied to a component without causing any impact. In such cases, both the maximum stress (σ_{max}) and the minimum stress (σ_{min}) are equal, with a stress ratio R =1.0.
- Reversed and repeated stress: This phenomenon entails alternating between equal magnitudes of tension and compression in consecutive cycles. In this scenario, $\sigma_{\min} = -\sigma_{\max}$, with a stress ratio of $R = -1.0$, and an average stress of zero.
- Fluctuating stress: The component undergoes alternating tensions with an average value that is not zero.

All design methodologies must define the correlation between the stress exerted on a component and the material strength it will be manufactured with, while taking into account service conditions. The objective is to achieve a suitable design factor N (safety factor) to guarantee the component's integrity during operation. The primary methods for predicting failures are outlined in Table 3.1 (Mott et al., 2006).

Table 3.1: Methods of failure prediction. Information taken from (Mott et al., 2006).

Method	Type of stresses	Type of Materials
Maximum normal stress	Uniaxial static	Brittle
Modified Mohr	Biaxial static	Brittle
Yield strength	Uniaxial static	Ductile
Maximum shear stress	Biaxial static	Ductile
Strain energy	Biaxial or triaxial	Ductile
Goodman	Fluctuating	Ductile
Gerber	Fluctuating	Ductile
Soderberg	Fluctuating	Ductile

According to the literature, the most accurate method for estimating failures in ductile materials is the distortion energy method, as it considers stresses under static loads or for normal, shear, or fully reversible combined stresses. This method introduces the concept of

"Von Mises stress" (σ'), which is calculated for biaxial stresses with maximum and minimum principal stresses (σ_1 and σ_2), as shown in equation (3.1) (Mott et al., 2006).

$$\sigma^{'} = \sqrt{\sigma_1^2 + \sigma_2^2 - \sigma_1\sigma_2} \tag{3.1}$$

A failure occurs when $\sigma' > s_y$, where s_y is the yield strength. In the biaxial stress method, it is required that the applied stress in the third orthogonal direction, σ_z, be zero. For design purposes, the design factor N can be applied to the yield strength, and then equation (3.2) can be used.

$$\sigma^{'} < \sigma_d = \frac{s_y}{N} \tag{3.2}$$

From (3.2), it can be seen that the safety factor is as shown in equation (3.3):

$$N = \frac{s_y}{\sigma^{'}} \tag{3.3}$$

Therefore, to ensure maximum accuracy in the results of this evaluation, it is imperative to understand the service conditions to which the device is exposed.

Throughout the design process, it's imperative to integrate human factors engineering. This entails prioritizing the creation of devices that suit user needs, rather than requiring users to adapt to the machine, a fundamental principle of ergonomics. This approach involves considering a wide range of information about potential users, including body dimensions, age, gender, ability to tolerate certain conditions, among others (Norton, 2016).

In the design of exoskeletons, user-centered prioritization is paramount, requiring careful consideration of aspects pertaining to the kinematics and dynamics of the upper limb. Within this framework, grasping how the device interacts with human motion is vital to enhance its functionality and comfort. The subsequent section offers an in-depth exploration of the pivotal factors influencing the design and efficacy of the exoskeleton.

3.1.1 Human anatomy and physiology: Upper limb kinematics

The human body is constituted as an organic entity that encompasses the head, the trunk, and the upper and lower extremities. In these body segments, the anatomical elements consist of bones, muscles, joints, and other tissues that collaborate in vital functions such as movement, manipulation, and interaction with the environment (Drake et al., 2020; Tortora et al., 2002; Netter, 2023).

The upper limb comprises fundamental joint and bone components that extend from the shoulder (connecting the limb to the trunk) to the hand (the distal portion beyond the wrist joint), including the arm (extending from the shoulder joint to the elbow joint), the elbow, and the forearm (located between the elbow and the wrist joint), as visualized in Figure 3.1 (Drake et al., 2020; Kapandji, 2006; Pons, 2008).

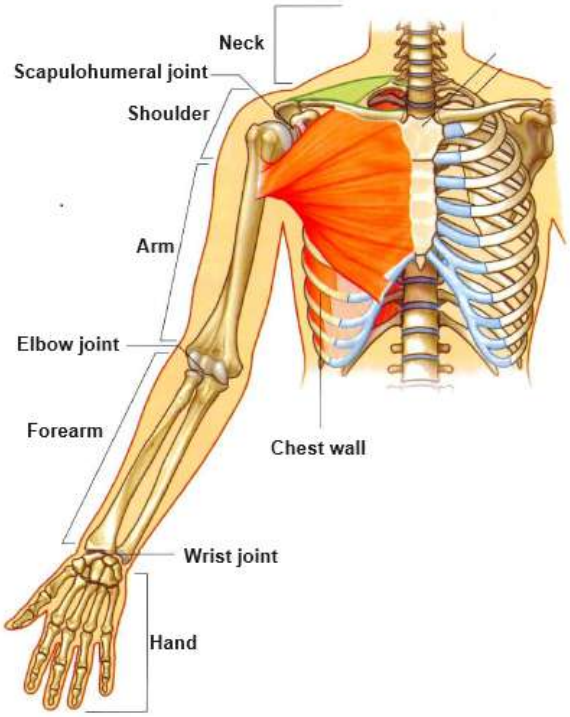

Figure 3.1: Anterior view of the upper limb. Figure adapted from (Drake et al., 2020).

Considering the above, generally seven degrees of freedom are recognized in the articular chain of the upper limb. The standard anatomical position, used to describe the location of bodily structures, is shown in Figure 3.2. In this position, the body is standing with the feet together, the arms at the sides, the face looking forward, and the palms of the hands facing forward, with the fingers straight and together (Drake et al., 2020; Pons, 2008).

Below are detailed the main physiological characteristics of the joints of the upper limb (Kapandji, 2006):

- **Shoulder Joint:** This proximal joint stands out as the most mobile among all the joints of the human body. It provides three degrees of freedom (DOF), allowing for the following movements:
  - Flexion (sagittal plane): It is the movement in which the arm is raised forward and upward from the anatomical position. Its range of motion is 180° (it can also be described as abduction of 180°). See Figure 3.3 a) right.
  - Extension (sagittal plane): Movement that takes the arm backward and downward from the anatomical position. Its range of motion is 45° to 50°. See Figure 3.3 a) left.
  - Abduction (frontal plane): It is the movement that involves moving the upper limb away from the trunk. This movement can reach 180°, with the arm positioned vertically above the trunk. See Figure 3.3 b).

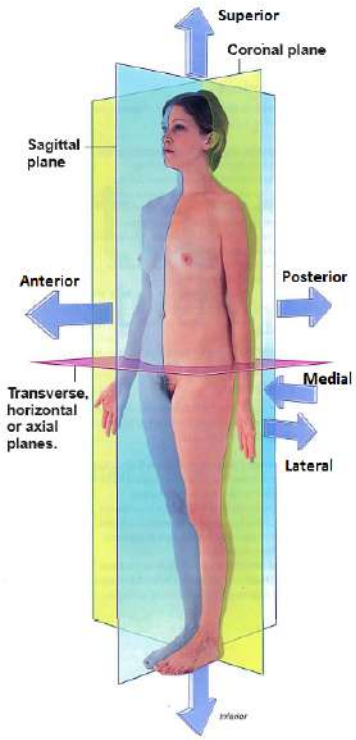

Figure 3.2: Anatomical position, planes, and terms of location and orientation. Figure taken from (Drake et al., 2020).

- Aduction (frontal plane): It is considered a movement opposite to abduction, that is, directed towards the inner part. From the anatomical position, aduction is not feasible unless it is associated with: a) an extension, allowing for very slight aduction, or b) a flexion, which allows aduction to reach between 30 and 45° (see Figure 3.3 c)). From any abduction position, aduction is termed "relative aduction" and is always possible in the frontal plane until reaching the anatomical position.
- Longitudinal rotation: It is possible in any shoulder position and involves the voluntary or associated rotation of joints that have three axes and three degrees of freedom. Generally, this rotation is measured when the arm hangs vertically along the body in the anatomical position (Figure 3.3 d: top view).

  To carry out the following movements, the elbow must be flexed at 90°.

- Internal rotation (transverse plane): It is a movement in which the arm rotates inward or towards the body. Its range of motion is usually 100° to 110°, and to achieve it, the forearm must pass behind the trunk, which implies a certain degree of extension in the shoulder. The freedom of this movement is crucial for the hand to reach the back (see Figure 3.3 d, bottom right).
- External rotation (transverse plane): This is a movement in which the arm rotates outward or away from the body. Its range of motion is typically 80° (see Figure 3.3 d, bottom left).

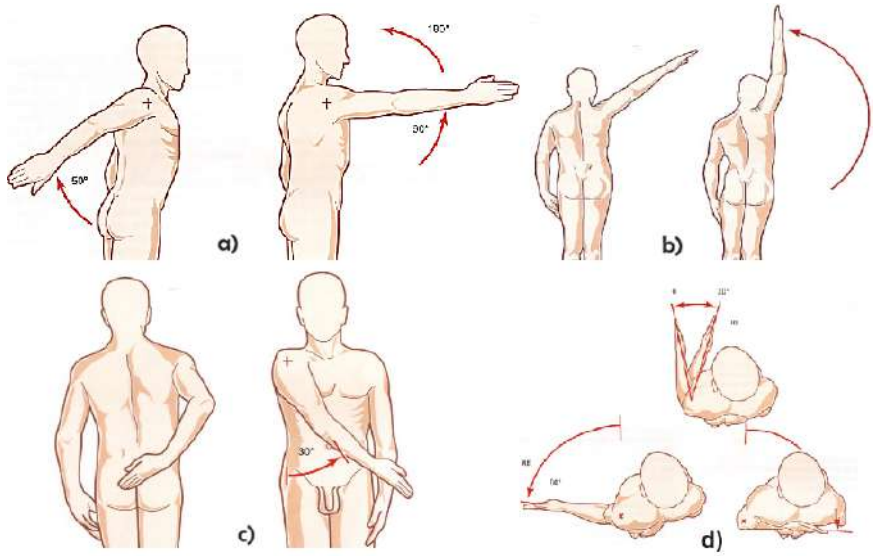

Figure 3.3: a) Flexion-extension in the sagittal plane, b) Abduction in the frontal plane, c) Adduction in the frontal plane, and d) Internal-external rotation in the transverse plane. Figures taken from (Kapandji, 2006).

  - Circumduction combines the fundamental movements around the three axes (see Figure 3.4). When it reaches its maximum range, the arm describes the space of an irregular cone, known as the cone of circumduction. This cone delineates in space an accessible spherical sector, where the hand can grasp objects without the need to move the trunk, allowing it to temporarily transport them towards the mouth.

- **Elbow Joint:** From an anatomical standpoint, this joint comprises solely a hinge joint. However, physiologically, flexion-extension and pronosupination can be distinguished. To measure the range of motion in these movements, the axis of the forearm aligns with the extension of the arm's axis.

  - Flexion: It is the movement that brings the forearm forward, so that the anterior surface of the forearm approaches the anterior surface of the arm. The range of active flexion is $140 - 145°$ (see Figure 3.5).

  - Extension: It's the movement that brings the forearm backward (refer to Figure 3.5). By definition, there's no amplitude in the case of elbow extension. However, relative extension is always possible from any position of elbow flexion. When an extension is incomplete, it's measured negatively.

  - Pronosupinacion: It's the rotation of the forearm around its longitudinal axis, adding a third degree of freedom to the wrist joint complex. This movement is only possible with the elbow flexed at 90° and close to the body.

    Actually, when the elbow is extended, the forearm aligns with the arm's extension, and the forearm's longitudinal rotation integrates with the arm's rotation around its longitudinal axis, facilitated by movements of shoulder external and internal rotation.

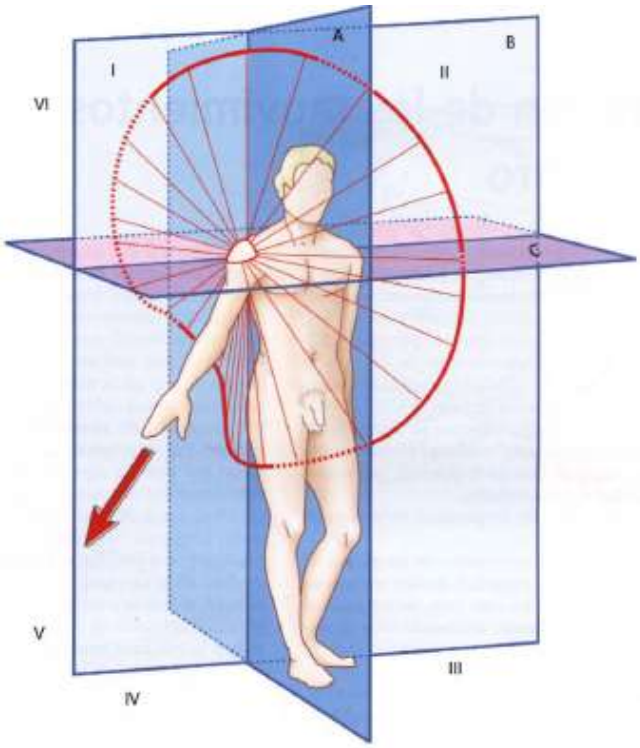

Figure 3.4: Shoulder movements in different planes. Figure taken from (Kapandji, 2006).

.

With the elbow flexed at 90°:

* The anatomical position (see Figure 3.6 a)) is established with the thumb pointing upward and the palm of the hand facing inward. From this position, the amplitudes of pronosupination movements are assessed.
* The supination position (see Figure 3.6 b)) is achieved when the palm of the hand is turned upward with the thumb pointing outward.
* The pronation position (see Figure 3.6 c)) is achieved when the palm of the hand faces downward and the thumb inward.

Hence, the complete range of authentic pronosupination (involving solely the axial rotation of the forearm) nears 180°. This motion holds significant importance for hand positioning control, crucial in activities like eating, protecting, and hygiene, and plays a pivotal role in all manual tasks, particularly during work-related activities.

- **Wrist Joint:** This joint constitutes the distal portion of the upper limb, facilitating the hand's ability to assume the optimal position for gripping. Initially, it possesses two degrees of freedom (DOF), and the incorporation of pronosupination adds a third DOF. This enables the hand to orient itself at any angle for grasping or holding objects. Its movements encompass:

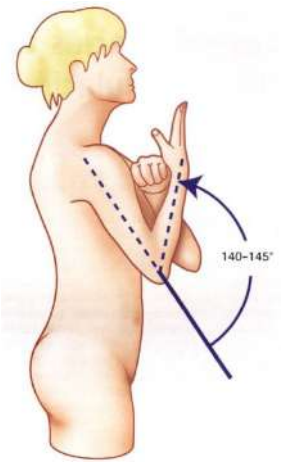

Figure 3.5: Anatomical position of the elbow. Figure taken from (Kapandji, 2006).

.

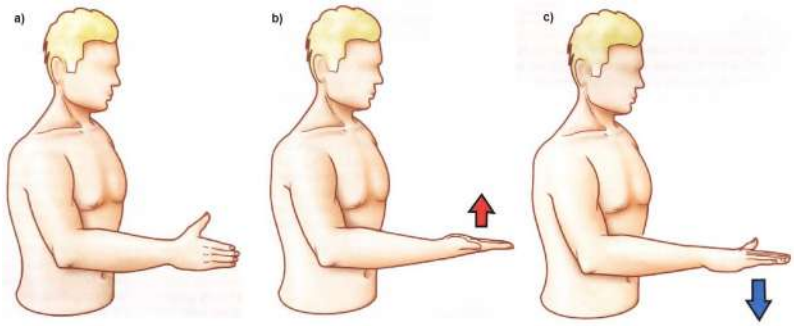

Figure 3.6: Pronosupination of the elbow: a) Anatomical position, b) Elbow supination, and c) Elbow pronation. Figures taken from (Kapandji, 2006).

.

- Flexion: Occurs when the anterior or palmar surface of the hand approaches the anterior surface of the forearm.
- Extension Occurs when the posterior or dorsal surface of the hand approaches the posterior surface of the forearm.

  Active flexion and extension exhibit a range of motion of 85°, as depicted in Figures 3.7-6 and 3.7-7. In passive flexion (Figure 3.7-8), it surpasses 90° in pronation (100°), while in passive extension (Figure 3.7-9), it exceeds 90° in both pronation and supination (95°).
- Adduction: Occurs when the hand approaches the body's axis. Its range of motion, as shown in Figure 3.7-4, is 45°, measured from the line connecting the center of the wrist to the distal portion of the third finger (dashed blue line).
- Abduction: Involves the hand moving away from the body's axis. Its range of motion, as shown in Figure 3.7-3, does not exceed 15°.

  Actually, the natural movements of the wrist are a combination of motions.

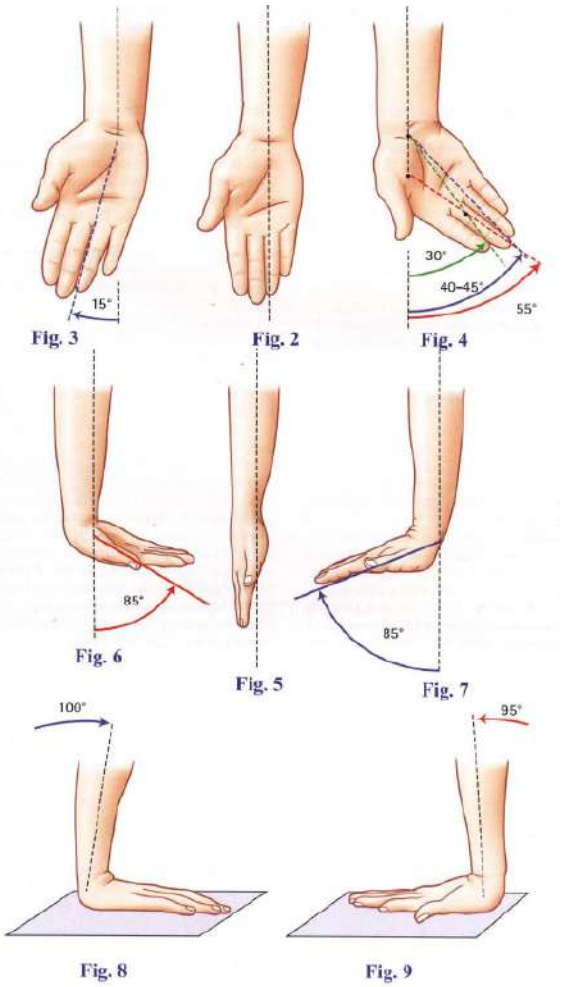

Figure 3.7: Wrist movements. Figures taken from (Kapandji, 2006).

.

– Circumduction: involves the simultaneous combination of flexion-extension with adduction-abduction movements in the wrist. This motion occurs concurrently concerning the two axes of the wrist joint. At its maximum range, the axis of the hand describes a conical surface in space, referred to as the circumduction cone (Figure 3.8-10).

Biomechanics serves as the bridge between mechanical principles and those governing the human body. Therefore, the following section will detail its main fundamentals.

3.1.2 Exoskeleton biomechanical modeling and simulation

Biomechanics integrates mechanical principles and methods into the analysis of the structure and function of the human body. It is thus responsible for describing, analyzing, and quantifying human movement, encompassing both kinematics, the study of how movement occurs, and dynamics, which investigates its origins (Knudson, 2007; Lippert, 2006; Pons, 2008; Winter, 2009).

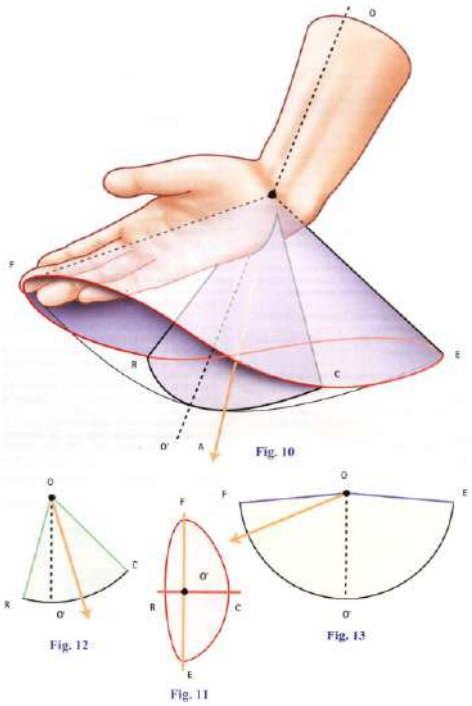

Figure 3.8: Wrist: Circumduction Movement. Figure taken from (Kapandji, 2006).

.

From this perspective, it is possible to represent human limbs as a parallel system to wearable robots (known as kinematic compatibility). This is because the human body can be conceptualized as a series of rigid segments connected by rotating joints. In this way, the principles of continuous mechanics, such as conservation of mass and energy, can be applied and specific equilibrium equations formulated to address the problem at hand (Zhao et al., 2023; Pons, 2008; Mahmoud and Saidi, 2022; Fei et al., 2017).

To develop an approximate mechanical model of the human skeletal system, utilizing the rigid body approach and upper limb anthropometry, Figure 3.9 serves as a reference. This process entails taking into account the weights of different body parts and their corresponding centers of gravity, as outlined in Tables 3.2 and 3.3.

Table 3.2: Segmental weight/body weight ratios from various studies. Information taken from (Le Veau et al., 1991).

Source	Braune %	Dempster %	Demster (adjusted) %	Clauser %
Head	7.0	7.9	8.1	7.3
Trunk	46.1	48.6	49.7	50.7
Arm	3.3	2.7	2.8	2.6
Forearm	2.1	1.6	1.6	1.6
Hand	0.8	0.6	0.6	0.7
Upper limb	6.2	4.9	5.0	4.9
Forearm and hand	2.9	2.2	2.2	2.3

Source	Braune %	Dempster %	Dempster (adjusted) %	Clauser %
Thigh	10.7	9.7	9.9	10.3
Leg	4.8	4.5	4.6	4.3
Foot	1.7	1.4	1.4	1.5
Lower limb	17.2	15.7	16.1	16.1
Leg and foot	6.5	6.0	6.1	5.8
Total	100.0	100.0	100.0	100.0

Table 3.3: Centers of mass: segment length ratio. Taken from (Le Veau et al., 1991).

Source	Braune and Fischer %	Dempster %	Clauser et al. %
Whole body	-	-	41.2
Head	-	43.3	46.6
Trunk	-	-	38.0
Arm	47.0	43.6	51.3
Forearm	42.1	43.0	39.0
Hand	-	49.4	48.0
Upper limb	-	-	41.3
Forearm and hand	47.2	67.7	62.6
Thigh	44.0	43.3	37.2
Leg	42.0	43.3	37.1
Foot	44.4	42.9	44.9
Lower limb	-	43.3	38.2
Leg and foot	52.4	43.7	47.5

The biomechanical model establishes a solid foundation for the design and control of robots with similar limbs, such as exoskeletons. These devices, portable and external to the user, aim to enhance or assist in physical movements. They are comprised of rigid elements, actuators, and sensors, whose primary goal is to improve individuals' strength, mobility, or endurance. Consequently, their application spans a wide range of purposes, from aiding individuals with physical disabilities to facilitating tasks such as lifting heavy loads for workers or optimizing athletes' performance (Siciliano et al., 2009; Correll et al., 2022; McKinnon, 2015).

Therefore, it is crucial to examine both the kinematics (direct and inverse) and dynamics of the robot to carry out tasks precisely and coordinately, effectively and safely. The fundamentals of these analyses within the field of robotics are then established.

Kinematic analysis

To enhance the design and control of exoskeletons, it's crucial to grasp how they function as multibody systems. Kinematic analysis involves scrutinizing the movement of each rigid

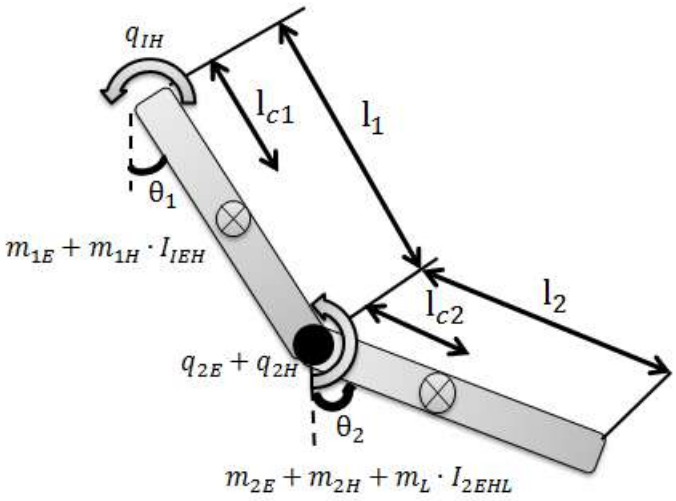

Figure 3.9: Mechanical equivalent of an exoskeleton attached to the arm. Figure taken from (Olaya, 2009).

.

component of the robot concerning a reference frame. This analysis encompasses both forward kinematics, which determines the position and orientation of the exoskeleton's end given the joint angles, and inverse kinematics, which calculates the joint angles needed to achieve a desired position and orientation of the end effector (Barrientos et al., 1997; Craig, 2005; Pons, 2008; Winter, 2009; Siciliano et al., 2009; Lynch and Park, 2017); Khatib et al., 2019).

The method developed by Denavit-Hartenberg (D-H) is the most commonly employed approach for solving the problem of forward kinematics in robotics. This technique outlines both the geometry and kinematics of a robotic manipulator using standard parameters, significantly simplifying the analysis and resolution of issues related to the robot's motion. It relies on the concept of homogeneous transformation matrices, which describe the relationship between two adjacent bodies using the rigid body model. Within this framework, specific coordinates and reference frames are defined at each joint of the robot, allowing for precise calculation of the position and orientation of the robot's end effector based on joint variables (Barrientos et al., 1997; Craig, 2005). The general form of the transformation matrix between two adjacent coordinate systems is represented as ${}^{i-1}A_i$ and is defined as:

$$ {}^{i-1}A_i = \begin{bmatrix} C\theta_i & -C\alpha_i S\theta_i & S\alpha_i C\theta_i & a_i C\theta_i \\ S\theta_i & C\alpha_i C\theta_i & -S\alpha_i C\theta_i & a_i S\theta_i \\ 0 & S\alpha_i & C\alpha_i & d_i \\ 0 & 0 & 0 & 1 \end{bmatrix} $$

Commonly, simplified models with 9 and 7 degrees of freedom are proposed to analyze the kinematics of the rigid body in the upper extremity. The latter includes 3 degrees of freedom for the shoulder, 2 for the elbow, and 2 for the wrist (see Figure 3.10). The associated D-H parameters are detailed in Table 3.4, where the values of a_i and d_i represent the constant lengths of the body segments. The range of motion for each degree of freedom is determined by the physiological range of the corresponding anatomical joint (described in Section 3.1.1).

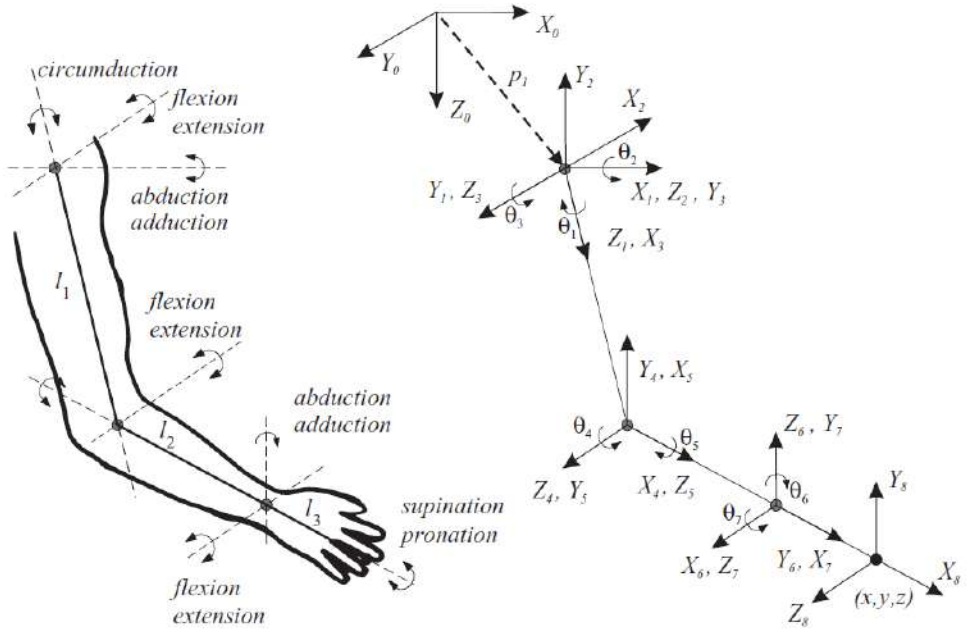

Figure 3.10: D–H notation for a human arm. Figure taken from (Pons, 2008).

Table 3.4: D-H parameters of the 7 DOF model of the upper limb. Taken from (Pons, 2008).

Joint	β_i	α_i	a_i	d_i	θ_i
Base	0	0	a_0	d_0	0
Shoulder	(-90) medial rotation/lateral rotation (+90)	-90	0	0	$\beta_1 + 90$
Shoulder	(-180) abduction/adduction (+50)	+90	0	0	$\beta_2 + 90$
Shoulder	(-180) flexion/extension (+80)	0	l_1	0	$\beta_3 + 90$
Elbow	(-10) extension/flexion (+145)	+90	0	0	$\beta_4 + 90$
Elbow	(-90) pronation/supination (+90)	+90	0	l_2	$\beta_5 + 90$
Wrist	(-90) flexion/extension (+70)	+90	0	0	$\beta_6 + 90$
Wrist	(-15) abduction/adduction (+40)	0	l_3	0	β_7

Once the D-H parameters have been established, it becomes possible to compute the relationships between the adjacent links of the robot using the transformation matrices A_i. By combining these transformations of successive joints, it becomes possible to determine the final position and orientation using the matrix $\boldsymbol{T}$=${}^0A_1, {}^1A_2, ..., {}^{n-1}A_n$. On the other hand, relationships between non-adjacent links are derived through the matrices $\boldsymbol{T}$, which result from the product of a set of matrices $\boldsymbol{A}$.

The purpose of solving the inverse kinematics problem is to find the values that the robot's joint coordinates, denoted as $q = [q_1, q_2, ..., q_n]^T$, must take so that the robot's end effector can be positioned and oriented according to a specific spatial location (Barrientos et al., 1997; Siciliano et al., 2009; Lynch and Park, 2017; Spong et al., 2020).

The resolution of this problem is closely linked to the specific configuration of the robot, which has driven the development of methods programmable based on its kinematics. However,

these methods often resort to iterative numerical techniques, whose speed and convergence assurance are not always guaranteed. Therefore, it is more appropriate to seek an analytical solution through a mathematical relationship in the following form (Barrientos et al., 1997):

$$q_k = f_k(x, y, z, \alpha, \beta, \gamma) \tag{3.4}$$

$$k = 1, ..., n(GDL) \tag{3.5}$$

This solution offers the following advantages:

- The problem is solved in real-time, for example, in trajectory tracking.
- Often, the solution to the inverse kinematics problem is not unique; that is, there are multiple combinations that position and orient the robot's end effector in the same way. Therefore, employing a closed-form solution may involve certain constraints to ensure that the obtained solution is the most suitable, such as limiting joint ranges.

Also common are the use of geometric methods, kinematic decoupling methods, or direct manipulation of the equations associated with the forward kinematics problem. This latter approach establishes the relationship:

$$\begin{bmatrix} n & o & a & p \\ 0 & 0 & 0 & 1 \end{bmatrix} = [t_{ij}]$$

Where the elements t_{ij} are functions of the joint coordinates $[q_1, ..., q_n]^T$. Through the 12 equations posed, the n joint variables q_i can be determined in terms of the components of the vectors **n,o,a,p**.

Once the expression t_{ij} corresponding to the robot has been established, that is, the matrix **T** that relates the reference frame S_0 associated with the base to the reference frame S_n associated with its end effector, and the expression of **T** has been obtained in terms of the joint coordinates (q_1, q_2, q_3), along with a presumed location of the robot's end effector defined by the vectors **n,o,a,p**, it is possible to manipulate directly the resulting 12 equations from **T** to solve for $q_1, ..., q_n$ in terms of **n,o,a,p**.

Jacobian analysis

In the previous sections, the kinematics of the robot have been described; However, the forces or torques acting on the robot, which can generate its movement, have not been taken into account. In this section, the fundamentals related to joint coordinate velocities will be addressed, as well as the position and orientation of the robot's end effector. The relationship between these two velocity vectors is obtained through the Jacobian matrix. The following points are highlighted (Barrientos et al., 1997):

- Direct Jacobian Matrix: Allows determining the velocities of the robot's end effector from the velocities of each joint.
- Inverse Jacobian Matrix: Allows determining the joint velocities necessary to achieve certain velocities at the robot's end effector.

The most direct way to establish the relationship between the velocities of the joints and those of the robot's end effector is to differentiate the equations of the corresponding direct kinematic model. Assuming that the equations solving the direct kinematic problem of an n-degree-of-freedom robot are known:

$$x = f_x(q_1, ..., q_n) \tag{3.6}$$
$$y = f_y(q_1, ..., q_n) \tag{3.7}$$
$$z = f_z(q_1, ..., q_n) \tag{3.8}$$
$$\alpha = f_\alpha(q_1, ..., q_n) \tag{3.9}$$
$$\beta = f_\beta(q_1, ..., q_n) \tag{3.10}$$
$$\gamma = f_\gamma(q_1, ..., q_n) \tag{3.11}$$

To obtain the inverse Jacobian, you can use the previously calculated Jacobian matrix (J). Assuming that the matrix **J** is square, it is possible to determine its value for a specific robot configuration and, by numerically inverting it, obtain the corresponding inverse Jacobian matrix for that configuration. However, there may be sets of joint coordinates $(q_1, ..., q_n)$ for which the matrix **J** is not invertible because its determinant (the Jacobian) is zero. These configurations are called singular configurations. Additionally, another problem may arise if the Jacobian matrix is not square, meaning that the number of degrees of freedom of the robot does not match the dimension of the task space. In such cases, the following situations arise (Barrientos et al., 1997):

- When the number of degrees of freedom is less than the dimension of the task space (the Jacobian matrix has more rows than columns), it indicates that the robot's movement is subject to certain constraints. This often occurs in cases where these constraints are not relevant.
- When the number of degrees of freedom is greater than the dimension of the task space (the Jacobian matrix has more columns than rows), it is known as redundant robots. In this case, there are unnecessary degrees of freedom, meaning they do not need to be moved to achieve the new positions or velocities required at the end effector.

In the case where the Jacobian matrix is not square, it is possible to use a pseudo-inverse matrix, such as $(JJ^T)^{-1}$. Another alternative to obtain the inverse Jacobian matrix is to repeat the procedure for obtaining the direct Jacobian, but this time starting from the inverse kinematic model.

Dynamic model

Dynamics involves studying the movement of a robot while taking into account the forces and moments influencing it. In the context of articulated multibody mechanisms like portable robots, dynamics entails analyzing motion in both configuration and workspace. This analysis considers internal forces, such as torque in each joint actuator, and external forces, such as interaction with the environment. As a result, a robot's dynamic model comprises a

mathematical representation that correlates applied forces and moments with the robot's positions, velocities, accelerations, and dimensional parameters (Barrientos et al., 1997; Craig, 2005; Pons, 2008; Siciliano et al., 2009; Lynch and Park, 2017)).

Equations of motion define how a system behaves over time. In robotics, the dynamic model plays a crucial role in various tasks, including motion simulation, designing and assessing mechanical structures, selecting actuators, and planning and evaluating dynamic control. Two main types of dynamic models can be identified:

- Forward dynamic model: Develops a representation of how joint and workspace coordinates change as forces and torques are applied. This model is defined as follows:

$$\ddot{r} = f(F, T) \tag{3.12}$$

$$\dot{r} = \int \ddot{r} dt \tag{3.13}$$

$$r = \int \dot{r} dt \tag{3.14}$$

- Inverse dynamic model: Presents the relationship between forces and torques with joint coordinates over time. Its expression can be as follows:

$$F = g(r, \dot{r}, \ddot{r}) \tag{3.15}$$

  The methodologies most commonly used to obtain the dynamic model of a robot are the Newton-Euler formulation, which utilizes vector functions, and the Lagrange-Euler formulation, which employs scalar functions.

The dynamics of a robot can be represented in the joint space as follows, according to (Craig, 2005):

$$M(q)\ddot{q} + C(q, \dot{q})\dot{q} + F(\dot{q}) + G(q) + \tau_d = \tau \tag{3.16}$$

$$F(\dot{q}) = F_u\dot{q} + F_d \tag{3.17}$$

where: $q \in \mathbb{R}^{n\times 1}$ is the vector of joint coordinates as a function of time, $\dot{q} \in \mathbb{R}^{n\times 1}$ is the vector of joint velocities as a function of time, $\ddot{q} \in \mathbb{R}^{n\times 1}$ is the vector of joint accelerations as a function of time. $M(q) \in \mathbb{R}^{n\times n}$ is a square inertia matrix representing the effect of joint acceleration on the generalized torque, $\tau \in \mathbb{R}^{n\times 1}$. $C(q, \dot{q}) \in \mathbb{R}^{n\times n}$ is centrifugal and Coriolis terms. $G(q) \in \mathbb{R}^{n\times 1}$ is a vector of gravity-related forces. $F(\dot{q}) \in \mathbb{R}^{n\times 1}$ is the friction term, $F_u \in \mathbb{R}^{n\times n}$ is a matrix of viscous friction coefficients, $F_d \in \mathbb{R}^{n\times 1}$ is the dynamic friction and $\tau_d \in \mathbb{R}^{n\times 1}$ is disturbance (represents inaccurately modeled dynamics).

Determining friction coefficients in a robot is generally challenging. Therefore, the mathematical model tends to be approximate, and the most common forms are:

- Neglect the friction terms in Equation 3.16, resulting in the following dynamic model:

$$M(q)\ddot{q} + C(q,\dot{q})\dot{q} + G(q) = \tau \tag{3.18}$$

- Unknown dynamics can be grouped within the disturbance term τ_d (see Equation 3.16), thus the resulting dynamic model can be expressed as follows:

$$M(q)\ddot{q} + N(q,\dot{q}) + \tau_d = \tau \tag{3.19}$$

  where the effects of nonlinear terms are represented by $N(q,\dot{q})$ as shown below:

$$N(q,\dot{q}) = C(q,\dot{q})\dot{q} + F(\dot{q}) + G(q)$$

3.1.3 Automatic Control

In previous sections, the procedure for deriving the kinematic and dynamic models of a robot has been explained. These models are designed to implement control strategies that optimize the precision of the robot's movements. Next, the fundamentals of the main control strategies will be discussed

Kinematic and dynamic Control

Kinematic control determines the trajectories that each joint of the robot should follow over time to reach the goals defined by the user. These trajectories are chosen considering the physical limitations inherent to the actuators and trajectory quality criteria, such as smoothness or precision. The functioning of kinematic control is explained below, and its scheme is presented in Figure 3.11 (Barrientos et al., 1997):

1. To specify the desired movement, input data are used, which may include: destination points in coordinates (x,y,z,α,β, γ), the type of desired trajectory, the expected time or velocity, endpoint accuracy, and Cartesian trajectory accuracy, among others.
2. Transforming the movement specification into an analytical trajectory in Cartesian space, where the Cartesian coordinates vary over time.
3. Discretize the Cartesian trajectory to obtain a finite set of points along that trajectory. Each point is represented by a tuple of six elements, commonly (x,y,z,α, β, γ).
4. Apply the inverse homogeneous transformation to convert each of these points into their respective joint coordinates (q_1,...,q_n). It is crucial to consider during this procedure the possibility of multiple solutions of the inverse homogeneous transformation, as well as the potential absence of a solution and the presence of singular points, to ensure the continuity of the trajectory.
5. The obtained joint points are then interpolated to generate a function $q_i(t)$ that passes through or approximates them. This function, feasible for the actuators, is transformed

into a Cartesian trajectory that aligns as closely as possible with the user's specification in terms of accuracy, speed, and other criteria.

6. Discretize the joint trajectory to create dynamic control references.

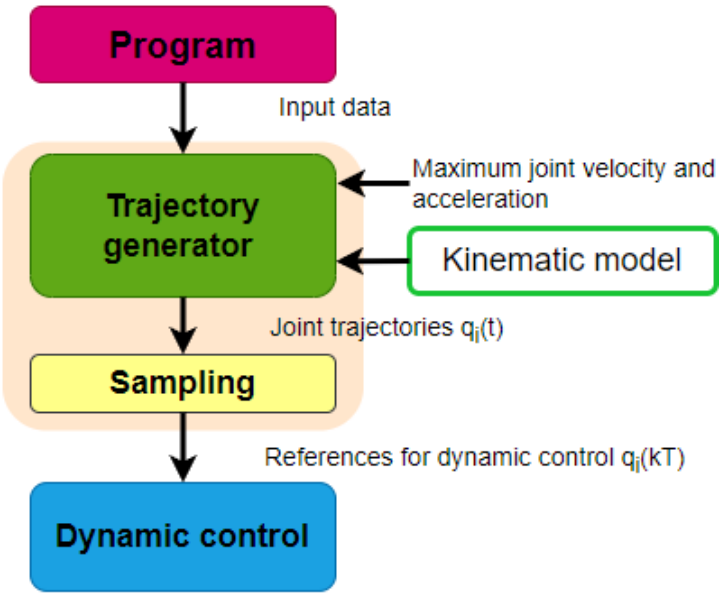

Figure 3.11: Operation of kinematic control (highlighted). Information taken from (Barrientos et al., 1997).

There are infinite spatial trajectories through which a robot can move from an initial point to a final one. The selection of the trajectory depends on various factors, such as its simplicity, suitability, or relevance to the task the robot must perform. Among the most common options are:

- Point-to-point trajectories: In this approach, each joint moves from an initial point to a final one without considering the state or movement of the other joints. In other words, each actuator positions its joint at the destination point in the shortest time possible. Within this approach, two cases can be distinguished: single-axis movement, where the joints move one at a time, and simultaneous axis movement, where all actuators simultaneously displace the robot's joints at a specific velocity each.
- Continuous trajectories: This strategy is employed when the user is familiar with the trajectory followed by the robot's end effector. In this case, the joint trajectories are calculated based on the known spatial trajectory.

In the field of rehabilitation, it's common for medical personnel to specify the movements that the robot must perform, detailing spatial locations, velocities, or types of trajectories. For the robot to effectively execute these movements, precise information about the initial point, intermediate points, and final point is crucial. It's essential for these points to be sufficiently close to each other to ensure maximum possible accuracy. Therefore, it's necessary to implement interpolators that utilize functions (typically polynomials), whose parameters are adjusted to the specific task conditions. The most commonly used interpolating functions

in joint space are (Barrientos et al., 1997):

- Linear: consists of maintaining a constant velocity between each successive pair of values (q^{i+1},q^i) of the joint. Therefore, the trajectory between the points can be described by Equation 3.20. This trajectory is continuous in position, but presents abrupt changes in joint velocity, resulting in infinite acceleration in practice, which is impossible.

$$q(t) = (q^i - q^{i-1})\frac{t - t^{i-1}}{t^i - t^{i-1}} + q^{i-1}, t^{i-1} < t < t^i \tag{3.20}$$

- Cubic: This trajectory is formed by a sequence of third-order polynomials, each valid between a pair of consecutive points, and these polynomials exhibit continuity both in position and velocity (known as splines). The equation describing the trajectory between two adjacent points is shown in Equation 3.21 (assuming that the joint starts and ends in a velocity-free situation).

$$q(t) = a + b(t - t^{i-1}) + c(t - t^{i-1})^2 + d(t - t^{i-1})^3, t^{i-1} < t < t^i \tag{3.21}$$

$$a = q^{i-1}$$

$$b = \dot{q}^{i-1}$$

$$c = \frac{3}{T^2}(q^i - a^{i-1}) - \frac{2}{T^2}\dot{q}^{i-1} - \frac{1}{T^2}\dot{q}^i$$

$$d = -\frac{2}{T^3}(q^i - q^{i-1}) + \frac{1}{T^2}(\dot{1}^{i-1} + \dot{q}^i)$$

$$T = t^i - t^{i-1}$$

- Other interpolators: Various interpolation methods have been proposed to connect the points of the trajectory using continuous functions, twice differentiable and computationally manageable. Among them, the use of sinusoidal functions stands out, which ensure continuity in all derivatives and can have the following form:

$$q(t) = a + bt + c\sin(\omega t) \tag{3.22}$$

  The determination of the coefficients is conditioned by the position, velocity, and acceleration constraints established.

Kinematic control selects trajectories that the robot ideally should follow in such a way that they best fit the motion specifications given by the user. In practice, the robot's motion

depends on its dynamic characteristics (inertia, friction, backlash, etc.), which are often unknown, leading to mismatches between the desired trajectory ($q_d(t)$) and the measured one **(q(t))**. Therefore, control algorithms aim to maximize the robot's speed and precision characteristics.

Consequently, the goal of dynamic control is to minimize the discrepancy between the trajectory executed by the robot and the suggested trajectory by kinematic control. To achieve this goal, the robot's dynamic model is employed along with different controllers, such as proportional integral derivative (PID) controllers or adaptive controllers. Due to the inherent complexity of the robot, its dynamic model is often highly nonlinear, multivariable, coupled, and with variable parameters. Therefore, in practice, it is common to use certain simplifications to reduce the complexity of the control model, leading to reasonably acceptable results.

Robot control can be performed in task or Cartesian space (when the robot comes into contact with the environment and experiences reaction forces) or in joint space (where its joint trajectories are controlled). In this context, the control techniques applied in joint space are briefly described, which can be single-joint (disregarding interaction between the robot's DOF) or multi-joint (considering the robot as a multivariable system).

In practice, the quality of the drive systems achieves a linear relationship between the control voltage (u) and the provided torque (τ) by the drive so that:

$$\tau = ku \tag{3.23}$$

Assuming the dynamic model of the robot is known, it is feasible to search for the control voltage **u(t)** that generates a pre-established trajectory **(q(t))**. In practice, it is common to employ a feedback control scheme, where the error is defined as the difference between the desired position and the measured position in the robot: $e = q_d(t) - q(t)$ (see Figure 3.12).

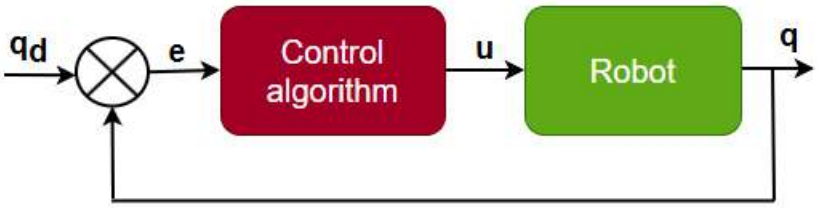

Figure 3.12: Control algorithm scheme. Information taken from (Barrientos et al., 1997).

Since most robots have a single controller tuned for specific conditions, any change in these conditions can affect their performance. Therefore, the effective application of a particular controller requires a detailed understanding of the dynamic model and/or operating conditions of the robot so that they can be properly adjusted to minimize errors in its performance. However, in practice, the parameters defining the models are rarely known precisely, as the robot's conditions can change over time or when the robot is coupled to a user, as in the case of exoskeletons. To address these types of challenges, adaptive control techniques emerge that can be applied under various operating conditions.

The premise of adaptive control is to adjust in real time the parameters defining the controller according to the instantaneous behavior of the robot, so that its movements always approximate the desired specifications. There are different schemes of adaptive control; however, all of them involve procedures for identifying the dynamic model of the robot and algorithms for calculating the controller parameters. Some examples are:

- Adaptive control with reference model: It performs an online comparison between the behavior of the real system and the desired one. The error between both behaviors is used to modify the controller parameters.
- Self-tuning adaptive control: Continuously recognizes the system model and employs a design algorithm to adapt the controller parameters.

3.1.4 Technology Integration

As previously observed, the development of a robotic exoskeleton involves the multidisciplinary integration of various fields, with particular emphasis on robotics and biomechanics (as they are human-centered devices designed to enhance the mobility and/or strength of their users). Since this process is multidisciplinary and aims to create increasingly efficient, safe, and tailored robotic exoskeletons to individuals' specific needs, it is crucial to establish ongoing interaction with users to obtain active feedback during their development. This process of continuous integration of technologies and systems to create more comprehensive, efficient, and versatile solutions is known as technological integration and plays a fundamental role in the development of complex systems.

This approach involves the convergence of various disciplines such as computer science, electronics, systems engineering, and artificial intelligence, which facilitates the creation of innovative and multifaceted solutions. In this way, technological integration allows for the maximization of available resources and enhances efficiency, productivity, and user experience across various applications (Dian et al., 2020; G. Chen et al., 2020; Manickam et al., 2022; Catchpole et al., 2024).

Digital Twin

A novel concept that establishes a connection between the digital and physical realms is the digital twin (DT). According to the definition by Singh et al. (Singh et al., 2021), it is described as "*a dynamic and self-evolving model, or a digital/virtual simulation of a real-world subject or object (whether it be a part, machine, process, human being, etc.), which accurately represents the current state of its physical counterpart at any given time through real-time data transfer and the preservation of historical records. Not only does the digital twin replicate its physical counterpart, but any modifications made to the digital twin are also reflected in the physical twin*". This definition allows for the distinction of two types of DTs based on when they are created:

Digital Twin Prototype (DTP): It includes the essential information needed to generate a physical replica from a virtual version (CAD models, materials, etc.). It can undergo various tests and analyses to identify potential undesired scenarios before the creation

of the physical twin, with the accuracy of the simulation model being crucial for the quality of the physical twin.

Digital Twin Instance (DTI): This type of digital twin arises during the production phase and is connected to its physical counterpart throughout its lifecycle. This allows for bidirectional data exchange between them, so that any modification in one will automatically be reflected in the other.

DT technology is considered the cornerstone of Industry 4.0, as it offers a series of key advantages, including error and uncertainty reduction, cost decrease in systems or processes, rapid prototyping and product redesign, solution optimization, enhanced maintenance, increased accessibility and safety compared to their physical counterparts, waste reduction, training, high fidelity, and its multidisciplinary nature, among others (Singh et al., 2021; Li et al., 2022; Baek, 2022; Mihai et al., 2022).

A DT is generated and utilized in the various stages of the product development process, encompassing each of the following aspects (Söderberg et al., 2017):

Design Phase: Involves robustness and tolerance analysis, utilizing geometric representations of parts and kinematic relationships, along with finite element analysis to conduct sensitivity and variation analysis.

Pre-production Phase: Serves as a foundation for inspection preparation, as well as for offline programming of coordinate measuring machines and scanners.

Production Phase: Utilizes the virtual assembly model in conjunction with inspection data to control production and detect, as well as correct errors.

Therefore, the generation of the DTP and the DTI represents different approaches to the creation and validation of products, systems, or processes. The former constitutes a precise virtual representation of a physical object or system, enabling simulation of its behavior, prediction of its performance, and testing in a controlled environment before actual implementation. In contrast, the latter refers to a tangible and materialized version of the product or system, providing a physical experience in realistic environments, allowing evaluation of aspects such as ergonomics, aesthetics, and functionality (Jones et al., 2020; Z. Huang et al., 2021, Semeraro et al., 2021;Tao et al., 2022; Attaran and Celik, 2023; X. Liu et al., 2023). Both approaches present their own advantages and challenges, and their strategic integration can provide a more comprehensive and efficient development process for a wide variety of industrial and consumer applications.

In the context of robotic device creation, Industry 4.0 has radically transformed how these devices are designed, manufactured, and operated, while also offering opportunities to optimize processes, customize products, and enhance operational efficiency. The adoption of advanced technologies such as digital twins, additive manufacturing, and intelligent production systems enables manufacturers to develop more flexible, adaptable, and autonomous robots capable of meeting the changing demands of the market and enhancing global competitiveness (Z. Gao et al., 2020; Goel and Gupta, 2020; Javaid et al., 2021; Khang et al., 2023;).

The main pillar of Industry 4.0 in manufacturing is additive manufacturing, which presents

significant advantages when creating complex and customized components, such as those required in exoskeletons. The synergy between Industry 4.0 and additive manufacturing represents a revolutionary approach that provides an agile and adaptable production environment, facilitating on-demand manufacturing, design optimization, and cost reduction (Hegab et al., 2023; Bhatia and Sehgal, 2023; Majd and Barari, 2023). Additive Manufacturing, technically known as 3D printing, encompasses various technologies that share the process of constructing three-dimensional objects by adding material. In other words, successive layers of material are applied to shape a tangible object from a digital file (Jorquera Ortega, 2016).

Therefore, once the DTI has been obtained through the pillars of Industry 4.0, it is imperative to design the human-machine interface that will facilitate interaction between the developed device and users. This aspect will be detailed in the following section.

Human-robot interface

The primary function of any robot is to support humans in any shared environment. Therefore, it is vital to establish effective interaction between them. Human-machine interfaces play a crucial role in facilitating communication between users and robots (Berg and Lu, 2020; Casas et al., 2020). In a robotic system, a human-robot interface (HRI) is a terminal that enables the human operator to program, control, monitor, and gather data from the system. In the context at hand, we will use the term HRI to refer to these human-robot interfaces (Berg and Lu, 2020).

Human-robot interfaces in the medical field have received significant attention, especially because users are not necessarily experts, making it imperative for the interface to be intuitive and efficient. In particular, in rehabilitation robotics, a field focused on improving and analyzing recovery processes through robotic systems (therapeutic training and sensorimotor performance evaluation), human-robot interaction generally encompasses three types of modalities as depicted in Figure 3.13 (Mohebbi, 2020):

1. Therapist-robot interaction: It involves monitoring, customization, and control of parameters of the therapeutic intervention.
2. Patient-robot interaction involves three main aspects: collecting patient information to assess their performance and provide feedback to the control system, communicating information to the patient about the procedure and their therapeutic progress.
3. Robot learning: The closed-loop control system is responsible for motion planning and ensures that the robot's behavior adjusts appropriately to the patient's movements.

Therefore, human-robot interaction plays a fundamental role in the effective integration of rehabilitation robots, emphasizing the importance of social, cognitive, and physical interactions. These aspects are crucial for the usability, ergonomics, and adaptability of these devices. Taking this into account, the design and development of interfaces require a deep understanding of both human and robot capabilities and limitations. In the case of exoskeleton interfaces for upper extremities, they focus on providing decoding approaches that enable precision and dexterity in a wide range of movements.

A strategy for designing a user interface with a focus on usability is to apply Jakob

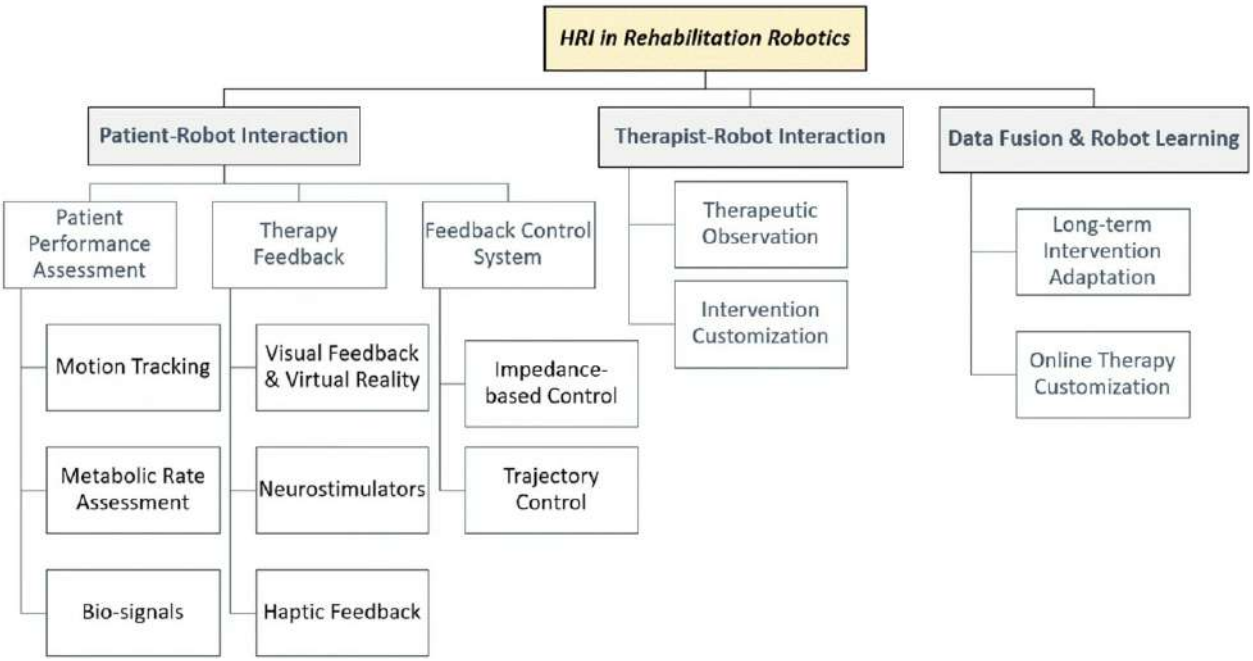

Figure 3.13: Category human-robot interaction modalities for rehabilitation robotics. Figure taken from (Mohebbi, 2020).

Nielsen's 10 general principles for interaction design. These principles, known as "heuristics," are detailed below (Nielsen, 1994):

1. System status visibility: It entails that the design should ensure users are consistently updated on what is happening, providing relevant feedback within an acceptable time-frame.
2. Familiar language for users: The design should employ terms and concepts that are familiar to them, and adhere to real-world conventions so that information is presented naturally and logically in an appropriate order.
3. User control and freedom: When errors occur, the design should provide a clearly marked exit that allows users to abandon an unwanted action without having to go through a long or complicated process.
4. Consistency and standards: Users should not have to wonder if different words, situations, or actions have the same meaning. It is essential to maintain consistency with the conventions established by the platform and the industry.
5. Error prevention: Effective error messages are fundamental. It's crucial to eliminate error-prone conditions or check them, providing users with a confirmation option before they commit to the action.
6. Recognition rather than recall: Reduce the burden on the user's memory by making elements, actions, and options visible. It shouldn't be necessary for the user to remember information from one part of the interface to another. The information required to use the design should always be visible or easily accessible when needed.

7. Flexibility and efficiency of use: Shortcuts can speed up interaction for both experienced and inexperienced users. Allow users to customize frequent actions.
8. Aesthetic and minimalist design: Interfaces should include relevant information. Every additional piece of information competes with the relevant elements, reducing their relative visibility.
9. Help users recognize, diagnose, and recover from errors: Error messages should use clear and understandable language, avoiding complexity of codes, accurately describing the problem, and providing constructive suggestions for resolution.
10. Help and documentation: In an ideal scenario, the system should be intuitive and not require additional instructions. However, at times it can be useful to provide documentation to assist users in understanding how to perform their tasks.

Usability in human-robot interfaces is crucial in the medical field. They should be intuitive, efficient, and safe, aiming to reduce learning time and minimize errors during use. Ensuring clear communication between the user and the robot is fundamental. Additionally, these interfaces should provide a high level of satisfaction by offering comfort and confidence in interacting with the robot, thus enhancing the overall experience. This approach significantly contributes to the adoption and acceptance of robots by users.

Since it's crucial to evaluate any device, conducting a comprehensive assessment covering various aspects of the exoskeleton, such as usability, effectiveness, and user satisfaction, among others, is essential. It is suggested to conduct these tests on a physical digital twin (DTI). Below, the main validation methodologies employed to evaluate the device developed in this work are described.

3.1.5 Exoskeleton Experimental Validation

Currently, the potential for the use of exoskeletons in rehabilitation is significant, offering new possibilities to enhance mobility and quality of life for individuals with physical limitations. However, two of the main obstacles hindering their acceptance among users are the complexity of their controls, which require specialized knowledge or training for operation, and their functionality (Moulaei et al., 2024).

Therefore, the evaluation of exoskeletons remains a challenge due to the diversity of perspectives and experiences among the involved subjects. While certain evaluations focus on physical interaction variables, the majority employ protocols with subjective elements, such as questionnaires, to assess the user's perception during the development of a training task. This practice is understandable since these devices are designed with the user in mind, implying that their evaluation is closely linked to the users' experience (Meyer et al., 2019). Some of the main aspects commonly evaluated include performance, usability, user satisfaction, and workload.

To reduce variability in measurements, it's essential to consider questionnaires based on international standards, such as ISO/IEC 9241, established by the International Organization for Standardization (ISO) and the International Electrotechnical Commission (IEC), which

focuses on the usability and ergonomics of human-computer interaction. Its main goal is to enhance user experience when using digital products or services through user-centered designs, ensuring they are intuitive, efficient, and satisfying. Its use has a positive impact on the quality and competitiveness of the products and services offered (Mena et al., 2022; Martínez et al., 2022).

The ISO 9241 standard, in its part II, defines usability as the extent to which specific users achieve their goals effectively, efficiently, and satisfactorily in a specific environment, where:

- Effectiveness is defined as the accuracy and completeness with which a user achieves a specific goal in a given environment. This implies that users complete a specific set of tasks, and the success or failure rate in their completion is evaluated.
- Efficiency is described as the correspondence between the resources used and the accuracy and difficulty of the goals achieved, which implies evaluating the time required by participants for their completion.
- Satisfaction refers to the comfort and acceptability of the system for both users and other individuals influenced by its use, and is used to evaluate overall usability.

In user-centered areas, primary metrics focus on usability as a quality indicator, and some of the most prominent ones are as follows:

- **Task success rate (users' ability to complete the task)**: This metric is used to evaluate the effectiveness of the provided solution, calculating the percentage of tasks that users successfully complete. It is computed by Equation 3.24.

$$TSR = \frac{N_{tcs}}{T_i} \tag{3.24}$$

  where: TSR represents the task success rate, N_{tcs} corresponds to the number of tasks completed successfully, and T_i represents the total attempts.

- **Time required to complete a task**: It is an indicator that evaluates the effectiveness of a system by determining the time needed for a user to complete a specific task. This parameter is calculated by Equation 3.25:

$$TTR = \frac{T_t}{N_u} \tag{3.25}$$

  where: TTR represents the task time rate, T_t indicates the total seconds, and N_u is the number of users involved.

- **User Error Rate**: This indicator is related to the effectiveness of the solution and focuses on analyzing the frequency of incorrect inputs during the task. It is calculated by Equation 3.26:

$$UER = \frac{T_e}{N_i * N_{AE}} \tag{3.26}$$

where: UER represents the user error rate, T_e indicates the total errors occurred from all users in the task, N_i is the number of attempts, and N_{AE} is the number of possible errors.

- **User Satisfaction** is based on the individual perspective of each user, which can be challenging to obtain due to potential subjectivity. Some approaches to evaluate it are:
  - After Scenario Questionnaire (ASQ): It consists of three questions designed to assess the satisfaction level with a particular scenario, and it is administered after the completion of that scenario.
  - Subjective Mental Effort Questionnaire (SMEQ), consists of a single question designed to evaluate the level of mental effort perceived by individuals in relation to a specific task.
  - Psychometric analysis of the NASA-TLX index is a widely used subjective and multidimensional assessment tool to measure perceived workload and evaluate task effectiveness. This methodology enables companies to assess workload, which refers to the effort required for a human operator to achieve a specific level of performance. In this context, workload is defined considering the interaction between task requirements, the circumstances in which it is performed, and the operator's skills, behaviors, and perceptions (Barrera-Gálvez et al., 2017). This index utilizes measures such as effort, frustration, mental load, temporal load, and stress to analyze the relationship between usability and utility in human-robot interaction systems (HRI).
- **Usability Magnitude Estimation (UME)**: Usability assessment often focuses on the user's effective interaction, frequently overlooking the influence of user expectations. However, these expectations provide valuable insights into usability as a whole, user satisfaction, and the significance of usability issues.

In assistive technologies, it's common to assess the overall usability of an object, device, or application through subjective evaluations. The most commonly used ones in user experience are the System Usability Scale (SUS) and the Quebec User Evaluation of Satisfaction with Assistive Technology (QUEST 2.0). The SUS consists of a 10-item questionnaire with reliable and valid results, where each item is scored from 1 (strongly disagree) to 5 (strongly agree). Scores range from 0 to 100, with usability considered high when surpassing 80 points. According to Lewis and Sauro (Lewis and Sauro, 2009), a minimum of 12 participants is recommended for comparative usability studies. Additionally, Julious (Julious, 2005) establishes a sample size of 12 per group when designing a clinical trial, based on reasons of feasibility, precision regarding the mean and variance, and regulatory considerations.

In usability analyses, it's common to use adapted questionnaires (in over 65% of cases), which limits evaluation options for reliably measuring the user experience in assistive technologies (Meyer et al., 2019). These questionnaires typically focus on assessing critical aspects

as determined by researchers, aiming to determine effectiveness and user satisfaction. This is relevant because during system use, much of the success depends on the strategies the user can modify or adjust to successfully complete the task, considering both user skills and device capabilities. Therefore, providing adequate feedback is essential (Barrera-Gálvez et al., 2017).

There are other techniques that eliminate the need for asking questions, such as Eye tracking, which enables observing a user's responses while interacting with a digital product (this document will not delve into this type of techniques).

Another fundamental aspect in the evaluation of assistive or rehabilitation devices is the assessment of the device's performance itself (precision, repeatability, and reproducibility), where the metrics predominantly used include: ranges of motion (Yurkewich et al., 2019, level of assistance Yurkewich et al., 2019, Z. Zhou et al., 2021), application of different controllers (accuracy, performance, etc.) (Costanzi et al., 2023, Morishita and Murakami, 2023, McDonald et al., 2020, Vélez-Guerrero et al., 2021, Z.-J. Chen et al., 2021).

Through a deep understanding of mathematical fundamentals, the groundwork has been laid to design and implement a robust and effective methodology aimed at addressing the challenges encountered in the development of a robotic exoskeleton applied in rehabilitation. By integrating detailed mathematical concepts such as optimal mechanical design, control theory, and comprehensive device evaluation in real-world settings, a theoretical framework supporting the research conducted in this thesis has been established. Now, with this solid mathematical foundation as a starting point, the development of the proposed methodology will commence, confident that the approach will be rigorous, efficient, and capable of generating significant results in practice.

Chapter 4

Comprehensive Development of Rehabilitation Devices: Full-Scope Methodology and Design Implementation

"The methodology in technological design is the engine driving innovation forward."

Albert Einstein.

This chapter establishes the conceptual and procedural framework that guides the development of this thesis. It details the research approach adopted, the analytical methods used, and the data collection techniques. Therefore, it is divided into two parts: the first describes the methodology, and the second addresses the practical implementation of the methodological design phase.

In the first part, a metaheuristic methodology is introduced for the development of a robotic exoskeleton aimed at upper limb rehabilitation, treating it as a mechatronic product. This methodology adapts and merges the user-centered approach outlined by Shetty et al. (Shetty et al., 2012) with the procedures described by Carvajal (Carvajal Rojas, 2005). And in the second phase, a comprehensive analysis is conducted on the results obtained by applying the methodology described in the first part, specifically regarding mechanical design. Consequently, a complete overview is provided of the processes, results, and challenges encountered in the creation of the virtual and physical prototype of the designed exoskeleton.

4.1 Methodology description

The proposed methodology consists of 12 stages integrated into 3 phases. The first phase begins with identifying the need and concludes with optimizing the design. The second phase

starts with the mathematical model of the final design from the first phase and ends with optimizing the device's operation. Finally, the third phase encompasses everything related to developing the physical prototype for the proposed device.

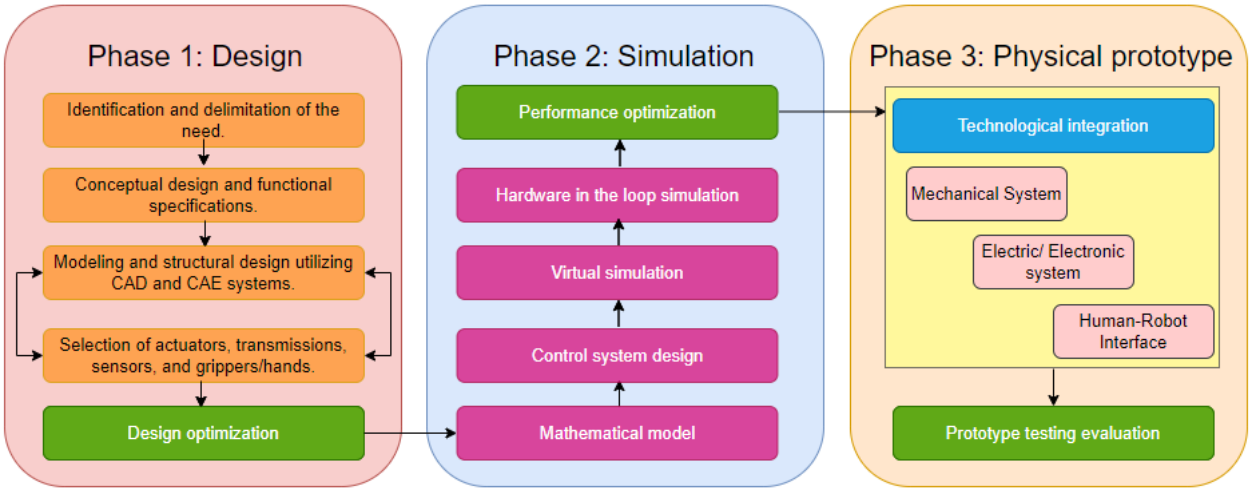

Figure 4.1: Proposed Methodology for the Development of the Rehabilitation Robot.

4.1.1 Phase 1: Design

The purpose of this phase is to obtain an optimized mechanical design for a rehabilitation robotic device, and it consists of the following stages:

1. Identification and delimitation of the need: It is essential to define the device's application environment, identify the end-user, and specify the objectives it must achieve.
2. Conceptual design and functional specifications: Once the robot's environment and tasks are defined, it is essential to establish its operating conditions or design metrics. At this stage, the robot's function has been determined, and the subsequent steps will focus on selecting and designing its mechanism.
3. Modeling and structural design utilizing computer-aided design (CAD) and computer-aided engineering (CAE) systems: In this stage, the basic structure of the robot is established, materials are chosen for each of its parts, the mechanism at the joints is defined, and static and/or dynamic load analyses are conducted. In summary, this stage involves configuring a virtual model using CAD systems and analyzing it using CAE systems.
4. Selection of actuators, transmissions, sensors, and grippers/hands: Based on the dynamic model of the robot, it is possible to estimate the torque and forces at the joints, enabling the selection of motors from commercial catalogs and the determination or design of corresponding transmissions. Additionally, control variables are defined, facilitating the selection of appropriate sensors. Upon completion of this stage, a design of the robot that meets the intended characteristics and functions is available, although optimization is also possible.

5. Design optimization: The purpose of this stage is to conduct engineering tests in order to achieve an optimal design of the device obtained in the previous phase. These tests adjust the parameters and/or variables of the robot to maximize or minimize certain characteristics. During this phase, the optimization of the device focuses on the mechanical design.

4.1.2 Phase 2: Simulation

During this phase, the kinematic behavior of the robot and several control strategies implemented in the virtual digital twin of the device (obtained in the previous stage) are simulated and analyzed. This phase consists of the following steps:

1. Mathematical model: They are generated to predict the behavior of the robot. These models may include obtaining Denavit-Hartenberg parameters, forward and inverse kinematics analysis, Jacobian, and analysis of its dynamic model (using Euler-Lagrange's or Newton-Euler's laws).
2. Control System Design: Upon validation of the robot, it becomes possible to develop a control system tailored to its mechanical characteristics and mathematical models, while also taking into account the conditions of its application.
3. Virtual Simulation: In this stage, a graphical representation of the robot's control system is generated on a computer (digital twin prototype, DTP) to visualize its animation and evaluate its performance. Specialized robot simulation software is used for this purpose.
4. Hardware-in-the-loop simulation: In certain contexts, such as systems interacting with humans (e.g., exoskeletons), creating entirely precise plant models can be challenging. In such situations, it becomes necessary to make assumptions, and conducting control system tests within the robot's environment proves beneficial. This approach is known as hardware-in-the-loop simulation, where real hardware components, such as mechanical and electrical parts, are used in the system control loop, acting as the plant being controlled. These tests provide the designer with confidence that the assumptions made in the robot's model were accurate.
5. Performance optimization: If any assumption made in the previous step proves to be incorrect, the designer has the opportunity to refine the design at the simulation level before creating the physical prototype of the device. In this case, the optimization focuses on the control system implemented in the device.

4.1.3 Phase 3: Physical Prototype

This stage represents the final step of the proposed methodology and focuses on building the physical prototype of the device (digital twin instance, DTI), taking into account the details related to the integration of all the systems that make up the device as well as the development of the human-robot interface. Below, each of the stages involved is detailed:

1. Technological integration: In this stage, each of the main systems comprising the device is examined in detail, along with their interrelationships. Subsequently, the integration

of all physical, mechanical, electrical/electronic, and computerized systems is carried out to configure a new device with the characteristics defined earlier.

2. Prototype Validation: This stage represents the culmination of the methodology and aims to carry out a comprehensive validation that assesses both the performance of the developed device and its usability for the different users involved. It is recommended to conduct validation tests in the application environment or under conditions as close to reality as possible.

4.2 Methodological Implementation: Designing the Digital Twin Prototype

The purpose of this stage is to obtain an optimized robotic exoskeleton for upper limb rehabilitation, considered as a mechatronic product. Therefore, the design stage is divided into two phases: in the first, a DTP is obtained considering the triad of design points of view (design requirements), then in the second stage the optimization of the DTP is developed (obtained in the first stage) through using the triad of pillars of Industry 4.0 (autonomous machines and systems, additive manufacturing and simulation of virtual environments). The description and the implementation of each of its steps are described below.

4.2.1 First phase: Identification and delimitation of the need

The exoskeleton is conceived as a support tool for physiotherapists, focusing on the passive rehabilitation of adults over 18 years old with limited mobility in the upper limb (due to stroke, musculoskeletal conditions, postoperative issues, among others). From this objective, the following conceptual design and its functional specifications are defined.

4.2.2 First phase: Conceptual design and functional specifications

These are based on the triad of design viewpoints (customer, designer and community), where the customers are medical institutions that offer physical and cognitive rehabilitation services. There are three categories of users: (1) the rehabilitation specialist, (2) the patient presenting the injury and (3) the medical institution that acquires the device. The requirements for each are described below:

1. First end user: Rehabilitation specialist (physical and/or cognitive).
    - Range: The device must comply with the functional ranges of joint movements to be rehabilitated (see Table 4.1). It must satisfy at least 80% of the ranges considered for a healthy person (taking into account what was mentioned in section 3.1.1 Human anatomy and physiology: Upper limb kinematics).
    - Usability: The device must be easy to operate.
    - Type of rehabilitation: The device is used passively with seated patients.
2. Second end user: Patient with injury (stroke, musculoskeletal, post-surgical, etc.).

- Ergonomic: The device must be adaptable to anthropometry. It must cover 50% of the ranges covering the 90th percentile of the adult population (Avila-Chaurand et al., 2007), see Table 4.2.

3. Client: Medical institution (administrative personnel).
   - Standardization: The device must be made of standard parts (easy replacement and minimal maintenance).
   - Affordability: The device must have an affordable cost.

Table 4.1: Joint movements.

Joint movements	Value
Shoulder internal–external rotation (S-IER)	$-30°$ to $+70°$
Shoulder abduction–adduction (S-AA)	$0°$ to $+90°$
Shoulder flexion–extension (S-FE)	$-50°$ to $+160°$
Elbow flexion–extension (E-FE)	$0°$ to $140°$
Wrist abduction–adduction (W-AA)	$-15°$ to $45°$

Table 4.2: Anthropometric measurements.

Parameters	Value
Weight (kg)	≤ 120.00
Arm length (m)	0.24–0.40
Forearm length (m)	0.25–0.39
Wrist to palm length (m)	0.06–0.15
Arm-forearm perimeter (m)	≤ 0.35

4.2.3 First phase: CAD design and component selection

A feature-based parametric design was considered to respond to customer requirements and model the relationships between its functions and physical solutions. The main design features considered by the designer and the community are the following:

1. Modular: Personalized, flexible, removable with a short manufacturing time.
2. Basic geometries: Flat, uniform (not degenerate) and low cost.
3. Type of mechanisms: Telescopic for variable length segments and bolted joints.
4. Manufacturing type: Additive manufacturing (3D printing).
5. Manufacturing materials: Filaments for 3D printing (mechanical properties).
6. Machinery and commercial parts: 3D printers (Raise3D Pro2 Plus and Ultimaker S5) and tubular profiles.

Figure 4.2 shows the first stage of the proposed methodology: where the main design features are obtained from the requirements (indicated above). Its selection is based on knowledge of the real-world problem, the result of this stage is the virtual digital twin

prototype (DTP) of the exoskeleton. An advantage of DTP is that it can perform engineering design evaluations, kinematics, dynamics and control. Furthermore, it can be optimized under various criteria such as weight, service life, bending and efficiency. This work focuses on optimizing the weight of a safe mechanical design and this is described below.

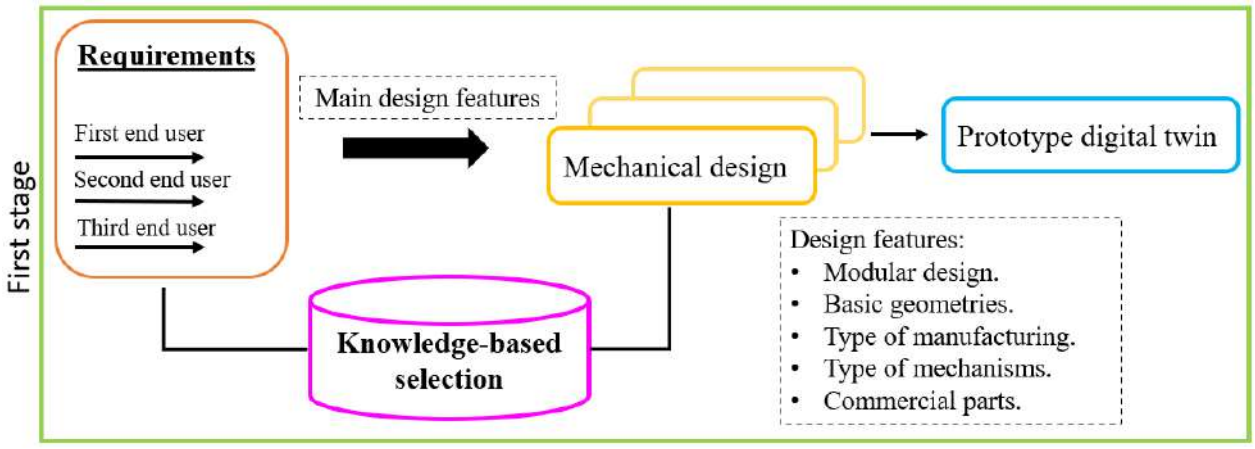

Figure 4.2: User-centered design methodology: first stage.

4.2.4 First phase: Obtaining the initial DTP

Figure 4.3 shows the DTP obtained in SolidWorks® (result of the first stage of the proposed methodology). On the left you can see the exoskeleton attached to the patient (on the arm and forearm), and on the right you can see the mechanical structure of the exoskeleton highlighting each of its parts, which are described below:

1. **Fixed base:** The device is anchored to a commercial wooden chair (see number 1 in Figure 4.3). This structure is placed inside the medical institution and must have an obstacle-free area of 1.5 m × 1.5 m around it for proper operation (portable device).

2. **Shoulder height adjustment:** The specialist manually adjusts the exoskeleton to the height of the patient's shoulder, the length of which can vary between 0.10 and 0.30 m (see number 2 in Figure 4.3).

3. **Shoulder movements:** A serial configuration of movements was implemented to minimize kinematic singularities when generating therapeutic routines, and the movement will be generated by a rotary actuator directly (taking into account high-power capacity, torque-to-weight ratio, precision and others). For this, links of different geometries were designed that comply with the anthropometric measurements of the target population (see Table 4.2) and also with the work area of the 3D printers: Raise3D Pro2 Plus and Ultimaker S5 (printers available at institutions). In addition, a model of simple rotary joints covering the 3 DOF of the shoulder was considered: (1) internal and external rotation (S-IER), (2) abduction–adduction (S-AA) and (3) flexion–extension (S-FE), as can be seen in Table 4.1 (see number 3 in Figure 4.3).

4. **Arm and forearm length adjustment:** Commercial carbon fiber telescopic tubular profiles are used and attached at their ends by a clamp; they allow variations in the

lengths of the arm and forearm (see Table 4.2). The physiotherapist performs the length adjustment manually and, finally, the patient is attached to the exoskeleton with Velcro bands (see numbers 4 and 6 in Figure 4.3).

5. **Elbow and wrist movement** The elbow (E-FE) and wrist (W-AA) joints attach to the ends of the arm and forearm structures, respectively. These parts are going to be manufactured from 3D-printed materials and their movements are going to be generated by a rotary engine directly (see numbers 5 and 7 in Figure 4.3 and Table 4.1).

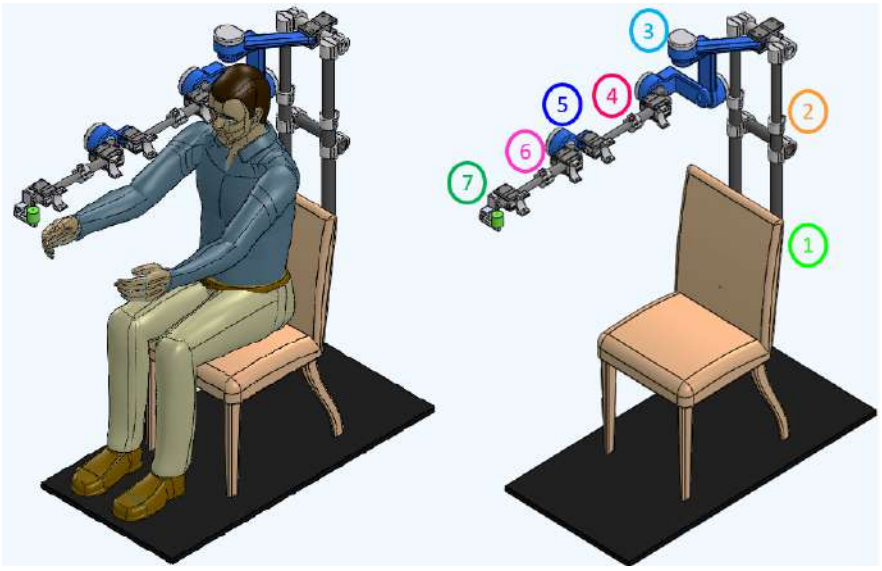

Figure 4.3: Virtual digital twin prototype (DTP): Exoskeleton with patient (left) and Exoskeleton (right): SolidWorks®.

4.2.5 Second Stage: Acquiring the optimized DTP

This section describes the second phase of the proposed methodology, which takes into account the triad referring to Industry 4.0:

- Autonomous machines and systems: Automating tasks with robots ensures precision and repeatability in movements, allowing personalized therapies for users.
- Additive manufacturing: This enables the creation of highly customized products, simplifying the production of iterative designs and the ease of modifying them.
- Simulation of virtual environments: This simplifies the testing and validation of concepts, designs and processes, eliminating the requirement for physical prototypes. This creates a secure environment for experimentation, enabling the identification of areas for improvement and optimization.

In this case, the DTP of the exoskeleton obtained in the previous stage through the SolidWorks® software (version 2018) is used. Its parts will be in 3D printing, so the materials assigned depend on it. The topological optimization of the exoskeleton was carried out at this stage, which has the following main objectives:

1. A safety factor greater than required (maximization).
2. Minimum total deformation (minimization).
3. Obtain a lightweight mechanical design (minimization).

A sequential methodology is proposed that considers conditional structures to satisfy the above objectives, through an objective function that includes the use of finite element analysis (FEA) simulations obtained from the SolidWorks® software (version 2018). FEA is a computerized method to predict how a real object would react to the presence of forces, heat and vibrations, among others; therefore you can know the internal stresses, and deformations that act on the object analyzed from the geometric and physical properties of each element. With the help of this information, the safety factor of the device as a whole is obtained. This is an advantage at the design stage because it provides an early estimate of the device's performance, which helps to propose significant changes considering the selected parameterized characteristics.

Because optimization goals are intrinsically related (they seek to reduce the mass of the design while smoothing the stress distribution) and are derived from the same static analysis, a weighted approach is used to scale the multi-objective problem into a single objective one. Algorithm 1 was developed for this purpose and is described below:

1. The material is assigned to the parts of the DTP (commercial and 3D-printed parts) and iterations are initiated.
2. The exoskeleton is analyzed through a static finite element analysis from which the values of safety factor (SF_k), maximum total deformation (MD_k) and total mass (TM_k) are obtained. These parameters are considered because they are the most representative of mechanical design (the initial values (k = 1) of SF, MD and TM are indicated by the subscript i).
3. A normalized weighted approach is used for the objective function (OF), considering the values of SF, MD and TM. First, it is assumed that the parts can be optimized, so the initial value of the OF is the unit and the following ones will represent the optimization relationship.
4. To modify the parts (change parts and material), they are individually modified in the order indicated in Figure 4.3 (starting with the telescopic tubes attached to the chair and ending with the parts that correspond to the movement of the wrist). Optimization is executed piece-by-piece iteratively and then evaluated for overall performance across the device.
5. The static analysis is run with the new changes and the OF value is returned to it. The process ends when the desired SF and OF are obtained (SF_d, OF_d).
6. Finally, the optimization process is evaluated through the value of the objective function (OF_k).

The decrease in the SF, as well as the decrease in the TM of the device, can generate an increase in its MD, which is consistent as the algorithm advances. The objective function

considers this behavior, so it is normalized and its change pattern is in accordance with the local search capacity of the parts and global features of the device, which converge in a minimization optimization problem.

The main strengths of Algorithm 1 are based on its methodology, which leverages a weighted objective function that integrates three objectives simultaneously that can be achieved with parts made by additive manufacturing (unlike most approaches that optimize only one objective). Moreover, its termination criteria rely on two factors (SF and OF), enabling the maximization of device performance. Additionally, it incorporates the utilization of virtual simulation outcomes that account for real application conditions, which is a feature often overlooked by other approaches that typically lack results from simulation environments operating under real conditions. In the next section, the proposed methodology will be executed and the results will be shown.

Algorithm 1 Topological optimization

Assigning materials to parts
$k \Leftarrow 1$
Device performance evaluation (SF_k, MD_k, TM_k)
do
    If $k = 1$
        $SF_i \Leftarrow SF_k$
        $MD_i \Leftarrow MD_k$
        $TM_i \Leftarrow TM_k$
        $OF_k \Leftarrow \frac{1}{3}\left(\frac{SF_k}{SF_i}\right) + \frac{1}{3}\left(\frac{MD_i}{MD_K}\right) + \frac{1}{3}\left(\frac{TM_k}{TM_i}\right)$
    Else
        Change parts and material.
        Device performance evaluation (SF_k, MD_k, TM_k)
        $OF_k \Leftarrow \frac{1}{3}\left(\frac{SF_k}{SF_i}\right) + \frac{1}{3}\left(\frac{MD_i}{MD_K}\right) + \frac{1}{3}\left(\frac{TM_k}{TM_i}\right)$
    End If
$k \Leftarrow k + 1$
While$((SF_k \geq SF_d)$ and $(OF_k \geq OF_d))$

The functions "Device performance evaluation (SF_k, MD_k, TM_k)" and "Change parts and material" are described below:

1. Function *"Device performance evaluation"* of Algorithm 1 considered the following:

    - The exoskeleton was analyzed by static analysis in the critical position (shoulder flexion at 90° and maximum design length). Criterion of the Von Mises tension was used to estimate the failure of the device (the coefficients of maximum stresses, maximum total deformation and maximum unit deformation belonging to the exoskeleton were obtained). The features taken into account in the analysis are shown in Table 4.3, where the torques of each actuator were obtained by considering the arm, forearm and wrist of the exoskeleton as cantilever beams. This last analysis considered the mechanical properties of the exoskeleton pieces, their maximum lengths, and as external forces, the percentage of the maximum weight of the

patient's upper limb (2.6% in the arm, 1.6% in the forearm and 0.7% in the wrist, according to what was indicated in section 3.1.2). The detailed analysis for sizing the actuators is presented in Annex .1.

Table 4.3: Finite element analysis features in SolidWorks®.

Parameter	Value
Gravity	9.81 $\frac{m}{s^2}$
Patient weight	120.00 kg
Actuator torque S-IER	10.86 Nm
Actuator torque S-AA	34.16 Nm
Actuator torque S-FE	33.45 Nm
Actuator torque E-FE	10.82 Nm
Actuator torque W-AA	0.30 Nm
Fixed restrictions	Attachment clamps to the chair and joints to the actuators
Mesh	Standard solid of 4 Jacobian points.

2. Function *"Change parts and material"* of the Algorithm 1: the DTP topological optimization is carried out in this function, it was performed through the change in the thicknesses of each of its parts (this generates uniform and non-degenerate basic geometries without post-manufacturing processes), in addition to the change in material. This process is carried out piece by piece iteratively. Once the piece is modified, its performance is evaluated in the global device assembly (function *"Device performance evaluation"*). Therefore, in SolidWorks® a design study was carried out in which parametric variables are selected at each part; the constraints were the safety factor (SF_d) and maximum stresses of the device, and the objective was to minimize the mass (the values of the constraints and objective initial considered the results of the DTP obtained in stage 1). Two types of parts were distinguished for optimization:

   - Commercial parts
     - Telescopic joints: Commercial tubular profiles of different materials were selected. For their optimization, their internal and external diameters were chosen as parametric variables, which were varied in a range of ±20 mm with steps of 1 mm. From the options generated, the pair of commercial profiles was selected that were adjusted telescopically through a clamp and presented the minimum mass (minimum local feasible).
   - Manufactured parts
     - Serial parts (see 3, 5 and 7 in Figure 4.3): In the first instance, the printing area of the printers is considered for the lengths of the pieces (Raise3D Pro2 Plus and Ultimaker S5). The initial thickness is random (characteristic of the stochastic method), and the optimization consists of modifying it within a range of ±20 mm of the initial value with intervals of 2 mm. To select the best candidate from the generated options (minimum local feasible), the following features were considered: that the thickness had the lowest mass and that the alignment to the center of rotation of each of the joints was maintained.

To join the pieces, removable joints (screws) were chosen, since they can withstand cutting forces, tensile forces or a combination of these.

Firstly, to apply the Algorithm 1, it is assumed that the parts can be optimized. The desired safety factor was set as 1 (mechanically safe device) and a value for the target function was 0.4 (weighted ratio of objectives). Table 4.4 shows the materials used in the design study in Solidworks® and results obtained from some iterations of Algorithm 1. Iterations $k = -2$ and $k = -1$ are shown as antecedents of iteration $k = i$ due to the following: (1) they use the DTP generated in stage 1 of this methodology and (2) the manufacturing method is subtractive manufacturing.

The $k = i$ iteration represents the initial DTP, which initially assigns steel for the fixed parts and aluminum for the arm and forearm components. Initially, tubular profiles with an external diameter of 50 mm and a thickness of 4 mm were considered and were available in the laboratory. Subsequently, the topological optimization process described above was applied to these profiles. Iterations with $k > 1$ display optimized results. The materials were selected because they are the most widely used due to their mechanical properties, while the last column ($k = n$) showcases the attributes of the selected final prototype.

The differences between the original DTP and the optimized version are illustrated in Figures 4.4-4.7 and 4.8-4.11, which show the results of static analyses performed in SolidWorks®. Furthermore, the SF decreases by 62%, resulting in a 127% increase in maximum stress. This increase contributes to rises in total and unit deformations by 127% and 351%, respectively, compared to the initial prototype (see Table 4.5).

Table 4.4: Conditions and results of topology optimization.

Parameter	k=-2	k=-1	k=i	k=2	k=3	k=n
Material: commercial fixed base parts	S-1020	Al-6061	S-1020	DI	S-1020	Al-6061
Material: commercial pieces for the arm and forearm	S-1020	Al-6061	Al-6061	Al-6061	Al-6061	CF
Material: manufactured parts	S-1020	Al-6061	ABS-CF10	ABS-CF10	ABS-CF10	ABS-CF10
FS_k	10.81	7.84	2.90	2.40	2.32	1.1
MD_k	0.01	0.03	0.74	1.29	1.14	2.06
TM_k	75.88	28.56	19.20	19.01	19.5	9.74
OF_k	27.22	9.61	1.00	0.79	0.77	0.41

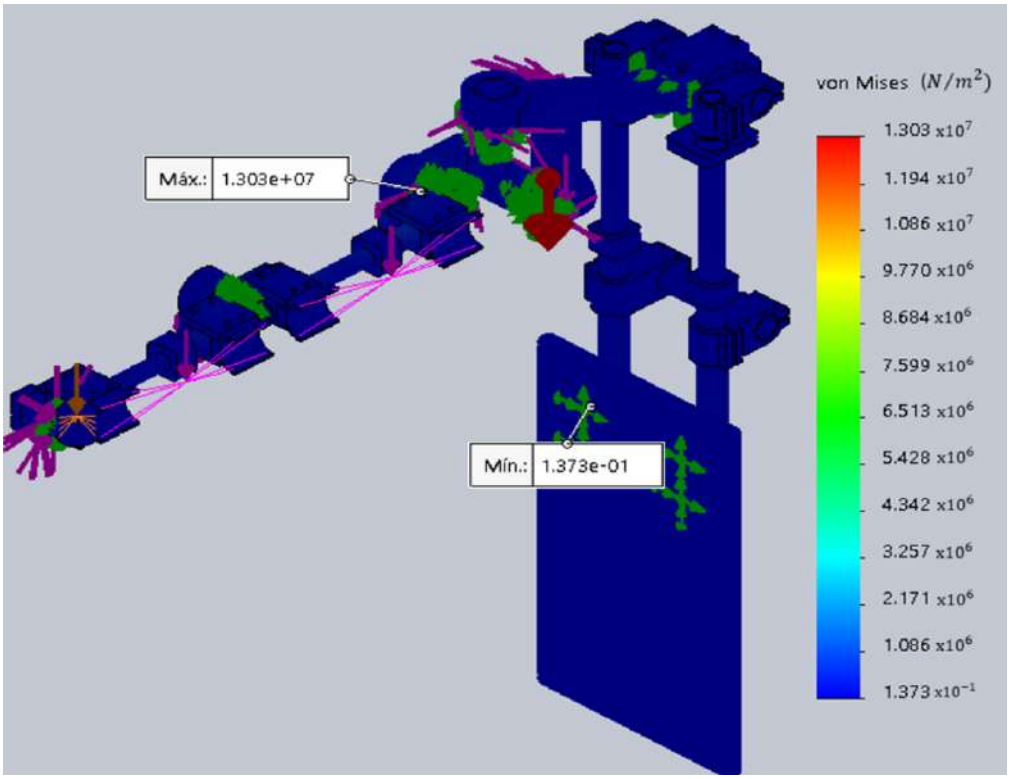

Figure 4.4: Initial DTP (SolidWorks®): Von Mises Stress (red indicates maximum and blue indicates minimum.

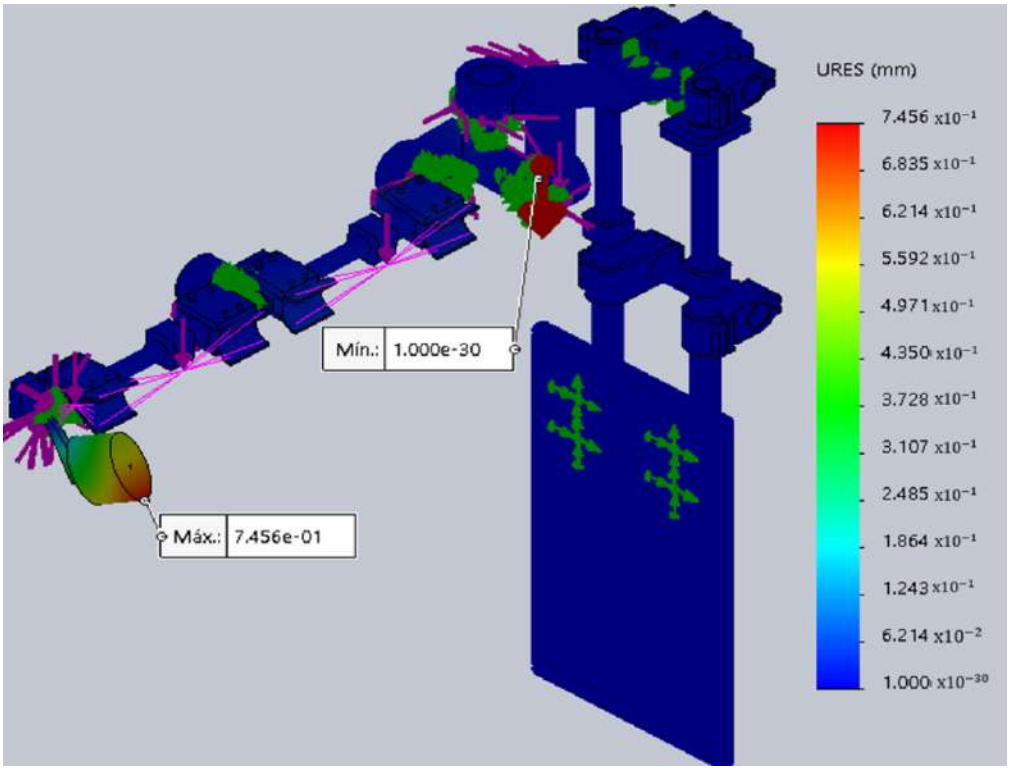

Figure 4.6: Initial DTP (SolidWorks®): Total deformation (red indicates maximum and blue indicates minimum).

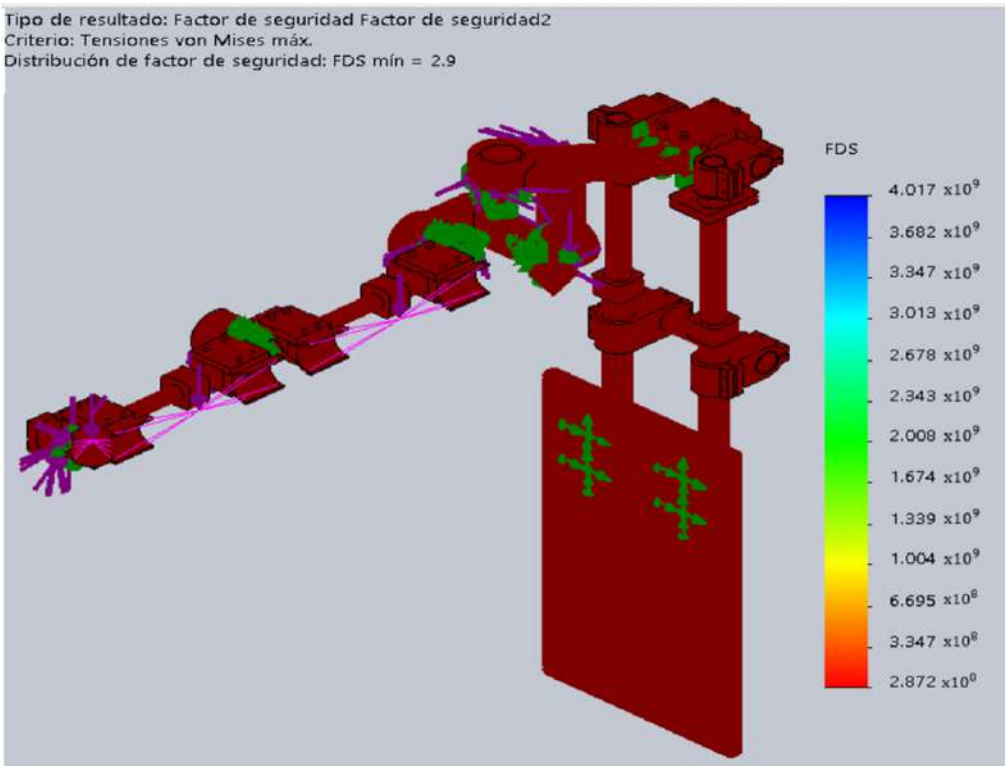

Figure 4.5: Initial DTP (SolidWorks®): SF (red indicates minimum FS).

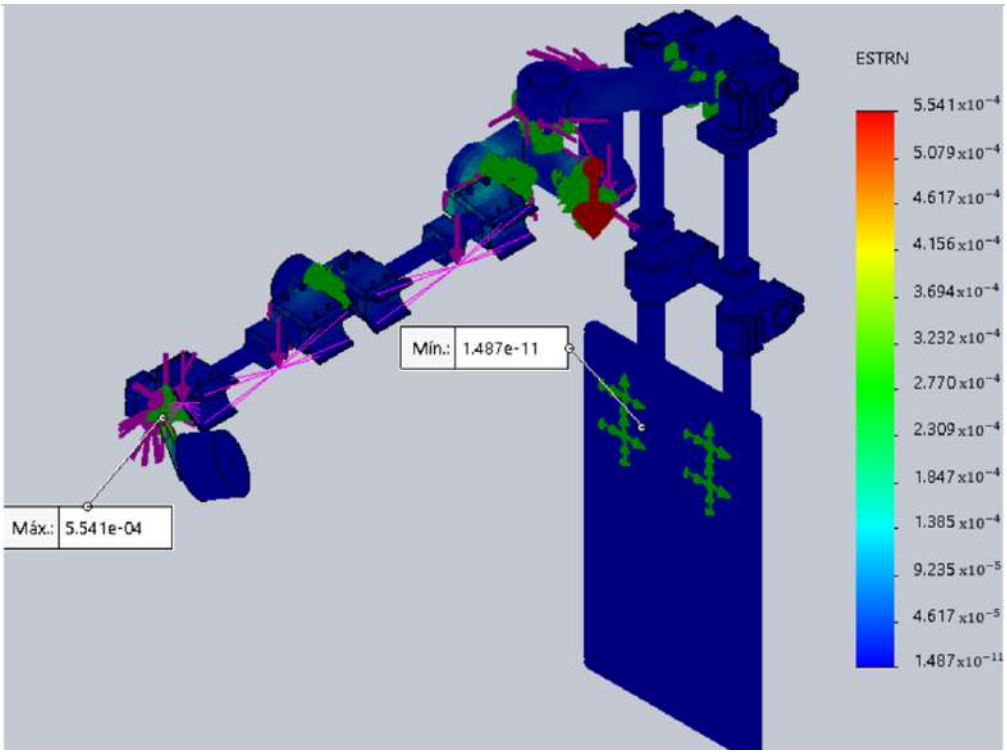

Figure 4.7: Initial DTP (SolidWorks®): Unit deformation (red indicates maximum and blue indicates minimum).

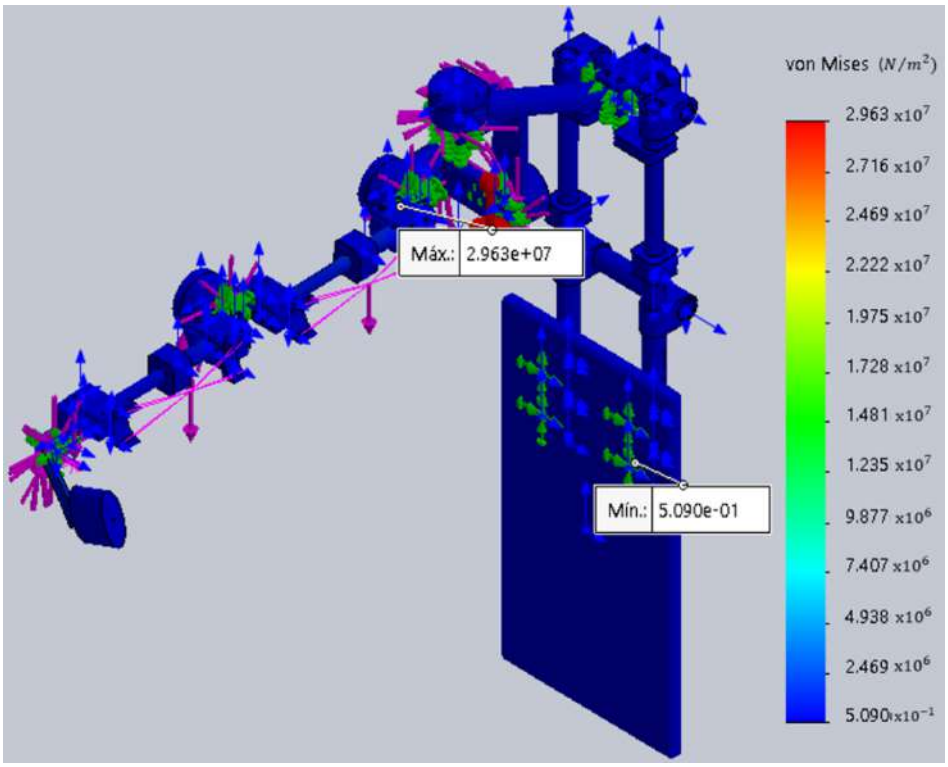

Figure 4.8: Optimized DTP (SolidWorks®): Von Mises Stress (red indicates maximum and blue indicates minimum.

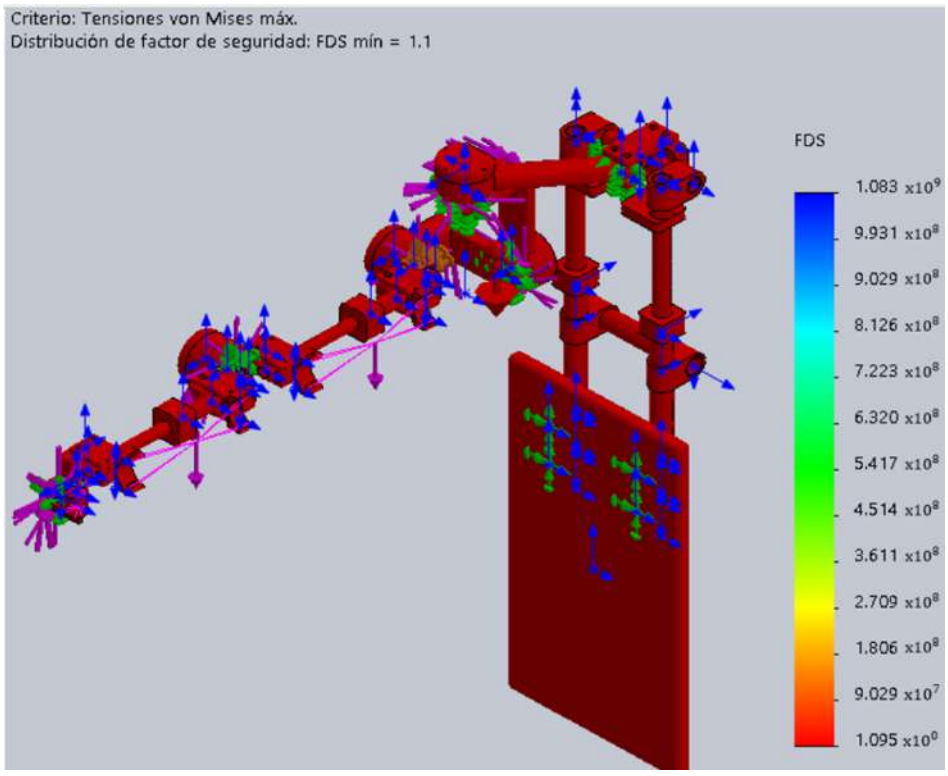

Figure 4.9: Optimized DTP (SolidWorks®): SF (red indicates minimum FS).

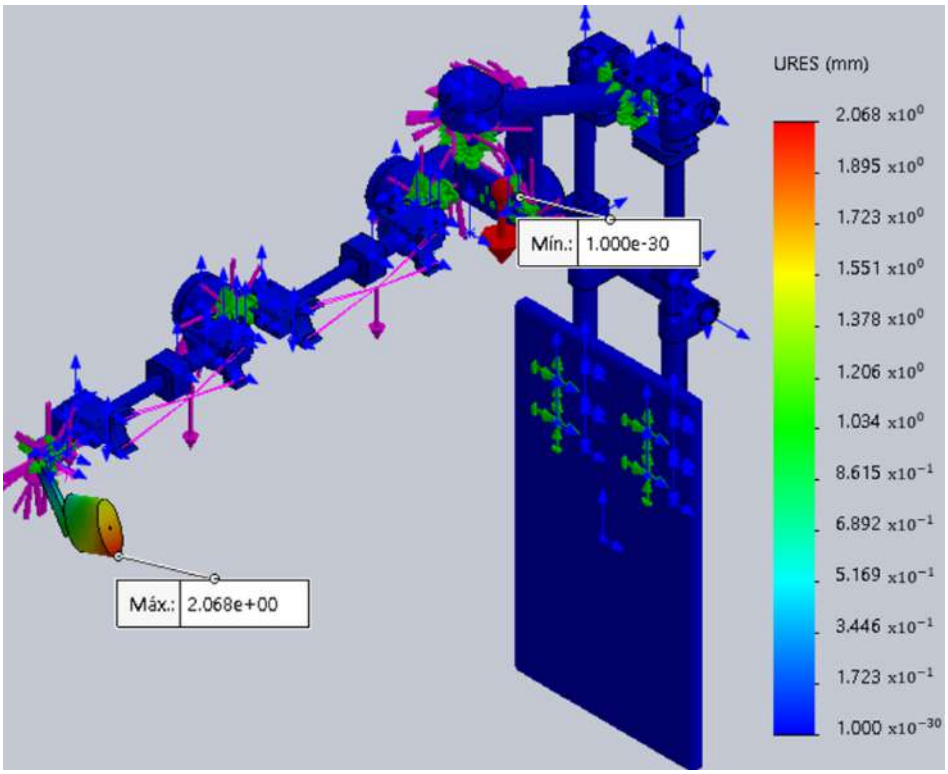

Figure 4.10: Optimized DTP (SolidWorks®): Total deformation (red indicates maximum and blue

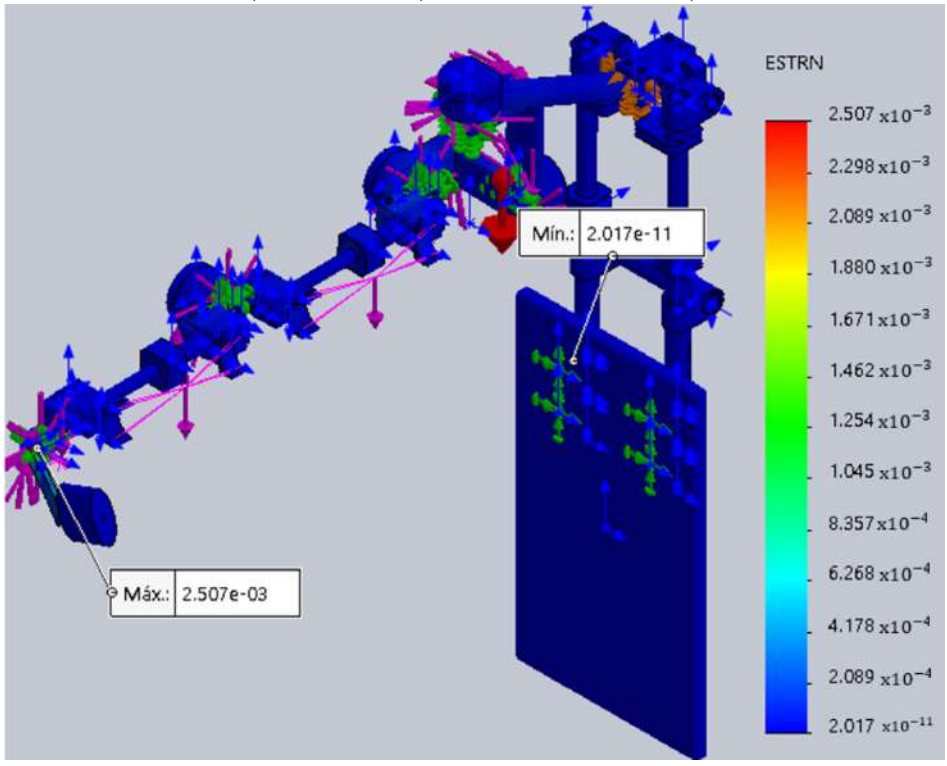

Figure 4.11: Optimized DTP (SolidWorks®): Unit deformation (red indicates maximum and blue indicates minimum).

Table 4.5: Optimization results.

Parameter	Initial DTP	Optimized DTP
Mass	19.20 kg	9.70 kg
Maximum stress (pieces), MPa	13.03 (ABS-CF10 parts)	29.63 (ABS-CF10 parts)
Maximum total deformation (position)	0.74 mm (palm)	2.06 mm(palm)
Maximum unit deformation	554.10 μm	2500.00 μm
Minimum safety	2.90	1.10

Furthermore, the results indicate a 49% reduction in the weight of the optimized DTP compared to the initial DTP (iterations k = i and k = n). This decrease is primarily due to the disparity in densities among the materials employed. For instance, the density of aluminum is approximately one-third that of steel, while the densities of CF and ABS-CF10 are even lower than that of steel. In addition, the value of the objective function is 0.41 and this shows the weighted relationship of the objectives to be met (SF, MD and TM).

For each parts groups shown in Table 4.4, commercial materials that present a good relationship between density and resistance were chosen. In this case, it was decided to use a single type of material and not a combination of them for the pieces made in 3D printing. The material selected for the final pieces made in 3D printing was ABS-CF10 because it is one of the most resistant and lightweight materials, and for commercial parts (1) Al-6061 for the pieces that join the fixed base and (2) carbon fiber for arm and forearm pieces were chosen. The results obtained demonstrated the feasibility and efficiency of the proposed methodology.

Figure 4.12 shows a graphical depiction of the proposed methodology (left): the initial stage centers around users, drawing inspiration from the human body (highlighted in yellow), while the subsequent stage aims to optimize the device's weight (highlighted in purple). Lastly, the prototype constructed based on the outcomes of the proposed methodology is displayed on the right. To offer a visual representation of the digital twin instance (DTI) with users, Figure 4.13 is provided.

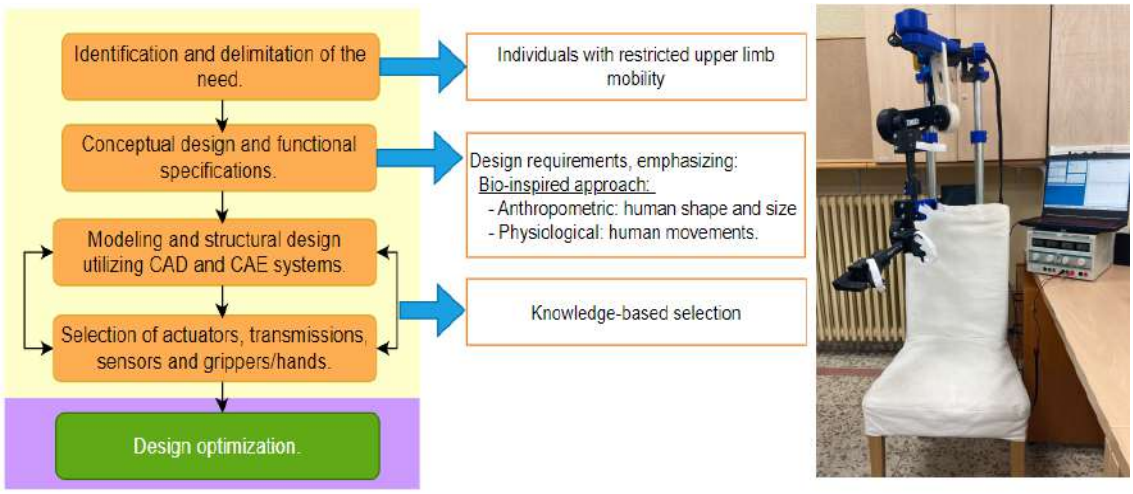

Figure 4.12: Design methodology and digital twin instance (DTI).

Figure 4.13: DTI with subjects: Subject 1 and subject 2.

Figure 4.14 shows the stages of DT utilization. In this context, the DTP was utilized during the design phase, primarily for 3D modeling (encompassing design validation and optimization) and kinematic modeling (comprising forward kinematics (Section 5.1.3), inverse kinematics (Section 5.1.4) and Jacobian (Sección 5.1.5) and strategies of automatic control (Section 5.2). Following the acquisition of the optimized DTP, we proceeded to the production phase, with additive manufacturing serving as the principal manufacturing method. Following the production phase, the DTI is generated, which is intended for experimental validation under real-world conditions. For this purpose, a human–robot interface was developed to streamline DTI operation, incorporating industrial controllers. Furthermore, personalized therapies can be scheduled based on the medical specialist's specifications. Further elaboration on DTI validation will be provided in Section 6.

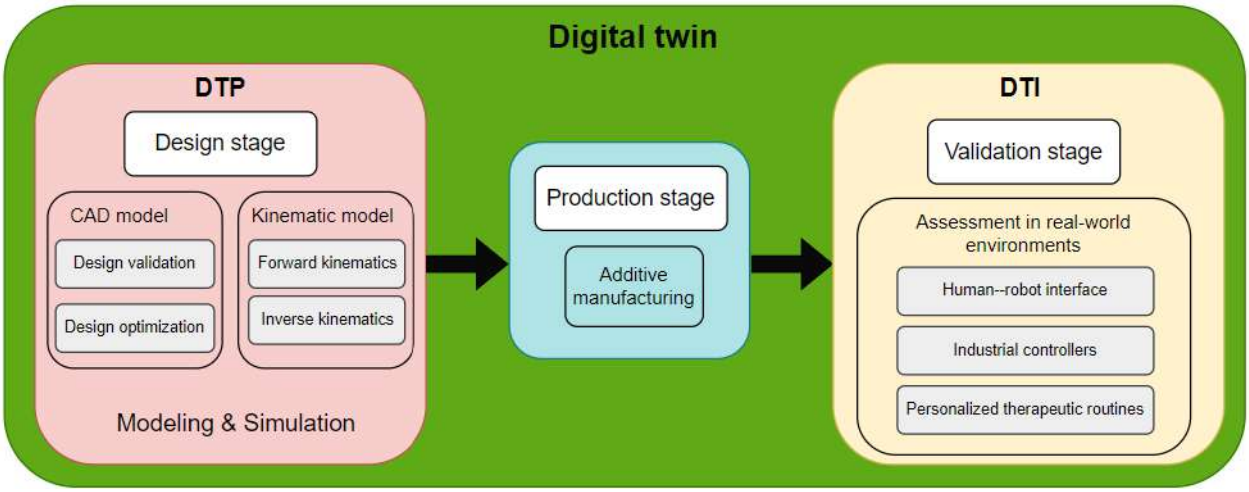

Figure 4.14: Development and application of the digital twin (DTP and DTI).

Below, the detailed process of obtaining the physical prototype of the optimized exoskeleton obtained in the design stage is described.

4.3 Methodological Implementation: Acquiring Physical Prototype (Digital Twin Instance)

To evaluate the performance of the exoskeleton designed in section 4.2.5, a prototype was fabricated using 3D printing, serving as a digital twin instance (DTI). For its construction, changes were necessary due to the materials available in the UPM laboratory. The main changes focused on the 3D printing materials and the actuators used, as detailed below:

- The materials used for the 3D printed parts are Acrylonitrile Styrene Acrylate (ASA) and Acrylonitrile Butadiene Styrene with 10% carbon fiber (ABS-CF10).
- The actuators used are GIM6010, with a nominal torque of 18 Nm.

Due to the changes made, the performance of the exoskeleton designed in section 4.2.5 will be affected. However, the generated DTI will help validate the concepts and establish future improvements. The characteristics of the generated DTI are detailed below.

4.3.1 Mechanical system: Manufacturing and Assembly

The aim of this stage is to achieve the mechanical structure of the DTI for the exoskeleton as outlined in section 4.2.5. Therefore, the manufacturing processes are described below: (1) process operations (which transform a work material from one stage to a more advanced stage using energy) and (2) assembly operations (which join two or more components to create a new entity called an assembly).

In this case, the manufacturing method is 3D printing, which utilizes the rapid prototyping technique known as Fused Deposition Modeling (FDM). Through this process, a full-scale piece designed on the computer is created by layer-by-layer plastic extrusion and three-dimensional tool positioning. Its main features include error reduction, decreased product development costs and lead times (up to 70%), as well as a 90% reduction in time to market.

Figure 4.15 depicts the DTI of the optimized exoskeleton. The cyan and yellow parts are manufactured through 3D printing, while the brown parts are commercial carbon fiber profiles and the gray tubular profiles are made of ductile iron. The assembly of the parts was performed using metric screws of various sizes and lengths.

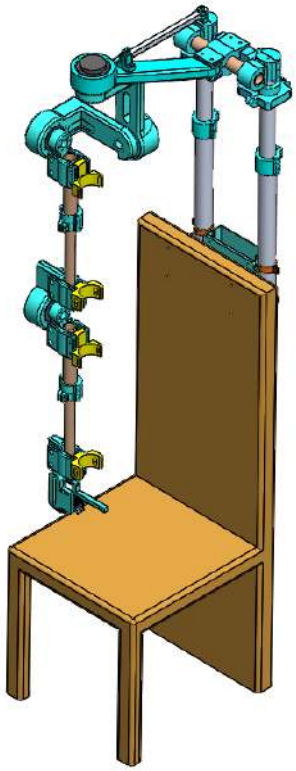

Figure 4.15: Exoskeleton DTI: Solidworks°

The parts manufactured through 3D printing were produced using two 3D printers: Raise3D Pro2 Plus and Ultimaker S5. Figures 4.16 - 4.19 showcase the parts manufactured with these printers.

Figure 4.16: Raise3D Pro2 Plus Printer

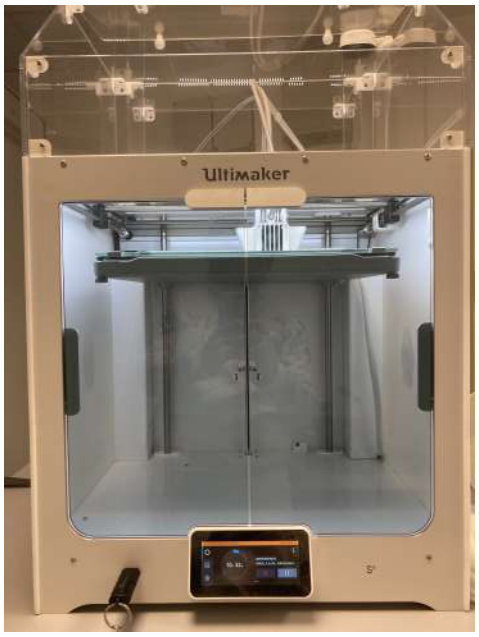

Figure 4.17: Ultimaker S5 Printer

Figure 4.18: Parts made of ABS-CF10

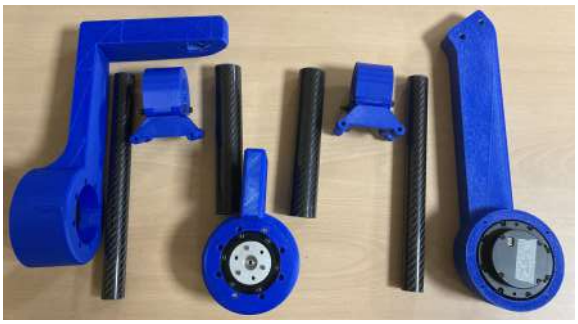

Figure 4.19: Carbon fiber tubular profiles and parts made of ASA

Once all the parts were obtained, both those manufactured through 3D printing and the commercial ones, assembly by parts was carried out (see Figures 4.20 to 4.21).

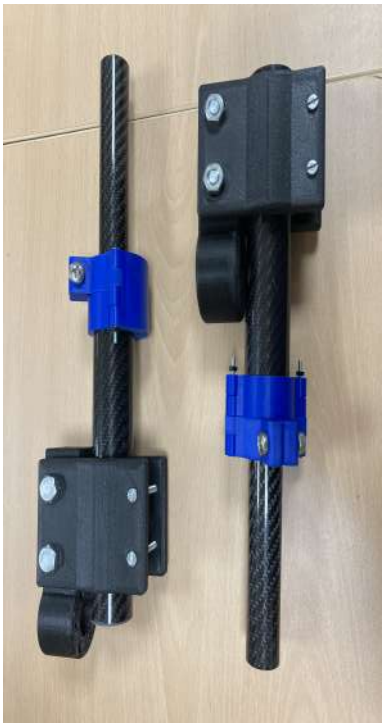

Figure 4.20: Subassemblies for the arm and forearm of the exoskeleton

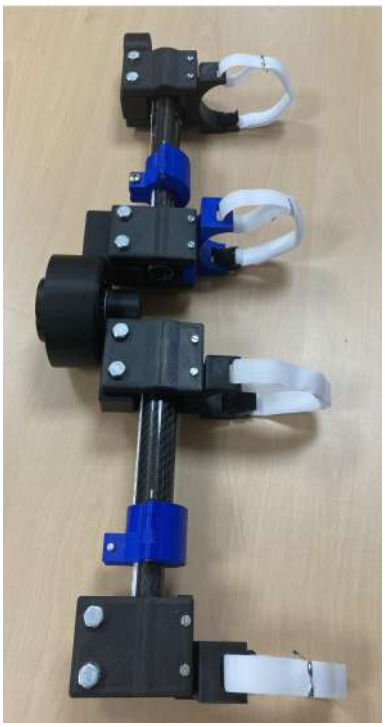

Figure 4.21: Subassembly for the upper limb of the exoskeleton

Once the corresponding subassemblies were completed, the total assembly was carried out, which has an approximate weight of 7.5 kg (excluding the chair). The exoskeleton was attached to a commercial wooden chair using commercial clamps (see Figure 4.22).

Figure 4.22: Exoskeleton DTI (Physical Prototype)

It is worth mentioning that the parts made of ABS-CF10 were produced at the Advanced Technologies Unit in Design and 3D Printing of the Hospital Universitario 12 de Octubre, using the Ultimaker S5 printer. On the other hand, the rest of the parts were manufactured at the laboratories of the Higher Technical School of Engineering and Industrial Design (ETSIDI), belonging to the UPM.

During the manufacturing of the exoskeleton parts, compliance with the NOM-241-SSA1-2012 standard was ensured. Additionally, the machinery meets standards for quality, installation, favorable operating conditions, and maintenance.

Additionally, the physical prototype complies with ISO 13482 in terms of mechanical design. This is because it lacks moving parts during operation, and the parts joined by mechanical fastening and press fit require tools for removal. The device operates effectively within the workspace. Therefore, the software operating it must consider the exoskeleton's workspace, as well as its load and speed limitations. Safety measures related to actuators, electronic components, and control strategies are taken into account when creating the human-robot interface (described in section 5.3).

The following sections will detail the stages of mathematical modeling, applied control strategies, virtual environment simulation, and development of the human-robot interface. The integration of these results leads to the evaluation of the device in real environments.

Chapter 5

Methodological Implementation: Mathematical modeling, control architecture and human-robot interface

"In the information age, technological design is the key to transforming knowledge into practical solutions."

Stephen Hawking.

Following the production phase, the DTI was successfully obtained for experimental validation under real-world conditions. To achieve this, a human-robot interface was designed to streamline DTI operation and enable the programming of personalized therapies according to the medical specialist's directives. This chapter presents the fundamental equations, modeling assumptions, and mathematical techniques used to solve and validate the model. Additionally, it addresses the control strategies implemented in simulation environments, accompanied by a detailed description of the human-robot interface aspects. Thus, a comprehensive overview of the processes, results, and challenges encountered throughout the project development is provided.

5.1 Mathematical modeling

In this section, we will discuss the workspace of the previously obtained exoskeleton, along with its direct and inverse kinematic models, as well as its Jacobian analysis and dynamic model. These evaluations will help assess its performance in the workspace and formulate strategies for implementing industrial controllers and trajectory planning.

5.1.1 Denavit-Hartenberg representation

The exoskeleton was designed in Solidworks®, it allows the movements: shoulder, elbow and wrist, it is assumed that the robot is aligned with the patient during the execution of the movements (the starting position of all movement is when the patient is seated with the upper limb hanging from the side of the body with the palm of the hand facing inwards). It is a serial device that utilizes Figure 5.1 to obtain the Denavit-Hartenberg (D-H) parameters shown in Table 5.1.

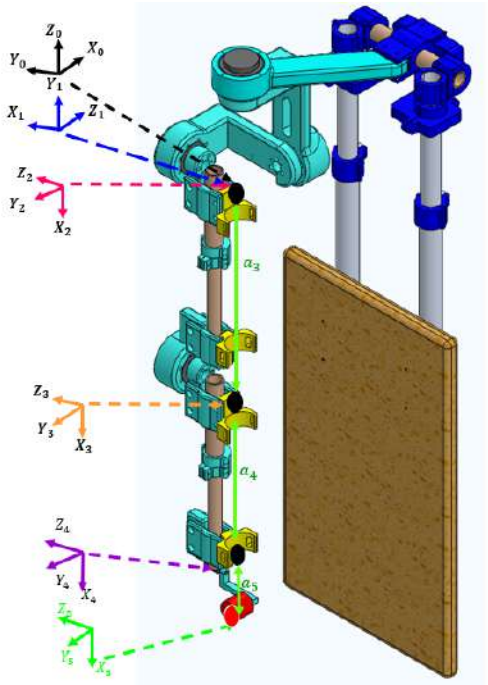

Figure 5.1: D-H notation for upper limb exoskeleton.

Table 5.1: D-H parameters of the upper limb exoskeleton.

Joint	Motion (q_i)	q_i	d_i	a_i	α_i
Shoulder	Internal–external rotation q_1 ($-30°$ to $70°$)	$q_1 + 90°$	0	0	$+90°$
Shoulder	Abduction–adduction q_2 ($0°$ to $90°$)	$q_2 - 90°$	0	0	$-90°$
Shoulder	Flexion–extension q_3 ($-50°$ to $160°$)	q_3	0	a_3 (24-40 cm)	0
Elbow	Flexion–extension q_4 ($0°$ to $140°$)	q_4	0	a_4 (25-39 cm)	0
Wrist	Abduction–adduction q_5 ($-15°$ to $45°$)	q_5	0	a_5 (6-15cm)	0

where: q_1 to q_5 represent the joint movements of shoulder internal-external rotation, shoulder abduction-adduction, shoulder flexion-extension, elbow flexion-extension, and wrist abduction-adduction, respectively. Parameter a_3 corresponds to the length of the patient's arm (shoulder-elbow segment), parameter a_4 corresponds to the length of the patient's forearm (elbow-wrist segment), and parameter a_5 corresponds to the length of the patient's hand (wrist-center of the palm segment).

5.1.2 Exoskeleton workspace

Table 5.2 shows the workspace (volume of space that the end effector can reach) for which the exoskeleton was designed, as indicated in the second column of Table 5.1. The initial cells present the workspace for each individual movement, and the last cell shows the complete workspace of the exoskeleton, considering the maximum lengths of the arm and forearm, as well as the full ranges of motion of each joint (red and blue colors). However, in this work, only the positions that are in front of the patient (blue color) are considered as the achievable workspace

Table 5.2: Exoskeleton workspace in Matlab®

Shoulder: Internal-external rotation	Shoulder: Abduction-adduction
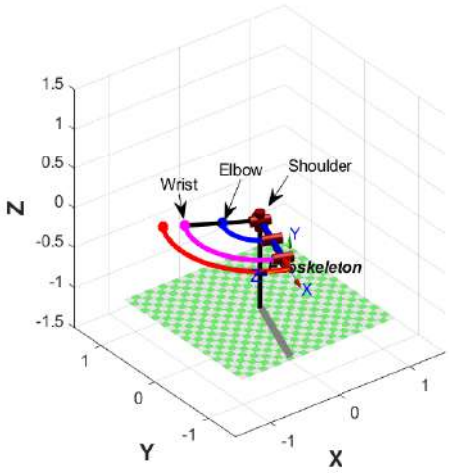	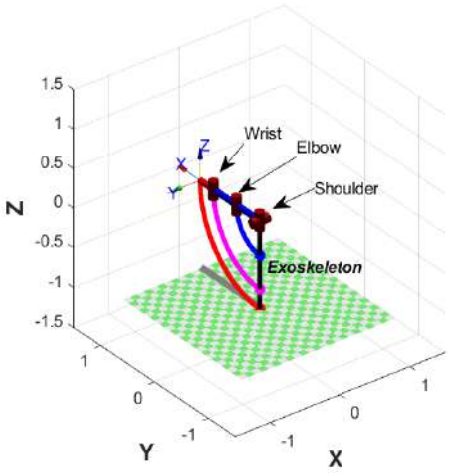
Shoulder: Flexion-extension	**Elbow: Flexion-extension**
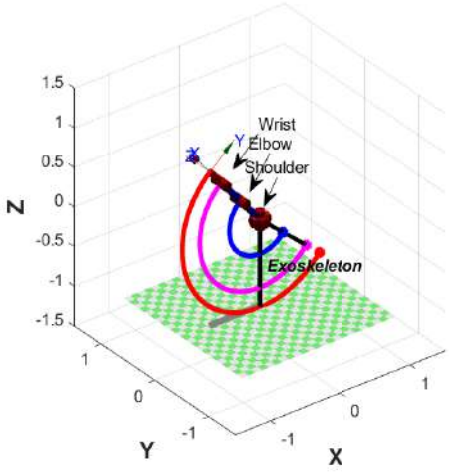	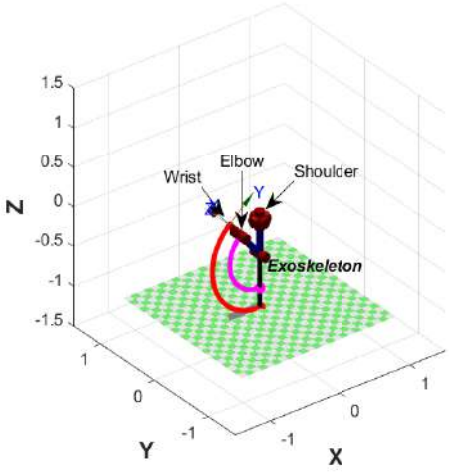

Wrist: Abduction-adduction

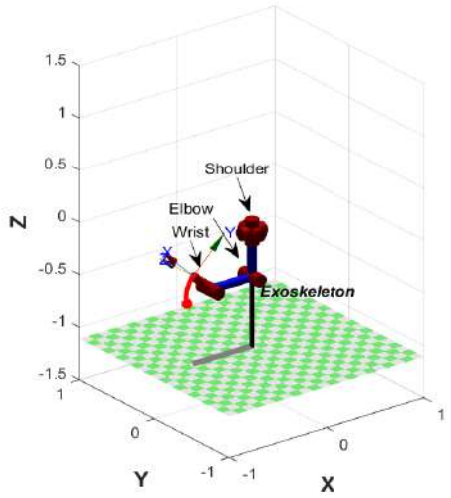

Full and achievable workspace

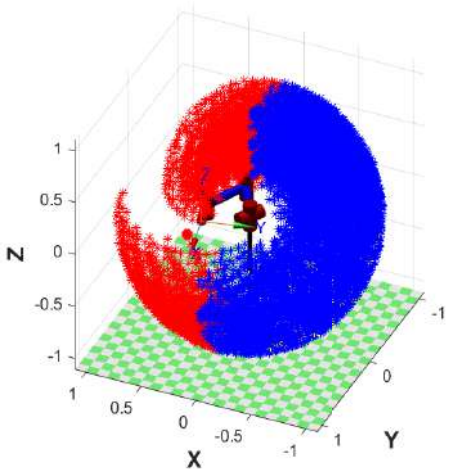

5.1.3 Forward Kinematics

Acquiring the kinematic model of the exoskeleton is crucial for predicting its movement and spatial positioning. This model establishes mathematical relationships linking input variables (joint positions) to output variables (position and orientation of the exoskeleton's end effector).

Once the D-H parameters of the exoskeleton are known (Table 5.1), the homogeneous transformation matrices ${}^{i-1}A_i$ and the matrices ${}^{0}T_i$ are calculated. The results of these matrices are shown below.

$$
{}^{0}\mathrm{A}_1 = \begin{bmatrix} \cos(q_1+\frac{\pi}{2}) & -\cos(\alpha_1)*\sin(q_1+\frac{\pi}{2}) & \sin(\alpha_1)*\sin(q_1+\frac{\pi}{2}) & a_1*\cos(q_1+\frac{\pi}{2}) \\ \sin(q_1+\frac{\pi}{2}) & \cos(\alpha_1)*\cos(q_1+\frac{\pi}{2}) & -\sin(\alpha_1)*\cos(q_1+\frac{\pi}{2}) & a_1*\sin(q_1+\frac{\pi}{2}) \\ 0 & \sin(\alpha_1) & \cos(\alpha_1) & d_1 \\ 0 & 0 & 0 & 1 \end{bmatrix}
$$

$$
{}^{1}\mathrm{A}_2 = \begin{bmatrix} \cos(q_2-\frac{\pi}{2}) & -\cos(\alpha_2)*\sin(q_2-\frac{\pi}{2}) & \sin(\alpha_2)*\sin(q_2-\frac{\pi}{2}) & a_2*\cos(q_2-\frac{\pi}{2}) \\ \sin(q_2-\frac{\pi}{2}) & \cos(\alpha_2)*\cos(q_2-\frac{\pi}{2}) & -\sin(\alpha_2)*\cos(q_2-\frac{\pi}{2}) & a_2*\sin(q_2-\frac{\pi}{2}) \\ 0 & \sin(\alpha_2) & \cos(\alpha_2) & d_2 \\ 0 & 0 & 0 & 1 \end{bmatrix}
$$

$$
{}^{2}\mathrm{A}_3 = \begin{bmatrix} \cos(q_3) & -\cos(\alpha_3)*\sin(q_3) & \sin(\alpha_3)*\sin(q_3) & a_3*\cos(q_3) \\ \sin(q_3) & \cos(\alpha_3)*\cos(q_3) & -\sin(\alpha_3)*\cos(q_3) & a_3*\sin(q_3) \\ 0 & \sin(\alpha_3) & \cos(\alpha_3) & d_3 \\ 0 & 0 & 0 & 1 \end{bmatrix}
$$

$$
{}^{3}\mathrm{A}_{4} = \begin{bmatrix} \cos(q_4) & -\cos(\alpha_4) * \sin(q_4) & \sin(\alpha_4) * \sin(q_4) & a_4 * \cos(q_4) \\ \sin(q_4) & \cos(\alpha_4) * \cos(q_4) & -\sin(\alpha_4) * \cos(q_4) & a_4 * \sin(q_4) \\ 0 & \sin(\alpha_4) & \cos(\alpha_4) & d_4 \\ 0 & 0 & 0 & 1 \end{bmatrix}
$$

$$
{}^{4}\mathrm{A}_{5} = \begin{bmatrix} \cos(q_5) & -\cos(\alpha_5) * \sin(q_5) & \sin(\alpha_5) * \sin(q_5) & a_5 * \cos(q_5) \\ \sin(q_5) & \cos(\alpha_5) * \cos(q_5) & -\sin(\alpha_5) * \cos(q_5) & a_5 * \sin(q_5) \\ 0 & \sin(\alpha_5) & \cos(\alpha_5) & d_5 \\ 0 & 0 & 0 & 1 \end{bmatrix}
$$

The corresponding matrix ${}^{0}T_{5}$ is:

$$
{}^{0}T_{5} = \begin{bmatrix} T_{11} & T_{12} & T_{13} & T_{14} \\ T_{21} & T_{22} & T_{23} & T_{24} \\ T_{31} & T_{32} & T_{33} & T_{34} \\ T_{41} & T_{42} & T_{43} & T_{44} \end{bmatrix}
$$

where:

$$
\begin{aligned}
T_{11} &= cos(q_1)sin(q_3)sin(q_4)sin(q_5) - cos(q_1)cos(q_3)cos(q_5)sin(q_4) - \\
&\quad cos(q_1)cos(q_4)cos(q_5)sin(q_3) - cos(q_1)cos(q_3)cos(q_4)sin(q_5) - \\
&\quad cos(q_3)cos(q_4)cos(q_5)sin(q_1)sin(q_2) + cos(q_3)sin(q_1)sin(q_2)sin(q_4)sin(q_5) + \\
&\quad cos(q_4)sin(q_1)sin(q_2)sin(q_3)sin(q_5) + cos(q_5)sin(q_1)sin(q_2)sin(q_3)sin(q_4) \\
T_{21} &= sin(q_1)sin(q_3)sin(q_4)sin(q_5) - cos(q_3)cos(q_5)sin(q_1)sin(q_4) - \\
&\quad cos(q_4)cos(q_5)sin(q_1)sin(q_3) - cos(q_3)cos(q_4)sin(q_1)sin(q_5) + \\
&\quad cos(q_1)cos(q_3)cos(q_4)cos(q_5)sin(q_2) - cos(q_1)cos(q_3)sin(q_2)sin(q_4)sin(q_5) - \\
&\quad cos(q_1)cos(q_4)sin(q_2)sin(q_3)sin(q_5) - cos(q_1)cos(q_5)sin(q_2)sin(q_3)sin(q_4) \\
T_{31} &= cos(q_2)cos(q_3)sin(q_4)sin(q_5) - cos(q_2)cos(q_3)cos(q_4)cos(q_5) + \\
&\quad cos(q_2)cos(q_4)sin(q_3)sin(q_5) + cos(q_2)cos(q_5)sin(q_3)sin(q_4) \\
T_{41} &= 0 \\
T_{12} &= cos(q_1)cos(q_3)sin(q_4)sin(q_5) - cos(q_1)cos(q_3)cos(q_4)cos(q_5) + \\
&\quad cos(q_1)cos(q_4)sin(q_3)sin(q_5) + cos(q_1)cos(q_5)sin(q_3)sin(q_4) + \\
&\quad cos(q_3)cos(q_4)sin(q_1)sin(q_2)sin(q_5) + cos(q_3)cos(q_5)sin(q_1)sin(q_2)sin(q_4) + \\
&\quad cos(q_4)cos(q_5)sin(q_1)sin(q_2)sin(q_3) - sin(q_1)sin(q_2)sin(q_3)sin(q_4)sin(q_5) \\
T_{22} &= cos(q_3)sin(q_1)sin(q_4)sin(q_5) - cos(q_3)cos(q_4)cos(q_5)sin(q_1) + \\
&\quad cos(q_4)sin(q_1)sin(q_3)sin(q_5) + cos(q_5)sin(q_1)sin(q_3)sin(q_4) - \\
&\quad cos(q_1)cos(q_3)cos(q_4)sin(q_2)sin(q_5) - cos(q_1)cos(q_3)cos(q_5)sin(q_2)sin(q_4) - \\
&\quad cos(q_1)cos(q_4)cos(q_5)sin(q_2)sin(q_3) + cos(q_1)sin(q_2)sin(q_3)sin(q_4)sin(q_5) \\
T_{32} &= cos(q_2)cos(q_3)cos(q_4)sin(q_5) + cos(q_2)cos(q_3)cos(q_5)sin(q_4) +
\end{aligned}
$$

$$
\begin{aligned}
& cos(q_2)cos(q_4)cos(q_5)sin(q_3) - cos(q_2)sin(q_3)sin(q_4)sin(q_5) \\
T_{42} &= 0 \\
T_{13} &= -cos(q_2)sin(q_1) \\
T_{23} &= cos(q_1)cos(q_2) \\
T_{33} &= sin(q_2) \\
T_{43} &= 0 \\
T_{14} &= a_5cos(q_1)sin(q_3)sin(q_4)sin(q_5) - a_4cos(q_1)cos(q_3)sin(q_4) - \\
& a_4cos(q_1)cos(q_4)sin(q_3) - a_3cos(q_3)sin(q_1)sin(q_2) - \\
& a_5cos(q_1)cos(q_3)cos(q_4)sin(q_5) - a_5cos(q_1)cos(q_3)cos(q_5)sin(q_4) - \\
& a_5cos(q_1)cos(q_4)cos(q_5)sin(q_3) - a_4cos(q_3)cos(q_4)sin(q_1)sin(q_2) - \\
& a_3cos(q_1)sin(q_3) + a_4sin(q_1)sin(q_2)sin(q_3)sin(q_4) - \\
& a_5cos(q_3)cos(q_4)cos(q_5)sin(q_1)sin(q_2) + a_5cos(q_3)sin(q_1)sin(q_2)sin(q_4)sin(q_5) + \\
& a_5cos(q_4)sin(q_1)sin(q_2)sin(q_3)sin(q_5) + a_5cos(q_5)sin(q_1)sin(q_2)sin(q_3)sin(q_4) \\
T_{24} &= a_3cos(q_1)cos(q_3)sin(q_2) - a_3sin(q_1)sin(q_3) - a_4cos(q_3)sin(q_1)sin(q_4) - \\
& a_4cos(q_4)sin(q_1)sin(q_3) + a_4cos(q_1)cos(q_3)cos(q_4)sin(q_2) - \\
& a_5cos(q_3)cos(q_4)sin(q_1)sin(q_5) - a_5cos(q_3)cos(q_5)sin(q_1)sin(q_4) - \\
& a_5cos(q_4)cos(q_5)sin(q_1)sin(q_3) - a_4cos(q_1)sin(q_2)sin(q_3)sin(q_4) + \\
& a_5sin(q_1)sin(q_3)sin(q_4)sin(q_5) + a_5cos(q_1)cos(q_3)cos(q_4)cos(q_5)sin(q_2) - \\
& a_5cos(q_1)cos(q_3)sin(q_2)sin(q_4)sin(q_5) - a_5cos(q_1)cos(q_4)sin(q_2)sin(q_3)sin(q_5) - \\
& a_5cos(q_1)cos(q_5)sin(q_2)sin(q_3)sin(q_4) \\
T_{34} &= a_4cos(q_2)sin(q_3)sin(q_4) - a_4cos(q_2)cos(q_3)cos(q_4) - a_3cos(q_2)cos(q_3) - \\
& a_5cos(q_2)cos(q_3)cos(q_4)cos(q_5) + a_5cos(q_2)cos(q_3)sin(q_4)sin(q_5) + \\
& a_5cos(q_2)cos(q_4)sin(q_3)sin(q_5) + a_5cos(q_2)cos(q_5)sin(q_3)sin(q_4) \\
T_{44} &= 1
\end{aligned}
$$

The matrix T_0^5 presents the kinematic equations that relate the base system to the end of the robot in terms of the joint coordinates. The first 9 elements of this matrix contain the orientation of the end-effector, and the first 3 elements of the fourth column contain the position (x,y,z) of the end-effector.

5.1.4 Inverse Kinematics

Determining the inverse kinematics relies on the kinematic model derived in the preceding section and involves determining the values of the joint variables q_1, q_2, q_3, q_4 and q_5 of the exoskeleton. First, the position of the wrist will be considered as the final position, and using the transformation matrix ${}^0T_4$ (Equation (5.1)), the value of q_4 was found.

$$ {}^{0}T_4 = \begin{bmatrix} N_{w_x} & O_{w_x} & A_{w_x} & P_{w_x} \\ N_{w_y} & O_{w_y} & A_{w_y} & P_{w_y} \\ N_{w_z} & O_{w_z} & A_{w_z} & P_{w_z} \\ 0 & 0 & 0 & 1 \end{bmatrix} \tag{5.1} $$

In this case, the method indicated in (Tolani and Badler, 1996) was used, where the position of the wrist $[P_{w_x}, P_{w_y}, P_{w_z}]$ is considered fixed in space, the elbow joint rotates around a defined axis from wrist to shoulder, and the shoulder positions are defined (s in [0,0,0]), elbow (e) and wrist (w). Solving analytically, q_4 is shown in Equation (5.2).

$$ q_4 = \pi - arccos\left(\frac{||w-s||^2 - d_e^2 - d_w^2}{-2 * d_e * d_w}\right) \tag{5.2} $$

where d_e and d_w are the maximum lengths of the arm and forearm, respectively.

The values of q_2 (Equation (5.3)), q_1 (Equation (5.4)) and q_3 (Equation (5.5)) were obtained by considering the position of the elbow as a function of them, as follows:

$$ {}^{0}T_3 = \begin{bmatrix} se_x & n_{2x} & n_{1x} & e_x \\ se_y & n_{2y} & n_{1y} & e_y \\ se_z & n_{2z} & n_{1z} & e_z \\ 0 & 0 & 0 & 1 \end{bmatrix} $$

where:

$$ se = \left(\frac{e-s}{||e-s||}\right), \qquad ew = \left(\frac{w-e}{||w-e||}\right), \qquad n_1 = se \times ew, \qquad n_2 = n_1 \times \ se $$

The result is:

$$ q_2 = arctan\left(\frac{n_{1z}}{\sqrt{n_{1x}^2 + n_{1y}^2}}\right) \tag{5.3} $$

$$ q_1 = arctan\left(\frac{-n_{1x}}{n_{1y}}\right) \tag{5.4} $$

$$ q_3 = arctan\left(\frac{e_y cos(q_1) sin(q_2) - e_z sin(q_1) sin(q_2)}{-e_x cos(q_1) - e_y sin(q_1)}\right) \tag{5.5} $$

Finally, we consider: $({}^4T_5)^{-1}T =^0 A_1^1 A_2^2 A_3^3 A_4$, where $({}^4A_5)^{-1}$ is the inverse matrix of the matrix ${}^4A_5$ and $T_w =^0 A_1^1 A_2^2 A_3^3 A_4$, to find q_5 (Equation (5.6))

$$q_5 = arcsin\left(\frac{p_y T_{w_{14}} - p_x T_{w_{24}} + p_y a_5}{p_x^2 + p_y^2}\right) \tag{5.6}$$

where p_x, p_y and p_z are the known palm positions at x, y and z, respectively.

The results derived from this model enable the acquisition of joint variable values utilized to track predefined trajectories.

5.1.5 Jacobian

To understand the relationship between joint velocities and those of the robot's end-effector, the Jacobian matrix representing its differential model is computed. A crucial aspect of this matrix is its determinant (the Jacobian), as it allows for the identification of singular configurations of the robot when the Jacobian is zero.

Highlighting two types of Jacobian matrices: the forward, which allows for calculating the velocities of the robot's end-effector from joint velocities, and the inverse, which enables determining the joint velocities necessary to achieve the velocities of the end-effector.

Direct Jacobian Matrix

This involves differentiating with respect to time the equations of the direct kinematic model (${}^0T_5$), resulting in the following matrix expression:

$$\begin{pmatrix} \dot{x} \\ \dot{y} \\ \dot{z} \\ w_x \\ w_y \\ w_z \end{pmatrix} = J \begin{pmatrix} \dot{q_1} \\ \dot{q_2} \\ \dot{q_3} \\ \dot{q_4} \\ \dot{q_5} \end{pmatrix}$$

where:

$\dot{x}$, $\dot{y}$, $\dot{z}$ They are the components of the linear velocity of the end effector along the x, y and z axes, respectively.

w_x, w_y, w_z They are the components of the angular velocity of the end effector along the x, y and z axes, respectively.

In this case, all joints of the exoskeleton are simple revolute, so to calculate the x, y and z components of the linear and angular velocity, the information provided in Table 5.3 is used.

Table 5.3: Linear and angular velocity for prismatic and revolute joints.

Velocity	Prismatic	Revolute
Linear	$R_{i-1}^0 \begin{bmatrix} 0 \\ 0 \\ 1 \end{bmatrix}$	$R_{i-1}^0 \begin{bmatrix} 0 \\ 0 \\ 1 \end{bmatrix} \times \left(d_n^0 - d_{i-1}^0\right)$
Angular	$\begin{bmatrix} 0 \\ 0 \\ 0 \end{bmatrix}$	$R_{i-1}^0 \begin{bmatrix} 0 \\ 0 \\ 1 \end{bmatrix}$

where:

$$J = \begin{bmatrix} R_0^0 \begin{bmatrix} 0 \\ 0 \\ 1 \end{bmatrix} \times \left(d_5^0 - d_0^0\right) & R_1^0 \begin{bmatrix} 0 \\ 0 \\ 1 \end{bmatrix} \times \left(d_5^0 - d_1^0\right) & \cdots & R_4^0 \begin{bmatrix} 0 \\ 0 \\ 1 \end{bmatrix} \times \left(d_5^0 - d_4^0\right) \\ R_0^0 \begin{bmatrix} 0 \\ 0 \\ 1 \end{bmatrix} & R_1^0 \begin{bmatrix} 0 \\ 0 \\ 1 \end{bmatrix} & \cdots & R_4^0 \begin{bmatrix} 0 \\ 0 \\ 1 \end{bmatrix} \end{bmatrix}$$

$$J = \begin{bmatrix} J_{11} & J_{12} & J_{13} & J_{14} & J_{15} \\ J_{21} & J_{22} & J_{23} & J_{24} & J_{25} \\ J_{31} & J_{32} & J_{33} & J_{34} & J_{35} \\ J_{41} & J_{42} & J_{43} & J_{44} & J_{45} \\ J_{51} & J_{52} & J_{53} & J_{54} & J_{55} \\ J_{61} & J_{62} & J_{63} & J_{64} & J_{65} \end{bmatrix}$$

The coefficients of the resulting Jacobian matrix (J) are shown in Annex .2.

As can be observed, the matrix J is not square, so it is not possible to calculate its determinant (Jacobian). This is because the number of degrees of freedom is less than that of the task space. Therefore, the robot's movement presents certain restrictions, which will be analyzed in the following section.

Inverse Jacobian Matrix

This matrix facilitates the calculation of the joint velocities required to achieve a specific movement of the robot's end effector. Additionally, it helps identify singular configurations of the mechanism, which are common in manipulator robots (such as exoskeletons) and occur when the Jacobian matrix becomes singular.

There are two types of singularities: 1) those found at the boundary of the workspace (present in all manipulators) and 2) those occurring within the workspace, resulting from the alignment of two or more joint axes. When a manipulator is in a singular configuration, it loses one or more degrees of freedom, meaning that, from the Cartesian space perspective, there are certain directions (or subspaces) where it is impossible to move the robot's hand, regardless of the selected joint configurations.

In this case, the resulting direct Jacobian matrix is non-square, which prevents the calculation of the Jacobian inverse. Therefore, assessing the manipulability of the exoskeleton

will be done by calculating the manipulability index (Moreno et al., 2012), as shown in equation 5.7. This performance index quantifies a robot's ability to generate velocities at its end effector and is proportional to the volume of the velocity ellipsoid.

$$w = \sqrt{det(JJ^T)} \tag{5.7}$$

In general terms, the exoskeleton will be in a singular configuration when it is completely straight down (that is, when all joint values are equal to zero), and the axes of rotation of the joints are aligned with each other. It should be noted that control algorithms based on joint space do not require a Jacobian matrix or its inverse; therefore, singularities do not pose a significant problem in this case. However, control approaches based on Cartesian coordinates do require the Jacobian or Jacobian inverse matrices, so it is necessary to adequately consider singularities.

5.2 Control Architecture

According to the objective of the application, the implemented controller must follow the trajectories applied in physical rehabilitation (defined by the specialist doctor). The dynamic model of the exoskeleton in the joint space and a PD controller (minimizes steady-state error and ascent time) were implemented; are shown in the equations (7.1) and (5.9).

$$M(q)\ddot{q} + C(q,\dot{q})\dot{q} + G(q) = \tau + \tau_u \tag{5.8}$$

$$K_p e(t) + K_d \dot{e}(t) = \tau \tag{5.9}$$

where: $q \in \mathbb{R}^{n\times 1}$ containing the joint angular position, $\dot{q} \in \mathbb{R}^{n\times 1}$ vector containing the joint angular velocity, $\ddot{q} \in \mathbb{R}^{n\times 1}$ vector containing the joint angular acceleration, M(q) $\in \mathbb{R}^{n\times n}$ is the inertial matrix, $C(q,\dot{q}) \in \mathbb{R}^{n\times n}$ is centrifugal and Coriolis terms, G(q) $\in \mathbb{R}^{n\times 1}$ is gravitational forces, $\tau \in \mathbb{R}^{n\times 1}$ denotes the generalized torque vector, $\tau_u \in \mathbb{R}^{n\times 1}$ is the vector of unknown disturbing forces, $e \in \mathbb{R}^{n\times 1}$ is is the tracking error calculated by $e = q_d - q$, where q_d is the desired trajectory and q is the measured trajectory and $\dot{e} \in \mathbb{R}^{n\times 1}$ is the tracking error in velocity, with $n = 5$ as the number of joints (M, C and G are shown in detail in Annex .3).

The exoskeleton is considered a support tool for rehabilitation medical staff, facilitating passive therapy for patients with mobility issues in the right upper limb. In this context, and based on the kinematic control shown in Figure 3.11, it is initially necessary to generate the trajectories that the exoskeleton should follow. Table 5.4 presents some of the main trajectories used in physical rehabilitation, classified into two groups: 1) simple movements and 2) complex movements, allowing for third and fifth-order trajectories in both cases.

Table 5.4: Physical Rehabilitation Trajectories.

Movement	Equations in Cartesian Space [m]
Simple Movements	
Shoulder Internal-External Rotation	$x = 0.48\cos(p)$ $y = 0.48\sin(p)$ $z = 0$
Shoulder abduction-adduction	$x = 0$ $y = 0.79\sin(p)$ $z = -0.79\cos(p)$
Shoulder flexion-extension	$x = -0.91\sin(p)$ $y = 0$ $z = -0.91\cos(p)$
Elbow flexion-extension	$x = -0.48\sin(p)$ $y = 0$ $z = -0.48\cos(p)$
Wrist abduction-adduction	$x = -0.05\sin(p)$ $y = 0$ $z = -0.05\cos(p)$
Complex Movements	
Diagonal	$x = -45.00p$ $y = -0.26p$ $z = -0.53 + 0.53p$
Half Circle and Circle	$x = r\cos(p)$ $y = r\sin(p)$ $z = 0$
Infinity	$x = -0.50r\cos(p)$ $y = r(\frac{\sin(2p)}{2})$ $z = 0$

where: r represents the radius of the circle to be constructed, while p denotes the coefficients of a third or fifth-order polynomial, depending on the specification provided by the medical staff.

Figure 5.2 shows the control scheme used in the simulation to validate the trajectories listed in Table 5.4. Below, this scheme is described:

- Input data: the movement to be performed (taking into account the workspace of the exoskeleton), the final position (assuming the initial position is zero), the desired time to reach the final position, and the order of the trajectory (third or fifth).
- Trajectory generator: It employs inverse kinematics to determine the desired joint trajectories ($q_{di}(t)$), which are considered as inputs for the dynamic control.
- Dynamic control: It employs a proportional-derivative controller for each joint, with the following gains: kp=[30 300 300 300 300 1.2] and kd=[5 40 40 40 0.15]. This controller takes as inputs $q_{di}(t)$ (obtained from the trajectory generator) and $q_{sim}(t)$ (obtained from

the virtual DTP of the exoskeleton, which considers the detailed mechanical properties in Annex .3).

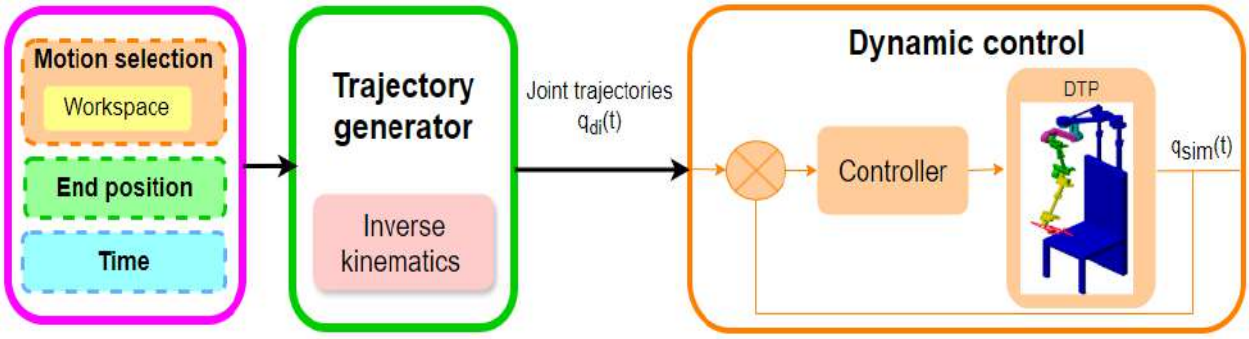

Figure 5.2: Control scheme for path tracking (utilizing the exoskeleton's DTP).

Several movements listed in Table 5.4 were performed, using different sets of input data covering both third and fifth-order polynomials. Table 5.5 displays the corresponding joint RMSEs for each of these movements implemented with third-order polynomials. Additionally, Table 5.6 provides the maximum joint torques obtained for those same movements. Figures 5.3-5.9 present the joint tracking, tracking error, and torques obtained in the simulation of each movement.

Table 5.5: RMSE: 3rd-order trajectory tracking

Movement	Trajectory features	$q_1[rad]$	$q_2[rad]$	$q_3[rad]$	$q_4[rad]$	$q_5[rad]$	Mean
S-IER	From ≈0 to 30° in 3 s	0.003	0.005	0.013	0.191	0.008	0.044
S-AA	From ≈0 to 90° in 5 s	0.005	0.004	0.020	0.005	0.006	0.008
S-FE	From ≈0 to 90° in 10 s	0.002	0.003	0.022	0.005	0.006	0.008
E-FE	From ≈0 to 120° in 5 s	0.003	0.004	0.006	0.004	0.006	0.005
Diagonal	From [-0.029,-0.005,-0.853] to [0.639, -0.408, 0.013] in 10 s	0.002	0.004	0.019	0.005	0.006	0.007
Circle	r=0.3m, in 4 s	0.005	0.005	0.017	0.040	0.011	0.016
Infinity	r=0.25m, in 4 s	0.006	0.005	0.001	0.004	0.007	0.005
Mean		0.003	0.004	0.014	0.036	0.007	0.013

Table 5.6: Maximum torques: 3rd-order trajectory tracking

Movement	$q_1[Nm]$	$q_2[Nm]$	$q_3[Nm]$	$q_4[Nm]$	$q_5[Nm]$
S-IER	0.999	9.773	18.000	18.000	0.199
S-AA	1.236	2.718	11.421	3.141	0.018
S-FE	1.396	1.690	12.458	3.644	0.018
E-FE	1.389	1.690	3.642	3.695	0.017
Diagonal	1.448	1.707	11.384	6.923	0.019
Circle	1.026	2.180	18.000	18.00	0.202
Infinity	1.141	1.994	0.956	3.142	0.013

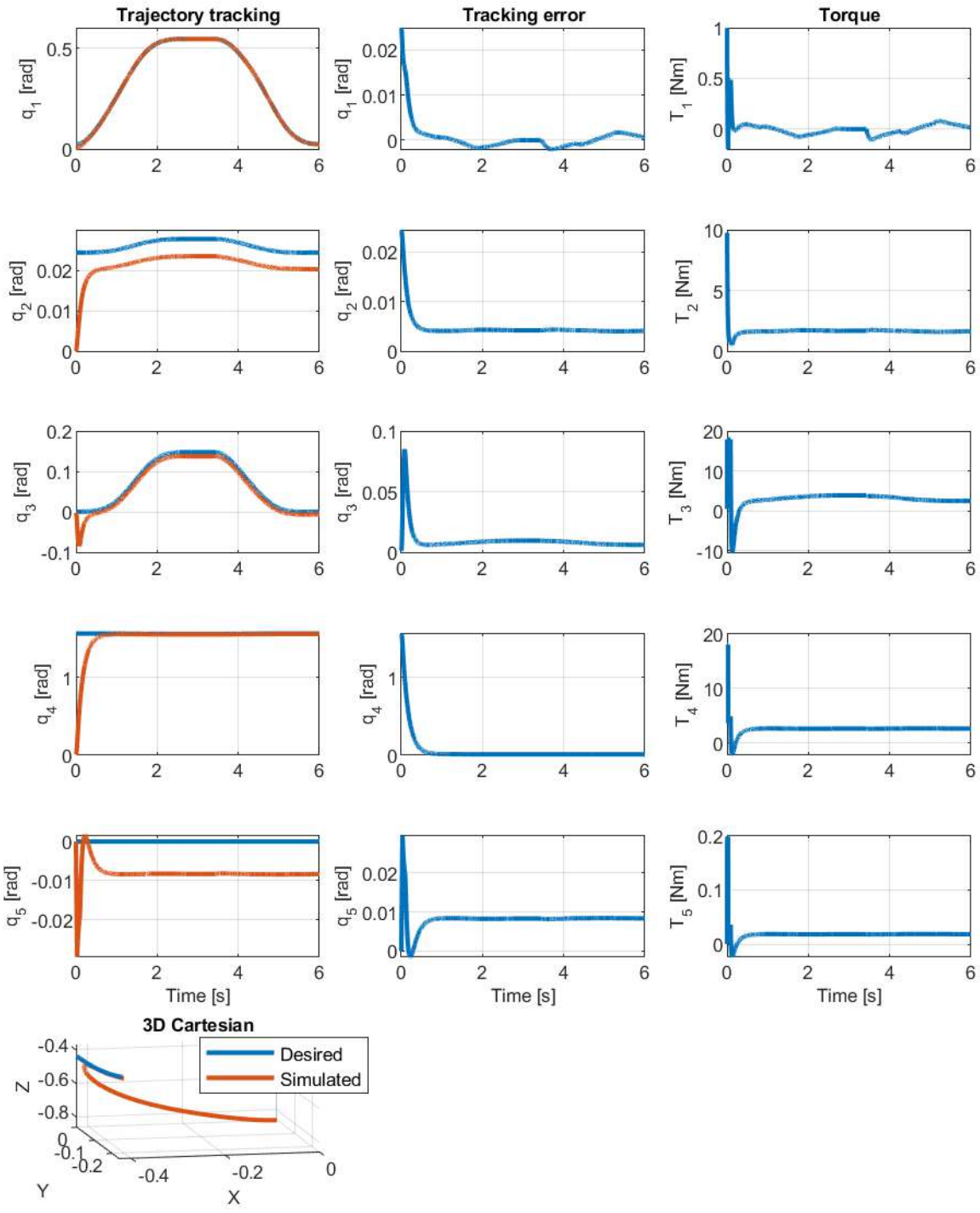

Figure 5.3: S-IER movement: DTP performance in simulation using a 3rd-order trajectory (desired trajectory (blue color) and simulated trajectory (orange color)).

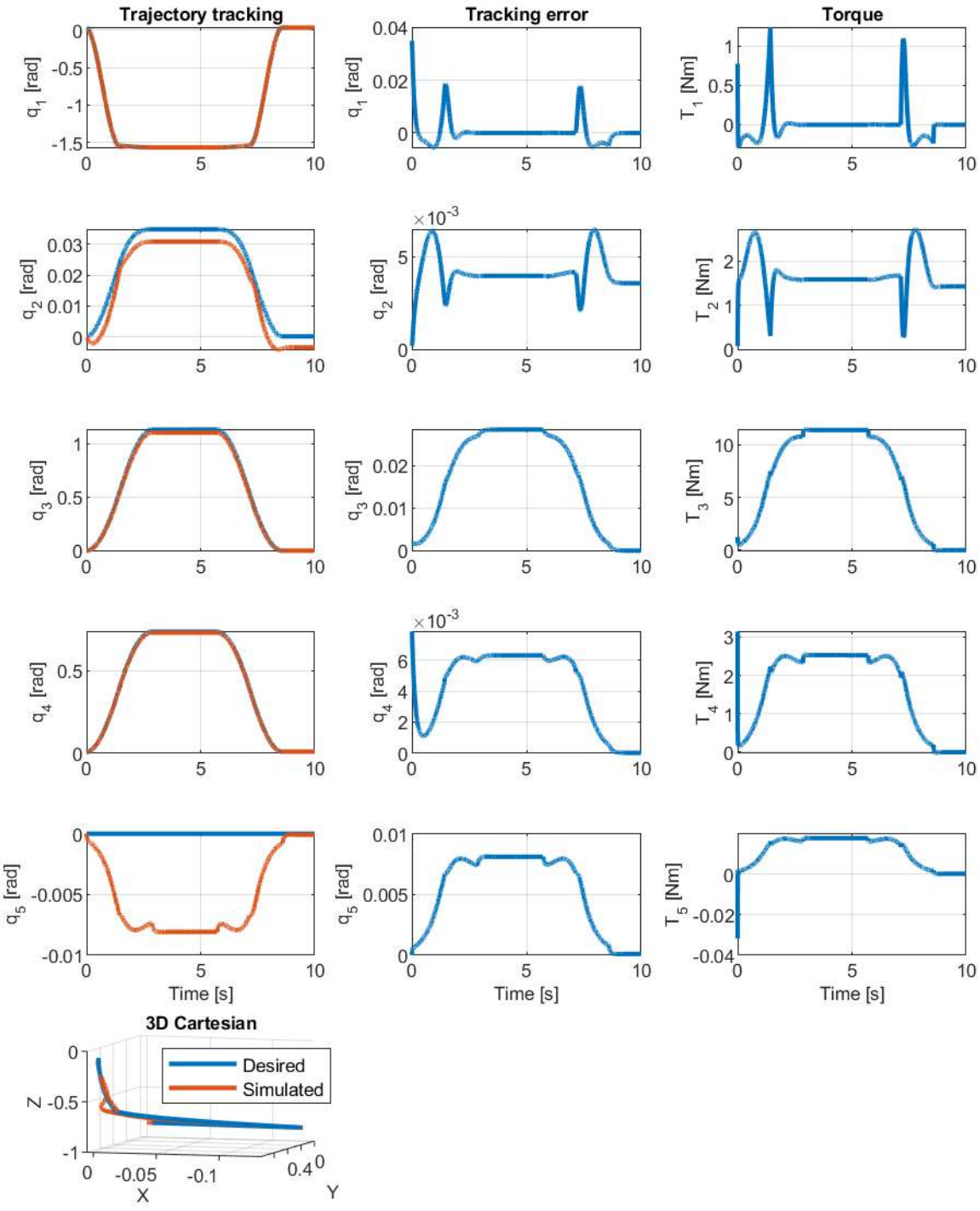

Figure 5.4: S-AA movement: DTP performance in simulation using a 3rd-order trajectory (desired trajectory (blue color) and simulated trajectory (orange color)).

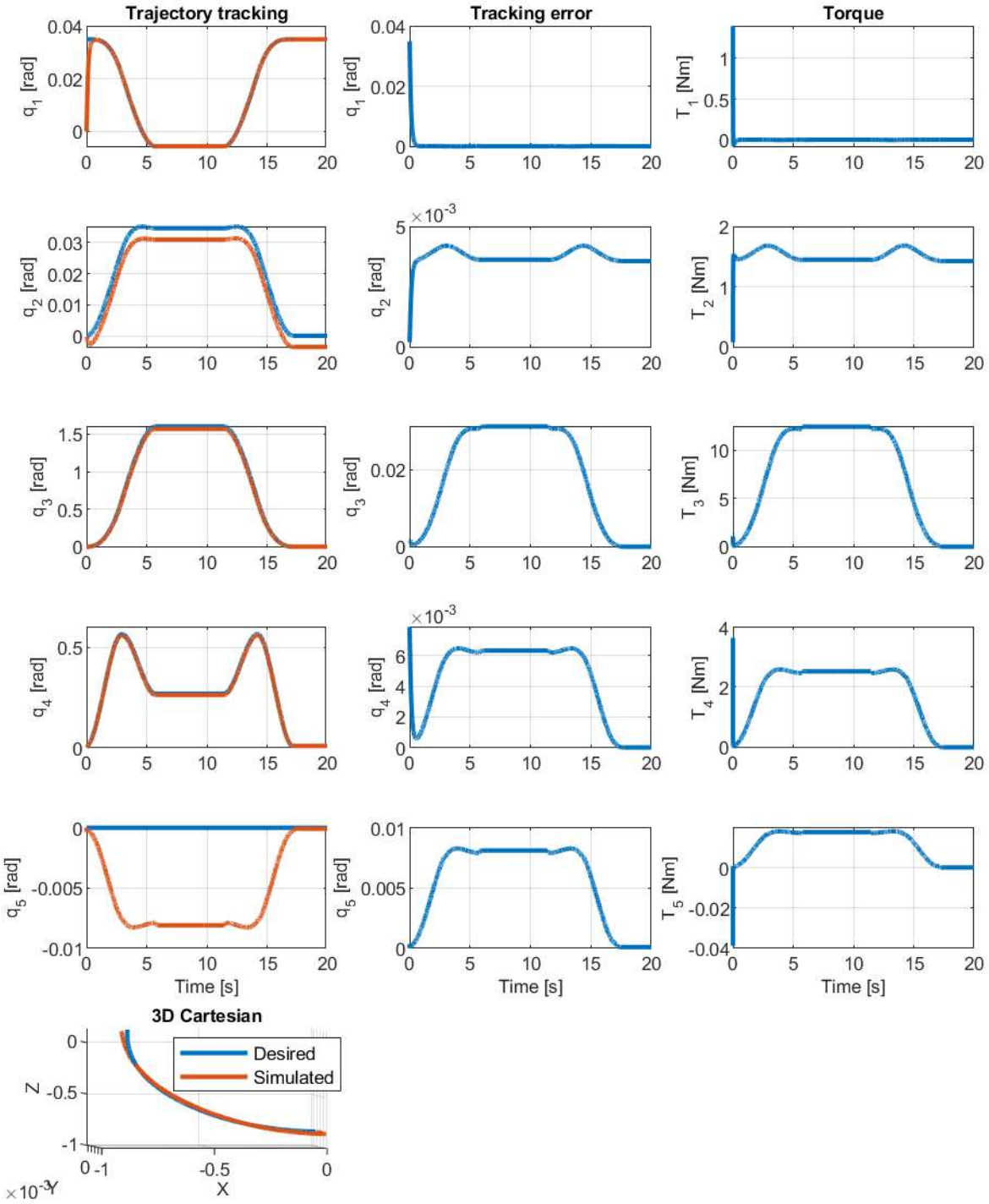

Figure 5.5: S-FE movement: DTP performance in simulation using a 3rd-order trajectory (desired trajectory (blue color) and simulated trajectory (orange color)).

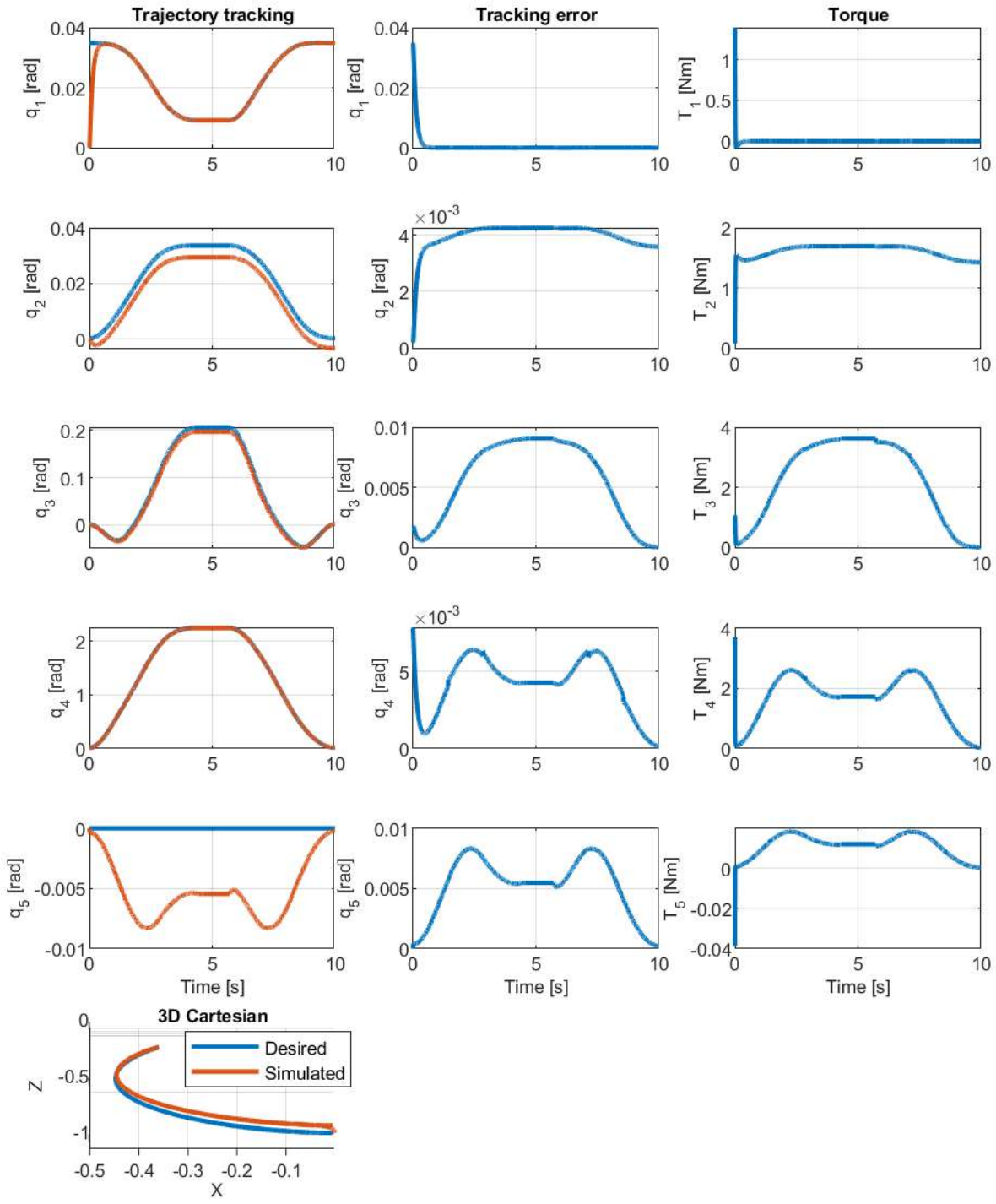

Figure 5.6: E-FE movement: DTP performance in simulation using a 3rd-order trajectory (desired trajectory (blue color) and simulated trajectory (orange color)).

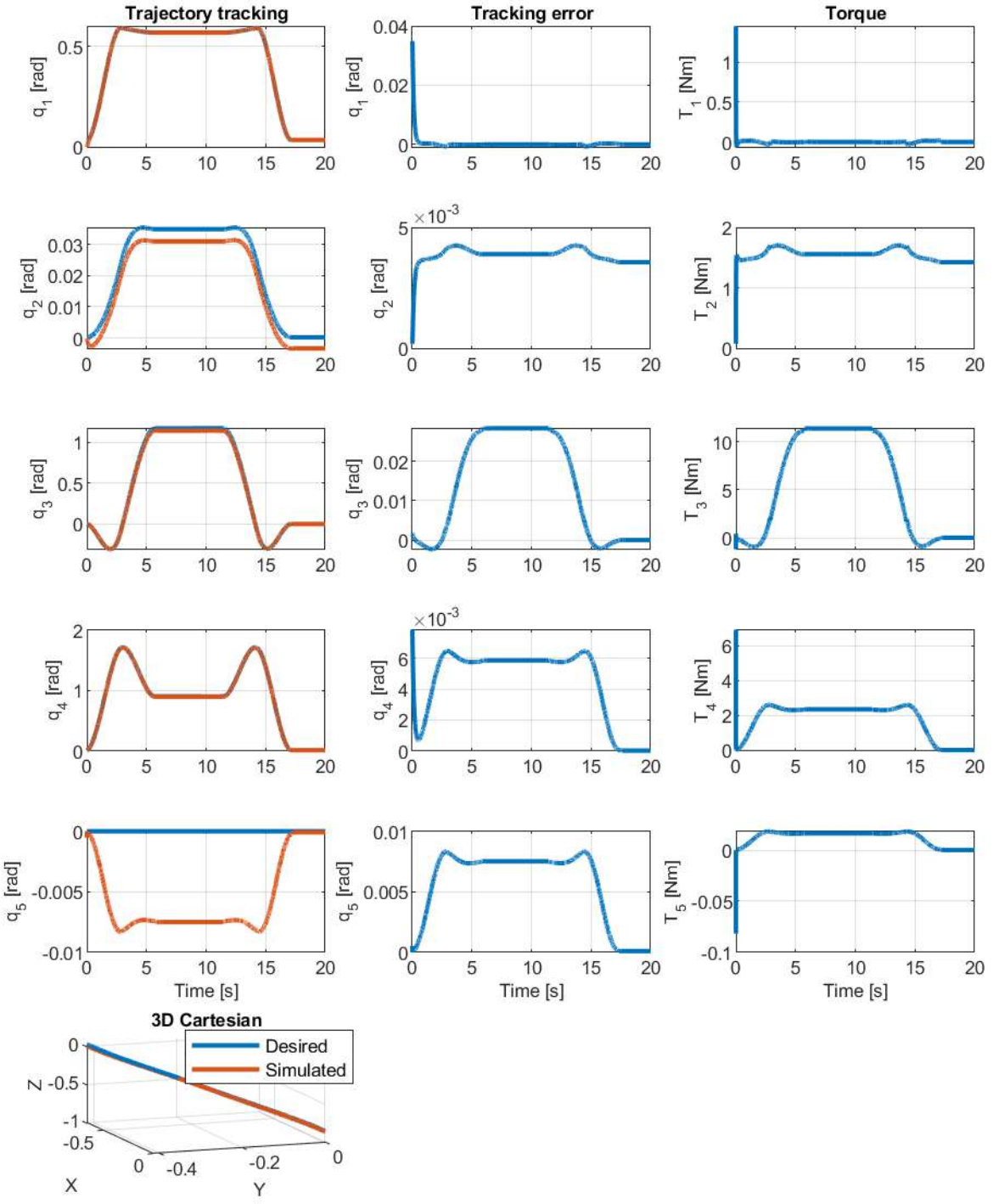

Figure 5.7: Diagonal movement: DTP performance in simulation using a 3rd-order trajectory (desired trajectory (blue color) and simulated trajectory (orange color)).

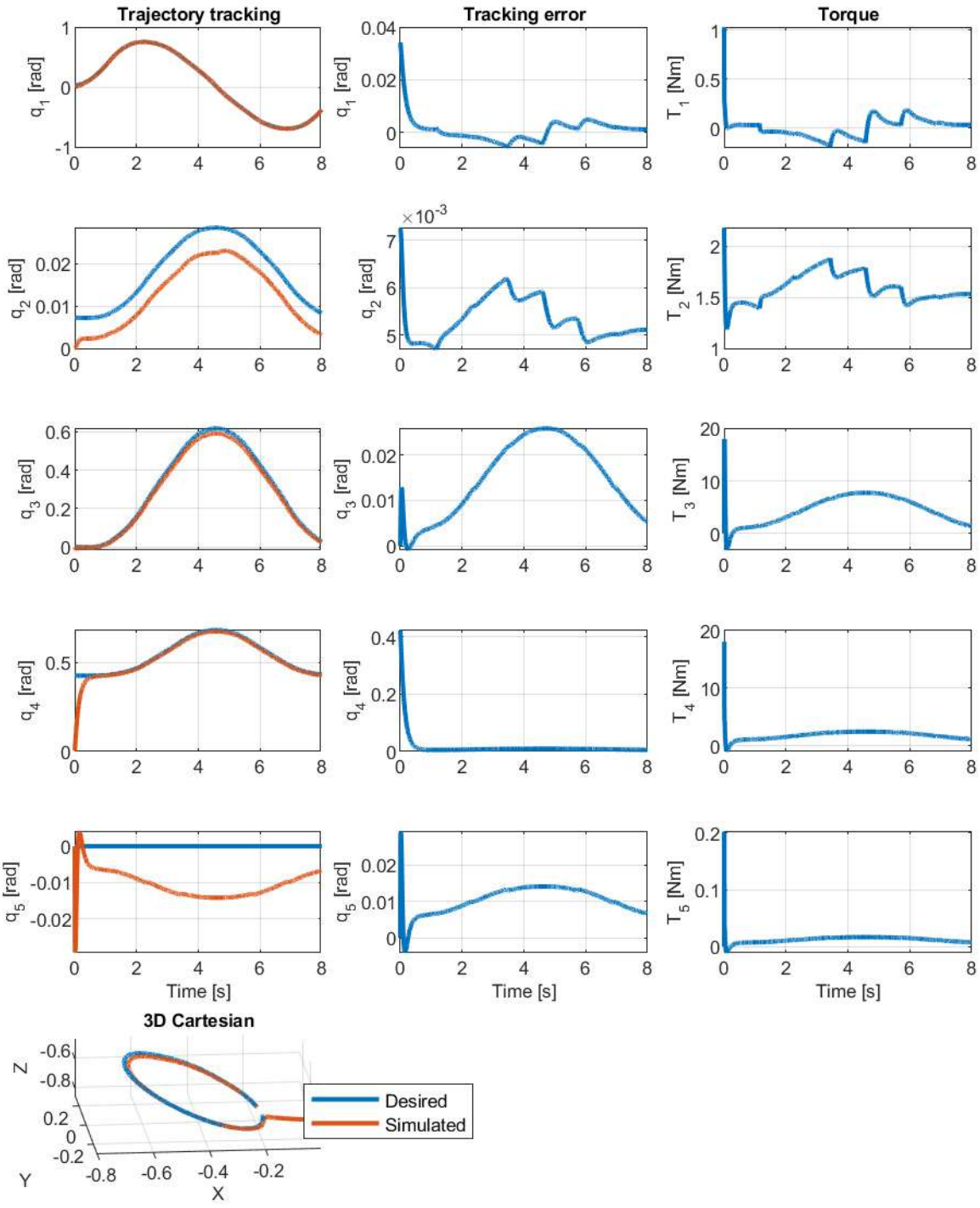

Figure 5.8: Circle movement: DTP performance in simulation using a 3rd-order trajectory (desired trajectory (blue color) and simulated trajectory (orange color)).

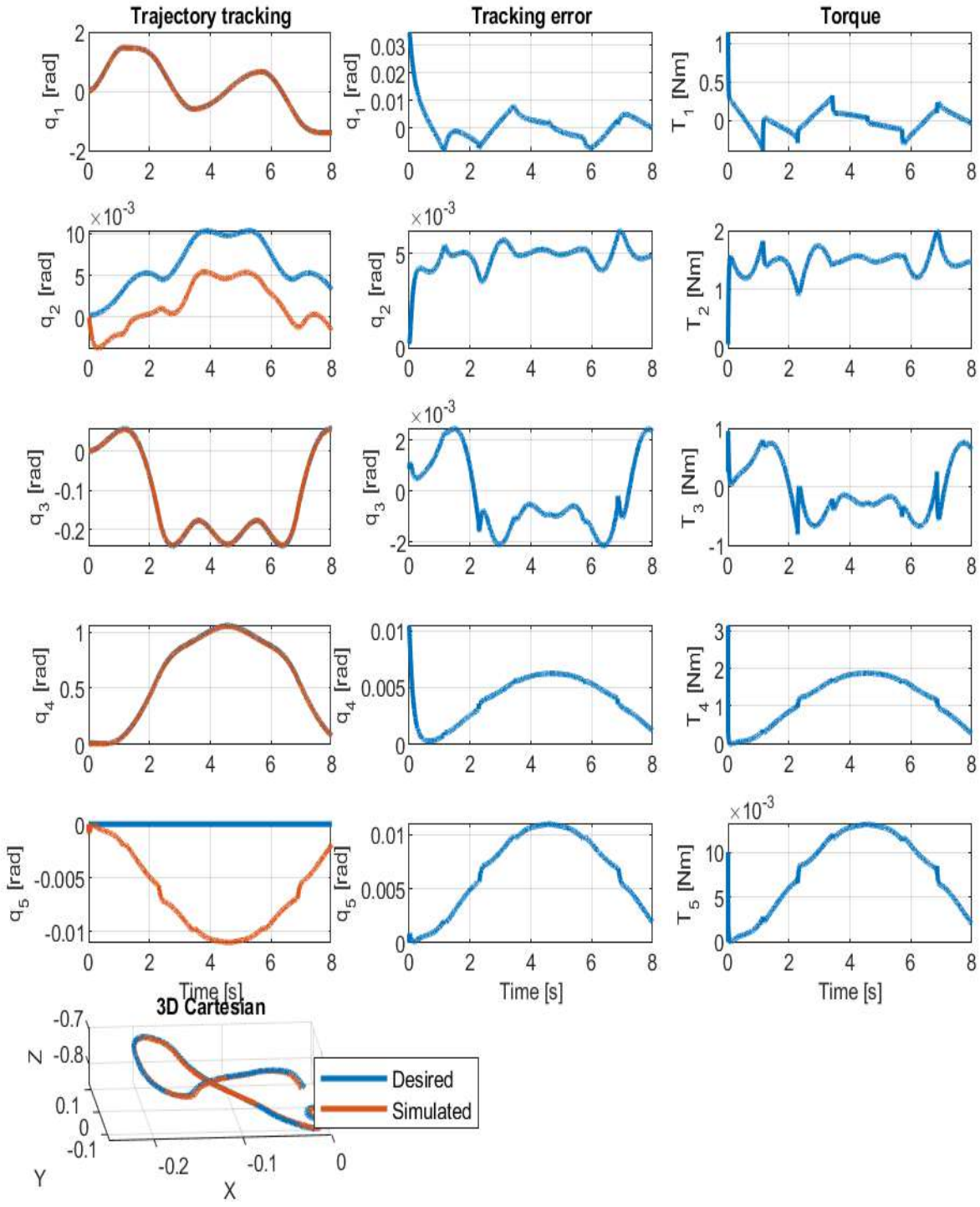

Figure 5.9: Infinity movement: DTP performance in simulation using a 3rd-order trajectory (desired trajectory (blue color) and simulated trajectory (orange color)).

Table 5.7 displays the corresponding joint RMSEs for each of these movements implemented with fifth-order polynomials. Additionally, Table 5.8 provides the maximum joint torques obtained for those same movements. Figures 5.10-5.16 present the joint tracking, tracking error, and torques obtained in the simulation of each movement.

Table 5.7: RMSE: 5th-order trajectory tracking

Movement	Trajectory features	$q_1[rad]$	$q_2[rad]$	$q_3[rad]$	$q_4[rad]$	$q_5[rad]$	Mean
S-IER	From ≈0 to 30° in 3 s	0.004	0.006	0.016	0.184	0.016	0.045
S-AA	From ≈0 to 90° in 5 s	0.005	0.006	0.027	0.006	0.011	0.011
S-FE	From ≈0 to 90° in 10 s	0.002	0.005	0.030	0.007	0.011	0.011
E-FE	From ≈0 to 120° in 5 s	0.003	0.005	0.009	0.006	0.010	0.007
Diagonal	From [-0.029,-0.005,-0.853] to [0.639, -0.408, 0.013] in 10 s	0.002	0.005	0.025	0.007	0.012	0.010
Circle	r=0.30m, in 4 s	0.005	0.005	0.015	0.040	0.010	0.015
Infinity	r=0.25m in 4 s	0.006	0.005	0.001	0.004	0.007	0.005
Mean		0.004	0.005	0.017	0.036	0.011	0.015

Table 5.8: Maximum torques: 5th-order trajectory tracking

Movement	$q_1[Nm]$	$q_2[Nm]$	$q_3[Nm]$	$q_4[Nm]$	$q_5[Nm]$
S-IER	0.745	7.330	18.000	18.000	0.203
S-AA	1.162	2.662	11.391	2.546	0.018
S-FE	1.047	1.685	12.467	2.573	0.018
E-FE	1.047	1.688	3.629	2.586	0.018
Diagonal	1.047	1.698	11.359	2.664	0.019
Circle	1.024	2.180	18.000	18.000	0.202
Infinity	1.047	1.965	0.940	3.142	0.013

The movements with the lowest mean RMSE, whether using third or fifth-order polynomials, are elbow flexion-extension and infinity, while shoulder internal-external rotation exhibits the highest error. Joint q_1 has the lowest mean RMSE, while joint q_4 shows the highest error. Regarding maximum torques, these are higher when using third-order polynomials compared to fifth-order ones, which aligns with expectations due to the order of implemented trajectories. Additionally, the joints $q_3(t)$ and $q_4(t)$ exhibit the highest maximum torques. Generally, these maximum torques are reached at the beginning of the trajectories, decreasing thereafter.

In general, mean RMSE of all performed movements was 0.015 radians, which is considered acceptable for the application. It is important to note that these simulations only take into account the behavior of the exoskeleton, meaning they exclude the effect of forces generated by patients during movement execution.

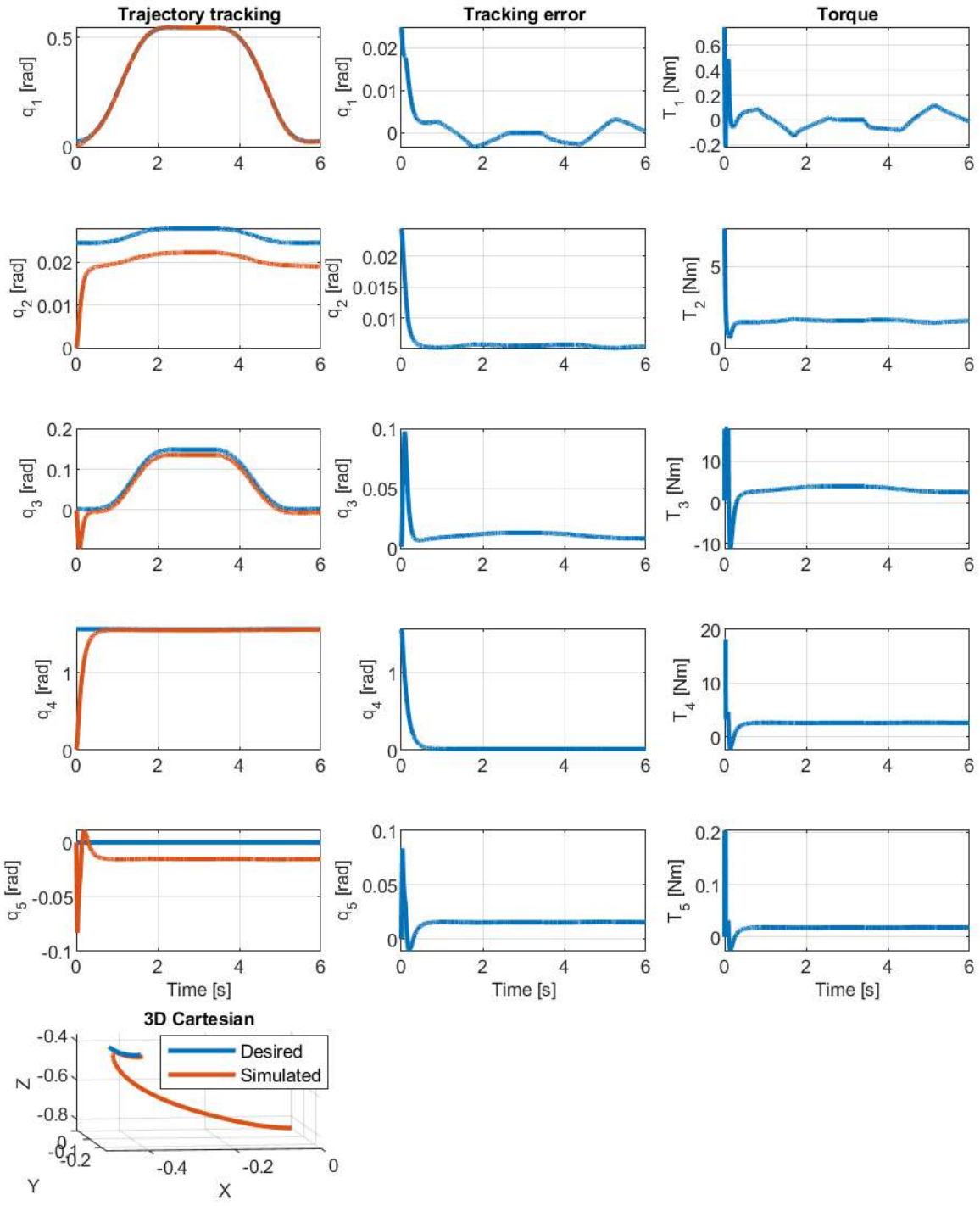

Figure 5.10: S-IER movement: DTP performance in simulation using a 5th-order trajectory (desired trajectory (blue color) and simulated trajectory (orange color)).

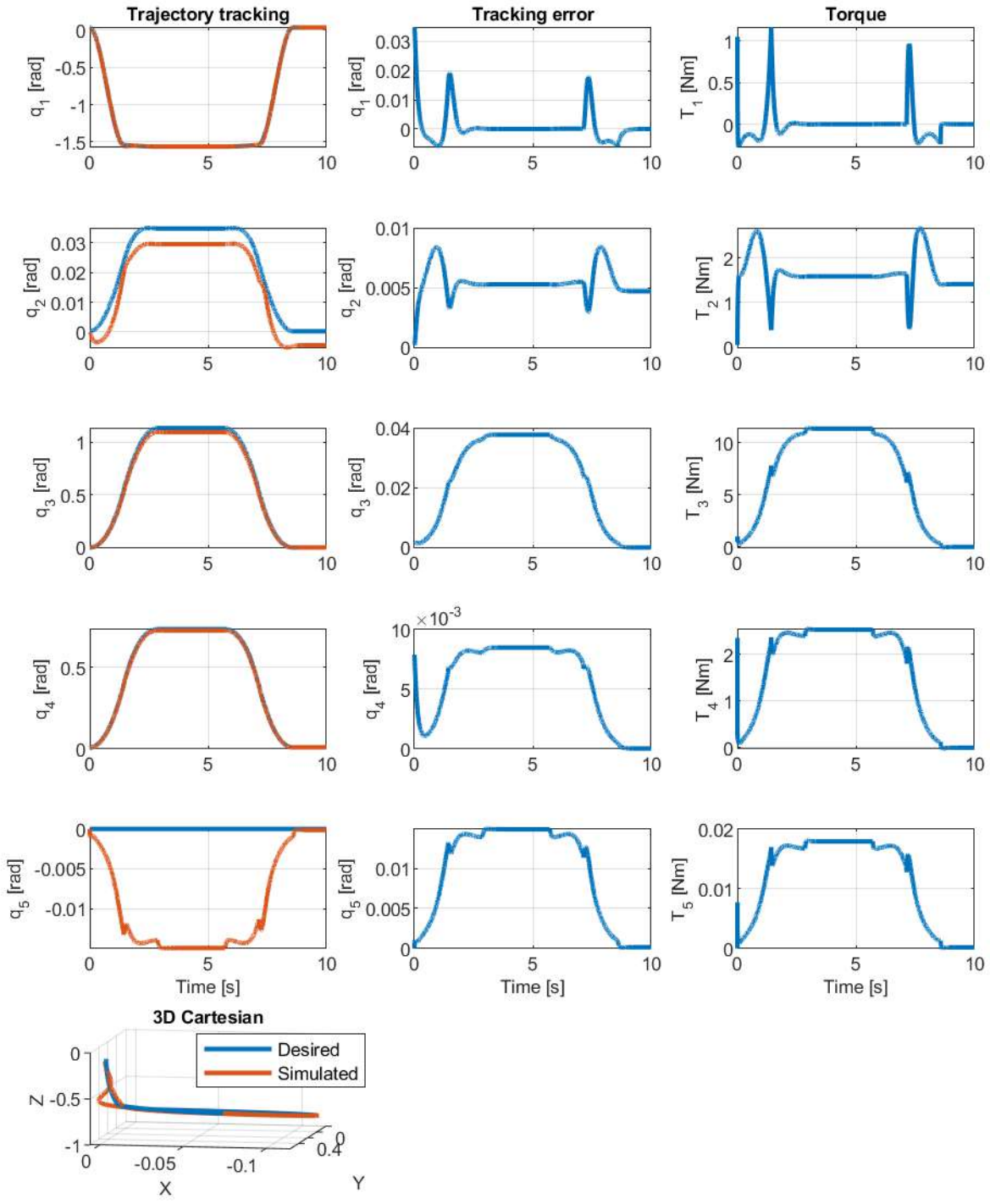

Figure 5.11: S-AA movement: DTP performance in simulation using a 5th-order trajectory (desired trajectory (blue color) and simulated trajectory (orange color)).

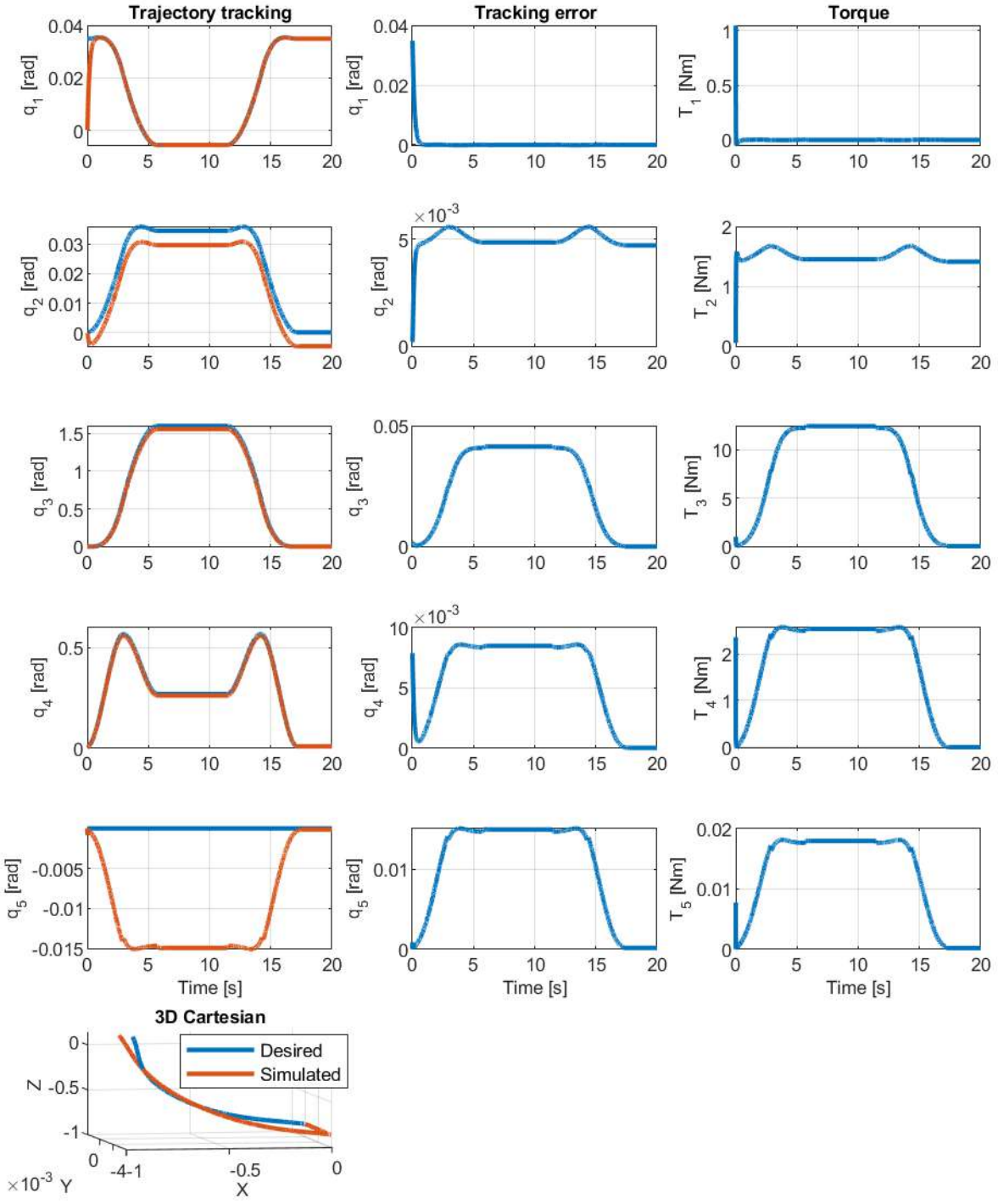

Figure 5.12: S-FE movement: DTP performance in simulation using a 5th-order trajectory (desired trajectory (blue color) and simulated trajectory (orange color)).

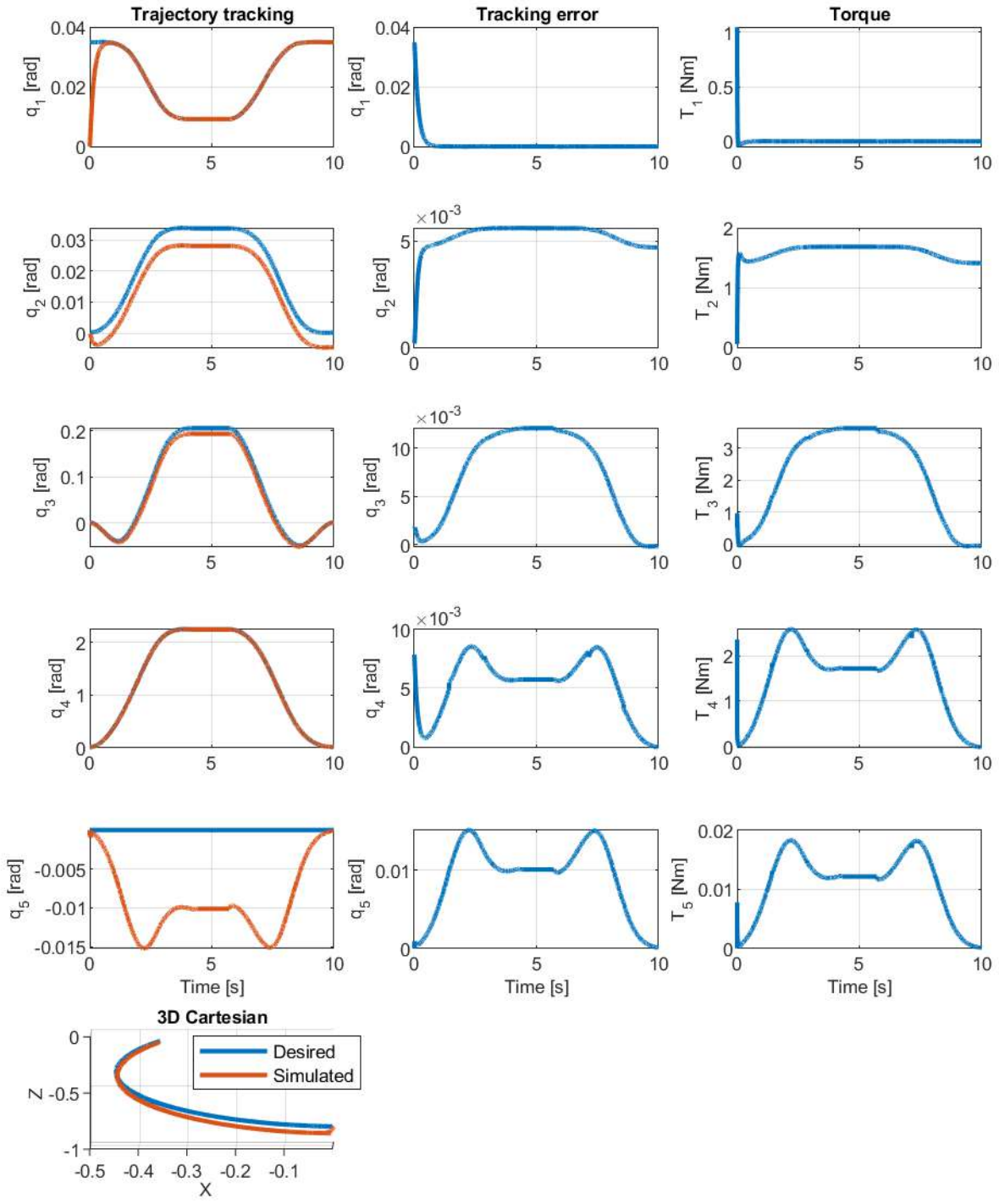

Figure 5.13: E-FE movement: DTP performance in simulation using a 5th-order trajectory (desired trajectory (blue color) and simulated trajectory (orange color)).

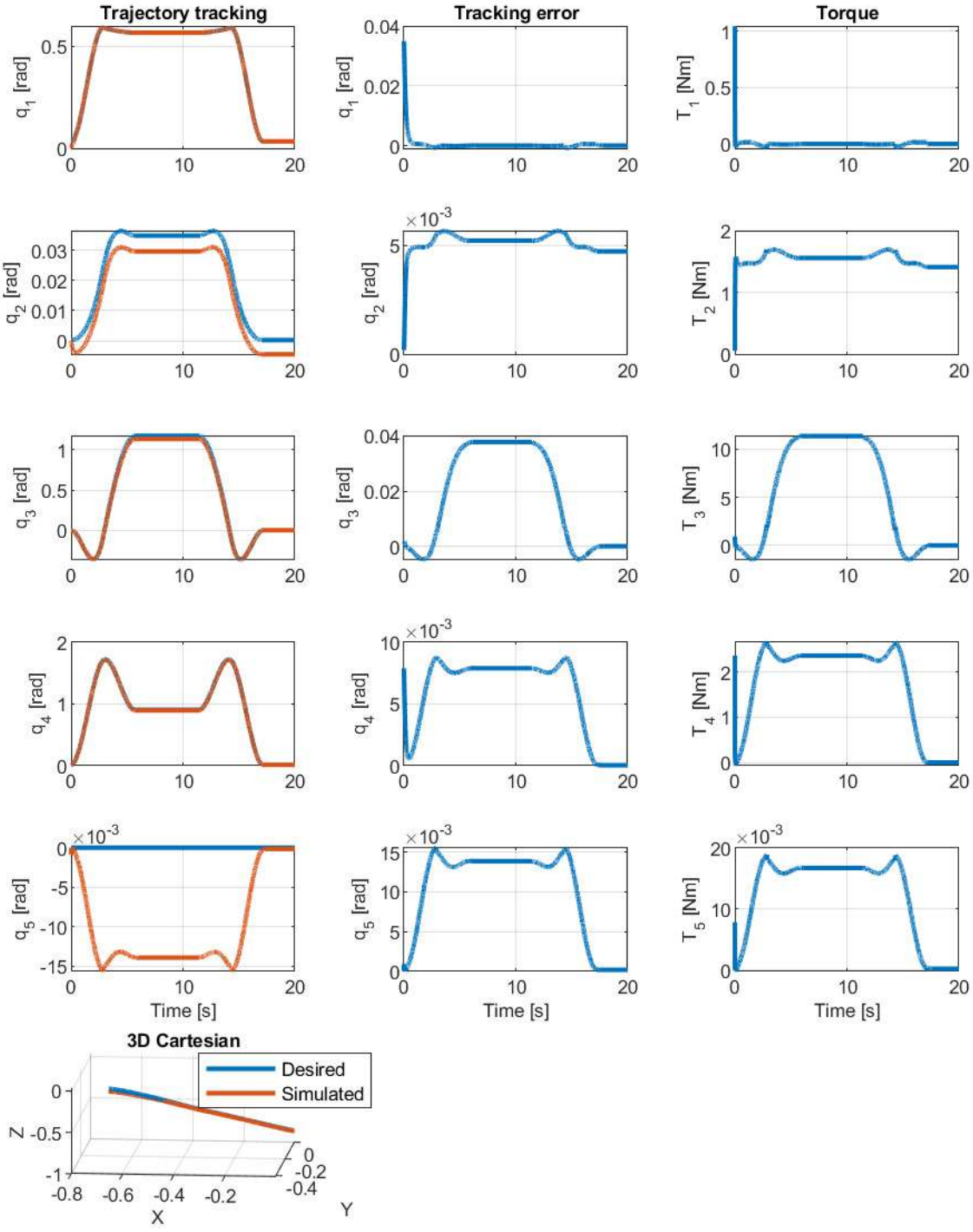

Figure 5.14: Diagonal movement: DTP performance in simulation using a 5th-order trajectory (desired trajectory (blue color) and simulated trajectory (orange color)).

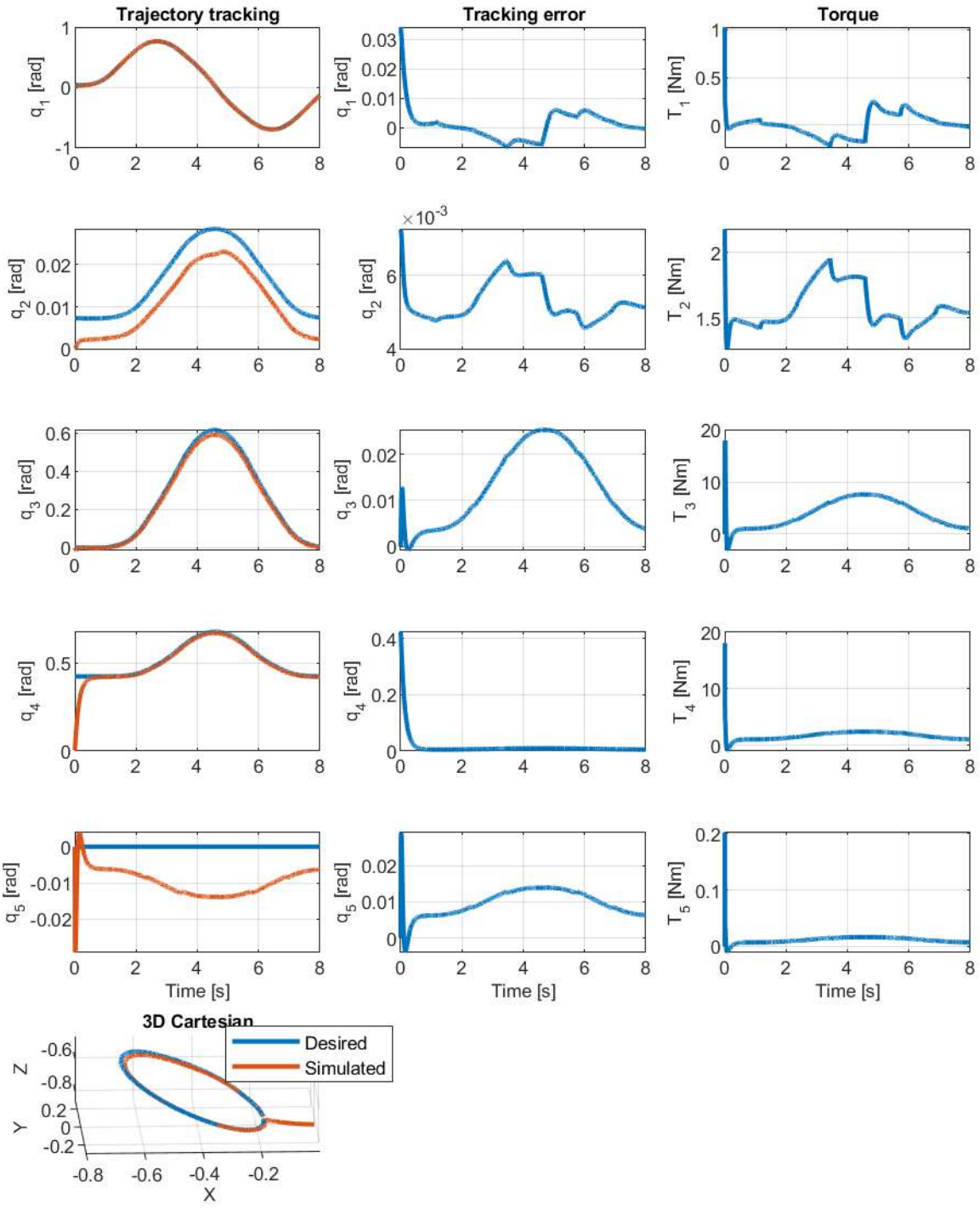

Figure 5.15: Circle movement: DTP performance in simulation using a 5th-order trajectory (desired trajectory (blue color) and simulated trajectory (orange color)).

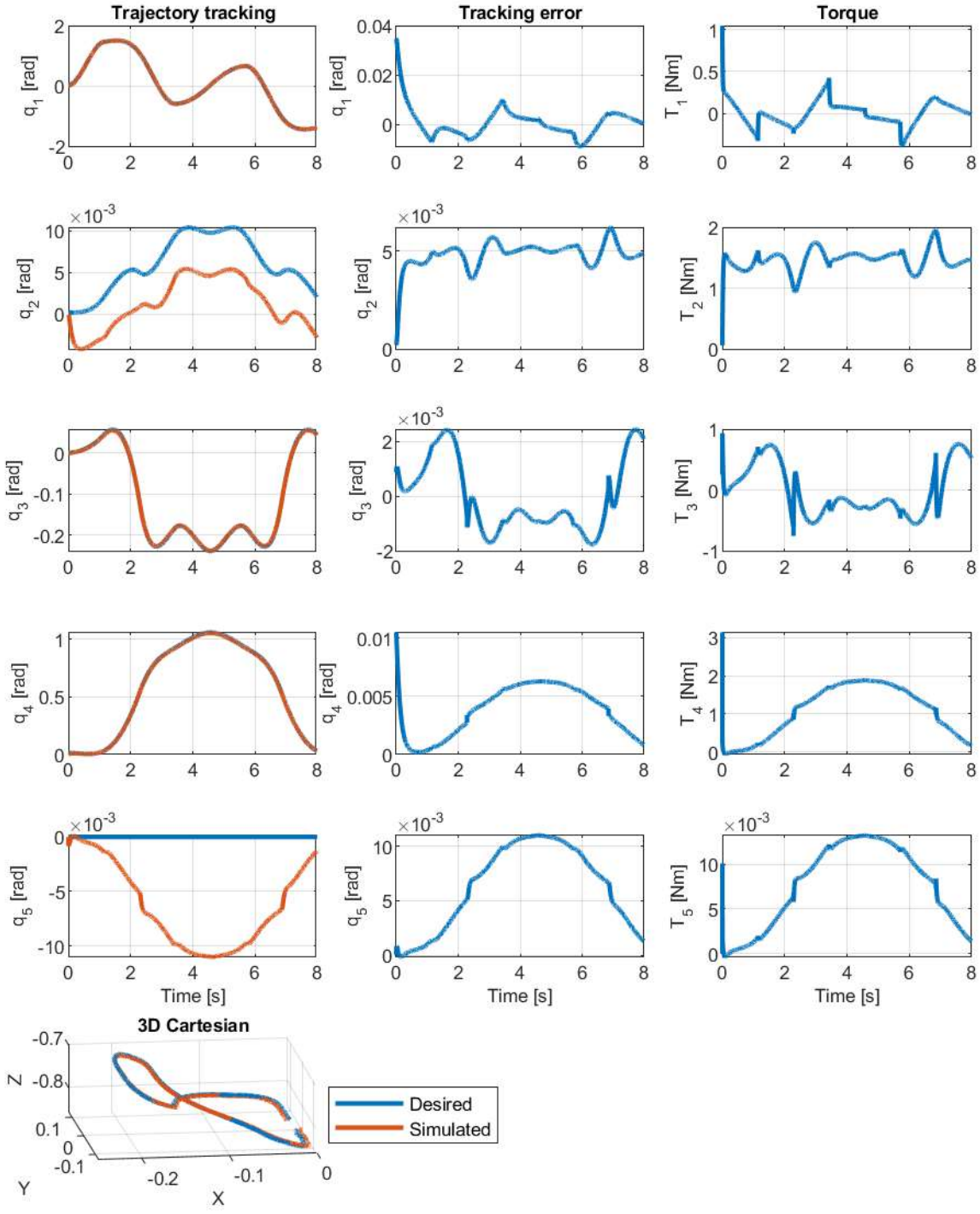

Figure 5.16: Infinity movement: DTP performance in simulation using a 5th-order trajectory (desired trajectory (blue color) and simulated trajectory (orange color)).

5.3 Human–Robot Interface: Design and Functionality.

The interface has been designed with a user-centered approach, specifically targeting medical personnel. Its primary goal is to provide a versatile tool that minimizes the amount of necessary data, while the collected data facilitates the creation of a detailed medical history. This interface integrates technical engineering aspects with clinical aspects related to therapeutic treatments, all while considering Jakob Nielsen's 10 general principles (Nielsen, 1994), enabling the execution of treatments that include retraining of movement patterns.

The user interface has been developed as an application in Matlab® and runs on a laptop computer. Data exchange between the virtual and physical digital twins is carried out through a wired data network using the CAN protocol via the serial port. Therefore, operating the exoskeleton is achieved by configuring and programming the system through the interface in two stages. The first stage involves simulating and graphically visualizing movement using the virtual digital twin (DTP) of the exoskeleton, while the second stage enables the execution of movements through the physical digital twin (DTI), see Figure 5.17.

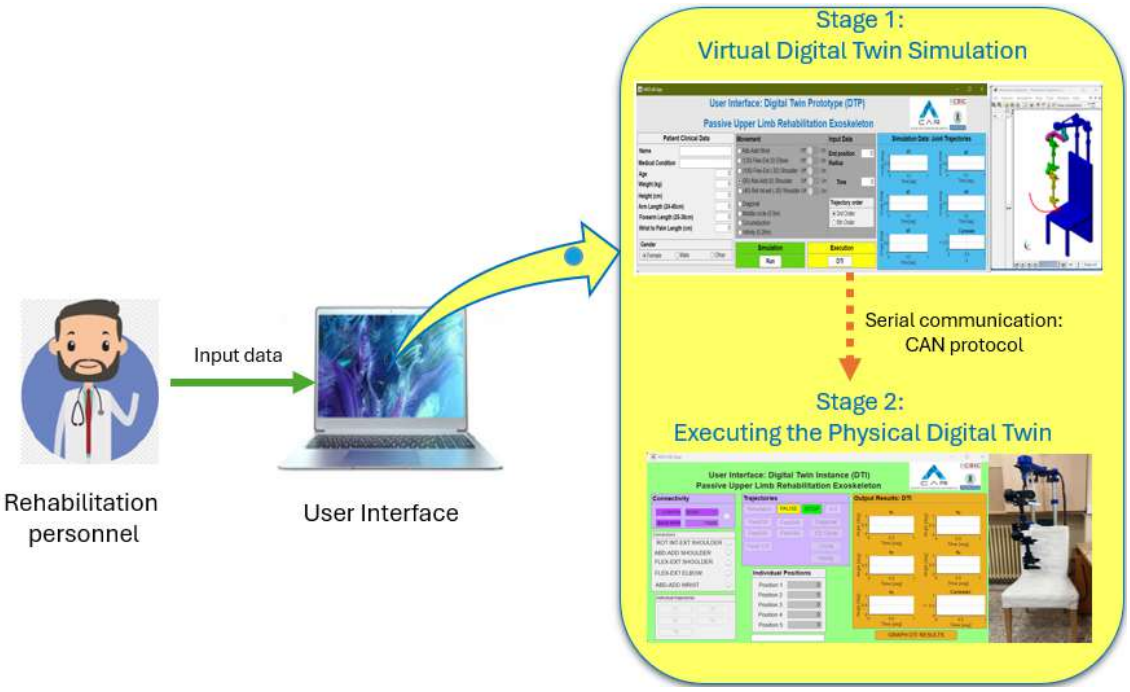

Figure 5.17: Human-robot interaction.

The user interface consists of a main screen and a secondary one. The main screen initiates the first contact with the user and presents the following features in sequence (refer to Figure 5.18):

1. It facilitates the input of users' clinical data (number 1 in Figure 5.18).
2. It allows configuring therapeutic movements once medical personnel selects the movement to execute, as well as the final position and the time at which said final position must be reached. This is done considering 2 modes of operation (number 2 in Figure 5.18).

(a) Mode 1: Decoupled movements, where the movement is performed exclusively by the selected joint, following a smooth joint trajectory defined by the rehabilitation medical personnel (third or fifth order).

(b) Mode 2: Coupled movements, where all joints execute the motion through smooth trajectories, thus generating a more natural and human-like movement (utilizing the inverse kinematics solution described in Section 5.1.4).

3. Once the therapeutic movements have been defined, the interface allows for a simulation of the exoskeleton's virtual DTP. In this simulation, users can visually observe the obtained joint and Cartesian trajectories, as well as a 3D visualization of the device executing the movement previously configured by medical personnel (number 3 in Figure 5.18).

4. It enables communication with the secondary interface, which allows for control of the DTI (number 4 in Figure 5.18).

5. It enables automatic storage of the user's clinical data, as well as the data for each therapeutic movement performed during the simulation of the exoskeleton's DTP.

The secondary screen enables communication and control of the digital twin instance (physical prototype). Below, its features are detailed in the corresponding order of the process (see Figure 5.19).

1. It facilitates the establishment of serial communication between the interface and the DTI (number 1 in Figure 5.19).

2. It allows executing the movements that have been previously simulated on the main screen, as well as the movements that have been predefined (identified as number 2 in Figure 5.19).

3. It facilitates the execution of specific joint movements at each of the joints of the DTI (Induction Therapy Device). Entering the final angular position in degrees is required, and the DTI will perform, in a single motion, the transition from the initial position to the position indicated by the user (number 3 in Figure 5.19).

4. It provides a visual representation of the performance of the physical prototype through joint and Cartesian graphs (number 4 in Figure 5.19).

5. It enables automatic storage of the output data from each therapeutic movement performed by the DTI of the exoskeleton.

In addition to the functions mentioned on the secondary screen, it also includes a pause button that allows the user to interrupt and then resume movement, and a stop button that aborts the movement and completely halts the actuators. These functions are activated by medical personnel as safety measures during DTI operation. As a result, the interface can operate the exoskeleton both in simulation and in the physical world.

The following section presents a comprehensive assessment covering the perspectives of the user, the physiotherapist, and the device's performance as a product.

Figure 5.18: Main screen of the interface developed in Matlab®.

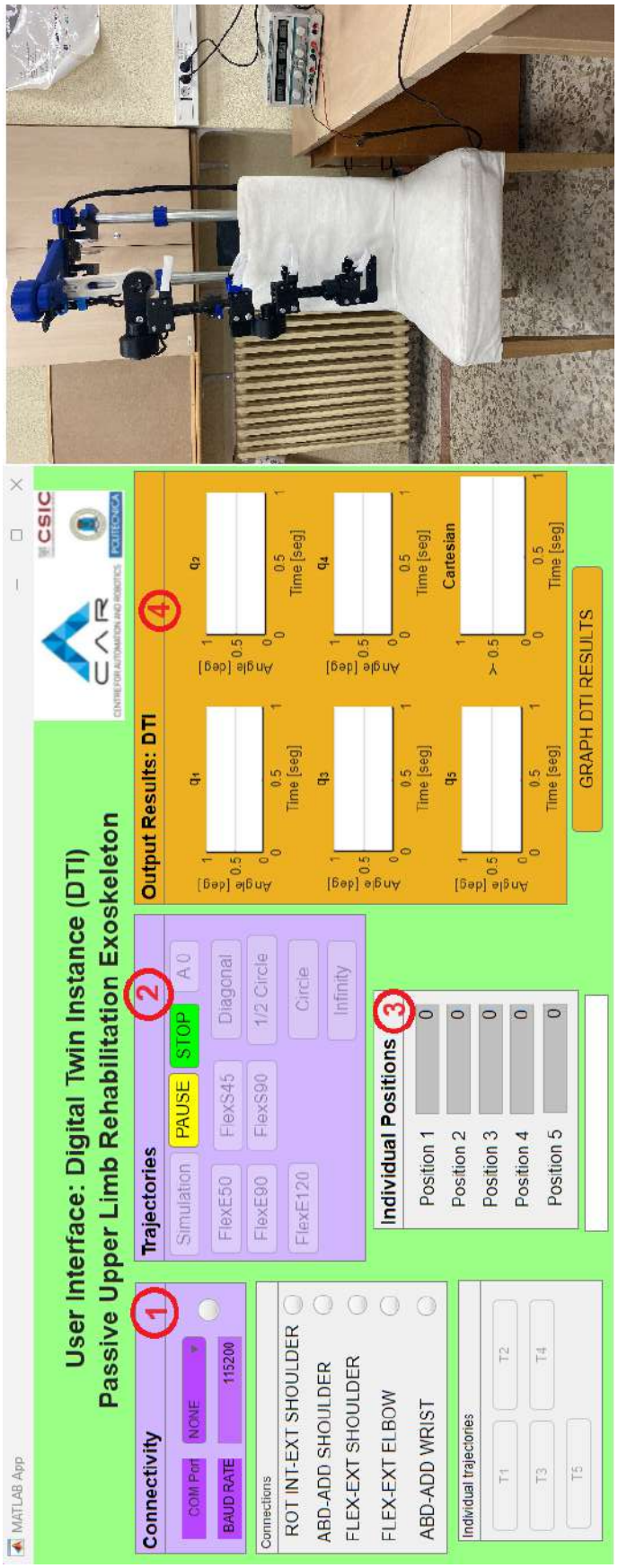

Figure 5.19: Secondary screen of the interface developed in Matlab®.

Chapter 6

Methodological Implementation: Exoskeleton evaluation in a clinical environment

"Science is not learned from books, but through experience".

Julio Verne.

The thorough assessment of rehabilitation exoskeletons is vital for ensuring their effectiveness, safety, and acceptance within clinical settings. By examining biomechanical, functional, and user experience factors, this evaluation yields essential insights that inform the design, deployment, and ongoing enhancement of these devices. Therefore, this section presents a comprehensive evaluation of the exoskeleton's DTI, encompassing its performance and user perceptions, including feedback from rehabilitation professionals and end users. The following outlines the process.

6.1 Description of the Full-Scope evaluation methodology

Initially, the device was installed in a rehabilitation room at the Hospital Universitario 12 de Octubre (HU12O) in Madrid, Spain (see Figure 6.1). The exoskeleton was controlled using a laptop equipped with an 11th generation Intel(R) Core(TM) i7-11800H processor, running at 2.30GHz, and 16GB of RAM were allocated.

Figure 6.1: Installation of the exoskeleton's DTI at HU12O

The rehabilitation medical personnel operated the device to provide assistance to the participants during the rehabilitation sessions. In this context, the term "users" encompasses both patients with injuries to the right upper limb and healthy individuals. All involved parties, including physiotherapists and users, were provided with comprehensive information about the study and gave their consent to participate voluntarily in the research. For users, this consent was formalized by signing an informed consent document.

The physiotherapists selected users based on the following inclusion criteria: individuals weighing under 80 kg, experiencing impairment in the right upper limb, and undergoing post-surgical recovery, or those suffering from tendinopathy. Exclusion criteria were applied to patients whose participation could be detrimental to their well-being, those who refused consent, as well as those with secondary conditions such as mental illnesses or experiencing any type of pain. Once users were selected, rehabilitation sessions were conducted during which they utilized the exoskeleton to perform a variety of movements, both simple and complex. The main features of the users who participated in the study are detailed in Table 6.1.

Table 6.1: Features of Test Users

User	User Type	Gender	Age [years]	Height [cm]	Weight [kg]
1	Patient	Female	53	157.00	55.00
2	Patient	Female	39	155.00	71.00
3	Patient	Male	56	165.00	59.50

User	User Type	Gender	Age [years]	Height [cm]	Weight [kg]
4	Patient	Male	46	171.00	70.00
5	Patient	Male	65	174.00	69.00
6	Patient	Female	58	160.00	55.00
7	Patient	Female	61	167.00	53.00
8	Patient	Male	62	167.00	65.00
9	Patient	Female	37	173.00	75.00
10	Patient	Female	60	153.00	73.00
11	Healthy user	Male	20	170.00	67.00
12	Healthy user	Female	20	157.00	52.00

According to the data presented in Table 6.1, the test was conducted with the participation of 10 patients and 2 healthy users (7 females and 5 males). The average age was 48 years old (standard deviation of 15.16), with an average height of 164 cm (standard deviation of 7.07), and an average weight of 63.70 kg (standard deviation of 8.00). It is important to note that none of the users had previous experience in using exoskeletons during their rehabilitation process.

With the aim of conducting a comprehensive and thorough evaluation of the developed system, the perception of both users and rehabilitation medical personnel, as well as the performance of the exoskeleton, were taken into consideration. To achieve this, qualitative and quantitative measures of the system were employed through standardized and/or customized questionnaires, which were administered after the tests. These questionnaires aimed to measure the usability and perceived workload of the rehabilitation staff, as well as the system's performance.

To conduct this assessment, it was proposed to employ the methodologies shown in Figure 6.2, which are described below:

6.2 Evaluations conducted by medical personnel

To carry out these evaluations, it was essential to inform the rehabilitation service staff about the requirements and tests associated with the study. Consequently, the tests were conducted by volunteers who consented to participate in the process.

This study was structured into two phases: the first one focused on training the physiotherapists, while the second one centered on operating the prototype and collecting data. Below, each of these stages is described in detail:

1. **Training:** Its aim is to instruct the rehabilitation service personnel at HU12O who will be using the device. This training took place at the hospital's facilities and was divided into two phases:
    - Phase 1: Physiotherapists were trained on the operation of the interface through an in-person demonstration. Subsequently, each of them used the interface individually.
    - Phase 2: Five physiotherapists from the previous group were selected to receive

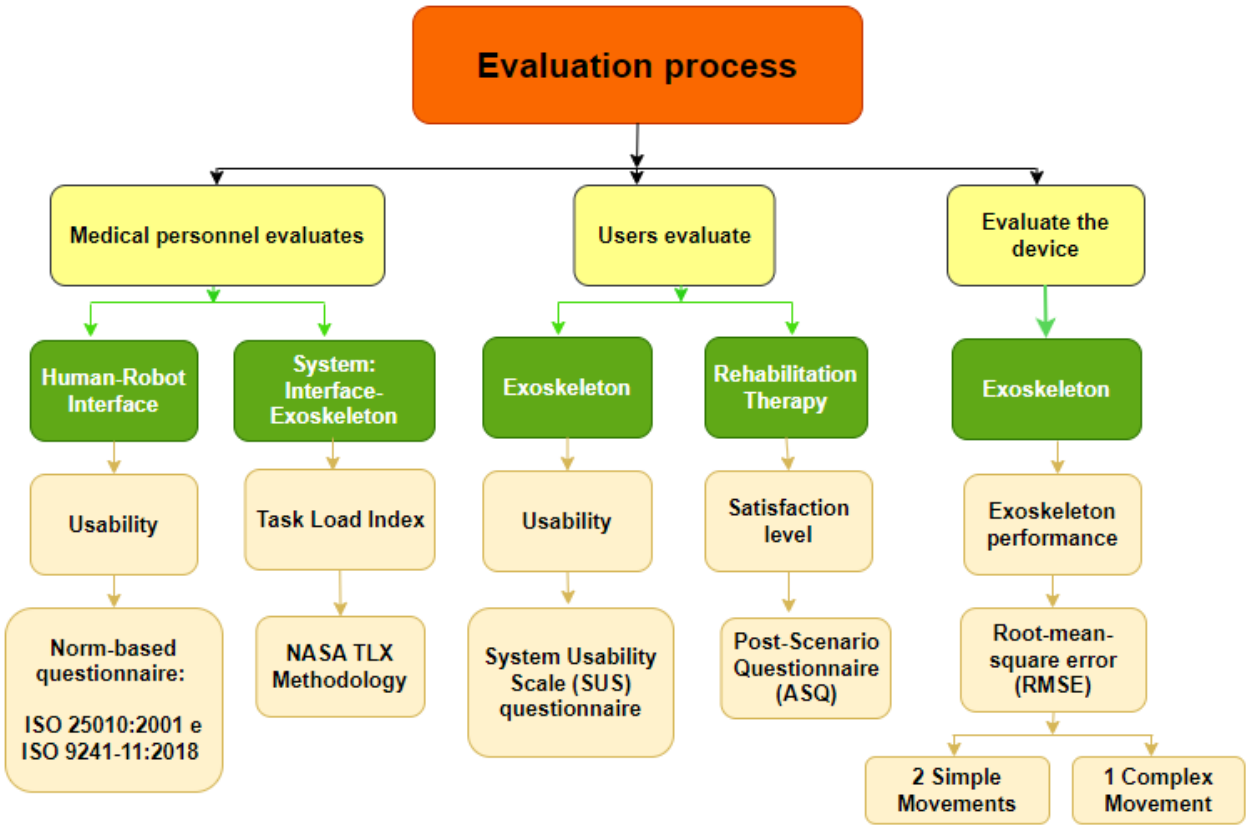

Figure 6.2: System Evaluation Process: Interface-Exoskeleton

training in the donning and use of the exoskeleton on patients. They were chosen because, at that time, the majority of their patients were undergoing upper limb rehabilitation. During the demonstration, one physiotherapist assumed the patient's position while another operated the device.

During both training phases, physiotherapists had the support of the device developer to clarify any doubts and address their comments.

2. **Operation of the device and data collection:** In phase 2 of the study, physiotherapists used the device during rehabilitation sessions with patients who had provided their signed consent. During these sessions, physiotherapists programmed personalized movements, both simple and complex, designed to support the patient's rehabilitation treatment (the movements are detailed in the section on assessments performed on the exoskeleton). Data on the movements executed by the device were recorded and stored for subsequent analysis regarding its performance.

At the end of each training phase, participants were asked to evaluate usability and workload index. The aspects of each evaluation are detailed below:

1. Human-Robot Interface: The usability of the interface was evaluated using a customized questionnaire based on ISO 25010-2011 and ISO 9241-11:2018 standards (see Annex .4). This evaluation was conducted by 12 physicaltherapists (PTs) who completed phase 1

of the training (25% men and 75% women), of whom only 16% had previous experience with exoskeletons. The average age of the physical therapists was 48 years old, with a standard deviation of 2.44 (see Table 6.2).

Table 6.2: Physiotherapists features

PT	Gender	Age [years]	Previous experience using exoskeletons
1	Male	49	No
2	Female	49	No
3	Female	52	No
4	Female	51	No
5	Female	46	Yes
6	Female	44	No
7	Male	49	No
8	Female	46	No
9	Male	47	Yes
10	Female	50	No
11	Female	45	No
12	Female	48	No

The customized questionnaire to assess the usability of the interface comprises 22 questions addressing the detailed aspects in Table 6.3. For each aspect, two questions were assigned, which are answered using a 5-point Likert scale.

Table 6.3: Aspects evaluated in the interface usability questionnaire

Num	Aspect	Question Number
1	Ease of learning	1-2
2	Ease of use	3-4
3	Comprehension capacity	5-6
4	Visual appeal	7-8
5	Responsiveness	9-10
6	Ease of navigation	11-12
7	Flexibility and adaptability	13-14
8	System feedback	15-16
9	System errors	17-18
10	Error recovery capacibility	19-20
11	User satisfaction	21-22

Figure 6.3 shows the number of physiotherapists and the Likert scale rating assigned to

each question in the questionnaire. The following are the conclusions for each aspect of the interface:

Ease of Learning 75% of the physiotherapists found it easy to learn how to use.

Ease of Use 83% of the physiotherapists found it easy to use.

Comprehensibility Over 60% of the physiotherapists could easily understand how to interact with the system.

Visual Appeal 75% of the physiotherapists found it attractive and visually pleasing.

Responsiveness Approximately 60% of the physiotherapists observed a quick response from the interface to their actions, while only 16% experienced delays or a lack of response.

Ease of Navigation Approximately 70% of the physiotherapists found the interface's navigation structure intuitive and could easily move through it.

Flexibility and Adaptability Approximately 40% of the physiotherapists agreed that the interface allowed them to adapt it to their preferences and make useful customizations.

System Feedback Approximately 70% of the physiotherapists agreed that the feedback provided by the interface was clear and helpful.

System Errors Only 16% of the physiotherapists experienced any errors while using the interface.

Error Recovery Capability One-third of the physiotherapists believed that the interface provides options to correct errors and recover from them, based on the percentage of physiotherapists who experienced some type of error.

User Satisfaction Approximately 60% of the physiotherapists found their satisfaction with the interface acceptable and would recommend it to other physiotherapy colleagues.

Taking into account the results obtained and aiming to enhance both the usability and adoption of the interface, it is suggested primarily to increase the level of acceptance regarding customization. Consequently, the inclusion of the capability to create sequences of simple and complex movements is proposed, allowing for adjusting the speed of each movement according to the joint ranges.

2. Interface-Exoskeleton System: The workload index experienced by physiotherapists was assessed using the NASA TLX methodology. This evaluation was conducted by the physiotherapists who participated in phase 2 of the training, specifically the first 5 physiotherapists mentioned in Table 6.2, and was performed after using the device during rehabilitation sessions with their patients. The results of the six scales of this methodology are presented in Table 6.4.

Figure 6.3: Usability questionnaire results graph evaluating the device interface (Annex .4 presents the entire questionnaire).

Table 6.4: Task Load Index Results (NASA TLX)

	Physiotherapist					
Variable	1	2	3	4	5	Mean
Mental demand	250	50	150	10	75	107
Physical demand	10	100	150	15	30	61
Temporal demand	50	0	125	0	200	75
Performance	105	75	50	15	100	69
Effort	25	300	0	15	25	73
Frustration	75	80	50	20	0	45
Total	515	605	525	75	430	430
Load Level	Medium	Medium	Medium	Low	Low	

The analysis of the results obtained from the physiotherapists who used the device revealed that mental demand was the most pronounced, followed by temporal demand and effort, while frustration was the lowest (see Figure 6.4). Furthermore, the findings suggest that improving the work environment could be beneficial, as most physiotherapists showed a medium level of workload.

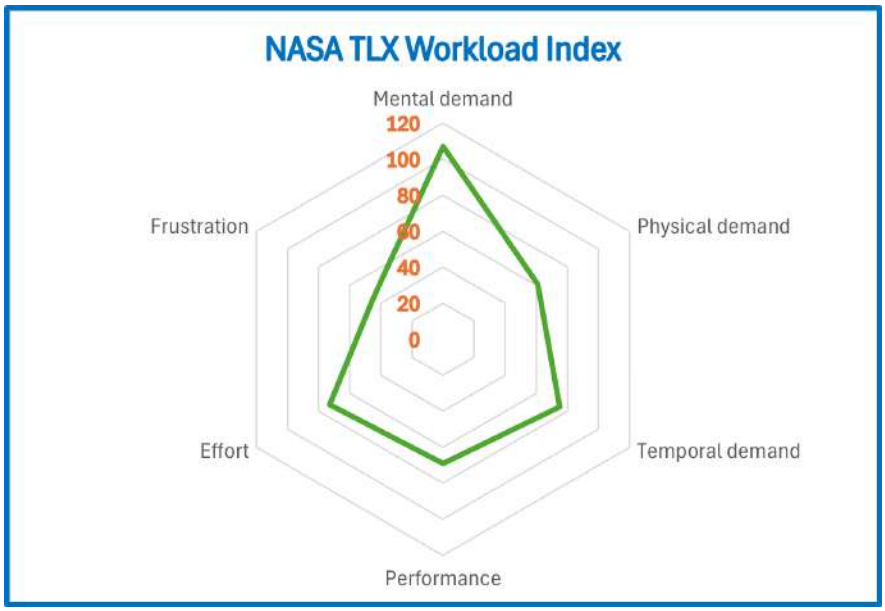

Figure 6.4: Resulting Task Load Index: NASA-TLX.

6.3 Evaluations conducted by users (patients and healthy users)

1. Exoskeleton: The usability of the exoskeleton was evaluated using the System Usability Scale. A 10-question survey using a 5-point Likert scale was employed for this purpose. The 12 users completed the survey after a rehabilitation session with the exoskeleton, and the results are presented in Table 6.5.

Table 6.5: SUS questionnaire results for each question

	Question									
User	1	2	3	4	5	6	7	8	9	10
1	3	3	2	5	3	4	1	1	3	5
2	3	3	4	5	4	3	4	3	5	4
3	4	2	4	5	4	2	3	2	4	2
4	4	3	4	2	4	3	4	2	4	2
5	4	5	3	4	3	3	3	4	3	3
6	4	2	4	3	3	3	4	2	4	3
7	1	3	4	3	2	4	4	2	2	2
8	4	2	5	5	4	3	3	3	4	2
9	3	3	4	4	3	3	4	3	3	3
10	5	1	5	5	5	1	1	5	5	1
11	4	3	5	2	3	2	4	2	4	1
12	1	2	3	5	4	2	3	3	2	4
Mean	3.33	2.66	3.91	4.00	3.50	2.75	3.16	2.66	3.58	2.66

According to the results obtained from the users, the following conclusions can be drawn: a) it is necessary to have the support of a professional, specifically a physical therapist, for the use of the device, as they control its operation through the interface; b) users do not find the exoskeleton difficult to use, as they only need it to be donned on the upper limb; c) they experienced a sense of security when using the device; and d) they did not need to acquire much prior knowledge before starting to use it.

Figure 6.5 presents the SUS result for each patient, with an average value of 56.87. This result can be considered below average since is lower than 68. This relatively low scoring can be mainly associated to the fact that the exoesqueleton was still at a prototype stage when validating it in a real scenario. This also suggests that the usability of the device needs improvement, particularly regarding the integration of functions and the coupling between the user and the exoskeleton.

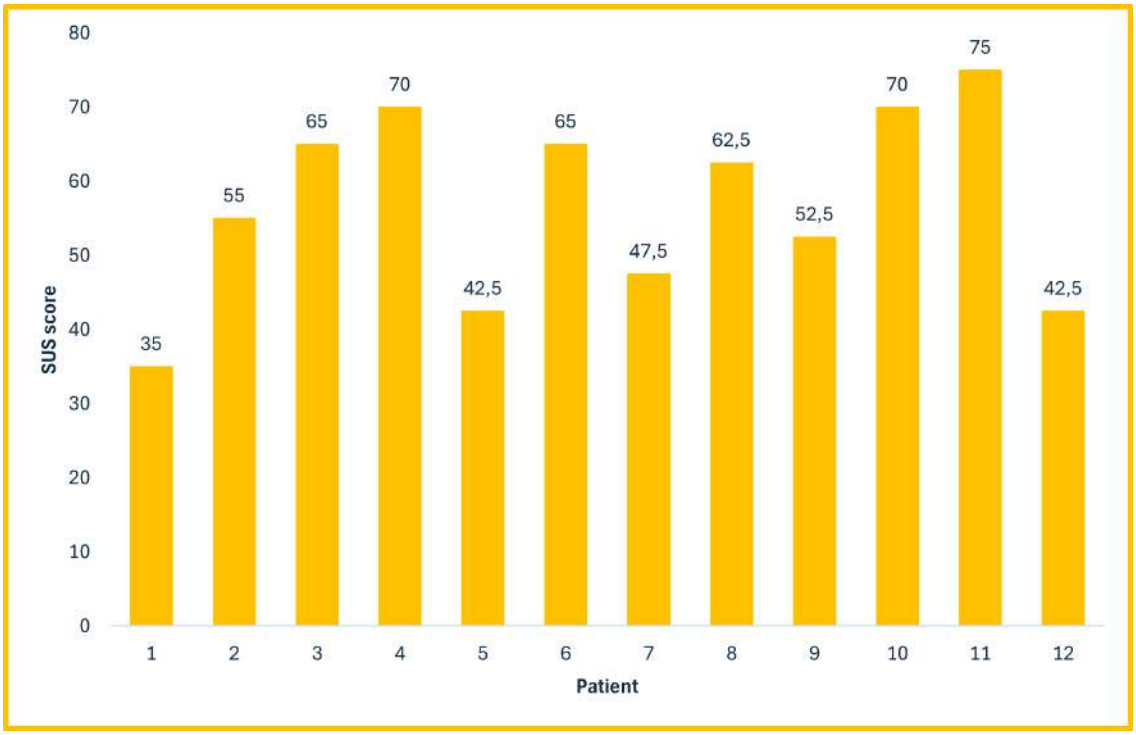

Figure 6.5: Result of the SUS questionnaire applied to the patients

2. Rehabilitation Therapy: Participant satisfaction with the therapeutic session was assessed using the post-session ASQ questionnaire. This questionnaire includes three objective questions rated on a five-point Likert scale.

   All participants completed the ASQ questionnaire at the end of the therapeutic session (see Figure 6.6), and their results are detailed in Table 6.6. In all questions, more than 50% of respondents expressed agreement, suggesting an acceptable level of satisfaction.

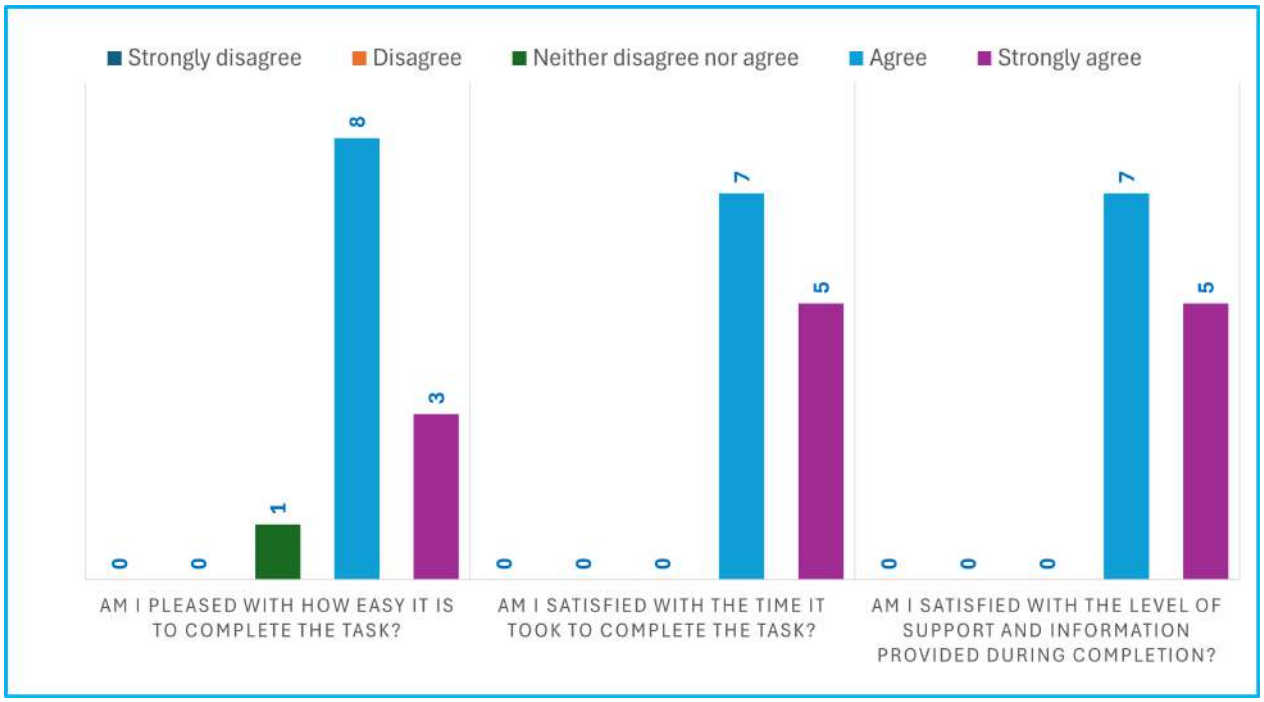

Figure 6.6: Results of the ASQ questionnaire administered to the patients

Table 6.6: ASQ questionnaire results for each question

	Question		
User	1	2	3
1	4	4	4
2	4	5	5
3	5	5	5
4	4	4	4
5	4	4	4
6	4	4	4
7	5	5	5
8	4	4	4
9	3	4	5
10	5	5	5
11	4	5	4
12	4	4	4
Mean	4.16	4.16	4.16

6.4 Evaluations conducted on the exoskeleton

1. Exoskeleton: The evaluation of the exoskeleton's performance was based on the precision, repeatability, and reproducibility of movements. Two simple movements were performed: 1) elbow flexion-extension and 2) shoulder internal-external rotation, in addition to a complex movement: the diagonal. The latter was only executed by those patients capable of performing it. Details of each movement are described in Table 6.7 and Figure 6.7 illustrates a patient using the exoskeleton, while the physiotherapist configures the interface.

Figure 6.7: Exoskeleton being used by the patient, with the interface being configured by the physiotherapist.

Table 6.7: Movements applied in rehabilitation and carried out through the use of the exoskeleton.

Movement		Users	Description	Speed [°/s]		
				Min	Max	Mean
Simple	Elbow flexion - extension	All users (see Table 6.1)	• Coupled movement. • Third-order articular trajectories. • Different finishing positions at different times.	6.00	20.00	15.08
	Shoulder internal-external rotation			2.00	20.00	9.83
Complex	Diagonal	Users from 5 to 9 (see Table 6.1)	• Coupled movement. • Third-order articular trajectories. • Different finishing positions at different times.	4.00	12.00	7.00

The data from Table 6.7 reveals that the device achieved a maximum speed of 20.00 $°/s$ and a minimum of 2.00 $°/s$. This highlights the wide range of speeds available on the device, as well as its versatility, flexibility, and ability to customize the therapeutic routines recommended by physiotherapists. This adaptability enables meeting the individual needs of each user.

Figures 6.8, 6.9, and 6.10 display the tracking of joint trajectories for each user during elbow flexion-extension, shoulder internal-external rotation, and diagonal movements, respectively. These figures depict the different final positions achieved by the users and the time taken to reach them, thus illustrating the varied execution speeds.

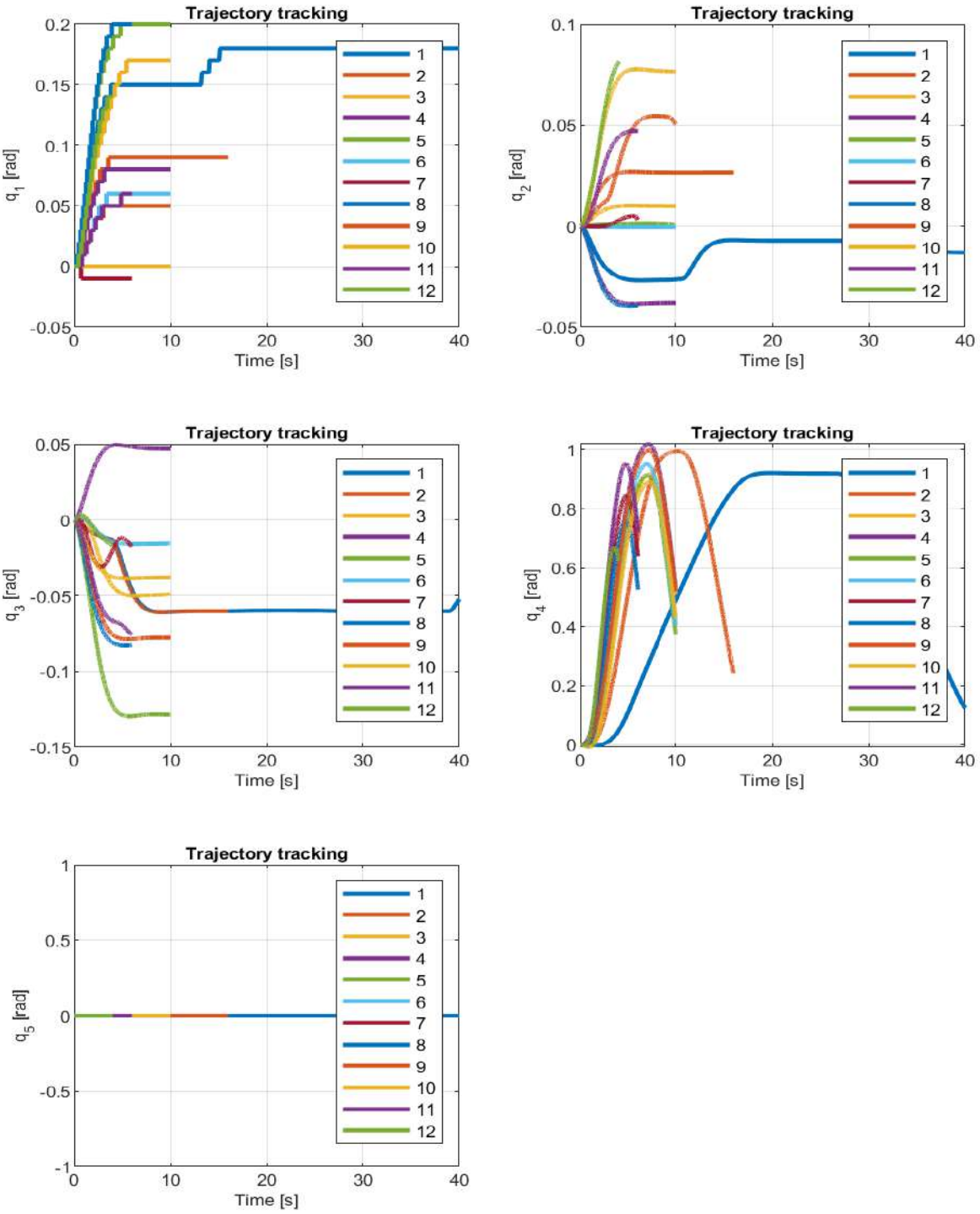

Figure 6.8: Users trajectory tracking: Elbow flexion-extension movement

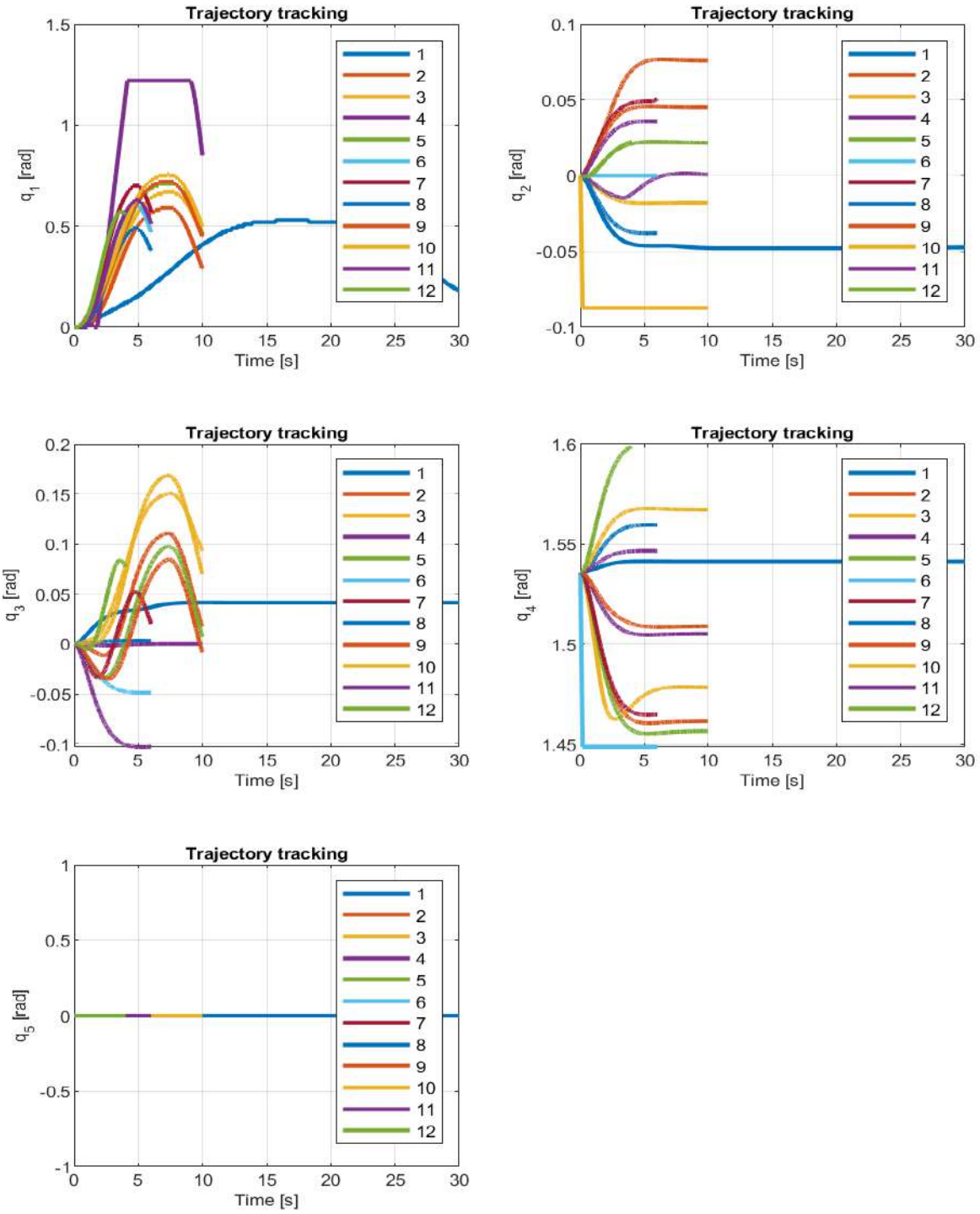

Figure 6.9: Users trajectory tracking: Shoulder internal-external rotation movement

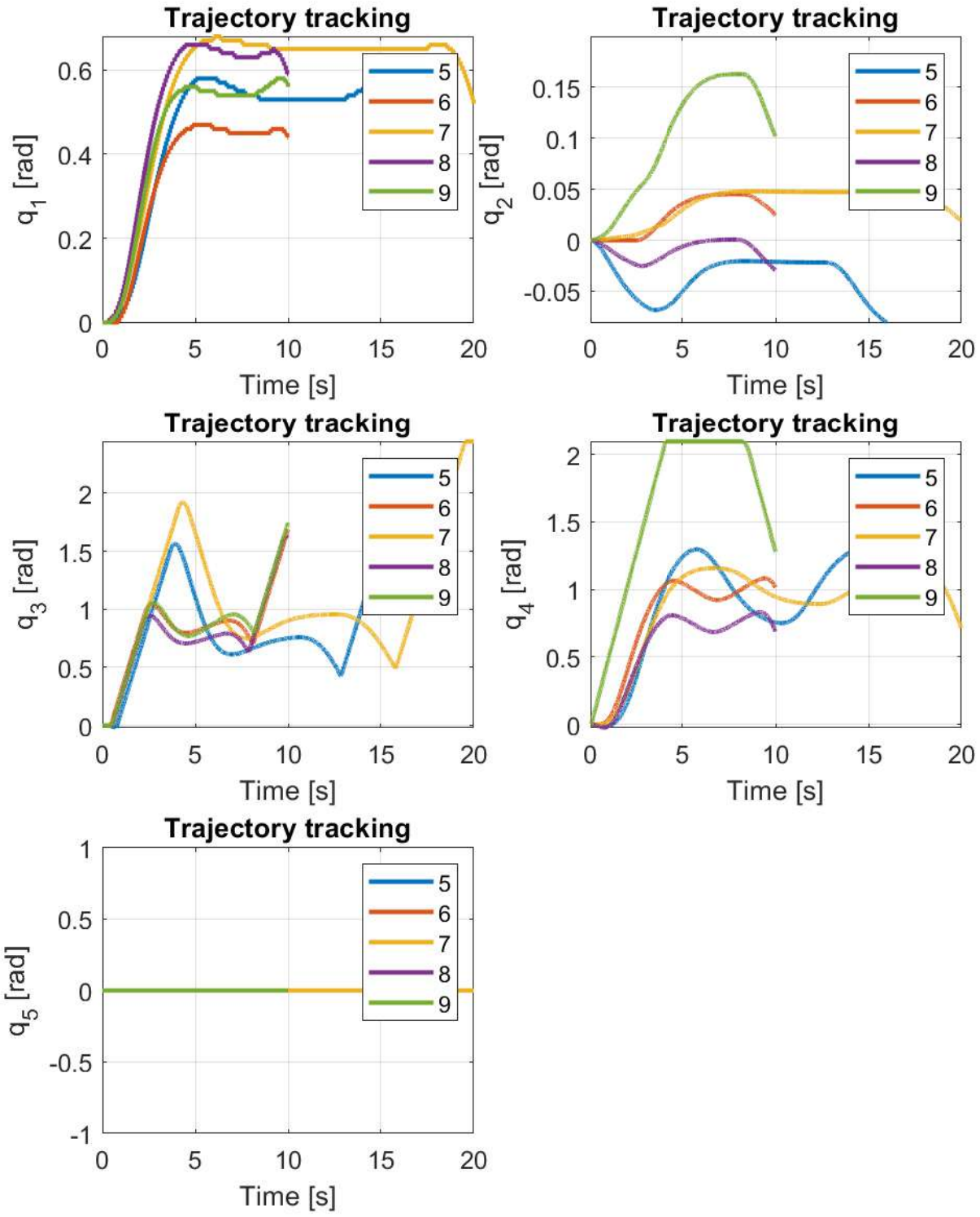

Figure 6.10: Users trajectory tracking: Diagonal movement

After carrying out all the mentioned therapeutic movements, the performance of the device was evaluated by calculating the root mean square error (RMSE) obtained for each user in each of those movements. The desired trajectories used are those obtained during the interface simulation stage (exoskeleton considers only its own weight). The measured trajectories correspond to those obtained from the exoskeleton after executing each of the movements. As an example, the behavior of user 6, who performed all three movements, is illustrated (see Figures 6.11, 6.12, and 6.13).

Tables 6.8, 6.9 and 6.10 present the mean RMSE results of all users for each movement.

Table 6.8: RMSE: Simple movement (elbow flexion-extension)

User	$q_1[rad]$	$q_2[rad]$	$q_3[rad]$	$q_4[rad]$	$q_5[rad]$
1	0.10	0.02	0.03	0.16	0.00
2	0.03	0.01	0.03	0.25	0.00
3	0.08	0.05	0.02	0.38	0.00
4	0.02	0.05	0.07	0.37	0.00
5	0.11	0.01	0.08	0.36	0.00
6	0.03	0.01	0.02	0.35	0.00
7	0.07	0.01	0.02	0.48	0.00
8	0.10	0.04	0.04	0.49	0.00
9	0.03	0.02	0.04	0.37	0.00
10	0.07	0.01	0.01	0.39	0.00
11	0.03	0.02	0.03	0.47	0.00
12	0.05	0.04	0.02	0.50	0.00
Mean	0.06	0.02	0.03	0.38	0.00

Table 6.9: RMSE: Simple movement (shoulder internal-external rotation)

User	$q_1[rad]$	$q_2[rad]$	$q_3[rad]$	$q_4[rad]$	$q_5[rad]$
1	0.11	0.09	0.04	0.02	0.00
2	0.23	0.02	0.09	0.09	0.00
3	0.25	0.06	0.08	0.09	0.00
4	1.28	0.05	0.09	0.06	0.00
5	0.25	0.02	0.11	0.10	0.00
6	0.30	0.04	0.16	0.12	0.00
7	0.31	0.01	0.13	0.08	0.00
8	0.25	0.07	0.07	0.02	0.00
9	0.25	0.01	0.11	0.05	0.00
10	0.27	0.13	0.09	0.01	0.00
11	0.32	0.02	0.20	0.02	0.00
12	0.35	0.03	0.12	0.02	0.00
Mean	0.34	0.05	0.11	0.06	0.00

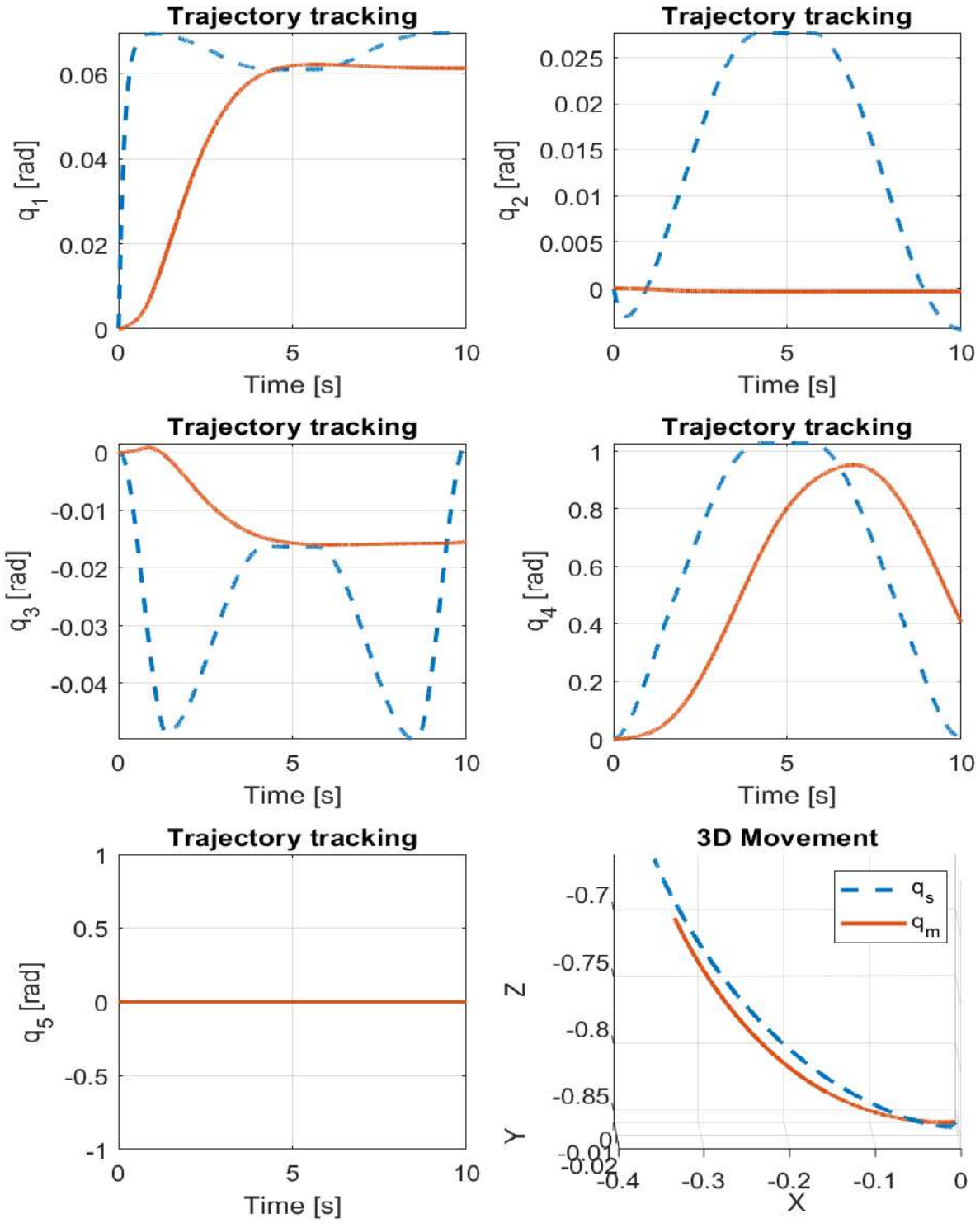

Figure 6.11: User 6: Trajectory tracking (elbow flexion-extension movement). Simulated trajectory (blue dashed line) and measured trajectory (orange line).

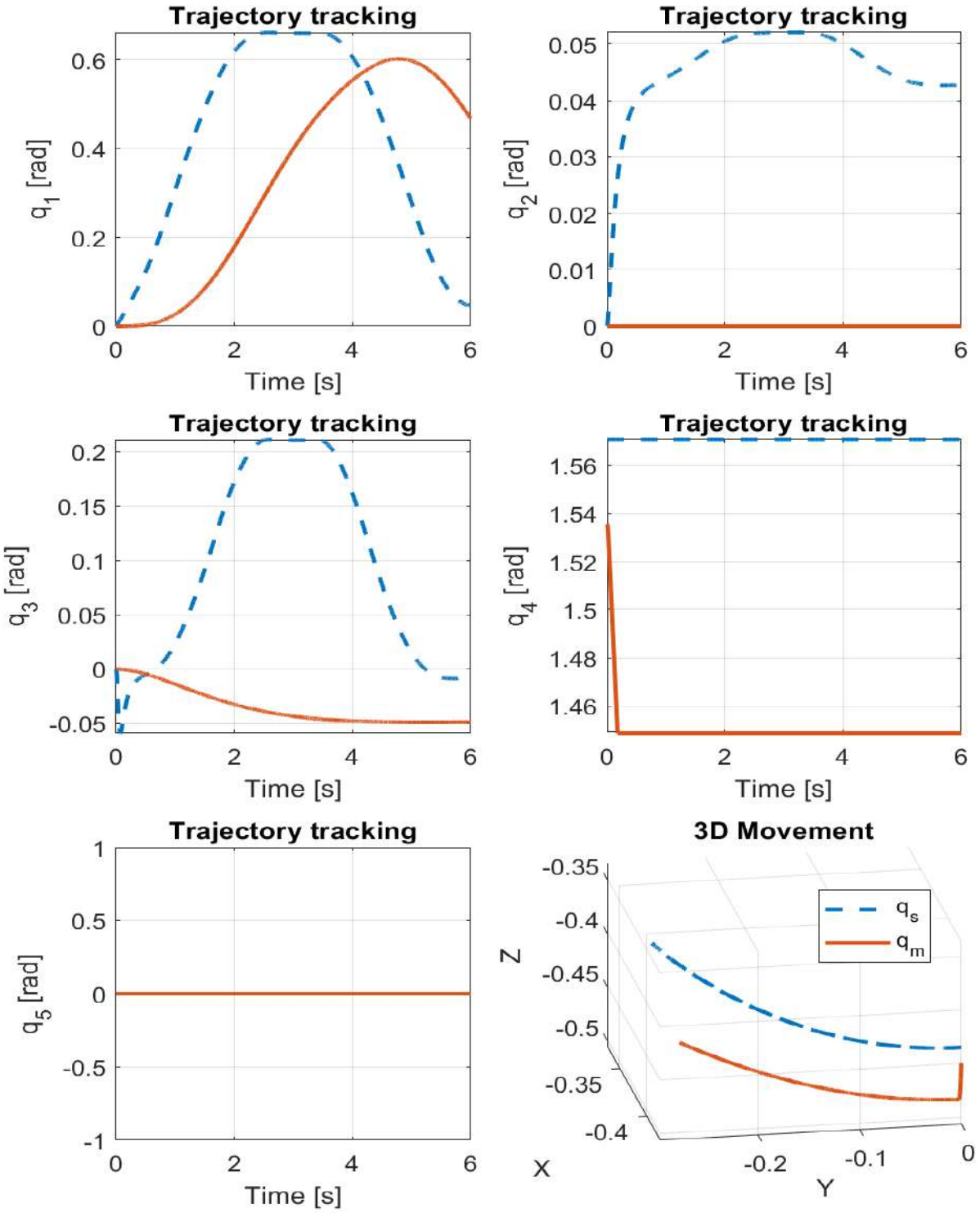

Figure 6.12: User 6: Trajectory tracking (shoulder internal-external rotation movement). Simulated trajectory (blue dashed line) and measured trajectory (orange line).

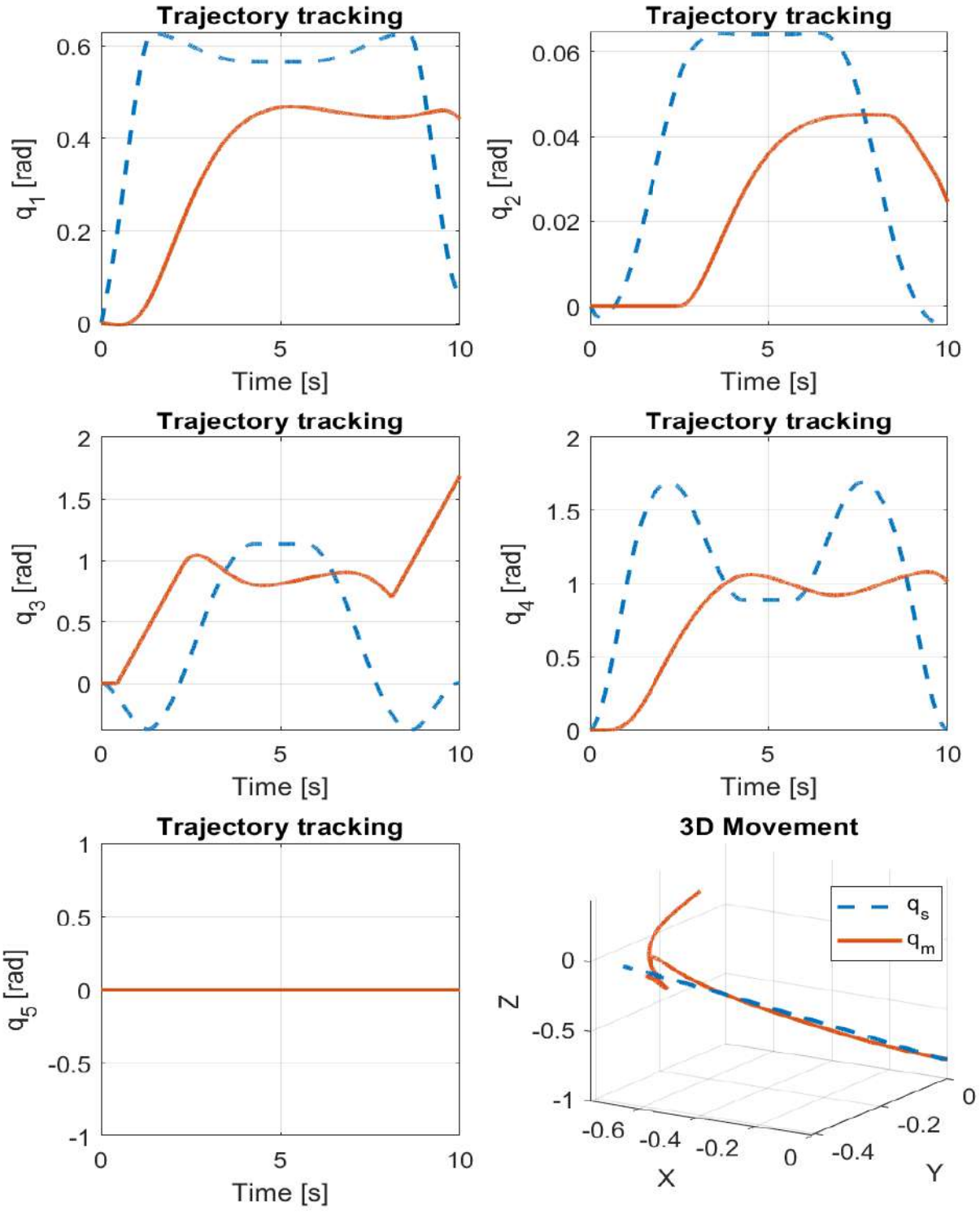

Figure 6.13: User 6: Trajectory tracking (diagonal movement). Simulated trajectory (blue dashed line) and measured trajectory (orange line).

It is worth noting that, in the case of user 4 (refer to Table 6.9), a significant RMSE was observed in the internal-external rotation movement of the shoulder, attributable to the user's particular health condition.

Table 6.10: RMSE: Complex movement (diagonal)

User	$q_1[rad]$	$q_2[rad]$	$q_3[rad]$	$q_4[rad]$	$q_5[rad]$
5	0.19	0.08	0.91	0.58	0.00
6	0.26	0.03	0.78	0.65	0.00
7	0.16	0.02	1.13	0.46	0.00
8	0.22	0.05	0.78	0.74	0.00
9	0.23	0.08	0.81	0.83	0.00
Mean	0.21	0.05	0.88	0.65	0.00

The RMSE data shows that the mean errors were 0.09 radians, 0.11 radians, and 0.35 radians for the elbow flexion-extension, shoulder internal-external rotation, and diagonal movements, respectively.

In single movements, it is noticeable that the joint directly involved in the motion exhibits a higher average error than the others. On the other hand, in the case of complex movements, a greater error is recorded compared to single movements. This disparity is due to the serial design of the robot (where an error in one joint directly affects the following ones) and the technical specifications of the actuators used.

Figures 6.14, 6.15, and 6.16 illustrate the torque estimation behavior of each user in every movement. It is important to note that torque behavior is influenced by the users' individual features, as errors vary depending on the movements executed by each individual.

Due to the nature of the application, it is necessary to use an optimal controller. Therefore, an advanced control technique is proposed that combines adaptive control with sliding modes and particle swarm optimization. This combination offers robustness and efficiency in handling complex and nonlinear systems. Sliding mode control provides a robust strategy against system uncertainties and disturbances, ensuring stable and precise performance. On the other hand, particle swarm optimization, inspired by the social behavior of animals such as birds and fish, dynamically and efficiently optimizes system parameters.

By applying these techniques in the context of an upper limb exoskeleton, the aim is to improve user assistance and rehabilitation, achieving more natural movements that adapt to the individual needs of each patient. This strategy will be developed and described in Chapter 7, within the context of the ETS-MARSE exoskeleton, created by the École de technologie supérieure (ÉTS) in Montreal, where I completed a stay.

In addition to conducting the evaluation described in Figure 6.2, an analysis of the device as a product designed to fulfill a specific objective in a particular environment was carried out. This analysis focused on the tests conducted on users to gather data for evaluating the quality indicators of the developed device. To achieve this, the process outlined in Figure 6.17 was followed, and the results obtained are presented in Table 6.11.

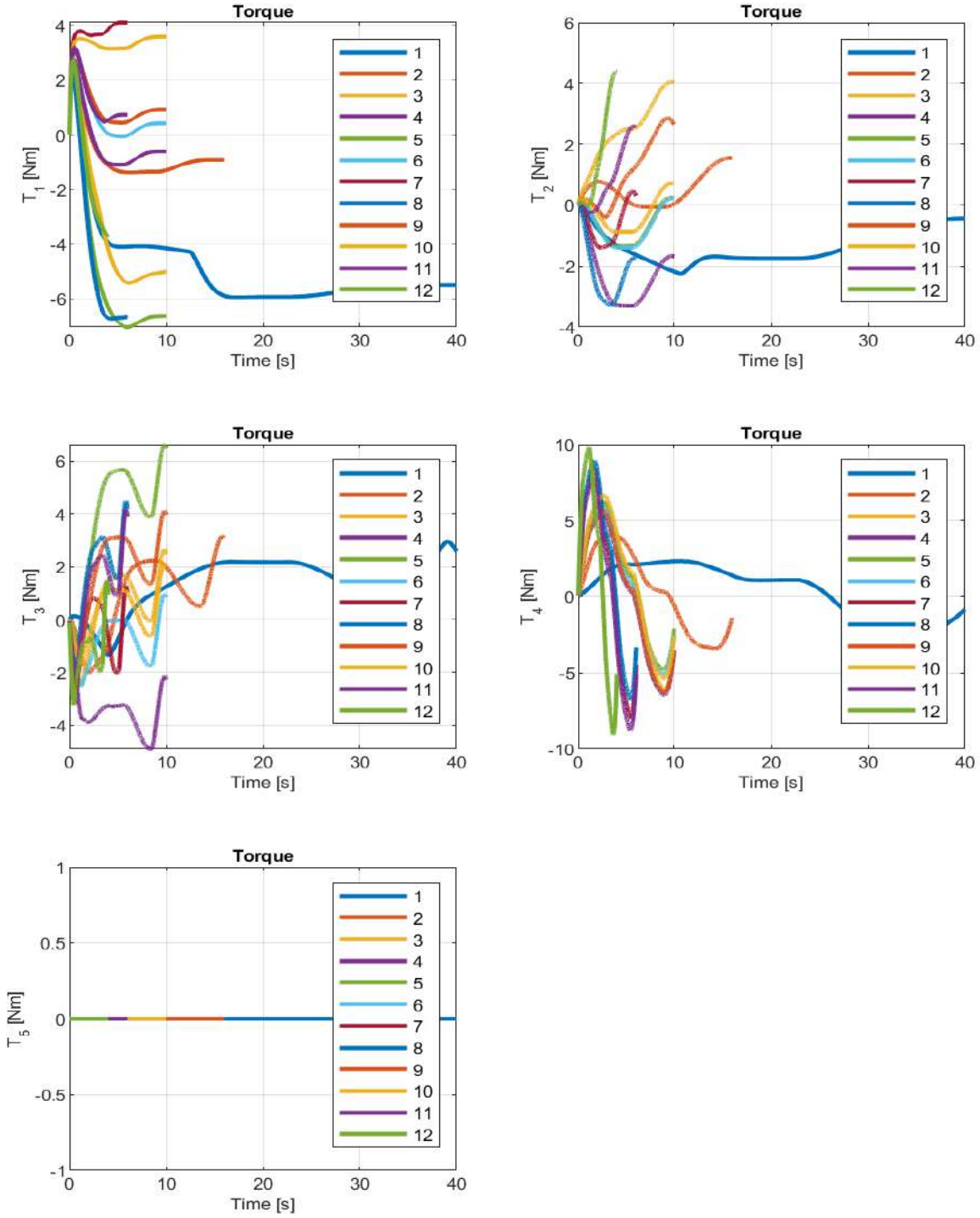

Figure 6.14: Users Torque: Elbow flexion-extension movement

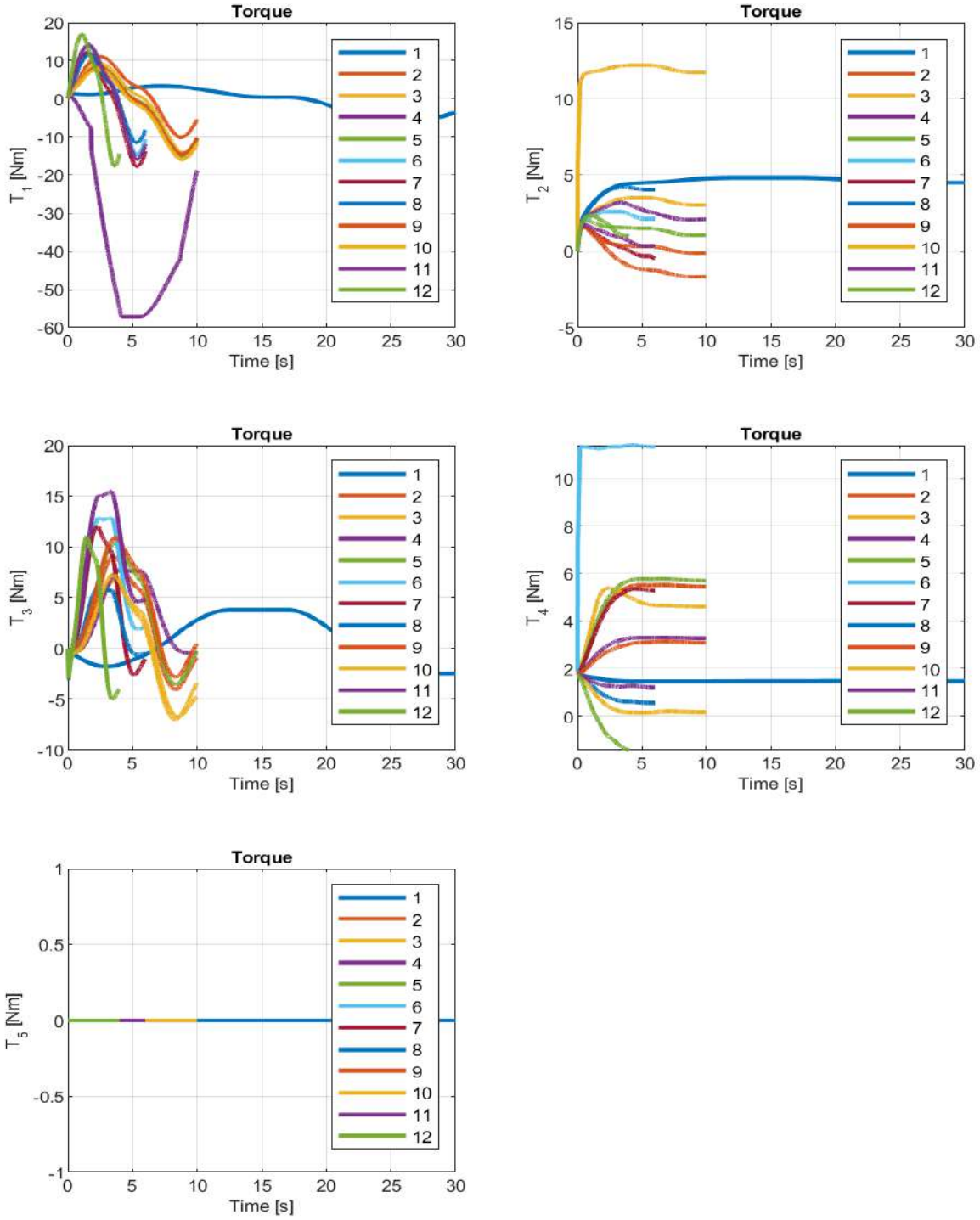

Figure 6.15: Users Torque: Shoulder internal-external rotation movement

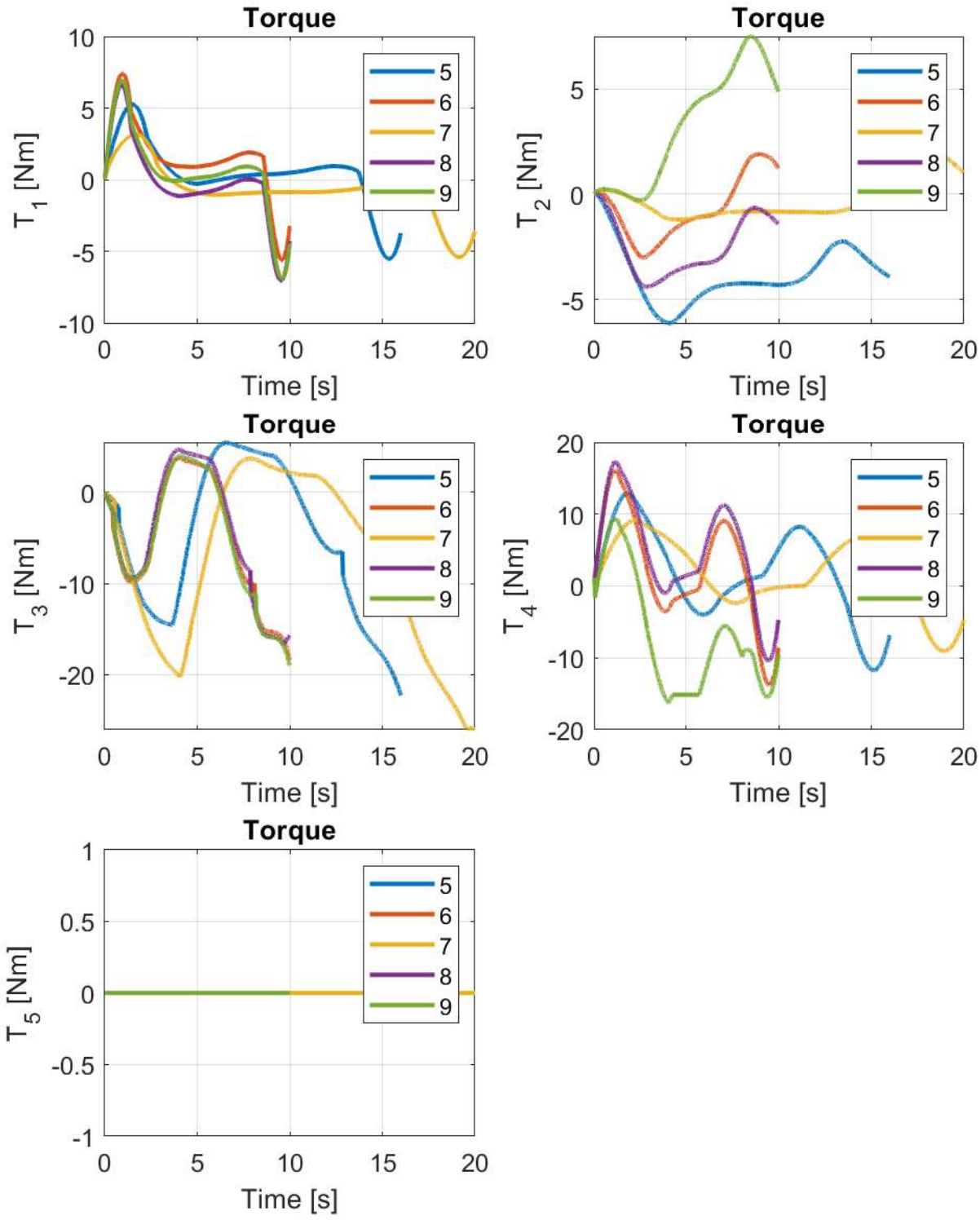

Figure 6.16: Users Torque: Diagonal movement

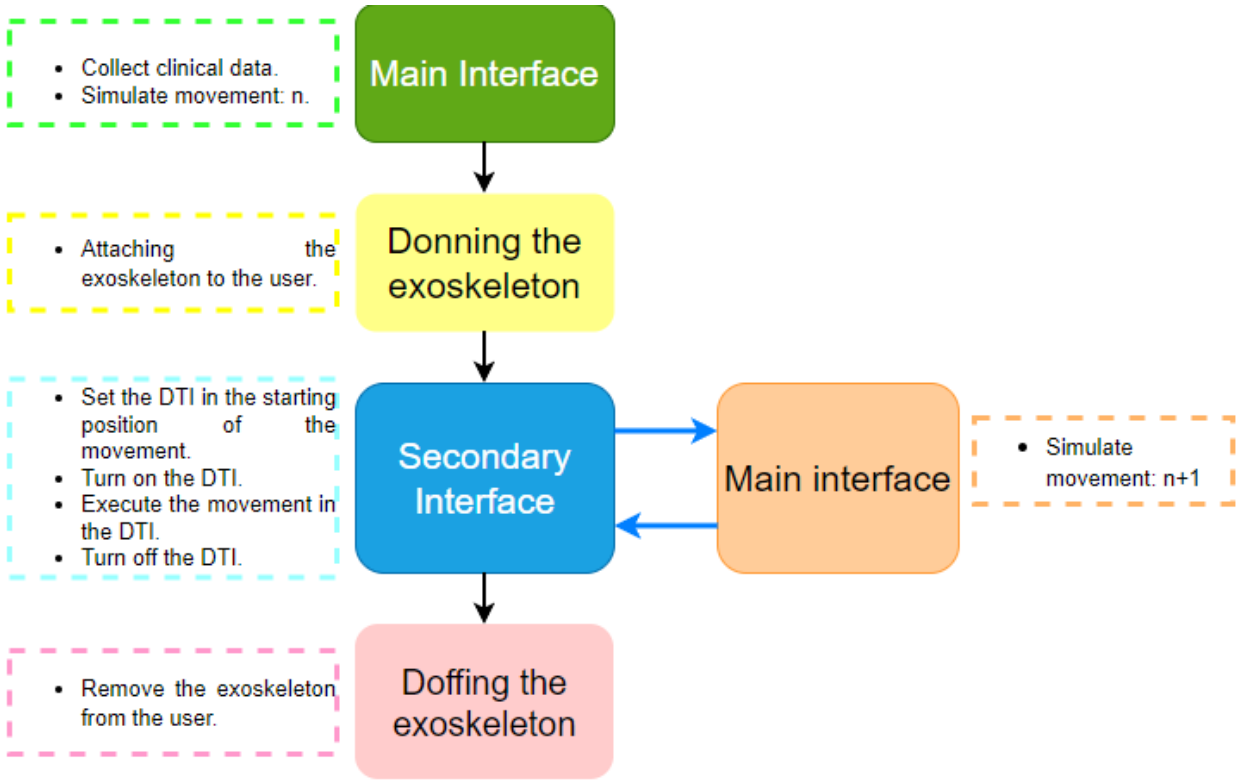

Figure 6.17: Procedure carried out in the tests with patients

Table 6.11: Description of the attempts made with the system (TE= It took two attempts due to technical errors in the device. PTE= The physiotherapist finished the task with 1 error. OP= Opposition to the movement.)

Attempt	Time [s]					Remarks
	Main Interface	Donning the exoskeleton	Secondary interface	Doffing the exoskeleton	Total	
U1-EF	96.00	125.00	84.00	18.00	503.00	
U1-ER	82.00		98.00			
U2-EF	115.00	90.00	33.00	13.00	386.00	TE
U2-ER	70.00		65.00			
U3-EF	62.00	81.00	56.00	24.00	308.00	PTE
U3-ER	35.00		50.00			
U4-EF	240.00	192.00	56.00	26.00	620.00	PTE
U4-ER	57.00		49.00			OP.
U5-EF	142.00	101.00	66.00	25.00	664.00	
U5-ER	48.00		78.00			
U5-D	62.00		142.00			PTE
U6-EF	184.00	81.00	39.00	24.00	526.00	
U6-ER	33.00		87.00			TE
U6-D	32.00		46.00			

Attempt	Time [s]					
	Main Interface	Donning the exoskeleton	Secondary interface	Doffing the exoskeleton	Total	Remarks
U7-EF	155.00	96.00	63.00	19.00	528.00	
U7-ER	36.00		67.00			
U7-D	41.00		51.00			
U8-EF	151.00	59.00	82.00	22.00	549.00	PTE
U8-ER	66.00		53.00			
U8-D	54.00		62.00			
U9-EF	108.00	105.00	40.00	14.00	399.00	
U9-ER	46.00		31.00			PTE
U9-D	26.00		29.00			TE
U10-EF	108.00	169.00	34.00	15.00	401.00	
U10-ER	32.00		43.00			
U11-EF	105.00	44.00	36.00	12.00	241.00	
U11-ER	21.00		23.00			
U12-EF	88.00	44.00	21.00	14.00	222.00	
U12-ER	36.00		19.00			

The results presented in Table 6.11 indicate that the average times for donning and doffing the exoskeleton from the patient were 98.91 seconds (1.64 minutes) and 18.83 seconds (0.31 minutes), respectively. Additionally, the mean time for patients who performed two movements was 383 seconds (6.38 minutes), while for those who performed three movements, it was 533.20 seconds (8.88 minutes).

The mean time each physiotherapist used the device with each patient was 445.58 seconds (7.42 minutes), and the mean time to perform each movement was 184.37 seconds (3.07 minutes). It is important to note that the execution times of each activity, as shown in Figure 6.17, depend on the individual skills of each physiotherapist and the conditions of each patient. Overall, it was observed that the times taken for each activity were faster in the case of healthy users.

Below are the main usability metrics considered as quality indicators. In this context, each individual movement performed by the device was regarded as an attempt.

Task success rate (TSR): Evaluates the effectiveness of the device based on the percentage of tasks completed successfully. As indicated in Table 6.11, three technical failures were observed. Therefore, out of the 32 attempts made, 29 were successful, resulting in a success rate of 90.62% (see Equation 6.1).

$$TSR = \frac{29}{32} = 90.62\% \tag{6.1}$$

Time required to complete a task (TTR): Measures the effectiveness of the device by

determining the time needed to complete a specific movement. In this case, the average time required for a therapist to perform a movement was 3.07 minutes (see Equation 6.2).

$$TTR = \frac{5347}{29} = 184.37s \tag{6.2}$$

User Error Rate (UER): Evaluates the effectiveness of the device by examining the frequency of failed inputs during attempts. In this situation, user errors refer to those indicated in the interface to physiotherapists during its use. Since the total number of possible errors in the interface is 14, the obtained result was 1.11% (see Equation 6.3).

$$UER = \frac{5}{32 * 14} = 1.11\% \tag{6.3}$$

According to the results obtained in TSR and UER, it was observed that the rate of technical errors was less than 10% in the conducted tests. Furthermore, the percentage of error attributable to users (physiotherapists) was 1.11%, suggesting that the device's effectiveness is acceptable.

Although the device has been comprehensively evaluated, it is important to note that the study presented some limitations: a) the time and number of tests to evaluate the interface and exoskeleton were limited. To reduce or avoid the number of errors by physiotherapists, it would be necessary to use the device and its interface for a longer period, which would contribute to improving the learning curve and adaptability of the device. b) The number of participants in the study was the minimum required for usability testing, so it is suggested to increase their quantity in future work. c) The clinically significant rehabilitation outcomes in the treatment of upper limb pathologies were not evaluated due to the limited duration of the trials.

Thanks to the results obtained in this evaluation stage, the effectiveness of the device regarding its mechanical design, implemented control strategies, and developed human-robot interface was confirmed, as well as its usability and the satisfaction level of users and physiotherapists. Although areas for improvement were identified in these aspects, an initial comprehensive engagement with all stakeholders was achieved, and improvement points were defined to be addressed in future work.

Chapter 7

ETS-MARSE: Sliding Mode Controller Gain Tuning Using Particle Swarm Optimization

"Optimization is essential to overcome the most challenging obstacles and reach new horizons in research".

Stephen Hawking.

This doctoral thesis aims to get the international mention, then according to the regulation, a research intership was carried out at the École de Technologie Supérieure (ETS) in Montreal, Canada.

Two primary challenges in controlling robotic rehabilitation devices are the uncertainties in mathematical models and, more importantly, the need for controllers capable of adapting to dynamic changes in human-robot interaction. To tackle these issues, this section proposes employing the particle swarm optimization (PSO) algorithm for the real-time adjustment of gains in the sliding mode controller (SMC) based on the exponential reaching law (ERL). The proposed approach was designed for a 7 DOF robotic exoskeleton used in upper-limb physical rehabilitation (Figure 7.1). The optimization algorithm aims to minimize tracking errors in rehabilitation exercises, through the robust ERL controller applied to nonlinear systems with external perturbations. Below are the mathematical analyses of this approach (Exoskeleton's uncertain dynamic model, convergence of algorithms, etc).

The following sections show the dynamical model of the exoskeleton (nonlinear considering external perturbations), the controller (features, stability analysis, etc.), the mathematical aspects of the PSO algorithm, the implementation conditions, experimental results and analyses obtained.

Figure 7.1: ETS-Marse Exoskeleton

7.1 Mathematical foundations

7.1.1 Exoskeleton's uncertain dynamic model

During physical therapy treatments, patients wear the exoskeleton for purposes that may be rehabilitation and/or assistance. Due to this, there are coupled systems with two different dynamics (human and exoskeleton), so they must be considered in the real application.

An adaptive controller is required for nonlinear systems that adapt to model uncertainties and external disturbances. So, the dynamics of the ETS-MARSE robot are presented in joint space as follows (Bedolla-Martinez et al., 2023):

$$M(\theta)\ddot{\theta} + C(\theta,\dot{\theta})\dot{\theta} + G(\theta) + F(\dot{\theta}) = \tau_o + \tau_d \tag{7.1}$$

where: $\theta \in \mathbb{R}^{n\times 1}$ containing the joint angular position, $\dot{\theta} \in \mathbb{R}^{n\times 1}$ vector containing the joint angular velocity, $\ddot{\theta} \in \mathbb{R}^{n\times 1}$ vector containing the joint angular acceleration, $M(\theta) \in \mathbb{R}^{n\times n}$ is the inertial matrix, $C(\theta,\dot{\theta}) \in \mathbb{R}^{n\times n}$ is centrifugal and Coriolis terms, $G(\theta) \in \mathbb{R}^{n\times 1}$ is gravitational forces, $F(\dot{\theta}) \in \mathbb{R}^{n\times 1}$ is characterizing nonlinear Coulomb friction, $\tau_o \in \mathbb{R}^{n\times 1}$ denotes the generalized torque vector, and $\tau_d \in \mathbb{R}^{n\times 1}$ represents the vector of unknown disturbing forces originating from the patient with n equal to 7 (number of joints). Consider the following relations:

$$M = M_o + M_u \tag{7.2}$$
$$C = C_o + C_u \tag{7.3}$$
$$G = G_o + G_u \tag{7.4}$$

where: the terms with subscript "o" represent the nominal part and terms with subscript "u" represent the unknown part for M, C, and G.

Isolating $\ddot{\theta}$ from Equation (7.1), we obtain Equation (7.5):

$$\ddot{\theta} = M_o^{-1}(\theta)[\tau_o - C_o(\theta, \dot{\theta})\dot{\theta} - G_o(\theta)] + U_u \tag{7.5}$$

where: U_u includes the unknown variables shown in Equation (7.6), and $M_o(\theta)$ is a symmetric matrix that is positive definite, ensuring the availability of $M_o^{-1}(\theta)$.

$$U_u = M_o^{-1}(\theta)[\tau_d - M_u(\theta)\ddot{\theta} - C_u(\theta, \dot{\theta})\dot{\theta} - G_u(\theta) - F(\dot{\theta})] \tag{7.6}$$

A compensatory torque derived from the nominal components of (7.1) is:

$$\tau_o = M_o(\theta)\nu(t) + C_o(\theta, \dot{\theta})\dot{\theta} + G_o(\theta) \tag{7.7}$$

where $\nu(t)$ represents the virtual control that guides the system toward the goal of control, to be designed later. Substituting Equation (7.7) in Equation (7.5), the following uncertain linear system is obtained.

$$\ddot{\theta} = \nu(t) + U_u \tag{7.8}$$

7.1.2 Proposed controller

The initial step involves selecting the sliding surface S based on the tracking error, as expressed in Equation (7.9). This indicates that upon reaching the sliding surface, the tracking error decreases to zero. The rate of convergence is linked to the value of Λ_i.

$$S_i = \Lambda_i e_i + \dot{e}_i \tag{7.9}$$

where the tracking error is calculated as $e_i = \theta_{di} - \theta_i$, where θ_{di} denotes the desired trajectory, and θ_i represents the measured angular position.

The subsequent phase includes choosing the control law ν that facilitates the error convergence toward the sliding surface. To achieve this, the following condition must be fulfilled:

$$S_i \dot{S}_i < 0 \qquad \forall t$$

A controller based on sliding modes with ERL was chosen for nonlinear systems, whose typical reaching law is as shown in Equation (7.10):

$$\begin{aligned} \dot{S}_i =& -\frac{K_i}{D(S_i)} \text{sign}(S_i) \\ D(S_i) =& \varsigma_i + (1-\varsigma_i) e^{-\rho_i |S_i|^{h_i}} \end{aligned} \tag{7.10}$$

$$\text{sign}(S_i) = \begin{cases} 1, & \text{for } S_i > 0 \\ 0, & \text{for } S_i = 0 \\ -1, & \text{for } S_i < 0 \end{cases}$$

where K_i is a strictly positive gain, ς_i is a strictly positive offset less than one ($0 < \varsigma_i < 1$), h_i is a positive integer greater than zero ($h_i > 0$), and ρ_i is also a positive integer greater than zero ($\rho_i > 0$).

Relation (7.10) has the following features:

- In the event of an increase in $|S_i|$, $D(S_i) \to \varsigma_i$, leading to the convergence of $K_i/D(S_i)$ towards K_i/ς_i. Consequently, during the reaching phase, $K_i/D(S_i)$ increases, resulting in a faster attraction towards the sliding surface.
- In the case of a decrease in $|S_i|$, $D(S_i) \to 1$, causing $K_i/D(S_i)$ to converge to K_i. Consequently, $K_i/D(S_i)$ gradually decreases, thereby mitigating chattering.

Thus, the ERL does not impact the stability of control through sliding modes since $D(S_i)$ remains strictly positive. Additionally, it enables the controller to dynamically adapt to changes in the sliding surface by permitting the variation of $K_i/D(S_i)$ within the range of K_i to K_i/ς_i.

It is crucial to emphasize that the abrupt term $K_i sign(S_i)$ in Equation (7.10) frequently results in heightened control activity, commonly referred to as chattering (an undesirable phenomenon). To address this concern, the paper employs a smoothed fragmented term in the control input, as illustrated in Equation (7.11):

$$\dot{S}_i = -\frac{K_i}{D(S_i)} \text{sat}\left(\frac{S_i}{\psi_i}\right) \qquad \forall t, K_i > 0 \tag{7.11}$$

where:

$$\text{sat}\left(\frac{S_i}{\psi_i}\right) = \begin{cases} 1, & \text{for } S_i \geq \psi_i \\ \frac{S_i}{\psi_i}, & \text{for } -\phi_i \leq S_i \leq \psi_i, \forall t, 0 < \psi_i \ll 1 \\ -1, & \text{for } S_i \leq \psi_i \end{cases}$$

By employing this substitution, the system's convergence is restricted to a boundary layer surrounding the sliding surface. The size of this neighborhood is directly determined by the parameter ψ_i. Therefore, the Equation (7.11) effectively addresses chattering issues and enhances tracking performance.

According with the Equations (7.5), (7.9) and (7.11), we obtain ν_i :

$$\nu_i = \ddot{\theta}_{di} + \Lambda_i \dot{e}_i + \frac{K_i}{D(S_i)} \text{sat}\left(\frac{S_i}{\psi_i}\right) \tag{7.12}$$

The online tuning process will determine the optimal values of the variables K_i and Λ_i, which adjust to changes during the trajectory tracking.

Controller stability analysis

To assess the stability of the controller, Equation (7.13) is chosen as the Lyapunov function.

$$H(S_i) = \frac{1}{2} S_i^2 \tag{7.13}$$

Hence, if $\dot{H} < 0$, it indicates $\dot{S}_i < 0$ for $S_i > 0$ and $\dot{S}_i > 0$ for $S_i < 0$ (refer to Equation (7.14)). This leads to the emergence of a switching phenomenon to uphold the condition $S_i \dot{S}_i < 0$.

$$\dot{H}(S_i) = S_i \dot{S}_i \tag{7.14}$$

where:

$$\dot{S}_i = \Lambda_i \dot{e}_i + \ddot{e}_i \tag{7.15}$$

$$\ddot{e}_i = \ddot{\theta}_{di} - \ddot{\theta}_i \tag{7.16}$$

Replacing Equations (7.15), (7.16) and (7.12) into (7.14), we obtain:

$$\dot{H}(S_i) = S\left(\frac{-K_i}{D(S_i)} \text{sat}\left(\frac{S_i}{\psi_i}\right) - U_{ui}\right) \tag{7.17}$$

To ensure asymptotic stability the following inequality must be satisfied:

$$|U_{ui}| < \frac{K_i}{D(S_i)} \tag{7.18}$$

where: U_{ui} represents the unknown dynamics (external disturbances and model uncertainties), which is assumed to be locally continuous and limited by $Umax_i$ (Equation (7.19))

$$0 < |U_{ui}| \leq Umax_i < \infty \tag{7.19}$$

7.1.3 Particle swarm optimization algorithm

Kennedy and Eberhart introduced the conventional PSO algorithm in 1995. This metaheuristic draws inspiration from the collaborative behavior observed in fish and birds, relying on the cooperation of agents through the sharing of information. Within the PSO algorithm, every agent is regarded as a particle, functioning as a potential solution in an optimization problem (Gopal et al., 2020, Trelea, 2003).

The fundamental model involves initializing a population with randomly selected solutions within the search space. The objective is to discover the optimal solution, with each particle continuously refining its behavior over iterations, leveraging its own experiences and insights gleaned from the top-performing particles within the swarm (Belkadi et al., 2017, J. Wang et al., 2021). Every particle is defined by vectors representing its position and velocity (Equation (7.20)).

$$X_i(t+1) = X_i(t) + V_i(t+1) \tag{7.20a}$$
$$V_i(t+1) = \omega V_i(t) + c_1 s_1 [P_b(t) - X_i(t)] + c_2 s_2 [P_g(t) - X_i(t)] \tag{7.20b}$$

where: X_i denotes the particle position, V_i denotes the particle velocity, P_b denotes the best individual position of each particle i, P_g stands for the best global position of the entire swarm, and ω denotes the inertia weight assigned to each particle, c_1 and c_2 denote the cognitive and social acceleration coefficients specific to each particle, where s_1 and s_2 denote two random numbers chosen independently from the interval [0,1], respectively.

The main three parameters of the PSO algorithm are: 1) inertial weight (ω), 2) the cognitive acceleration parameter (c_1) and 3) the social acceleration (c_2).These parameters impact the algorithm's ability to conduct both global and local searches, and their summarization is as follows: 1) the global search is enhanced with a large inertial weight, whereas the local search is enhanced with a small inertial weight; 2) if $c_1 > c_2$ then the global search is facilitated, and 3) if $c_2 > c_1$ then the local search is improved.

Convergence analysis

As the PSO is a stochastic algorithm, it is important to provide an overview of the convergence analysis. To this end, this subsection considers its deterministic version and presents its converge analysis based on the discrete-time dynamic system theory (Gopal et al., 2020, Chuan and Quanyuan, 2007, Belkadi et al., 2015, Belkadi et al., 2016).

In this case, the random numbers are replaced by their average (0.5), so Equation (7.20) can be written as below:

$$X_i(t+1) = X_i(t) + V_i(t+1) \tag{7.21a}$$
$$V_i(t+1) = \omega V_i(t) + c[P(t) - X_i(t)] \tag{7.21b}$$

where:

$$P(t) = \frac{c_1 P_b(t) + c_2 P_g(t)}{c_1 + c_2} \tag{7.22a}$$
$$c = \frac{c_1 + c_2}{2} \tag{7.22b}$$

The equations (7.21a)-(7.21b) are reformulated in matrix form as follows:

$$\begin{bmatrix} X_i(t+1) \\ V_i(t+1) \end{bmatrix} = A \begin{bmatrix} X_i(t) \\ V_i(t) \end{bmatrix} + BP(t) \tag{7.23}$$

$$A = \begin{bmatrix} 1-c & \omega \\ -c & \omega \end{bmatrix}, B = \begin{bmatrix} c \\ c \end{bmatrix}$$

where: $P(t)$ is the external input, while A and B correspond to the dynamical matrix and input matrix, respectively.

So, the time-dependent behavior of the PSO algorithm relies on the eigenvalues of the dynamic matrix A. These eigenvalues can be computed using Equation (7.24).

$$\det(\eta I - A) = 0 \tag{7.24}$$

The result of Equation (7.24) is shown in equation (7.25)

$$\eta^2 + (c - 1 - \omega)\eta + \omega = 0 \tag{7.25}$$

The eigenvalues $\eta_{1,2}$ are shown in equation (7.26)

$$\eta_{1,2} = \frac{\omega + 1 + c \pm \sqrt{\Delta}}{2} \tag{7.26}$$

where: $\Delta = (\omega + 1 - c)^2 - 4\omega$. Therefore, the effectiveness and convergence of the algorithm rely on the values assigned to the parameters ω and c.

The conditions derived from the eigenvalues given in Equation (7.26) are as follows: 1) $\omega < 1$, 2) $c > 0$, and 3) $2\omega - c + 2 > 0$.

The convergence region is illustrated in the (ω, c) plane, as depicted in Fig. 7.2 a). Regardless of the initial position and velocity, the particle will converge to its equilibrium position, as defined by Equations (7.22a) and (7.32), only if the algorithm parameters fall within this triangular region.

Before the convergence, the particle may exhibit the following behaviors:

1. When the eigenvalues of matrix A take on complex values, harmonic oscillations manifest around the equilibrium point. This equivalence is represented by Equation (7.27), and its domain in the plane is illustrated in Fig. 7.2 b).

$$\omega^2 + c^2 - 2\omega c - 2\omega - 2c + 1 < 0 \tag{7.27}$$

2. The oscillating pattern resembling zigzagging emerges near the equilibrium point when there is at least one eigenvalue of matrix A with a negative real part, whether it is a real or complex value. This relationship is expressed by either Equations (7.28) or (7.29), and its region in the plane is illustrated in Fig. 7.2 c).

$$\omega < 0 \tag{7.28}$$

$$\omega - c + 1 < 0 \tag{7.29}$$

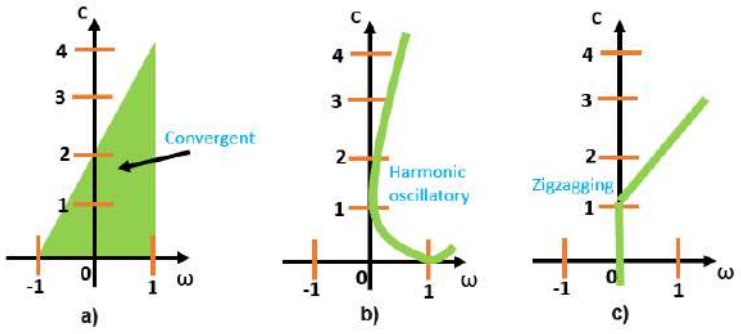

Figure 7.2: Region of dynamic behavior within the parameter space (ω, c): a) Convergence region, b) Harmonic oscillatory behavior and c) Zigzagging behavior. Information taken from (Trelea, 2003)

Equilibrium point

Typically, the particle's initial state is not in a state of equilibrium. In practice, it is crucial to determine whether the particle will eventually reach equilibrium, signifying the convergence of the optimization algorithm, and the trajectory it will traverse in the state space while exploring for optimal points.

Equation (7.23), can be written as follows:

$$Y_{(k+1)} = AY_k + BP(t) \tag{7.30}$$

where: $Y_k = [X_k, V_k]^T$

For an equilibrium point to exist, the Equation (7.31) must be satisfied for any k.

$$Y^{eq}_{(k+1)} = Y^{eq}_k \tag{7.31}$$

In the deterministic analysis, the particle must possess zero velocity and be positioned at the attraction point P (Eq. (7.22a)). Consequently, we derive Equation (7.32):

$$Y^{eq} = [P, 0]^T \tag{7.32}$$

It means $X^{eq} = P$ and $V^{eq} = 0$. Therefore, the equilibrium point is stable if and only if both eigenvalues of matrix A (real or complex) have magnitudes less than 1.

7.2 Implementation

In this study, the optimization of the ERL controller's tuning parameters (gains K_i and Λ_i) in the presence of external disturbances, such as initial offsets and variations among users, is formulated as an optimization problem and addressed using the PSO algorithm.

7.2.1 Exoskeleton description

The controller is applied to the ETS-MARSE (École de Technologie Supérieure - Motion Assistive Robotic-exoskeleton for Superior Extremity) with 7 DOF (Rahman, 2012), see Fig. 7.3. This exoskeleton facilitates rehabilitation by assisting movements for individuals with impaired upper extremities. Its design takes into account the alignment of the upper extremity, featuring 3 degrees of freedom (DOF) for the shoulder (S), 1 DOF for the elbow (E), and 3 DOF for the wrist (W). The modified Denavit-Hartenberg parameters (D-H) for the exoskeleton are detailed in Table 7.1.

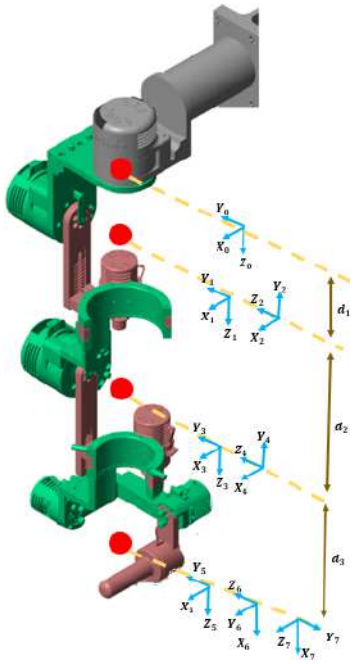

Figure 7.3: ETS MARSE: Exoskeleton.

Table 7.1: Modified D-H parameters

Movement	θ_i	a_{i-1}	α_{i-1}	d_i	Range [deg]
S: Horizontal Flex-Ext	θ_1	0	0	d_1	-20 to 70
S: Vertical Flex-Ext	θ_2	0	$-\frac{\pi}{2}$	0	-5 to 120
S: Int rot- Ext rot	θ_3	0	$+\frac{\pi}{2}$	d_2	-85 to 80
E: Ext-Flex	θ_4	0	$-\frac{\pi}{2}$	0	-5 to 115
W: Pron-sup	θ_5	0	$+\frac{\pi}{2}$	d_3	-85 to 85
W: Ext-Flex	$\theta_6 - \frac{\pi}{2}$	0	$-\frac{\pi}{2}$	0	-25 to 20
W: Ulnar-radial deviation	θ_7	0	$-\frac{\pi}{2}$	0	-55 to 60

The real-time system of the exoskeleton consists of three processing units, detailed as follows:

- Host PC (Intel Core i7-4770 CPU @3.4 GHz, and 16GB RAM): facilitates the transmission of higher-level controls to the exoskeleton via the human-machine interface (created in LabView 2017).
- A real-time PC (NI PXI-8108, Intel dual-core @2.53GHz processor and 8GB RAM): operates the top-level control and manages the dynamics of the exoskeleton with a sampling time of 1 ms.
- FPGA (NI PXI-7813R): Utilized for handling analog and digital inputs and outputs to the actuators and sensors, executing the low-level control (PI) current control loop with a sampling time of 50 μs.

The robot utilizes brushless DC motors, specifically Maxon EC-45 and Maxon EC-90, in combination with harmonic drives. Motors 1 and 2 have a gear ratio of 120:1, while motors 3-7 have a gear ratio of 100:1.

7.2.2 Tests description

In this section, we will describe the tests to be performed, which consider the following: A trajectory for passive rehabilitation will be executed on two healthy users (see Table 7.2 and Figure 7.4). This trajectory encompasses the motion of all exoskeleton joints, taking into account the modified D-H parameters as outlined in Table 7.1. The initial configuration positions the elbow joint at 90°.

Table 7.2: Users features

User	Sex	Age (years old)	Weight [kg]	Height [cm]
$User_1$	Male	33	75	160
$User_1$	Female	33	54	154

Figure 7.4: Exoskeleton with users: a) user 1 and b) user 2

To demonstrate the efficiency of using the PSO algorithm in adjusting the ERL controller gains, the following test will be performed:

1. Assess the performance of the ERL controller under pre-tuned gains, denoted as PT conditions.
2. Assess the real-time performance of the ERL controller through online tuning using PSO, denoted as PSO conditions.

3. Assess the performance of the ERL controller using the globally optimized gains obtained after applying the PSO algorithm, denoted as PSOG conditions.

First test

The gains were chosen heuristically and theirs values are shown in Table 7.3.

Table 7.3: ERL: Pre-tuned gains

Metric	q_1	q_2	q_3	q_4	q_5	q_6	q_7
K_i	50.0	20.0	90.0	60.0	250.0	500.0	450.0
Λ_i	90.0	40.0	70.0	20.0	25.0	10.0	10.0
ς_i	0.5	0.5	0.5	0.5	0.5	0.5	0.5
ρ_i	2.0	2.0	2.0	2.0	2.0	2.0	2.0
h_i	2.0	2.0	2.0	2.0	2.0	2.0	2.0
ψ_i	0.5	0.5	0.5	0.5	0.5	0.5	0.5

Second test

The ERL controller parameters vary over time and are adaptively tuned online. This flexibility allows for efficient tracking of trajectories, even when confronted with external disturbances like patient forces or physiotherapist assistance. The control scheme is depicted in Fig. 7.5.

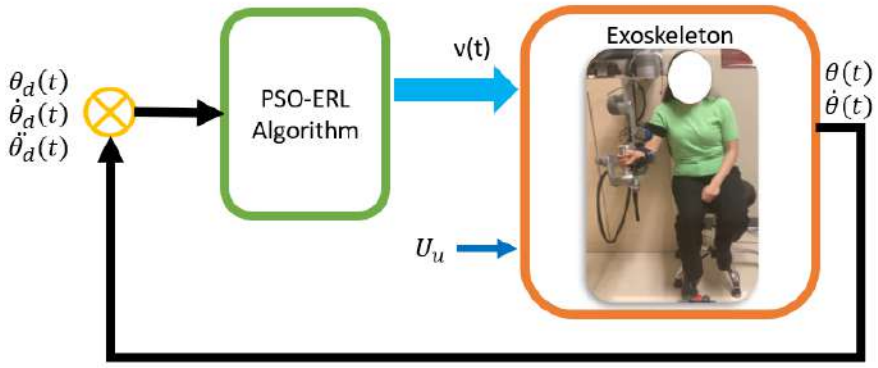

Figure 7.5: Control scheme.

Commonly, to address the optimization problem, a single objective function is used that encompasses all DOF. In this work, a weighted objective function is employed, it includes position and velocity errors for each degree of freedom (DOF), where position error is prioritized. So, the function targeted as the objective in the PSO algorithm is presented in equation (7.33).

$$f(e, \dot{e}) = \alpha\|e\| + \beta\|\dot{e}\| \tag{7.33}$$

Here, $\alpha + \beta = 1$, with α and β constrained to the ranges of 0 to 1.

In this scenario, each particle comprises the following two gains K_i and Λ_i. The goal is to dynamically identify the optimal particle in real-time, minimizing the objective function ($f(e, \dot{e})$). Algorithm 2 introduces the proposed robust PSO-ERL algorithm.

Algorithm 2 Proposed robust PSO-ERL algorithm.

1: Define the number of particles in the swarm, n.
2: Initialize the swarm with random values.
3: i←1
4: **repeat**
5: Insert a particle i (K_i, Λ_i)
6: Compute ν using the ERL approach Eq. (7.12)
7: Calculate $\tau_0(t)$ using Eq. (7.7).
8: Utilize τ_0 as the input for the system.
9: Compute the objective function f using Eq. (7.33).
10: Store the value of f for particle i.
11: i←i+1
12: **until i>m**
13: Determine $P_i(t)$ and $P_g(t)$.
14: Resolve Equation (7.20).
15: **GOTO 4**

In this case, Equation (7.20a) represents the value of the gain (K_i or Λ_i) and Equation (7.20b) represents the change rate of the value of the corresponding gain. The initial values of the particles (K_i and Λ_i) are randomly generated within their respective search space, as defined in Table 7.4. Subsequently, the objective function is calculated in each iteration to assess each particle, iteratively guiding the PSO-ERL to find the optimal solution. The particle exhibiting the minimum value of the objective function corresponds to the best global gain.

Table 7.4: Search space

Gains constraints	q_1	q_2	q_3	q_4	q_5	q_6	q_7
K_{min}	25	10	70	40	200	460	430
K_{max}	70	60	130	80	320	540	550
Λ_{min}	70	30	60	2	20	5	1550
Λ_{max}	100	80	110	28	70	40	1950

The remaining parameters for the PSO algorithm and the experimental conditions of the controller are detailed in Table 7.5.

To select the parameters in Table 7.5, we considered the following:

- $\omega \approx 1$: Promotes global exploration.
- $c_2 > c_1$: Global optimum is prioritized.
- $\gamma > \beta$: Prioritizing position error minimization.

Table 7.5: Experimental conditions (online gain tuning with PSO)

Metric	Value
Initial offset	5 [deg] in each joint
External disturbances (see Table 7.2)	2 healthy users
Number of particles (m)	30.0
ω (inertial factor of PSO)	0.9
c_1 (personal acceleration parameter of PSO)	0.1
c_2 (group acceleration parameter of PSO)	0.3
γ (objective function, f)	0.7
β (objective function, f)	0.3
ς (controller parameter, ERL)	0.5
ρ (controller parameter, ERL)	2.0
h (controller parameter, ERL)	2.0
ψ (controller parameter, ERL)	0.5

Once the second test was completed (applying the PSO algorithm to determine the gains K_i and Λ_i of the controller) the values of the global gains were obtained for each user, which are shown in Table 7.6.

Table 7.6: Global gains tuned with ERL+PSO

Metric	q_1	q_2	q_3	q_4	q_5	q_6	q_7
K_{User_1}	52.1	47.4	101.3	68.6	289.8	460.0	550.0
K_{User_2}	25.0	50.5	70.0	63.5	253.4	492.9	503.0
Λ_{User_1}	88.4	37.6	79.5	8.4	46.5	26.7	1654.7
Λ_{User_2}	99.9	80.0	94.1	17.4	24.9	10.4	1664.6

Third test

It consists of executing the ERL controller with the values of the gains shown in Table 7.6.

So, in the next section we perform a comparative analysis of the results obtained in the three experiments.

7.2.3 Experimental results and comparative analysis

Figures 7.6-7.9 show the results of the trajectory tracking, tracking error, control signals, and cartesian tracking and error graphs of user 1, respectively. And Figures 7.10-7.13 correspond to user 2. In each figure, there are 3 signals, each one corresponding to the experiments carried out (PT, PSO and PSOG).

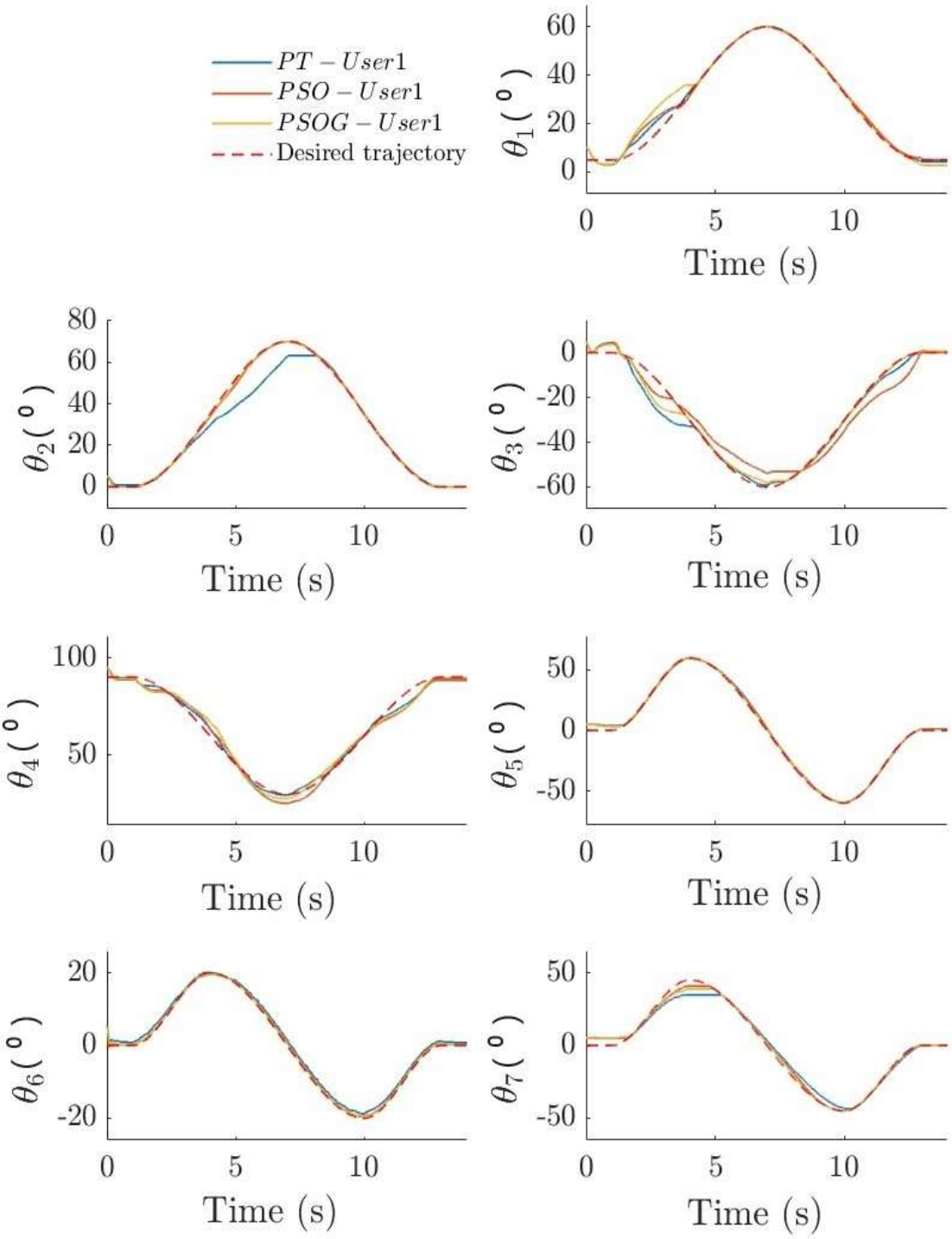

Figure 7.6: Trajectory tracking: User 1.

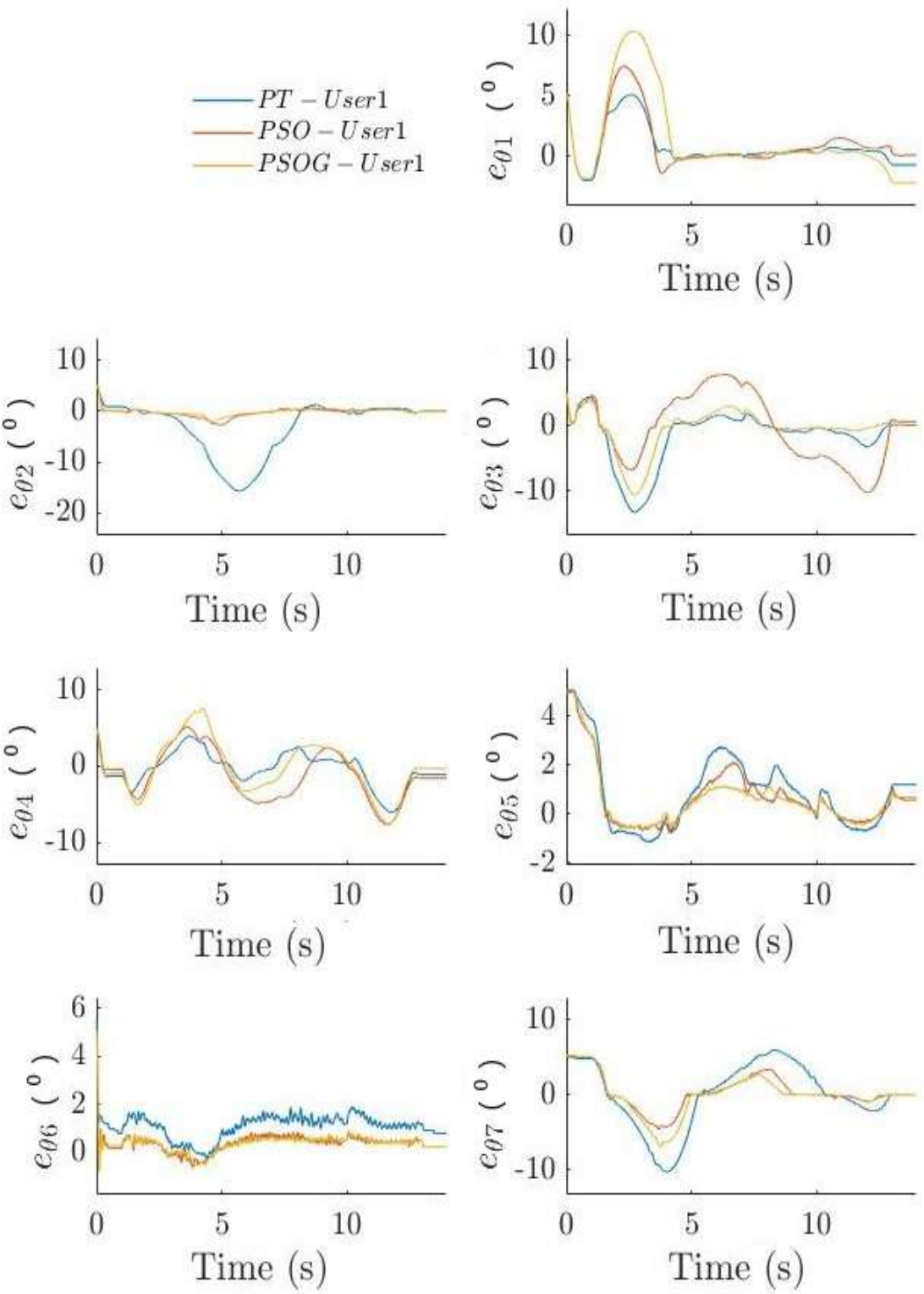

Figure 7.7: Tracking error: User 1.

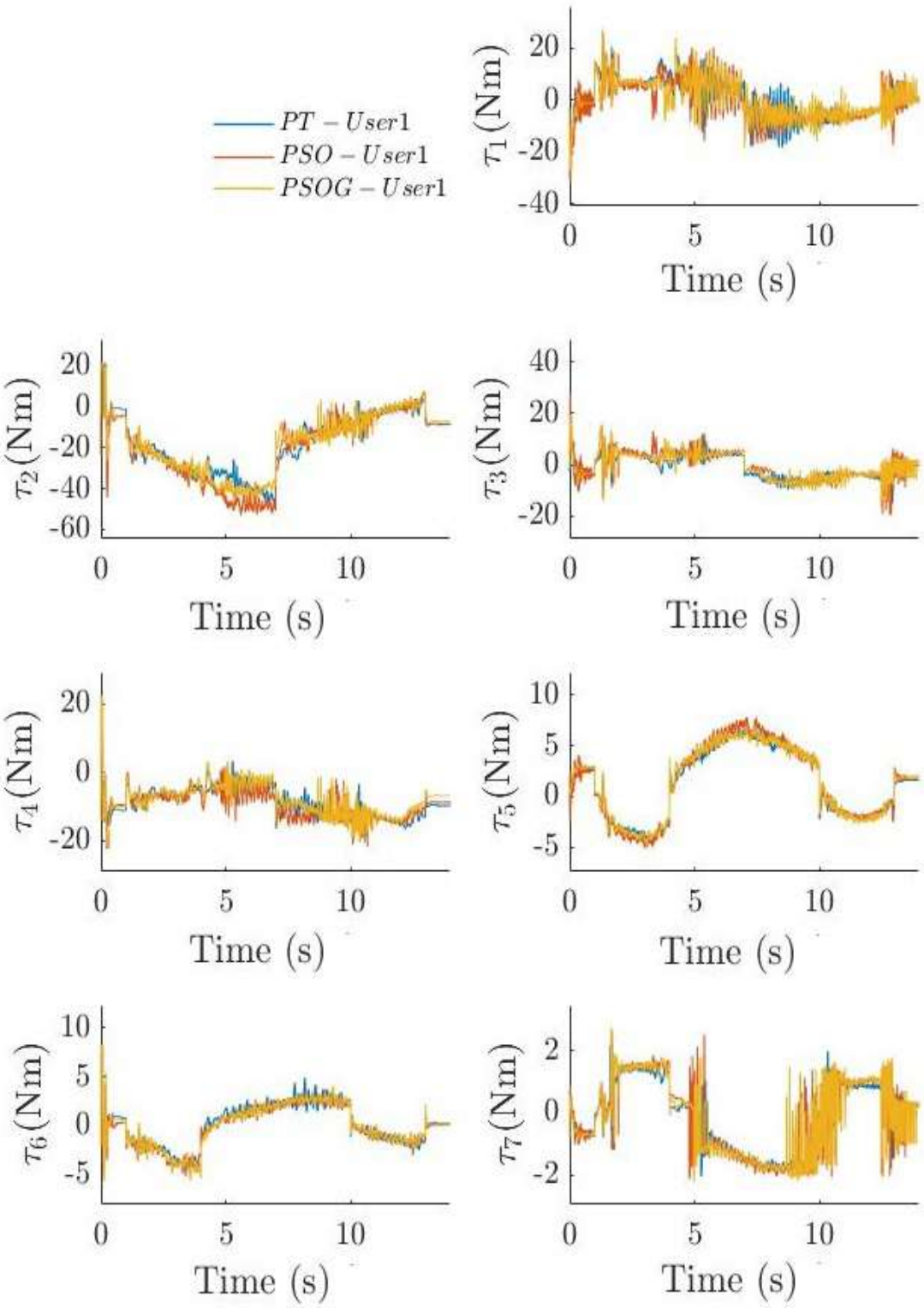

Figure 7.8: Control signal: user 1.

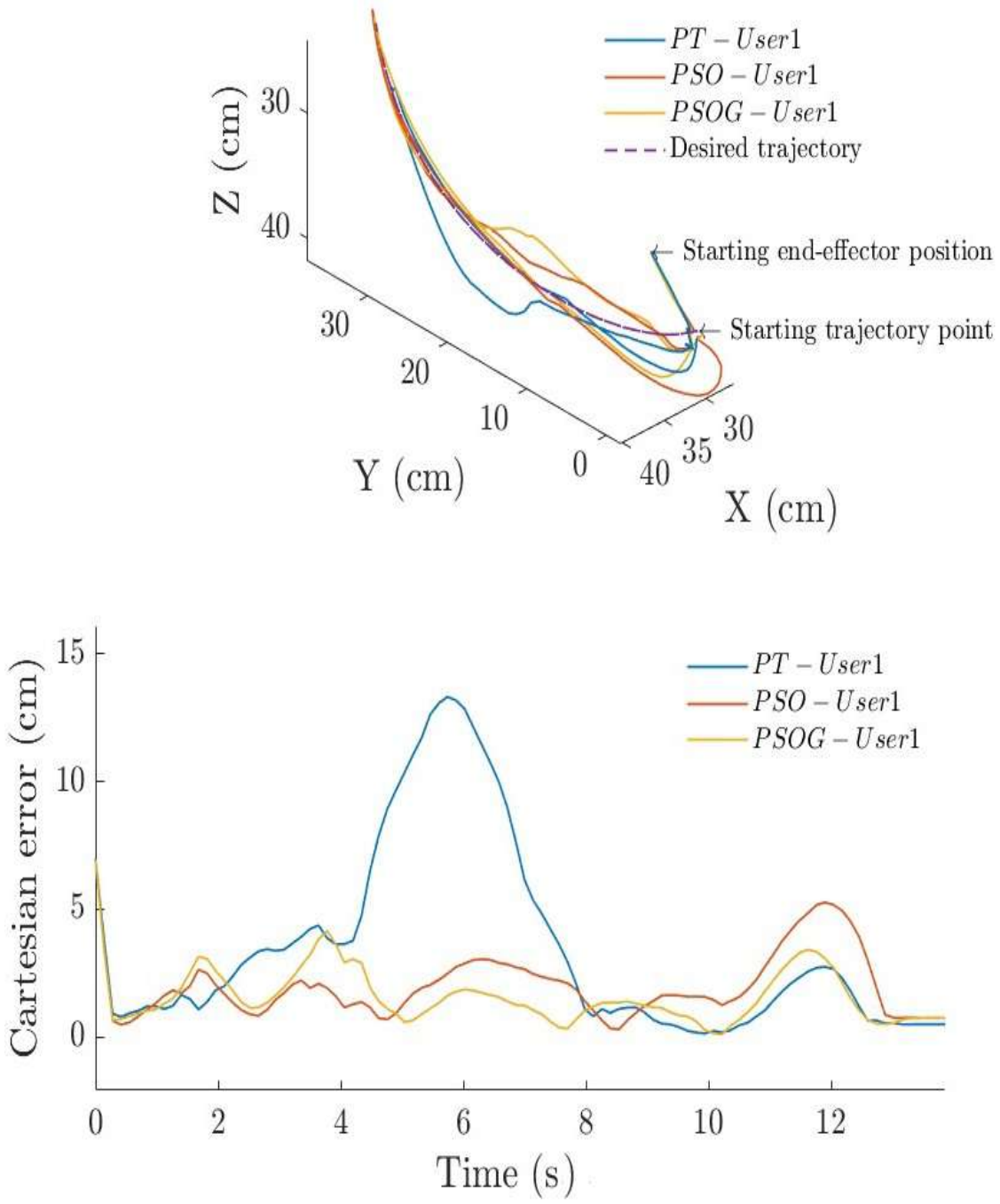

Figure 7.9: Cartesian tracking and error: user 1.

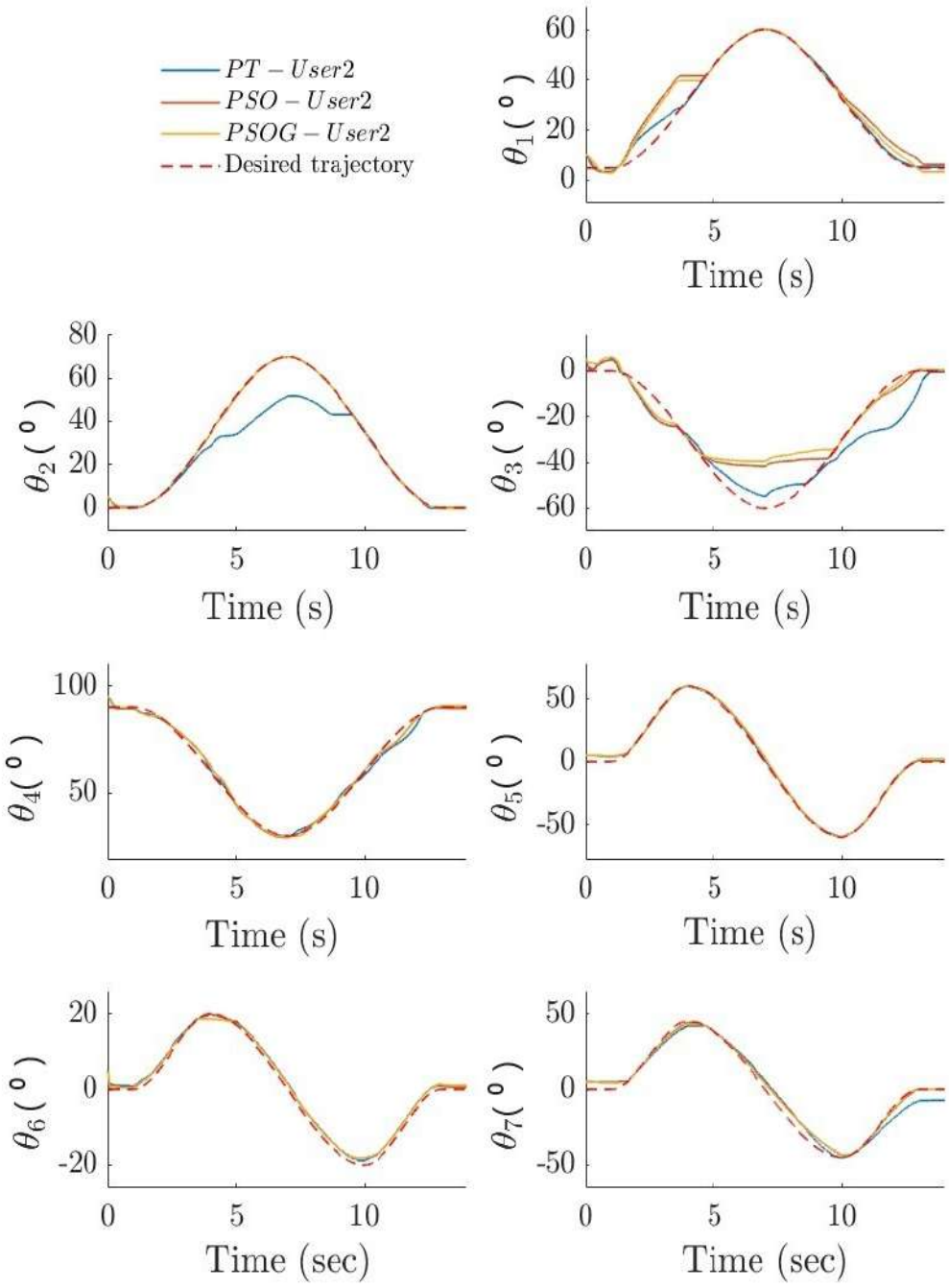

Figure 7.10: Trajectory tracking: User 2.

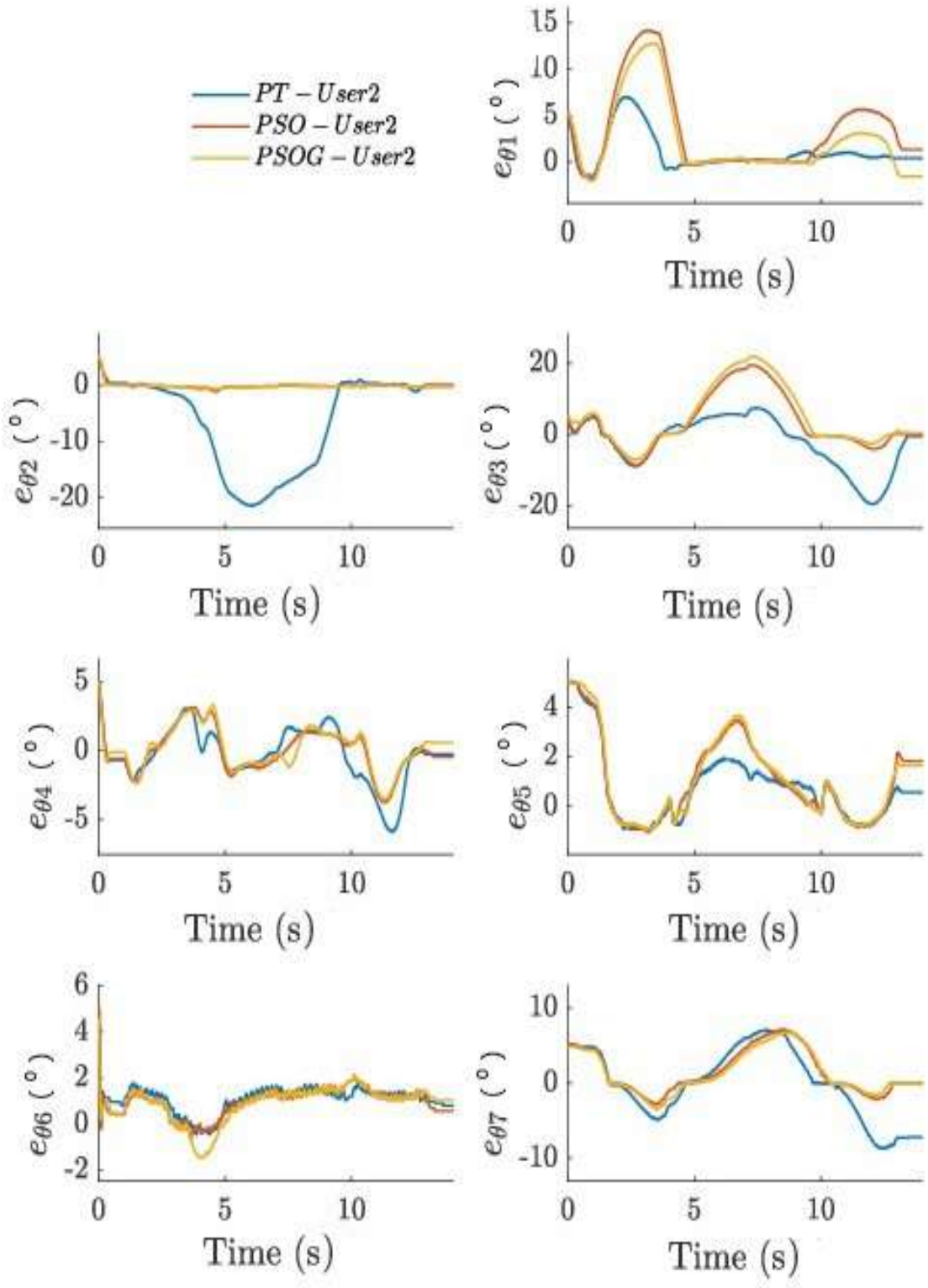

Figure 7.11: Tracking error: User 2.

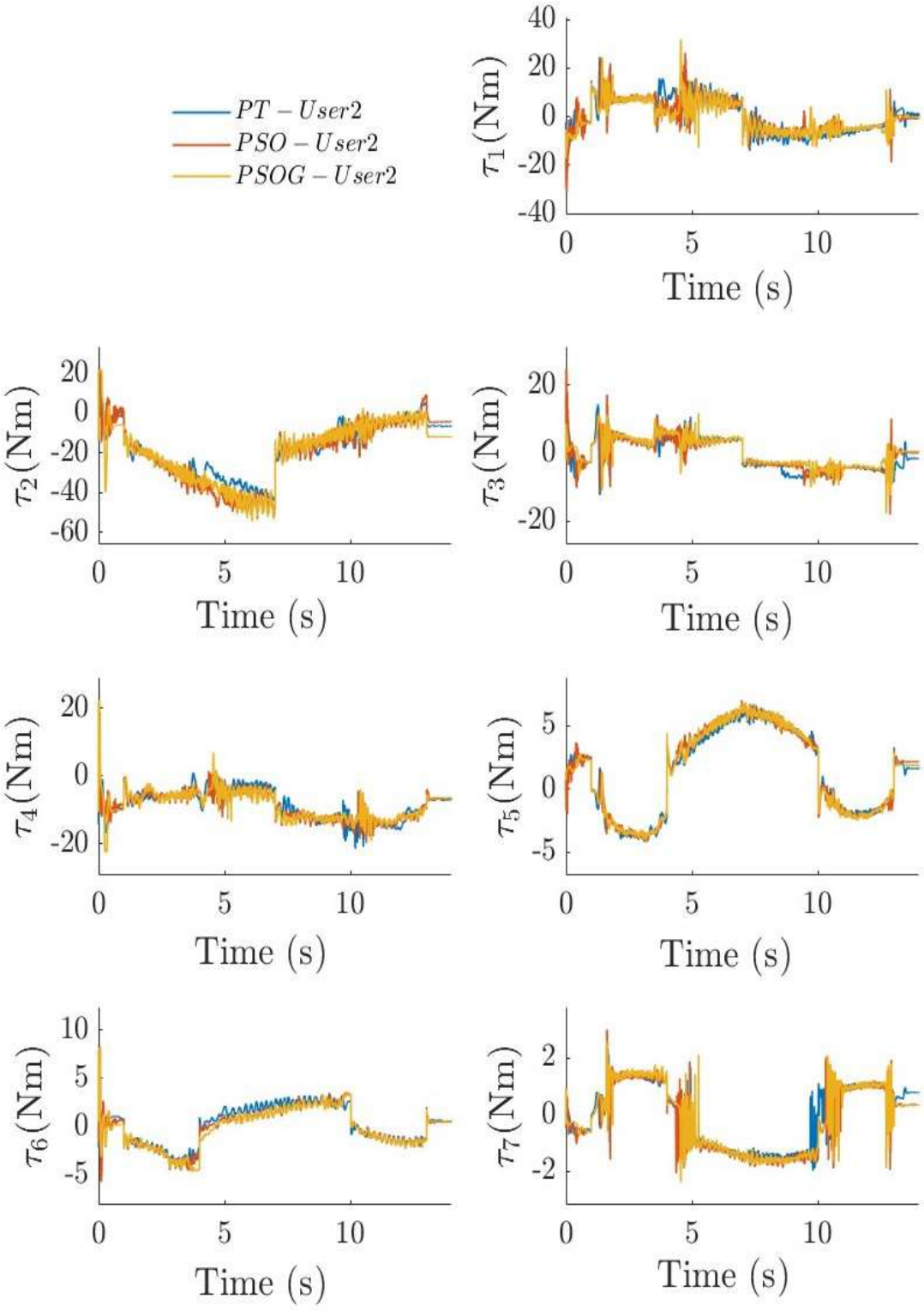

Figure 7.12: Control signal: user 2.

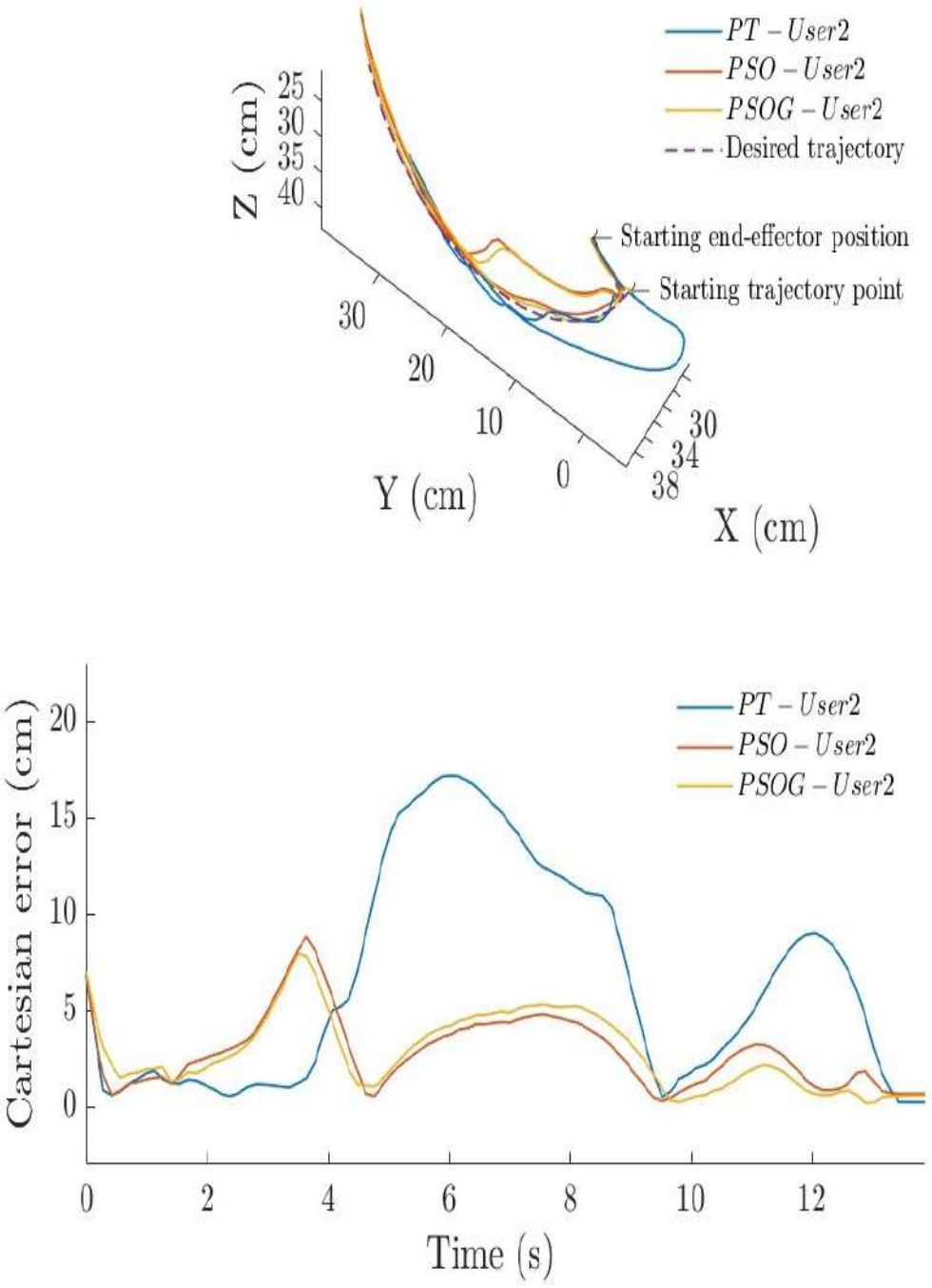

Figure 7.13: Cartesian tracking and error: user 2.

To evaluate the behavior of the PSO algorithm, Figures 7.14-7.15 show the behavior of a particle, which is an oscillatory and convergent behavior. We can also see that choosing the parameters ω, c_1, c_2 guarantee the deterministic convergence of the PSO algorithm, whose eigenvalues of the Equation (7.26) are equal to $\lambda_{1,2} = 0.85 \pm j0.42$.

According to the results obtained, the average RMSE (mean square error) for both users

in the first test was $[0.05, 0.07]rad$ and the average RMSE for the same users in the third test was $[0.03, 0.05]rad$. This shows that the proposed approach reduces the average RMSE of user 1 by 28.3% and by 23.5% for user 2.

It should be noted that chattering is not eliminated entirely, however, the average RMST (root mean square torque) for the same users in the first test was $[7.33, 7.21]$ and for the third test was $[7.36, 7.33]$. It is concluded that the RMST in the third experiment increased by 0.4% and 1.6% compared to the first test, which means a small increase in the control activity while greatly improving the tracking error.

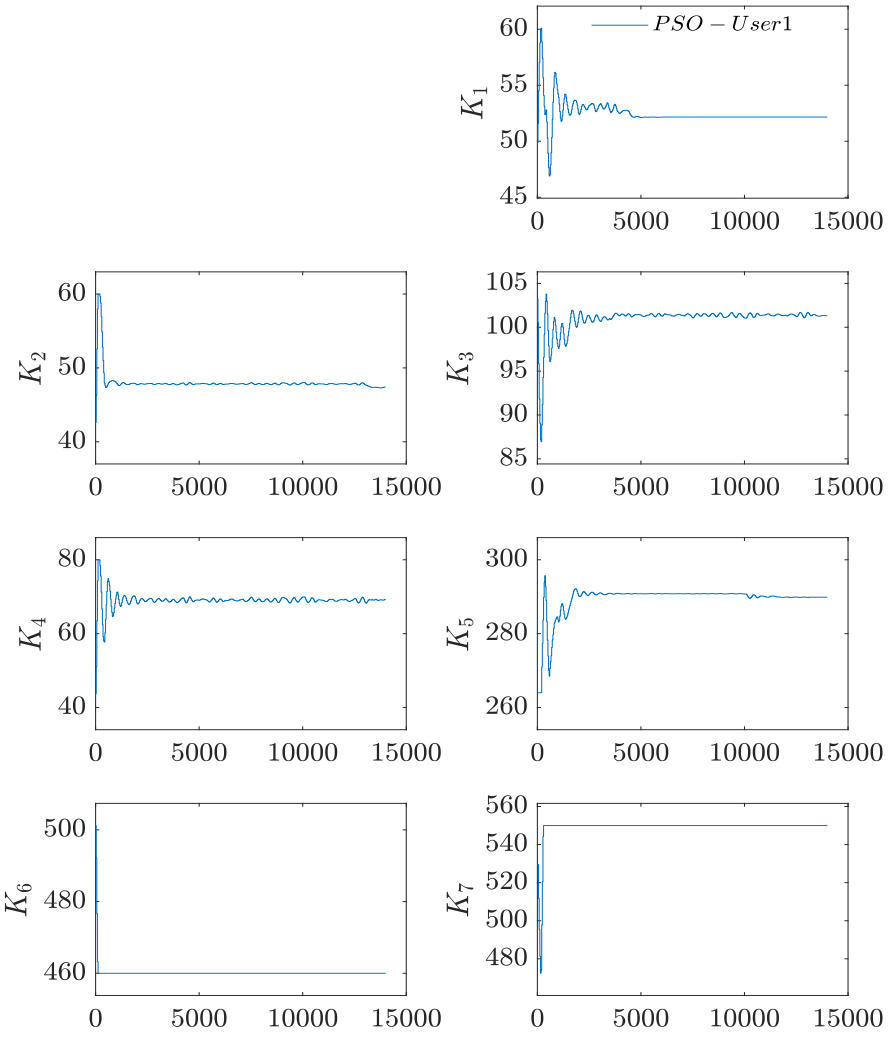

Figure 7.14: Global gain evolution: K_i

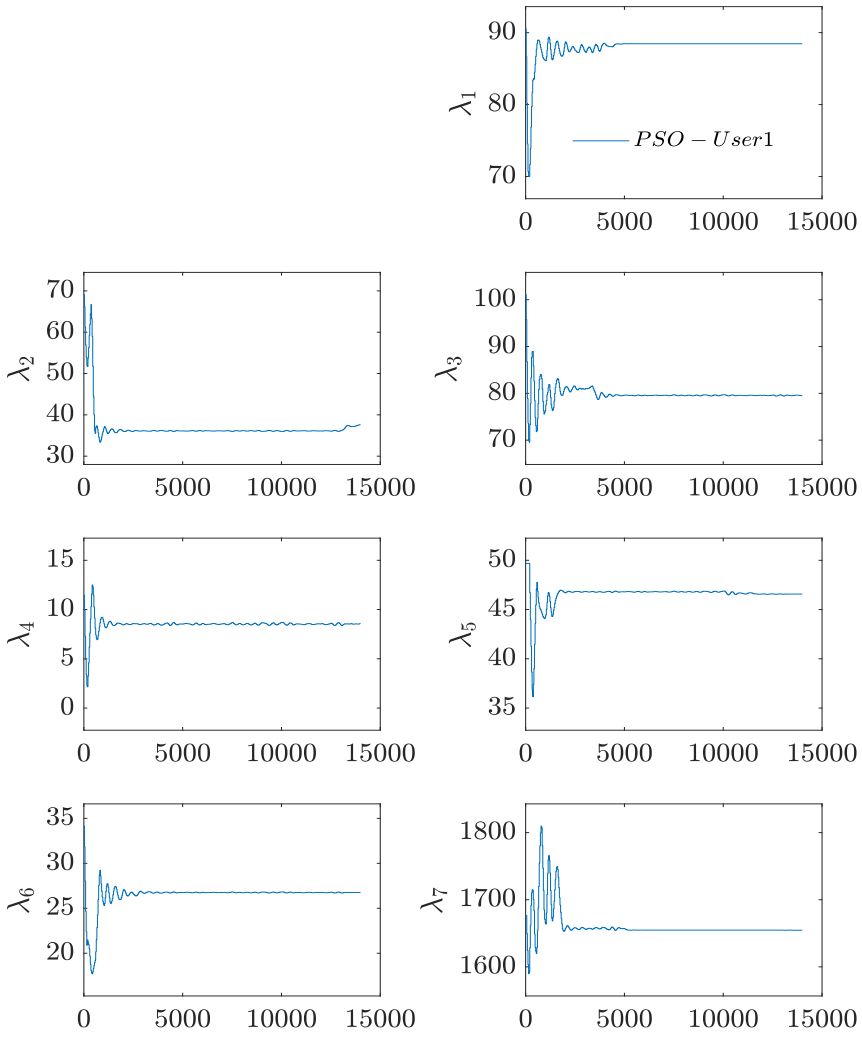

Figure 7.15: Global gain evolution: Λ_i

Tables 7.7-7.8 show the users' results for the RMSE and RMST of each joint, as well as their average for the first and third tests.

Table 7.7: Results: RMSE

Joint	$User_1$			$User_2$		
	PT	PSOG	%	PT	PSOG	%
q_1	0.03	0.06	+110.00	0.03	0.08	+109.55
q_2	0.10	0.01	-88.16	0.17	0.00	-94.82
q_3	0.07	0.05	-27.67	0.13	0.16	25.62

Joint	$User_1$			$User_2$		
	PT	PSOG	%	PT	PSOG	%
q_4	0.03	0.06	+52.43	0.03	0.02	-22.07
q_5	0.03	0.02	-23.41	0.02	0.03	23.33
q_6	0.02	0.00	-55.32	0.02	0.02	-1.71
q_7	0.07	0.04	-38.72	0.08	0.05	-33.06
Average	0.05	0.03	-28.31	0.07	0.05	-23.49

Table 7.8: Results: RMST

Joint	$User_1$			$User_2$		
	PT	PSOG	%	PT	PSOG	%
q_1	7.45	7.24	-2.71	7.56	6.47	-14.47
q_2	22.66	22.89	+1.02	22.05	24.36	+10.47
q_3	4.58	4.91	+7.24	4.75	4.20	-11.70
q_4	9.86	9.35	-5.13	9.52	9.54	+0.15
q_5	3.60	3.72	+3.57	3.51	3.59	+2.25
q_6	2.08	2.18	+4.76	2.01	1.99	-0.90
q_7	1.11	1.21	+9.23	1.10	1.16	+5.21
Average	7.33	7.36	+0.36	7.21	7.33	+1.56

In addition, it should be noted that the elapsed time for each of the trials of the first and third experiments was $238\mu s$, while for each of the tests of the second experiment it was 263μ seconds (11% increase).

In this study, a promising solution was provided for tuning robust controllers applied to coupled and time-changing systems. The controller's performance relies on the gains within the search space (according to the physical characteristics of the system). This implies that if the exoskeleton lacks robust dynamic stability and energy efficiency, the algorithm is unlikely to enhance control performance significantly.

Obtaining gains from the ERL controller via the PSO algorithm reduced the error in trajectory tracking by more than 20% in two users with different morphologies, allowing its application for different users with different motor conditions. Furthermore, the proposed controller allowed the chattering phenomenon to be attenuated even when the tracking error was improved. As future work, an improved version of the PSO algorithm is proposed to improve trajectory tracking as well as the minimization of energy consumption

Chapter 8

Discussion of contributions

"What we know is a drop of water; what we don't know is the ocean."

Isaac Newton.

In this chapter, we examine how the results obtained in this doctoral thesis compare with previous studies, identifying strengths, limitations, and possible clinical implications. The analysis will detail how the findings contribute to existing knowledge and what novel aspects they bring to the current literature on rehabilitation exoskeletons. Additionally, opportunities for development and optimization in the design and application of these devices will be explored, considering both technical and clinical perspectives.

Exoskeleton design methodology: optimization

Although the objective of the design methodology aligns with that of most reviewed methodologies, these often prioritize a single perspective when generating designs, meaning that the proposed solutions only cater to the viewpoint under which they were created (Chougrani et al., 2019; Dinh et al., 2021; Kaveh et al., 2020; Lagaros and Karlaftis, 2016; Ning et al., 2022; Papavasileiou and Charmpis, 2016; T. Wang et al., 2023). In this regard, the methodology proposed in this work fulfills the three engineering design perspectives (client, designer, and community). Additionally, it also incorporates the triad of pillars of Industry 4.0 (autonomous machines and systems, additive manufacturing, and virtual environment simulation). It is based on a real bioinspired problem and implements a metaheuristic optimization to meet the requirements, thus achieving a comprehensive tool that embraces a multidisciplinary approach and contributes to a high degree of usability and adoptability of the developed exoskeleton (Struijk et al., 2022).

A highlighted aspect of the proposed methodology is that its initial phase includes a stage for optimizing mechanical design. Throughout this process, multiple objectives are pursued, such as minimizing two aspects and maximizing another, through a weighted objective function. This methodology conducts a local search, evaluating the performance of the solution within

the broader context of the design. This leads to simultaneous solutions, based on population, which are updated through a memory-based search process, besides the design considers the parametric design approach based on characteristics, which allowed its optimization through defining the dimensions of each of the parts of the device. This feature distinguishes the methodology from approaches that solely focus on one optimization objective (L. Gao et al., 2022; Greco et al., 2023; Ning et al., 2022; Vélez-Guerrero et al., 2021).

Another significant consideration during the optimization process is the time and computational resources required to achieve the objectives. As the number of objectives increases, so does the time and resources needed to obtain a solution (Peres and Castelli, 2021). Therefore, a strategy to balance software and hardware resources in the proposed methodology was to employ a weighted objective function. This function allows for the combination of all requirements, using a minimal set of design variables and without the need for sensor data or kinematic analysis. As a result, the utilization of computational and temporal resources is minimized.

According to the design optimization carried out, it can be concluded that the exoskeleton proposed in this work presents a relationship between its exoskeleton weight and its degrees of freedom of 1.94 kg/DOF, which makes it lighter than other exoskeletons such as Armeo®Power (29.28 kg/DOF, DIH brand, 2024), Jace S603 (8.33 kg/DOF, GmbH., 2024), Harmony (2.23 kg/DOF, B. Kim and Deshpande, 2017), ANYexo (2.16 kg/DOF, Zimmermann et al., 2019) and Float (2.00 kg/DOF, Buccelli et al., 2022). Therefore, it is a lighter solution, with lower energy consumption and is therefore viable to use in physical rehabilitation. Therefore, advances in 3D printing technology and carbon polymer composites are a promising option for the development of lightweight exoskeleton robots, allowing companies to be competitive and profitable in the future (Carro Suárez et al., 2019).

Digital twin: prototype and instance

Digital twin prototype (DTP)

The generation and use of a DT make it possible to create sustainable work environments (they establish human–robot interaction in the modeling and simulation of the device), to evaluate the virtual prototype before manufacturing the physical device (reducing costs and manufacturing time) (Attaran and Celik, 2023; Z. Huang et al., 2021; X. Zhou and Zheng, 2021). They also offer a variety of options to ensure collaborative security in industrial environments. These can be divided into validation, analysis, prediction and improvement (Mazumder et al., 2023). In this study, a design validation approach is employed, utilizing finite element analysis to verify the mechanical feasibility of the device. Additionally, the DT was essential for validating control strategies and the device's operation in simulations under conditions similar to real-life scenarios. Once the device's efficiency was confirmed in the DTP, a low-cost DTI was constructed, allowing the evaluation of the designed exoskeleton's performance in a clinical setting. The results obtained were favorable and revealed potential improvements in both the device's functionality and usability. Thus, the proposed methodology can be adapted and implemented in different areas of product development due to its metaheuristic approach.

During the manufacturing process, Digital Twins (DTs) offer a range of options to ensure collaborative safety in industrial environments, spanning from validation and analysis to prediction and improvement (Mazumder et al., 2023). In this study, the design validation approach is employed, addressing crucial aspects such as the mechanical confirmation of the device through finite element analysis, as well as the validation of control strategies through simulation of movements used in physical rehabilitation therapies. Furthermore, the use of virtual DT allows its application in the training of medical personnel using the exoskeleton, thus enhancing its effectiveness and safety in clinical use.

One of the factors that stands out in the proposed methodology is the use of the digital twin combined with other pillars of industry 4.0, such as: autonomous machines and systems (robotic exoskeleton), additive manufacturing (allows the creation of customized and complex structures) and simulation of virtual environments (analogous to reinforcement learning), which potentiates and expands the areas where it can be implemented (X. Zhou and Zheng, 2021, Z. Huang et al., 2021, Attaran and Celik, 2023). In addition, although it was shown that it has real-world applications in the health area, where a multidisciplinary approach is necessary to achieve results that maximize the performance of the systems. There is currently still some preference for subtractive methods (Computer Numerical Control (CNC) machining and metal casting, extrusion and welding), mainly due to the costs derived from the use of new technologies. However, advances in 3D printing technology and carbon polymer composites are a promising option for the development of lightweight exoskeleton robots (Hussain et al., 2021). So, it is necessary to show the advantages achievable with this type of technologies, allowing companies to be competitive and profitable in the future (Carro Suárez et al., 2019).

However, there are still areas where the use of DTs is critical: especially in coordination and collaboration with multiple robots, mainly due to human safety and data standardization. The most significant challenges presented by DTs are: high implementation costs (software and sensors), increased demand for energy and storage, as well as integration and complexity (control, maintenance, among other). Despite the challenges DTs face, they are very useful throughout the product lifecycle. Some example projects are: Living Heart, which uses them for clinical diagnosis, testing, medical device design and education/training (Attaran and Celik, 2023), and the European project Change2Twin that supports manufacturing SMEs in their digitalization process by providing DTs solutions (Negri et al., 2017).

Digital twin instance (DTI)

To obtain a functional physical prototype, it is necessary to integrate the mechanical, electrical/electronic parts, as well as the human-robot interface that allows for communication and configuration of the exoskeleton. Therefore, the following points are highlighted:

- The human-robot interface in a rehabilitation exoskeleton acts as the communication channel between the robot and the user, in this case, the physical therapist. This interface enables precise and adaptive interaction to meet the individual needs of patients. The main difference of the interface developed in this thesis, compared to others, lies in the integration of a simulation stage prior to the execution of the therapeutic movements programmed in the robot. Most works only present interfaces that operate without

this simulation stage (Alguacil-Diego et al., 2021; Catalán et al., 2023; Dalla Gasperina et al., 2022; Ferrero et al., 2022; Longatelli et al., 2021; Nann et al., 2020; Park et al., 2020). Additionally, the generated interface is user-centered and, to ensure the required usability, its design is based on Jakob Nielsen's 10 principles of interaction (Nielsen, 1994).

- The human-robot interface developed in its simulation stage can be used to train medical personnel, especially students, promoting autonomous learning and greater engagement (Berisha-Gawlowski et al., 2021; Kaarlela et al., 2022; Liljaniemi and Paavilainen, 2020; Madni and Madni, 2022; Sepasgozar, 2020). Additionally, since the interface developed in this thesis can also be used in real environments, it enables the development of robotic technology to be flexible and applicable both in educational settings and practical situations.
- Although the obtained physical prototype is lightweight and offers 5 DOF, it is feasible to endow it with more degrees of freedom to enhance its manipulability and increase the number of allowed movements (Catalán et al., 2023; Ning et al., 2022; Tröster et al., 2020; Zeiaee et al., 2019). This is because its design is based on a modular approach. The construction of the prototype allowed the evaluation of various aspects, such as performance, usability, satisfaction degree, and ergonomics, among others. This is mainly achieved because it complies with the following safety measures:
  - The interface design complies with the main interface design standards.
  - The DTI reaches 80% of the range of motion of the shoulder, elbow, and wrist joints, considering the workspace of healthy subjects (initial verification on the interface).
  - It allows the programming of speeds and maximum displacements that are within the workspace allowed by the exoskeleton, enabling its programming to execute different therapeutic routines as defined by the physiotherapist.
- In this case, the device requires a power source that connects to the electrical outlet, which implies that it does not have its own autonomy. This particularity offers the advantage of prolonged use during rehabilitation sessions, provided that the necessary power is available.

Optimal control strategy

In the DTI of 5 DOF, independently adjusted PD controllers were implemented to maximize performance in each case and demonstrate the device's best capability in the experimental context. The gains of the actuator controllers were adjusted at the beginning of the tests to achieve the best possible resolution and precision. This feature has allowed the device to be used with users of diverse characteristics and has enabled the execution of different trajectories in the performed movements. Therefore, the use of this standard industrial controller through a human-robot interface has proven feasible in the application, allowing the adaptation of therapeutic routines to users by tracking feasible trajectories for each one (Ali and Tokhi,

2018; Aole et al., 2022; Fei et al., 2017; Fellag et al., 2017; Mahmoud and Saidi, 2022; Palazzi et al., 2022; Qureshi and Mudassir, 2021), adapting to their ranges of motion and reach times. However, it is possible to improve the controller by including online adaptive control techniques to cope with disturbances during therapeutic routines (Ali and Tokhi, 2018; Aole et al., 2022; Zhao et al., 2023).

Although the implementation of industrial controllers integrated into the actuators ensures good performance for certain applications, in this case, it restricted the option of using controllers different from those preset in the actuators. However, having the digital twin of the exoskeleton opens up the possibility of implementing these alternative controllers, at least in simulation environments.

In the 5DOF exoskeleton, it was only possible to implement the PD controller in each of the joints. To overcome this limitation, I conducted a research stay where I investigated a robust control approach that allowed for online adjustment of controller gains. This approach considers mathematical demonstrations that address uncertainties in mathematical modeling and disturbances, factors that affect the performance of exoskeletons (Narayan et al., 2022, G. Zhang et al., 2022, Silawatchananai and Howimanporn, 2020, Mahmoud and Saidi, 2022). The gain adjustment was performed using the PSO algorithm, a metaheuristic that does not require many resources and can be adapted to the specific application.

The advantages of this approach include a quick response to changes over time, resistance to changes in parameters, and ease of implementation. An exponential reaching law (Komurcugil et al., 2022, Brahmi et al., 2020) is used to simultaneously reduce chattering and reaching time without compromising the robustness of the SMC. Comparing this approach with others, it can be concluded that, to the best of our knowledge, this is the first instance in which this method is applied in a 7-DOF exoskeleton to adjust gains online in an SM controller, with healthy subjects of different morphologies, where the results demonstrated an improvement exceeding 20% in trajectory tracking.

Full-scope evaluation of a rehabilitation exoskeleton

It has been proven that the evaluation of exoskeletons, such as this type of robots, requires a multidisciplinary approach involving the participation of engineers, technicians, clinical personnel, patients, and healthy individuals. This evaluation must be carried out at all stages of development to enhance its effectiveness in rehabilitation, as well as its ease of use and acceptance by all involved parties (Alguacil-Diego et al., 2021; Ferrero et al., 2022; Semprini et al., 2022; Struijk et al., 2022). This approach becomes particularly important when tests are conducted under real conditions, as the results are more reliable and desirable. Therefore, the tests conducted in this thesis were carried out in a clinical environment.

En el caso de exoesqueletos de miembros superiores se destacan 4 niveles de interacción (Struijk et al., 2022):

1. Basic technical function: the metrics commonly used for its evaluation are: precision, range of motion, material, degree of freedom (DOF), power, and low-level control (Z.-J. Chen et al., 2021; Costanzi et al., 2023; McDonald et al., 2020; Morishita and Murakami,

2023; Vélez-Guerrero et al., 2021; Yurkewich et al., 2019; Z. Zhou et al., 2021).

2. Interaction with user: the main metrics used to evaluate it are: efficiency, high-level control, pathology, size, safety, movement, sound, usability, learnability, functionality, among others (Alguacil-Diego et al., 2021; Dalla Gasperina et al., 2022; Gandolla et al., 2021; H. K. Kim et al., 2021; Lambelet et al., 2020; Semprini et al., 2022).
3. Interaction with caregiver: the main metrics considered for these evaluations are: calibration, adjustment, donning and doffing.
4. Interaction with society: the main metrics considered for these evaluations are: aesthetics, robutness, mobility and versatility. ,

To ensure the comprehensive development of an exoskeleton, it's crucial to conduct evaluations that encompass multiple levels of application. However, due to their inherent complexity, these evaluations often tend to focus on a single domain, with technical issues and user interaction being the most common (Alguacil-Diego et al., 2021; Catalán et al., 2023; Dalla Gasperina et al., 2022; H. K. Kim et al., 2021; Nann et al., 2020; Pérez et al., 2022; Pérez-Rodríguez et al., 2019). In this context, one of the main contributions of this thesis is the evaluation of the exoskeleton as a product, in addition to its technical functions and its interaction with users.

Other advantages of the developed evaluation were as follows:

- Standardized and customized evaluation tools were used, based on standard quality norms, which were completed by users (both patients and healthy individuals) and physiotherapists after using the device in real-life scenarios. This is significant, as most customized instruments tend to exhibit biases and may not be applicable to all devices in this field, thereby creating a gap and potentially biasing results when making comparisons (Alguacil-Diego et al., 2021; Catalán et al., 2023; Lambelet et al., 2020; Meyer et al., 2019; Nann et al., 2020; Semprini et al., 2022).
- The population involved in the evaluations included patients, healthy individuals, and physiotherapists. In most studies, these groups are considered separately, focusing solely on patients (Alguacil-Diego et al., 2021; Catalán et al., 2023; Ferrero et al., 2022; Gandolla et al., 2021; Longatelli et al., 2021; Meyer et al., 2019; Nann et al., 2020; Park et al., 2020; Pérez et al., 2022), healthy individuals (Lambelet et al., 2020; Verdel et al., 2022), or medical personnel (Dalla Gasperina et al., 2022; H. K. Kim et al., 2021; Semprini et al., 2022). Few studies present evaluations involving all three types of participants, as done in this study.

The primary limitation of the conducted evaluation is that it does not address the evaluation of the therapy itself, as a longer period is required to carry out such tests.

Chapter 9

Conclusions and future work

"There is no barrier, lock, or bolt you can impose on the freedom of my mind".

Virginia Woolf.

9.1 Conclusions

This doctoral thesis focused on the design and development of a rehabilitation exoskeleton for upper limbs (it includes movements of the shoulder, elbow, and wrist). To achieve this, a user-centered methodology with multidisciplinary approaches was designed and implemented, aiming to create the most comprehensive device possible. Consequently, this doctoral thesis presents the following original contributions.

1. **Mechanical Design Methodology:** A user-centered and task-focused methodology (know-how) was designed and implemented, considering the premise that the exoskeleton has two users: patients and physiotherapists. This methodology can be applied in the development of any robotic device, whether for rehabilitation or assistance, simply by defining its goals, application, and users. By considering these aspects, the aim is for the device to be safe, reliable, affordable, and user-friendly.
2. **Optimized Design:** The methodology proposed in this document seeks optimal solutions through a metaheuristic process, making it applicable to different mechanical systems whose design is user-centered and based on specific characteristics. The implemented optimization satisfies the reduction of the device's mass and ensures a viable safety factor, while also seeking a balance between cost and manufacturing time (parts with basic geometries without a post-fabrication phase). The final optimized design addresses a healthcare need through bio-inspired design, adheres to all three engineering design perspectives, and leverages three pillars of Industry 4.0. As a result, it achieves a 49% decrease in mass compared to the initial design.
3. **Virtual DTP:** Having a digital twin prototype in virtual environments facilitated the completion of the following tasks (without the need to produce a physical prototype, resulting in time and cost savings):

- Perform the mechanical design of the device to visualize its spatial distribution and three-dimensional characteristics.
- Carry out the design optimization process, using the equivalent of the DTP to perform finite element analysis with specialized software, and thereby determine its feasibility (safety factor).

  The kinematic (forward and inverse) and dynamic model of the designed exoskeleton was validated through therapeutic routines implemented in simulation. The models used in the mathematical models consider biomechanical solutions that closely mimic natural movements under quasi-real conditions, as the equivalent DTPs allow simulating the mechanical properties of the device and also adding external forces to simulate the forces generated by the patient on the exoskeleton. The use of therapeutic routines allowed for customizing movements according to the characteristics indicated by physiotherapists (positions and timings).

4. **Control architecture:** Two control approaches were employed:
   - An industrial standard controller was utilized, with controller gains in the actuators adjusted at the beginning of the tests to achieve the highest resolution and precision allowed. This controller provided versatility in creating trajectories (speeds, functional ranges, etc.), with a maximum mean error obtained in simulation of 0.045 radians. Therefore, this approach proved to be viable in the application; however, it is also susceptible to improvement.
   - A robust control approach was implemented, allowing gain adjustment through a metaheuristic algorithm. Experimental results demonstrated an improvement of over 20% in precision when tracking trajectories. This approach is applicable in highly nonlinear systems with uncertainties in modeling and the presence of disturbances, as it uses a sliding mode controller with an exponential reach surface.
5. **Human-Robot Interaction Interface**: The interface created for managing the exoskeleton is based on the premise that the device does not replace the interpersonal connection between therapists and patients, but rather is used in standard treatment to enhance patient outcomes, reduce the physical workload of medical staff, and help meet the demand for rehabilitation services. In this regard, the therapist remains a key player in the rehabilitation program, supporting and supervising robot-assisted treatment and selecting the most suitable training profile. This optimization of therapist workload introduces a cost-effective advantage of robot-assisted therapy compared to traditional rehabilitation. According to the results obtained from the interface evaluation, approximately 60% of physiotherapists consider their satisfaction level acceptable, and further suggestions include adding more features for the customization of therapeutic routines.

   The developed interface enables the device to be used in three different modes (ensuring personalized treatments) and complies with safety aspects, thereby facilitating its usability and adaptability in medical environments.
6. **Digital twin instance (DTI)**

A 3D-printed device was constructed, combining mechanically resistant materials with reduced weight, making it lightweight and cost-effective compared to other methods. This design features 5 degrees of freedom (DOF); however, thanks to its modular design, it is feasible to add more DOF without compromising its workspace. Nonetheless, depending on the added components, it is possible that the performance of the current actuators may be diminished.

According to the conducted tests, a physical prototype is available for evaluation with both simple and combined therapeutic movements, in both injured and healthy subjects. The exoskeleton was able to achieve speeds ranging from 2 degrees per second to 20 degrees per second, allowing for a broad and effective customization of movements according to the application's objectives.

It is important to note that the motors currently installed in the 5-DOF exoskeleton are not capable of providing the necessary torque to lift the arm of a 120 kg patient (the weight for which the device was designed). Additionally, the material from which the device is made may break. Therefore, it is suggested to use the recommended materials during the design stage and employ different 3D printers to improve the quality and mechanical strength of the parts.

Furthermore, the exoskeleton currently lacks force/torque sensors in the joints, which prevents the performance of active therapies. However, overall, it complies with mechanical design and manufacturing standards, interface design, and exoskeleton quality evaluation as a product.

7. **Evaluation Methodology:** The proposed evaluation methodology analyzes the device from three perspectives: as a product, in technical terms, and in its interaction with users. The evaluations were conducted with the participation of three stakeholder groups: patients, healthy individuals, and physiotherapists. The customized instruments used are based on standard quality norms and are applicable to devices with the same purpose. In summary, the results were as follows:

    - Patient evaluations: The level of satisfaction with the device's use is acceptable. However, in terms of usability, it needs improvement by adding more features to the device, which is understandable considering that the evaluated device was a prototype. Furthermore, although the perceived sense of safety regarding the exoskeleton is acceptable, it is suggested to enhance it with manual control devices for medical staff and emergency stop systems for patients, as currently these aspects are only considered in the interface.
    - Assessments conducted by physiotherapists: They consider the user interface controlling the exoskeleton to be acceptable, as they find it easy to use (83%). Moreover, 75% of them deem it easy to learn and visually appealing, with only 16% experiencing errors when using it. Additionally, the workload index of physiotherapists who used the complete system (interface and exoskeleton) showed a moderate workload level, low frustration, and high mental demand, as it was their first time using an exoskeleton in their work.

- Assessments conducted on the exoskeleton: One advantage of the movements performed is that tests were carried out with two simple motions, one for the shoulder (internal-external rotation) and one for the elbow (flexion-extension), in addition to a combined movement (diagonal). All of them were executed at different speeds, and although most reached the same final positions, the times at which these positions were reached varied. According to the results, the joint that showed the greatest deviations in trajectory tracking was joint 4, with an RMSE of 0.38 radians, which is acceptable for the implemented rehabilitation trajectories

  The device exhibited a success rate of over 90%, with only 3 failed attempts during the tests and a user error rate of less than 2%. Additionally, the average time required for the device to complete a movement (including user data collection, exoskeleton donning/doffing, interface setup, and movement execution) was 3.07 minutes, indicating that these metrics are acceptable in terms of product usability.

Overall, the results indicate that both patients and physiotherapists were able to conduct the experimental sessions without experiencing physical or mental fatigue, and they expressed satisfaction with the use of the exoskeleton. Additionally, the results of the cross-validation are promising regarding the use of the created human-robot interface.

9.2 Future work

As future work, the following lines of research are suggested:

- Incorporate additional degrees of freedom to the exoskeleton to enhance its manipulability, workspace, and ergonomics.
- Enable the generation of movement sequences in the interface, allowing for the configuration of different speeds based on the range of motion, time, and number of repetitions. Add new movements to the interface according to the new degrees of freedom added to the physical prototype.
- To modify the patients' attachment system to the exoskeleton to ensure greater comfort and precision in movements. The current attachment may cause some discomfort in certain positions, so efforts are being made to enhance this aspect for improving the patient experience.
- Incorporating manual control devices for physiotherapists and manual emergency controls for the patients, as currently all these aspects are solely considered within the interface.
- To implement sensory feedback into the exoskeleton aiming to enhance the biomechanical interaction among the device, the therapist, and the patient, thereby boosting its performance and increasing the system's usability and adaptability.
- To explore enhancements to the control system through the utilization of real-time adaptive schemes and/or control based on biosignals.
- Conduct a more extensive evaluation involving a larger number of patients and physical therapists over an extended period to achieve more conclusive results

References

Aichaoui, M., & Ikhlef, A. (2022). Adaptive backstepping control for upper limb rehabilitation robot using pso tuning. *2022 19th International Multi-Conference on Systems, Signals & Devices (SSD)*, 601–608.

Alattas, R. J., Patel, S., & Sobh, T. M. (2019). Evolutionary modular robotics: Survey and analysis. *Journal of Intelligent & Robotic Systems*, *95*, 815–828.

Alguacil-Diego, I.-M., Cuesta-Gómez, A., Contreras-González, A.-F., Pont-Esteban, D., Cantalejo-Escobar, D., Sánchez-Urán, M. Á., & Ferre, M. (2021). Validation of a hybrid exoskeleton for upper limb rehabilitation. a preliminary study. *Sensors*, *21*(21), 7342.

Ali, S. K., & Tokhi, M. O. (2018). Control design of a de-weighting upper limb exoskeleton. *2018 International Conference on Applied Engineering (ICAE)*, 1–6.

Al-Waeli, K. H., Ramli, R., Haris, S. M., Zulkoffli, Z. B., & Amiri, M. S. (2021). Offline ann-pid controller tuning on a multi-joints lower limb exoskeleton for gait rehabilitation. *IEEE Access*, *9*, 107360–107374.

Amiri, M. S., Ramli, R., & Ibrahim, M. F. (2019). Hybrid design of pid controller for four dof lower limb exoskeleton. *Applied Mathematical Modelling*, *72*, 17–27.

Aole, S., Elamvazuthi, I., Waghmare, L., Patre, B., Bhaskarwar, T., & Prasetyo, T. (2022). Adrc for upper limb exoskeleton: A simulation study. *2022 IEEE 5th International Symposium in Robotics and Manufacturing Automation (ROMA)*, 1–6.

Asad, U., Khan, M., Khalid, A., & Lughmani, W. A. (2023). Human-centric digital twins in industry: A comprehensive review of enabling technologies and implementation strategies. *Sensors*, *23*(8), 3938.

Attaran, M., & Celik, B. G. (2023). Digital twin: Benefits, use cases, challenges, and opportunities. *Decision Analytics Journal*, *6*, 100165. https://doi.org/https://doi.org/10.1016/j.dajour.2023.100165

Avila-Chaurand, R., Prado-León, L., & González-Muñoz, E. (2007). Dimensiones antropométricas de población latinoamericana: México, cuba, colombia, chile. *Universidad de Guadalajara, México*.

Baek, M.-S. (2022). Digital twin federation and data validation method. *2022 27th Asia Pacific Conference on Communications (APCC)*, 445–446. https://doi.org/10.1109/APCC55198.2022.9943622

Bank, W. H. O.
bibinitperiod W. (2011). World report on disability. world health organization.

Barrera-Gálvez, R., Solano-Pérez, C., Arias-Rico, J., Sánchez-Padilla, M., & Díaz-Pérez, L. (2017). Un enfoque para el diagnóstico de estrés por medio del método de índice de carga de trabajo de la nasa (nasatlx). *Congreso Nacional de Tecnología Aplicada a Ciencias de la Salud*.

Barrientos, A., Peñin, L. F., Balaguer, C., & Aracil, R. (1997). *Fundamentos de robótica*. McGraw-Hill, Interamericana de España.

Bedolla-Martinez, D., Kali, Y., Saad, M., Ochoa-Luna, C., & Rahman, M. H. (2023). Learning human inverse kinematics solutions for redundant robotic upper-limb rehabilitation. *Engineering Applications of Artificial Intelligence*, *126*, 106966.

Belkadi, A., Ciarletta, L., & Theilliol, D. (2015). Particle swarm optimization method for the control of a fleet of unmanned aerial vehicles. *Journal of Physics: Conference Series*, *659*(1), 012015.

Belkadi, A., Ciarletta, L., & Theilliol, D. (2016). Uavs fleet control design using distributed particle swarm optimization: A leaderless approach. *2016 International Conference on Unmanned Aircraft Systems (ICUAS)*, 364–371.

Belkadi, A., Oulhadj, H., Touati, Y., Khan, S. A., & Daachi, B. (2017). On the robust pid adaptive controller for exoskeletons: A particle swarm optimization based approach. *Applied Soft Computing*, *60*, 87–100.

Belov, M. P., Truong, D. D., & Khoa, T. D. (2022). Self-tuning subordinate control system based on neural network for nonlinear electric drivers of lower limbs of exoskeleton. *2022 Conference of Russian Young Researchers in Electrical and Electronic Engineering (ElConRus)*, 549–553.

Bembli, S., Haddad, N. K., & Belghith, S. (2021). An exoskeleton–upper limb system control using a robust model free terminal sliding mode with emg signal. *2021 international conference on control, automation and diagnosis (ICCAD)*, 1–8.

Berg, J., & Lu, S. (2020). Review of interfaces for industrial human-robot interaction. *Current Robotics Reports*, *1*, 27–34.

Berisha-Gawlowski, A., Caruso, C., & Harteis, C. (2021). The concept of a digital twin and its potential for learning organizations. *Digital transformation of learning organizations*, 95–114.

Bhatia, A., & Sehgal, A. K. (2023). Additive manufacturing materials, methods and applications: A review [International Virtual Conference on Sustainable Materials (IVCSM-2k20)]. *Materials Today: Proceedings*, *81*, 1060–1067. https://doi.org/https://doi.org/10.1016/j.matpr.2021.04.379

Brahmi, B., El-Monajjed, K., Rahman, M. H., Ahmed, T., El-Bayeh, C., Khan, M. R., & Saad, M. (2020). Novel adaptive reaching law for sliding mode control of an upper limb exoskeleton robot. *2020 IEEE Region 10 Symposium (TENSYMP)*, 1432–1437.

Broad, A., Abraham, I., Murphey, T., & Argall, B. (2020). Data-driven koopman operators for model-based shared control of human–machine systems. *The International Journal of Robotics Research*, *39*(9), 1178–1195.

Buccelli, S., Tessari, F., Fanin, F., De Guglielmo, L., Capitta, G., Piezzo, C., Bruschi, A., Van Son, F., Scarpetta, S., Succi, A., et al. (2022). A gravity-compensated upper-limb exoskeleton for functional rehabilitation of the shoulder complex. *Applied Sciences*, *12*(7), 3364.

Carro Suárez, J., Flores Salazar, F., Flores Nava, I., & Hernández Hernández, R. (2019). Industry 4.0 and digital manufacturing: A design method applying reverse engineering. *Ingeniería*, *24*(1), 6–28.

Carvajal Rojas, J. H. (2005). Metodología de diseño mecatrónico de robots. *épsilon*, *1*(4), 91–101.

Casas, J., Cespedes, N., Múnera, M., & Cifuentes, C. A. (2020). Chapter one - human-robot interaction for rehabilitation scenarios. In A. T. Azar (Ed.), *Control systems design of bio-robotics and bio-mechatronics with advanced applications* (pp. 1–31). Academic Press. https://doi.org/https://doi.org/10.1016/B978-0-12-817463-0.00001-0

Catalán, J. M., Trigili, E., Nann, M., Blanco-Ivorra, A., Lauretti, C., Cordella, F., Ivorra, E., Armstrong, E., Crea, S., Alcañiz, M., et al. (2023). Hybrid brain/neural interface and autonomous vision-guided whole-arm exoskeleton control to perform activities of daily living (adls). *Journal of NeuroEngineering and Rehabilitation*, *20*(1), 61.

Catchpole, K., Cohen, T., Alfred, M., Lawton, S., Kanji, F., Shouhed, D., Nemeth, L., & Anger, J. (2024). Human factors integration in robotic surgery. *Human Factors*, *66*(3), 683–700.

Cha, J. S., Monfared, S., Stefanidis, D., Nussbaum, M. A., & Yu, D. (2020). Supporting surgical teams: Identifying needs and barriers for exoskeleton implementation in the operating room. *Human factors*, *62*(3), 377–390.

Chen, G., Wang, P., Feng, B., Li, Y., & Liu, D. (2020). The framework design of smart factory in discrete manufacturing industry based on cyber-physical system. *International Journal of Computer Integrated Manufacturing*, *33*(1), 79–101.

Chen, Z.-J., He, C., Guo, F., Xiong, C.-H., & Huang, X.-L. (2021). Exoskeleton-assisted anthropomorphic movement training (eamt) for poststroke upper limb rehabilitation: A pilot randomized controlled trial. *Archives of Physical Medicine and Rehabilitation*, *102*(11), 2074–2082.

Chougrani, L., Pernot, J.-P., Véron, P., & Abed, S. (2019). Parts internal structure definition using non-uniform patterned lattice optimization for mass reduction in additive manufacturing. *Engineering with Computers*, *35*(1), 277–289.

Choutri, K., Fareh, R., Rahman, M. H., Bettayeb, M., Fadloun, S., & Lagha, M. (2023). Reinforcement learning fractional order pid controller for upper limb rehabilitation robot. *2023 International Conference on Fractional Differentiation and Its Applications (ICFDA)*, 1–6. https://doi.org/10.1109/ICFDA58234.2023.10153385

Chuan, L., & Quanyuan, F. (2007). The standard particle swarm optimization algorithm convergence analysis and parameter selection. *Third International Conference on Natural Computation (ICNC 2007)*, *3*, 823–826.

Cieza, A., Causey, K., Kamenov, K., Hanson, S. W., Chatterji, S., & Vos, T. (2020). Global estimates of the need for rehabilitation based on the global burden of disease study 2019: A systematic analysis for the global burden of disease study 2019. *The Lancet*, *396*(10267), 2006–2017.

Clark, W. E., Sivan, M., & O'Connor, R. J. (2019). Evaluating the use of robotic and virtual reality rehabilitation technologies to improve function in stroke survivors: A narrative review. *Journal of rehabilitation and assistive technologies engineering*, *6*, 2055668319863557.

Coorey, G., Figtree, G. A., Fletcher, D. F., Snelson, V. J., Vernon, S. T., Winlaw, D., Grieve, S. M., McEwan, A., Yang, J. Y. H., Qian, P., et al. (2022). The health digital twin to tackle cardiovascular disease—a review of an emerging interdisciplinary field. *NPJ digital medicine*, *5*(1), 126.

Correll, N., Hayes, B., Heckman, C., & Roncone, A. (2022). *Introduction to autonomous robots: Mechanisms, sensors, actuators, and algorithms*. Mit Press.

Costanzi, D., Gandolla, M., & Calanca, A. (2023). Towards personalized myoelectric control strategies. *2023 IEEE International Conference on Metrology for eXtended Reality, Artificial Intelligence and Neural Engineering (MetroXRAINE)*, 858–863.

Craig, J. J. (2005). *Introduction to robotics: Mechanics and control*. Pearson.

Cruz Martínez, G. M., & Z.-Avilés, L. (2020). Design methodology for rehabilitation robots: Application in an exoskeleton for upper limb rehabilitation. *Applied Sciences*, *10*(16), 5459.

Dalla Gasperina, S., Longatelli, V., Panzenbeck, M., Luciani, B., Morosini, A., Piantoni, A., Tropea, P., Braghin, F., Pedrocchi, A., & Gandolla, M. (2022). Agree: An upper-limb robotic platform for personalized rehabilitation, concept and clinical study design. *2022 International Conference on Rehabilitation Robotics (ICORR)*, 1–6.

Dehio, N., Smith, J., Wigand, D. L., Mohammadi, P., Mistry, M., & Steil, J. J. (2022). Enabling impedance-based physical human–multi–robot collaboration: Experiments with four torque-controlled manipulators. *The International Journal of Robotics Research*, *41*(1), 68–84.

Delgado, P., Arachchige Don, T. A., Gomez, J., Miranda, V., & Yihun, Y. (2021). Design of bio-exoskeleton for elbow rehabilitation. *Frontiers in Biomedical Devices*, *84812*, V001T10A002.

de Medeiros, R. B., & Muñoz, D. M. (2022). Tuning of fp-pid controller based on pso algorithm applied to a human gait. *2022 Latin American Robotics Symposium (LARS), 2022 Brazilian Symposium on Robotics (SBR), and 2022 Workshop on Robotics in Education (WRE)*, 1–6.

Desplenter, T., Zhou, Y., Edmonds, B. P., Lidka, M., Goldman, A., & Trejos, A. L. (2020). Rehabilitative and assistive wearable mechatronic upper-limb devices: A review. *Journal of rehabilitation and assistive technologies engineering*, *7*, 2055668320917870.

Dian, F. J., Vahidnia, R., & Rahmati, A. (2020). Wearables and the internet of things (iot), applications, opportunities, and challenges: A survey. *IEEE access*, *8*, 69200–69211.

DIH brand, H. a. (2024). Armeo®power: Technical data sheet. [Accessed: 2024-02-21].

Dinh, V. B., Chau, N. L., Le, N. T., & Dao, T.-P. (2021). Topology-based geometry optimization for a new compliant mechanism using improved adaptive neuro-fuzzy inference system and neural network algorithm. *Engineering with Computers*, 1–30.

Drake, R. L., Vogl, A. W., & Mitchell, A. M. (2020). *Gray. anatomía para estudiantes*. Elsevier Health Sciences.

Elayan, H., Aloqaily, M., & Guizani, M. (2021). Digital twin for intelligent context-aware iot healthcare systems. *IEEE Internet of Things Journal*, *8*(23), 16749–16757.

Fallaha, C. J., Saad, M., Kanaan, H. Y., & Al-Haddad, K. (2010). Sliding-mode robot control with exponential reaching law. *IEEE Transactions on industrial electronics*, *58*(2), 600–610.

Fei, F., Wang, H., & Tian, Y. (2017). Robust time delay estimation based intelligent pid control of a 6dof upper-limb exoskeleton robot. *2017 9th International Conference on Intelligent Human-Machine Systems and Cybernetics (IHMSC)*, *2*, 386–389.

Fellag, R., Benyahia, T., Drias, M., Guiatni, M., & Hamerlain, M. (2017). Sliding mode control of a 5 dofs upper limb exoskeleton robot. *2017 5th International Conference on Electrical Engineering-Boumerdes (ICEE-B)*, 1–6.

Ferrero, L., Quiles, V., Ortiz, M., Iáñez, E., Megía, Á., Gil-Agudo, Á. M., & Azorín, J. M. (2022). Assessing user experience with bmi-assisted exoskeleton in patients with spinal cord injury. *2022 44th Annual International Conference of the IEEE Engineering in Medicine & Biology Society (EMBC)*, 4064–4067.

Fitzsimons, K., Kalinowska, A., Dewald, J. P., & Murphey, T. D. (2020). Task-based hybrid shared control for training through forceful interaction. *The International Journal of Robotics Research*, *39*(9), 1138–1154.

Franco, O. A. M., Crespo, J., Di Natali, C., Ortiz, J., & Caldwell, D. G. (2023). Integration of the user command interface to the industrial exoskeleton xotrunk. *2023 IEEE/SICE International Symposium on System Integration (SII)*, 1–7.

Franco, O. A. M., Park, D., Di Natali, C., Caldwell, D. G., & Ortiz, J. (2024). Integration and task assessment of the user command interface to the occupational exoskeleton shoulder-sidewinder. *2024 IEEE/SICE International Symposium on System Integration (SII)*, 1176–1182.

Gandolla, M., Dalla Gasperina, S., Longatelli, V., Manti, A., Aquilante, L., D'Angelo, M. G., Biffi, E., Diella, E., Molteni, F., Rossini, M., et al. (2021). An assistive upper-limb exoskeleton controlled by multi-modal interfaces for severely impaired patients: Development and experimental assessment. *Robotics and Autonomous Systems*, *143*, 103822.

Gao, L., Ma, C.-J., Zhou, N., & Zhao, L.-J. (2022). Optimization design method of upper limb exoskeleton cam mechanism's motion trajectory model. *Computers & Industrial Engineering*, *171*, 108427.

Gao, Z., Wanyama, T., Singh, I., Gadhrri, A., & Schmidt, R. (2020). From industry 4.0 to robotics 4.0 - a conceptual framework for collaborative and intelligent robotic systems [13th International Conference Interdisciplinarity in Engineering, INTER-ENG 2019, 3–4 October 2019, Targu Mures, Romania]. *Procedia Manufacturing*, *46*, 591–599. https://doi.org/https://doi.org/10.1016/j.promfg.2020.03.085

GmbH., J. S. (2024). Jace leben ist bewegung. [Accessed: 2024-02-21].

Goel, R., & Gupta, P. (2020). Robotics and industry 4.0. In A. Nayyar & A. Kumar (Eds.), *A roadmap to industry 4.0: Smart production, sharp business and sustainable development* (pp. 157–169). Springer International Publishing. https://doi.org/10.1007/978-3-030-14544-6_9

González-Mendoza, A., Quiñones-Urióstegui, I., Salazar-Cruz, S., Perez-Sanpablo, A.-I., López-Gutiérrez, R., & Lozano, R. (2022). Design and implementation of a rehabilitation upper-limb exoskeleton robot controlled by cognitive and physical interfaces. *Journal of Bionic Engineering*, *19*(5), 1374–1391.

Gopal, A., Sultani, M. M., & Bansal, J. C. (2020). On stability analysis of particle swarm optimization algorithm. *Arabian Journal for Science and Engineering*, *45*(4), 2385–2394.

Greco, C., Weerakkody, T. H., Cichella, V., Pagnotta, L., & Lamuta, C. (2023). Lightweight bioinspired exoskeleton for wrist rehabilitation powered by twisted and coiled artificial muscles. *Robotics*, *12*(1), 27.

Gull, M. A., Bai, S., & Bak, T. (2020). A review on design of upper limb exoskeletons. *Robotics*, *9*(1), 16.

Habiba, K. N., Arifin, A., Babgei, A. F., Risciawan, A., & Zazuli, M. I. (2022). Design of fuzzy-pi controller for shoulder exoskeleton with motoric progress of rehabilitation subject consideration. *2022 International Conference on Computer Engineering, Network, and Intelligent Multimedia (CENIM)*, 32–37.

Halim, I., Saptari, A., Abdullah, Z., Perumal, P., Abidin, M. Z. Z., Muhammad, M. N., & Abdullah, S. (2022). Critical factors influencing user experience on passive exoskeleton application: A review. *International Journal of Integrated Engineering*, *14*(4), 89–115.

Han, Y., Liu, C., Xiu, H., Li, Z., Shan, S., Wang, X., Ren, L., & Ren, L. (2022). Trajectory control of an active and passive hybrid hydraulic ankle prosthesis using an improved pso-pid controller. *Journal of Intelligent & Robotic Systems*, *105*(3), 48.

Hegab, H., Khanna, N., Monib, N., & Salem, A. (2023). Design for sustainable additive manufacturing: A review. *Sustainable Materials and Technologies*, *35*, e00576. https://doi.org/https://doi.org/10.1016/j.susmat.2023.e00576

Heidari, O., Wolbrecht, E. T., Perez-Gracia, A., & Yihun, Y. S. (2018). A task-based design methodology for robotic exoskeletons. *Journal of rehabilitation and assistive technologies engineering*, *5*, 2055668318800672.

Huang, P.-h., Kim, K.-h., & Schermer, M. (2022). Ethical issues of digital twins for personalized health care service: Preliminary mapping study. *Journal of Medical Internet Research*, *24*(1), e33081.

Huang, Z., Shen, Y., Li, J., Fey, M., & Brecher, C. (2021). A survey on ai-driven digital twins in industry 4.0: Smart manufacturing and advanced robotics. *Sensors*, *21*(19). https://doi.org/10.3390/s21196340

Hussain, F., Goecke, R., & Mohammadian, M. (2021). Exoskeleton robots for lower limb assistance: A review of materials, actuation, and manufacturing methods. *Proceedings of the Institution of Mechanical Engineers, Part H: Journal of Engineering in Medicine*, *235*(12), 1375–1385.

Javaid, M., Haleem, A., Singh, R. P., & Suman, R. (2021). Substantial capabilities of robotics in enhancing industry 4.0 implementation. *Cognitive Robotics*, *1*, 58–75. https://doi.org/https://doi.org/10.1016/j.cogr.2021.06.001

Jones, D., Snider, C., Nassehi, A., Yon, J., & Hicks, B. (2020). Characterising the digital twin: A systematic literature review. *CIRP Journal of Manufacturing Science and Technology*, *29*, 36–52. https://doi.org/https://doi.org/10.1016/j.cirpj.2020.02.002

Jorquera Ortega, A. (2016). *Fabricación digital: Introducción al modelado e impresión 3d*. Ministerio de Educación, Cultura y Deporte.

Julious, S. A. (2005). Sample size of 12 per group rule of thumb for a pilot study. *Pharmaceutical Statistics: The Journal of Applied Statistics in the Pharmaceutical Industry*, *4*(4), 287–291.

Juvinall, R. C., et al. (2013). Diseño de elementos de máquinas.

Kaarlela, T., Arnarson, H., Pitkäaho, T., Shu, B., Solvang, B., & Pieskä, S. (2022). Common educational teleoperation platform for robotics utilizing digital twins. *Machines*, *10*(7), 577.

Kapandji, A. I. (2006). *Fisiología articular 1: Miembro superior. 6ª edic* (E. médica Panamericana, Ed.). Maloine.

Kaveh, A., Hamedani, K. B., Hosseini, S. M., & Bakhshpoori, T. (2020). Optimal design of planar steel frame structures utilizing meta-heuristic optimization algorithms. *Structures*, *25*, 335–346.

Khan, J. S., Mohammadi, M., Rasmussen, J., Bai, S., & Struijk, N. L. A. (2022). A review on the design of assistive cable-driven upper-limb exoskeletons and their experimental evaluation. *2022 IEEE International Conference on Systems, Man, and Cybernetics (SMC)*, 59–64.

Khang, A., Rath, K. C., Satapathy, S. K., Kumar, A., Das, S. R., & Panda, M. R. (2023). Enabling the future of manufacturing: Integration of robotics and iot to smart factory infrastructure in industry 4.0. In *Handbook of research on ai-based technologies and applications in the era of the metaverse* (pp. 25–50). IGI Global.

Khatib, O., Siciliano, B., & Villani, L. (2019). *Springer handbook of robotics*. Springer.

Kim, B., & Deshpande, A. D. (2017). An upper-body rehabilitation exoskeleton harmony with an anatomical shoulder mechanism: Design, modeling, control, and performance evaluation. *The International Journal of Robotics Research*, *36*(4), 414–435.

Kim, H. K., Seong, S., Park, J., Kim, J., Park, J., & Park, W. (2021). Subjective evaluation of the effect of exoskeleton robots for rehabilitation training. *IEEE Access*, *9*, 130554–130561.

Knudson, D. (2007). *Fundamentals of biomechanics* (2nd). Springer Science & Business Media.

Komurcugil, H., Bayhan, S., Guler, N., & Abu-Rub, H. (2022). A new exponential reaching law approach to the sliding mode control: A multilevel multifunction converter application. *IEEE Transactions on Industrial Electronics*, *70*(8), 7557–7568.

La Bara, L. M. A., Meloni, L., Giusino, D., & Pietrantoni, L. (2021). Assessment methods of usability and cognitive workload of rehabilitative exoskeletons: A systematic review. *Applied Sciences*, *11*(15), 7146.

Lagaros, N. D., & Karlaftis, M. G. (2016). Life-cycle cost structural design optimization of steel wind towers. *Computers & Structures*, *174*, 122–132.

Lambelet, C., Temiraliuly, D., Siegenthaler, M., Wirth, M., Woolley, D. G., Lambercy, O., Gassert, R., & Wenderoth, N. (2020). Characterization and wearability evaluation of a fully portable wrist exoskeleton for unsupervised training after stroke. *Journal of neuroengineering and rehabilitation*, *17*, 1–16.

Le Veau, B., Williams, M., & Lissner, H. R. (1991). *Biomecánica del movimiento humano de williams y lissner*. Trillas.

Lewis, J. R., & Sauro, J. (2009). The factor structure of the system usability scale. In M. Kurosu (Ed.), *Human centered design* (pp. 94–103). Springer Berlin Heidelberg.

Li, L., Lei, B., & Mao, C. (2022). Digital twin in smart manufacturing. *Journal of Industrial Information Integration*, *26*, 100289. https://doi.org/https://doi.org/10.1016/j.jii.2021.100289

Liljaniemi, A., & Paavilainen, H. (2020). Using digital twin technology in engineering education–course concept to explore benefits and barriers. *Open Engineering*, *10*(1), 377–385.

Lippert, L. S. (2006). *Clinical kinesiology and anatomy* (4th). F.A. Davis.

Liu, J., Fang, H., & Xu, J. (2021). Online adaptive pid control for a multi-joint lower extremity exoskeleton system using improved particle swarm optimization. *Machines*, *10*(1), 21.

Liu, X., Jiang, D., Tao, B., Xiang, F., Jiang, G., Sun, Y., Kong, J., & Li, G. (2023). A systematic review of digital twin about physical entities, virtual models, twin data, and applications. *Advanced Engineering Informatics*, *55*, 101876. https://doi.org/https://doi.org/10.1016/j.aei.2023.101876

Liu, Y., Zhang, L., Yang, Y., Zhou, L., Ren, L., Wang, F., Liu, R., Pang, Z., & Deen, M. J. (2019). A novel cloud-based framework for the elderly healthcare services using digital twin. *IEEE access*, *7*, 49088–49101.

Longatelli, V., Antonietti, A., Biffi, E., Diella, E., D'Angelo, M. G., Rossini, M., Molteni, F., Bocciolone, M., Pedrocchi, A., & Gandolla, M. (2021). User-centred assistive system for arm functions in neuromuscular subjects (useful): A randomized controlled study. *Journal of neuroengineering and rehabilitation*, *18*, 1–16.

Lynch, K. M., & Park, F. C. (2017). *Modern robotics*. Cambridge University Press.

Madni, A., & Madni, C. (2022). Digital twin: Key enabler and complement to model-based systems engineering. In *Handbook of model-based systems engineering* (pp. 1–23). Springer.

Mahmoud, I., & Saidi, I. (2022). Trajectory tracking control of upper-limb rehabilitaion exoskeleton based on robust control. *2022 5th International Conference on Advanced Systems and Emergent Technologies (ICASET)*, 330–335.

Majd, Y. F., & Barari, A. (2023). Precision uncertainty due to infill in additive manufacturing of small-scale devices. *2023 IEEE 13th International Conference Nanomaterials: Applications and Properties (NAP)*, IMT12-1-IMT12–4. https://doi.org/10.1109/NAP59739.2023.10310711

Manickam, P., Mariappan, S. A., Murugesan, S. M., Hansda, S., Kaushik, A., Shinde, R., & Thipperudraswamy, S. (2022). Artificial intelligence (ai) and internet of medical things (iomt) assisted biomedical systems for intelligent healthcare. *Biosensors*, *12*(8), 562.

Martínez, M. S., Martínez, D. I., Filoniuk, V. R., Chiappori, G. G., Diz, A. C., & Arias, S. E. (2022). Aplicación de norma iso 9241-11 para la evaluación de la usabilidad en simuladores de vuelo. *Innovación y Software*, *3*(2), 70–80.

Mazumder, A., Sahed, M., Tasneem, Z., Das, P., Badal, F., Ali, M., Ahamed, M., Abhi, S., Sarker, S., Das, S., et al. (2023). Towards next generation digital twin in robotics: Trends, scopes, challenges, and future. *Heliyon*, *9*(2).

McDonald, C. G., Sullivan, J. L., Dennis, T. A., & O'Malley, M. K. (2020). A myoelectric control interface for upper-limb robotic rehabilitation following spinal cord injury. *IEEE Transactions on Neural Systems and Rehabilitation Engineering*, *28*(4), 978–987.

McKinnon, P. (2015). *Robotics: Everything you need to know about robotics from beginner to expert*. Peter McKinnon.

Mena, V. M. P., Freire, E. X. G., & Manzano, J. M. B. (2022). Usabilidad del software: Una revisión sobre su evolución conceptual y parámetros de evaluación. *Publicaciones en Ciencias y Tecnología*, *16*(2), 121–134.

Meyer, J. T., Schrade, S. O., Lambercy, O., & Gassert, R. (2019). User-centered design and evaluation of physical interfaces for an exoskeleton for paraplegic users. *2019*

IEEE 16th International Conference on Rehabilitation Robotics (ICORR), 1159–1166. https://doi.org/10.1109/ICORR.2019.8779527

Meza, C. A., Tamayo, F., & Franco, E. E. (2015). Optimización topológica aplicada al diseño de componentes estructurales mecánicos de peso reducido. *El hombre y la máquina*, (46), 72–79.

Mihai, S., Yaqoob, M., Hung, D. V., Davis, W., Towakel, P., Raza, M., Karamanoglu, M., Barn, B., Shetve, D., Prasad, R. V., Venkataraman, H., Trestian, R., & Nguyen, H. X. (2022). Digital twins: A survey on enabling technologies, challenges, trends and future prospects. *IEEE Communications Surveys & Tutorials*, *24*(4), 2255–2291. https://doi.org/10.1109/COMST.2022.3208773

Mohebbi, A. (2020). Human-robot interaction in rehabilitation and assistance: A review. *Current Robotics Reports*, *1*(3), 131–144.

Moreno, H. A., Saltarén, R., Carrera, I., Puglisi, L., & Aracil, R. (2012). Índices de desempeño de robots manipuladores: Una revisión del estado del arte. *Revista Iberoamericana de Automática e Informática industrial*, *9*(2), 111–122. https://doi.org/10.1016/j.riai.2012.02.005

Moreno Franco, O. A., Park, D., Di Natali, C., Caldwell, D. G., & Ortiz, J. (2023). Evaluation of visual and audio notifications in the user command interface integrated with the industrial exoskeleton shoulder-sidewinder. *2023 IEEE International Conference on Robotics and Biomimetics (ROBIO)*, 1–7. https://doi.org/10.1109/ROBIO58561.2023.10354678

Morishita, H., & Murakami, T. (2023). Assistance torque control based on musculoskeletal hexagon output distribution for upper limb exoskeleton. *2023 IEEE International Conference on Mechatronics (ICM)*, 1–6.

Morone, G., Cocchi, I., Paolucci, S., & Iosa, M. (2020). Robot-assisted therapy for arm recovery for stroke patients: State of the art and clinical implication. *Expert review of medical devices*, *17*(3), 223–233.

Mott, R. L., Pozo, V. G., Sánchez, S. S., Fernández, á. H., & Sánchez, J. V. (2006). Diseño de elementos de máquinas.

Moulaei, K., Bahaadinbeigy, K., Haghdoostd, A. A., Nezhad, M. S., & Sheikhtaheri, A. (2023). Overview of the role of robots in upper limb disabilities rehabilitation: A scoping review. *Archives of Public Health*, *81*(1), 84.

Moulaei, K., Moulaei, R., & Bahaadinbeigy, K. (2024). The most used questionnaires for evaluating the usability of robots and smart wearables: A scoping review. *Digital Health*, *10*, 20552076241237384.

Nann, M., Cordella, F., Trigili, E., Lauretti, C., Bravi, M., Miccinilli, S., Catalan, J. M., Badesa, F. J., Crea, S., Bressi, F., et al. (2020). Restoring activities of daily living using an eeg/eog-controlled semiautonomous and mobile whole-arm exoskeleton in chronic stroke. *IEEE Systems Journal*, *15*(2), 2314–2321.

Narayan, J., Bharti, R. R., & Dwivedy, S. K. (2022). Robust sliding mode control with reaching laws for a pediatric lower-limb exoskeleton system. *2022 Second International Conference on Power, Control and Computing Technologies (ICPC2T)*, 1–6.

Negri, E., Fumagalli, L., & Macchi, M. (2017). A review of the roles of digital twin in cps-based production systems [27th International Conference on Flexible Automation and Intelligent Manufacturing, FAIM2017, 27-30 June 2017, Modena, Italy]. *Procedia*

Manufacturing, *11*, 939–948. https://doi.org/https://doi.org/10.1016/j.promfg.2017.07.198

Netter, F. H. (2023). *Atlas de anatomía humana. abordaje regional*. Elsevier Health Sciences.

Nielsen, J. (1994). 10 usability heuristics for user interface design [Consult: May 13, 2024].

Ning, Y., Wang, H., Tian, J., Yan, H., Tian, Y., Yang, C., Wei, J., & Niu, J. (2022). An eight-degree-of-freedom upper extremity exoskeleton rehabilitation robot: Design, optimization, and validation. *Journal of Mechanical Science and Technology*, *36*(11), 5721–5733.

Norton, R. L. (2016). *Diseño de maquinaria*.

Olaya, A. F. R. (2009). *Sistema robótico multimodal para análisis y estudios en biomecánica, movimiento humano y control neuromotor* [Doctoral dissertation, Universidad Carlos III de Madrid] [En línea: http://e-archivo.uc3m.es/handle/10016/5636].

Organization., W. H. (2022). Musculoskeletal health. [Accessed: 2023-02-12].

Organization., W. H. (2024). Rehabilitation. [Accessed: 2024-05-22].

Ostuni, B. M., Caporaso, T., Grazioso, S., Palomba, A., Di Gironimo, G., & Lanzotti, A. (2023). Preliminary evaluation of an active soft bellow exoskeleton for industrial overhead tasks. *2023 IEEE International Workshop on Metrology for Industry 4.0 & IoT (MetroInd4.0&IoT)*, 227–232.

Palazzi, E., Luzi, L., Dimo, E., Meneghetti, M., Vicario, R., Luzia, R. F., Vertechy, R., & Calanca, A. (2022). An affordable upper-limb exoskeleton concept for rehabilitation applications. *Technologies*, *10*(1), 22.

Papavasileiou, G. S., & Charmpis, D. C. (2016). Seismic design optimization of multi–storey steel–concrete composite buildings. *Computers & Structures*, *170*, 49–61.

Park, J. H., Park, G., Kim, H. Y., Lee, J.-Y., Ham, Y., Hwang, D., Kwon, S., & Shin, J.-H. (2020). A comparison of the effects and usability of two exoskeletal robots with and without robotic actuation for upper extremity rehabilitation among patients with stroke: A single-blinded randomised controlled pilot study. *Journal of neuroengineering and rehabilitation*, *17*, 1–12.

Peres, F., & Castelli, M. (2021). Combinatorial optimization problems and metaheuristics: Review, challenges, design, and development. *Applied Sciences*, *11*(14), 6449.

Pérez, V. Z., Yepes, J. C., Vargas, J. F., Franco, J. C., Escobar, N. I., Betancur, L., Sánchez, J., & Betancur, M. J. (2022). Virtual reality game for physical and emotional rehabilitation of landmine victims. *Sensors*, *22*(15), 5602.

Pérez-Rodríguez, R., Moreno-Sánchez, P. A., Valdés-Aragonés, M., Oviedo-Briones, M., Divan, S., García-Grossocordón, N., & Rodríguez-Mañas, L. (2019). Friwalk robotic walker: Usability, acceptance and ux evaluation after a pilot study in a real environment. *Disability and Rehabilitation: Assistive Technology*.

Pons, J. L. (2008). *Wearable robots: Biomechatronic exoskeletons*. John Wiley & Sons.

Postol, N., Grissell, J., McHugh, C., Bivard, A., Spratt, N. J., & Marquez, J. (2021). Effects of therapy with a free-standing robotic exoskeleton on motor function and other health indicators in people with severe mobility impairment due to chronic stroke: A quasi-controlled study. *Journal of Rehabilitation and Assistive Technologies Engineering*, *8*, 20556683211045837.

Qureshi, M. U., & Mudassir, M. (2021). Robust control design for 3 degree of freedom fully actuated upper limb exoskeleton. *2021 16th International Conference on Emerging Technologies (ICET)*, 1–6.

Rahman, M. H. (2012). *Development of an exoskeleton robot for upper-limb rehabilitation* [Doctoral dissertation, École de technologie supérieure].

Ratiba, F., Mohamed, G., Mustapha, H., & Noura, A. (2022). Adaptive finite-time robust sliding mode controller for upper limb exoskeleton robot. *2022 19th International Multi-Conference on Systems, Signals & Devices (SSD)*, 1255–1260.

Rocon, E., & Pons, J. L. (2011). *Exoskeletons in rehabilitation robotics: Tremor suppression* (Vol. 69). Springer.

Safira, L. A., Arifin, A., Kusuma, H., Risciwan, A., & Zazuli, M. I. (2023). Adaptive pid controller based on sliding surface for controlling elbow joint robot rehabilitation. *2023 International Seminar on Intelligent Technology and Its Applications (ISITIA)*, 316–321.

Samala, R. K. (2023). Particle swarm optimization. In *Swarm intelligence-recent advances and current applications*. IntechOpen.

Sanjuan De Caro, J. D., Sunny, M. S. H., Muñoz, E., Hernandez, J., Torres, A., Brahmi, B., Wang, I., Ghommam, J., & Rahman, M. H. (2022). Evaluation of objective functions for the optimal design of an assistive robot. *Micromachines*, *13*(12), 2206.

Saveriano, M., Abu-Dakka, F. J., Kramberger, A., & Peternel, L. (2023). Dynamic movement primitives in robotics: A tutorial survey. *The International Journal of Robotics Research*, *42*(13), 1133–1184.

Semeraro, C., Lezoche, M., Panetto, H., & Dassisti, M. (2021). Digital twin paradigm: A systematic literature review. *Computers in Industry*, *130*, 103469. https://doi.org/https://doi.org/10.1016/j.compind.2021.103469

Semprini, M., Lencioni, T., Hinterlang, W., Vassallo, C., Scarpetta, S., Maludrottu, S., Iandolo, R., Carè, M., Laffranchi, M., Chiappalone, M., et al. (2022). User-centered design and development of twin-acta: A novel control suite of the twin lower limb exoskeleton for the rehabilitation of persons post-stroke. *Frontiers in neuroscience*, *16*, 915707.

Sepasgozar, S. M. (2020). Digital twin and web-based virtual gaming technologies for online education: A case of construction management and engineering. *Applied Sciences*, *10*(13), 4678.

Shetty, D., Manzione, L., & Ali, A. (2012). Survey of mechatronic techniques in modern machine design. *Journal of Robotics*, *2012*.

Shigley, J. E., Nisbett, J. K., & Budynas, R. G. (2019). *Diseño en ingeniería mecánica de shigley*. McGraw-Hill Interamericana.

Siciliano, B., Sciavicco, L., Villani, L., & Oriolo, G. (2009). *Robotics: Modelling, planning and control*. Springer.

Silawatchananai, C., & Howimanporn, S. (2020). Robust control design of arm exoskeleton based on sliding mode control. *2020 9th International Congress on Advanced Applied Informatics (IIAI-AAI)*, 542–547.

Silawatchananai, C., & Parnichkun, M. (2019). Haptics control of an arm exoskeleton for virtual reality using pso-based fixed structure h∞ control. *International Journal of Advanced Robotic Systems*, *16*(3), 1729881419849198.

Singh, M., Fuenmayor, E., Hinchy, E. P., Qiao, Y., Murray, N., & Devine, D. (2021). Digital twin: Origin to future. *Applied System Innovation*, *4*(2). https://doi.org/10.3390/asi4020036

Söderberg, R., Wärmefjord, K., Carlson, J. S., & Lindkvist, L. (2017). Toward a digital twin for real-time geometry assurance in individualized production. *CIRP Annals*, *66*(1), 137–140. https://doi.org/https://doi.org/10.1016/j.cirp.2017.04.038

Soleimani Amiri, M., Ramli, R., Ibrahim, M. F., Abd Wahab, D., & Aliman, N. (2020). Adaptive particle swarm optimization of pid gain tuning for lower-limb human exoskeleton in virtual environment. *Mathematics*, *8*(11), 2040.

Spong, M. W., Hutchinson, S., & Vidyasagar, M. (2020). *Robot modeling and control*. John Wiley & Sons.

Sreejeth, M., Kumar, R., Tripathi, N., & Garg, P. (2023). Tuning a pid controller using metaheuristic algorithms. *2023 8th International Conference on Communication and Electronics Systems (ICCES)*, 276–282.

Struijk, L. N. A., Kanstrup, A. M., Bai, S., Bak, T., Thøgersen, M. B., Mohammadi, M., Bengtson, S. H., Kobbelgaard, F. V., Gull, M. A., Bentsen, B., et al. (2022). The impact of interdisciplinarity and user involvement on the design and usability of an assistive upper limb exoskeleton-a case study on the exotic. *2022 International Conference on Rehabilitation Robotics (ICORR)*, 1–5.

Tao, F., Xiao, B., Qi, Q., Cheng, J., & Ji, P. (2022). Digital twin modeling. *Journal of Manufacturing Systems*, *64*, 372–389. https://doi.org/https://doi.org/10.1016/j.jmsy.2022.06.015

Tolani, D., & Badler, N. I. (1996). Real-time inverse kinematics of the human arm. *Presence: Teleoperators & Virtual Environments*, *5*(4), 393–401.

Tortora, G. J., Derrickson, B., Tzal, K., de los ángeles Gutiérrez, M., & Klajn, D. (2002). *Principios de anatomáa y fisiología* (Vol. 7). OXFORD University press.

Trelea, I. C. (2003). The particle swarm optimization algorithm: Convergence analysis and parameter selection. *Information processing letters*, *85*(6), 317–325.

Tröster, M., Wagner, D., Müller-Graf, F., Maufroy, C., Schneider, U., & Bauernhansl, T. (2020). Biomechanical model-based development of an active occupational upper-limb exoskeleton to support healthcare workers in the surgery waiting room. *International Journal of Environmental Research and Public Health*, *17*(14), 5140.

van Dijsseldonk, R. B., van Nes, I. J., Geurts, A. C., & Keijsers, N. L. (2020). Exoskeleton home and community use in people with complete spinal cord injury. *Scientific reports*, *10*(1), 15600.

Vélez-Guerrero, M. A., Callejas-Cuervo, M., & Mazzoleni, S. (2021). Design, development, and testing of an intelligent wearable robotic exoskeleton prototype for upper limb rehabilitation. *Sensors*, *21*(16), 5411.

Verdel, D., Sahm, G., Bastide, S., Bruneau, O., Berret, B., & Vignais, N. (2022). Influence of the physical interface on the quality of human–exoskeleton interaction. *IEEE Transactions on Human-Machine Systems*, *53*(1), 44–53.

Villarejo, J. J., Valencia-Jiménez, N. J., Arango-Hoyos, G. P., & Caicedo-Bravo, E. F. (2018). Biofeedback system for exoskeletqn assisted gait rehabilitation. *Revista Ingeniería Biomédica*, *12*, 47–57.

Wang, J., Tang, B., Pang, M., Xiang, K., & Ju, Z. (2021). Self-adaptive particle swarm optimization with human-in-the-loop for ankle exoskeleton control. *Sensors and Materials*, *33*.

Wang, T., Gasick, J., Sun, S., & Qian, X. (2023). A comparison of manufacturing constraints in 3d topologically optimized heat sinks for forced air cooling. *Engineering with Computers*, *39*(3), 1711–1733.

Winter, D. A. (2009). *Biomechanics and motor control of human movement* (Cuarta). John Wiley & Sons.

Wu, H., Su, W., & Liu, Z. (2014). Pid controllers: Design and tuning methods. *2014 9th IEEE Conference on industrial electronics and applications*, 808–813.

Yu, P., Gao, Y., Jiang, F. J., Johansson, K. H., & Dimarogonas, D. V. (2023). Online control synthesis for uncertain systems under signal temporal logic specifications. *The International Journal of Robotics Research*, 02783649231212572.

Yurkewich, A., Hebert, D., Wang, R. H., & Mihailidis, A. (2019). Hand extension robot orthosis (hero) glove: Development and testing with stroke survivors with severe hand impairment. *IEEE Transactions on Neural Systems and Rehabilitation Engineering*, *27*(5), 916–926.

Zeiaee, A., Soltani-Zarrin, R., Langari, R., & Tafreshi, R. (2019). Kinematic design optimization of an eight degree-of-freedom upper-limb exoskeleton. *Robotica*, *37*(12), 2073–2086.

Zhang, G., Wang, J., Yang, P., & Guo, S. (2022). A learning control scheme for upper-limb exoskeleton via adaptive sliding mode technique. *Mechatronics*, *86*, 102832.

Zhang, K., Chen, X., Liu, F., Tang, H., Wang, J., Wen, W., et al. (2018). System framework of robotics in upper limb rehabilitation on poststroke motor recovery. *Behavioural neurology*, *2018*.

Zhao, Y., Wu, H., Zhang, M., Mao, J., & Todoh, M. (2023). Design methodology of portable upper limb exoskeletons for people with strokes. *Frontiers in Neuroscience*, *17*, 1128332.

Zhou, X., & Zheng, L. (2021). Model-based comparison of passive and active assistance designs in an occupational upper limb exoskeleton for overhead lifting. *IISE transactions on occupational ergonomics and human factors*, *9*(3-4), 167–185.

Zhou, Z., Chen, W., Fu, H., Fang, X., & Xiong, C. (2021). Design and experimental evaluation of a non-anthropomorphic passive load-carrying exoskeleton. *2021 6th IEEE International Conference on Advanced Robotics and Mechatronics (ICARM)*, 251–256.

Zimmermann, Y., Forino, A., Riener, R., & Hutter, M. (2019). Anyexo: A versatile and dynamic upper-limb rehabilitation robot. *IEEE Robotics and Automation Letters*, *4*(4), 3649–3656.

Annexes

.1 Annex 1: Actuator Sizing

Once the CAD design is obtained, it is feasible to select the appropriate actuators for the robot. For this selection, a dynamic analysis of the prototype's structure was performed in the positions with the greatest lever arm for each movement. In this way, the system was divided into the following subsystems:

1. Wrist subsystem: abduction-adduction movement.
2. Forearm subsystem: flexion-extension movement.
3. Arm subsystem: flexion-extension movement.
4. Arm subsystem: abduction-adduction movement.
5. Arm subsystem: internal-external rotation movement.

To determine the minimum torque required to maintain the structure in static equilibrium, a dynamic analysis of each subsystem is performed. Each one is treated as a cantilever beam, considering the weight of the mechanical structure, the maximum lengths for which it was designed, the location where the greatest lever arm occurs, and the external forces affecting the components (which represent the maximum weights of each part of the human arm, see Table 3.3).

Wrist subsystem: Abduction-Adduction Movement.

This subsystem allows for the abduction-adduction movement of the wrist and is secured to the patient by Velcro straps (see Figure 1). It has a length of 6.00 cm and a mass of 0.20 kg, with the wrist positioned at 0°. The structure must support the weight of the hand of the upper limb, which has a mass of 0.84 kg (equivalent to 0.70% of the user's maximum mass), with the center of mass located at 0.02 m (representing 48.00% of the maximum length of the hand).

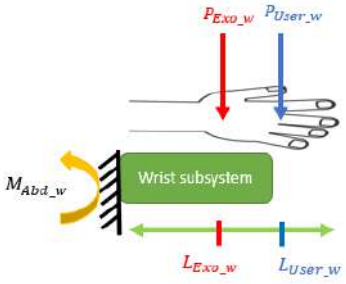

Figure 1: Free body diagram of the wrist subsystem.

$$\begin{aligned} \curvearrowleft +\Sigma M &= 0 \\ M_{Abd_w} - 1.96(0.03) - 8.24(0.09) &= 0 \\ M_{Abd_w} &= 0.30Nm \end{aligned} \tag{1}$$

The torque required for the wrist subsystem is shown in equation (1).

Forearm subsystem: flexion-extension movement.

It allows for the flexion-extension movement of the elbow and is secured to the patient by Velcro straps (see Figure 2). The corresponding mechanical structure has a length of 39.00 cm and an approximate mass of 1.10 kg, with the forearm positioned at a 90° elbow flexion. The forces it must withstand include the weight of the forearm and hand of the upper limb, which has a mass of 2.76 kg (equivalent to 2.30% of the patient's maximum mass), with the center of mass located at 0.28 m (representing 62.60% of the maximum length of the forearm and hand), in addition to a 0.20 kg motor located at the wrist to execute the movement of the anterior subsystem.

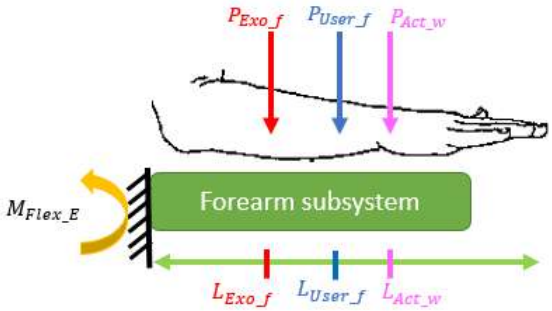

Figure 2: Free body diagram of the forearm subsystem.

.

$$\begin{aligned} \curvearrowleft +\Sigma M &= 0 \\ M_{Flex_E} - 10.79(0.22) - 27.07(0.28) - 1.96(0.39) &= 0 \\ M_{Flex_E} &= 10.82Nm \end{aligned} \tag{2}$$

The torque required for the forearm is shown in equation (2).

Arm subsystem: flexion-extension movement.

It allows for the flexion-extension movement of the shoulder and is secured to the patient by Velcro straps (see Figure 3). The mechanical structure is composed of the parts of the arm, forearm, and wrist subsystems. It has a maximum length of 86.00 cm and a mass of 2 kg. With the upper limb positioned at a 90° shoulder flexion, the structure supports a mass of 5.88 kg corresponding to the upper limb (4.9% of the user's maximum mass), with a center of mass at 0.36 m (41.30% of the maximum length of the upper limb). Additionally, it supports the motor of the forearm, weighing 0.60 kg and with a center of mass at 0.43 m, and the motor of the wrist, weighing 0.20 kg and with a center of mass at 0.86 m.

$$\begin{aligned} \curvearrowleft +\Sigma M &= 0 \\ M_{Flex_S} - 57.68(0.36) - 19.62(0.43) - 5.88(0.43) - 1.96(0.86) &= 0 \\ M_{Flex_S} &= 33.45Nm \end{aligned} \tag{3}$$

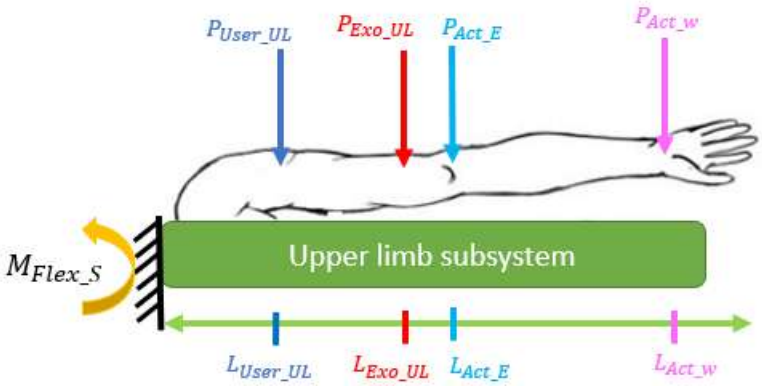

Figure 3: Free body diagram of the arm subsystem (flexion-extension movement).

.

The torque required for the flexion-extension movement of the upper limb is shown in equation (3).

Arm subsystem: abduction-adduction movement.

It allows for the abduction-adduction movement of the shoulder and is secured to the patient by Velcro straps (see Figure 4). The mechanical structure is composed of parts from the arm, forearm, and wrist subsystems, positioned in a 90° abduction. The forces supported by this structure correspond to the mass of the upper limb (5.88 kg) with a center of mass at 0.36 m. Additionally, it supports 0.60 kg of the forearm motor with a center of mass at 0.43 m, 0.20 kg of the wrist motor with a center of mass at 0.86 m, and the weight of the structure itself.

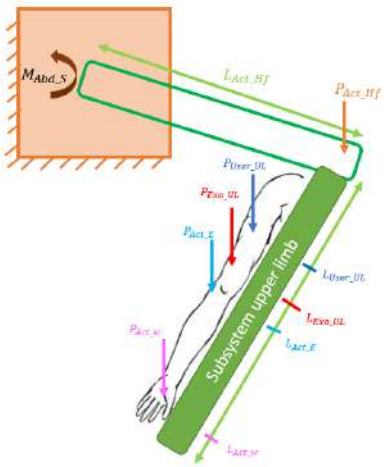

Figure 4: Free body diagram for the abduction-adduction movement of the shoulder.

.

$$\begin{aligned} \curvearrowleft +\Sigma M &= 0 \qquad (4) \\ M_{Abd_S} - 5.88(0.12) - 57.68(0.36) - 19.62(0.43) - 5.88(0.43) - 1.96(0.86) &= 0 \\ M_{Abd_S} &= 34.15Nm \end{aligned}$$

The torque required for the abduction-adduction movement of the upper limb is shown in equation (4).

Arm subsystem: internal-external rotation movement.

It allows internal and external rotation of the shoulder and attaches to the patient using Velcro straps. The upper limb is positioned in 90° shoulder flexion (see Figure 5). The structure is composed of parts from the subsystems of the arm, forearm, and wrist. The forces supported by this structure correspond to the mass of the shoulder flexion actuator, elbow flexion, and wrist abduction, in addition to the mass of the upper limb and the mass of the exoskeleton structure.

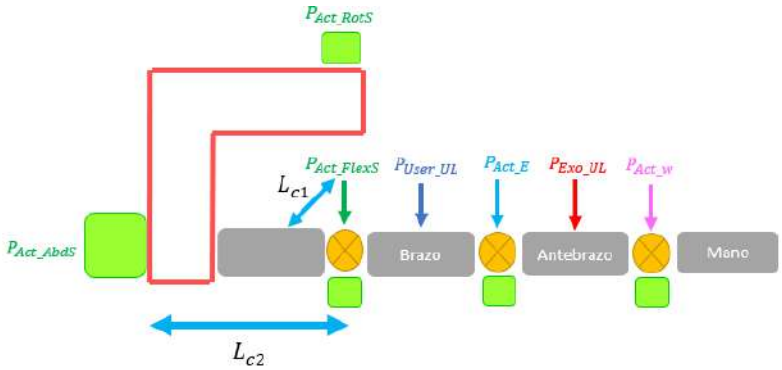

Figure 5: Free body diagram for internal-external rotation movement of the shoulder.

$$\begin{aligned} \dot{\curvearrowleft} +\Sigma M &= 0 \qquad (5) \\ M_{Rot_S} - 5.88(0.07) - 104.53(0.1) &= 0 \\ M_{Rot_S} &= 10.86Nm \end{aligned}$$

The torque required for the internal-external rotation of the upper limb is shown in equation (5).

.2 Annex 2: Direct Jacobian Matrix

The resulting Jacobian matrix is shown below:

$$J = \begin{bmatrix} J_{11} & J_{12} & J_{13} & J_{14} & J_{15} \\ J_{21} & J_{22} & J_{23} & J_{24} & J_{25} \\ J_{31} & J_{32} & J_{33} & J_{34} & J_{35} \\ J_{41} & J_{42} & J_{43} & J_{44} & J_{45} \\ J_{51} & J_{52} & J_{53} & J_{54} & J_{55} \\ J_{61} & J_{62} & J_{63} & J_{64} & J_{65} \end{bmatrix}$$

where:

$$
\begin{aligned}
J_{11} &= a_3 * sin(q_1) * sin(q_3) - a_3 * cos(q_1) * cos(q_3) * sin(q_2) + \\
&\quad a_4 * cos(q_3) * sin(q_1) * sin(q_4) + a_4 * cos(q_4) * sin(q_1) * sin(q_3) - \\
&\quad a_4 * cos(q_1) * cos(q_3) * cos(q_4) * sin(q_2) + a_5 * cos(q_3) * cos(q_4) * sin(q_1) * sin(q_5) + \\
&\quad a_5 * cos(q_3) * cos(q_5) * sin(q_1) * sin(q_4) + a_5 * cos(q_4) * cos(q_5) * sin(q_1) * sin(q_3) + \\
&\quad a_4 * cos(q_1) * sin(q_2) * sin(q_3) * sin(q_4) - a_5 * sin(q_1) * sin(q_3) * sin(q_4) * sin(q_5) - \\
&\quad a_5 * cos(q_1) * cos(q_3) * cos(q_4) * cos(q_5) * sin(q_2) + \\
&\quad a_5 * cos(q_1) * cos(q_3) * sin(q_2) * sin(q_4) * sin(q_5) + \\
&\quad a_5 * cos(q_1) * cos(q_4) * sin(q_2) * sin(q_3) * sin(q_5) + \\
&\quad a_5 * cos(q_1) * cos(q_5) * sin(q_2) * sin(q_3) * sin(q_4) \\
J_{12} &= -cos(q_2) * sin(q_1) * (a_4 * cos(q_3 + q_4) + a_3 * cos(q_3) + a_5 * cos(q_3 + q_4 + q_5)) \\
J_{13} &= a_4 * cos(q_1) * sin(q_3) * sin(q_4) - a_4 * cos(q_1) * cos(q_3) * cos(q_4) - \\
&\quad a_3 * cos(q_1) * cos(q_3) + a_3 * sin(q_1) * sin(q_2) * sin(q_3) - \\
&\quad a_5 * cos(q_1) * cos(q_3) * cos(q_4) * cos(q_5) + a_5 * cos(q_1) * cos(q_3) * sin(q_4) * sin(q_5) + \\
&\quad a_5 * cos(q_1) * cos(q_4) * sin(q_3) * sin(q_5) + a_5 * cos(q_1) * cos(q_5) * sin(q_3) * sin(q_4) + \\
&\quad a_4 * cos(q_3) * sin(q_1) * sin(q_2) * sin(q_4) + a_4 * cos(q_4) * sin(q_1) * sin(q_2) * sin(q_3) + \\
&\quad a_5 * cos(q_3) * cos(q_4) * sin(q_1) * sin(q_2) * sin(q_5) + \\
&\quad a_5 * cos(q_3) * cos(q_5) * sin(q_1) * sin(q_2) * sin(q_4) + \\
&\quad a_5 * cos(q_4) * cos(q_5) * sin(q_1) * sin(q_2) * sin(q_3) - \\
&\quad a_5 * sin(q_1) * sin(q_2) * sin(q_3) * sin(q_4) * sin(q_5) \\
J_{14} &= a_4 * cos(q_1) * sin(q_3) * sin(q_4) - a_4 * cos(q_1) * cos(q_3) * cos(q_4) - \\
&\quad a_5 * cos(q_1) * cos(q_3) * cos(q_4) * cos(q_5) + a_5 * cos(q_1) * cos(q_3) * sin(q_4) * sin(q_5) + \\
&\quad a_5 * cos(q_1) * cos(q_4) * sin(q_3) * sin(q_5) + a_5 * cos(q_1) * cos(q_5) * sin(q_3) * sin(q_4) + \\
&\quad a_4 * cos(q_3) * sin(q_1) * sin(q_2) * sin(q_4) + a_4 * cos(q_4) * sin(q_1) * sin(q_2) * sin(q_3) + \\
&\quad a_5 * cos(q_3) * cos(q_4) * sin(q_1) * sin(q_2) * sin(q_5) + \\
&\quad a_5 * cos(q_3) * cos(q_5) * sin(q_1) * sin(q_2) * sin(q_4) + \\
&\quad a_5 * cos(q_4) * cos(q_5) * sin(q_1) * sin(q_2) * sin(q_3) - \\
&\quad a_5 * sin(q_1) * sin(q_2) * sin(q_3) * sin(q_4) * sin(q_5) \\
J_{15} &= a_5 * cos(q_1) * cos(q_3) * sin(q_4) * sin(q_5) - a_5 * cos(q_1) * cos(q_3) * cos(q_4) * cos(q_5) + \\
&\quad a_5 * cos(q_1) * cos(q_4) * sin(q_3) * sin(q_5) + a_5 * cos(q_1) * cos(q_5) * sin(q_3) * sin(q_4) + \\
&\quad a_5 * cos(q_3) * cos(q_4) * sin(q_1) * sin(q_2) * sin(q_5) + \\
&\quad a_5 * cos(q_3) * cos(q_5) * sin(q_1) * sin(q_2) * sin(q_4) + \\
&\quad a_5 * cos(q_4) * cos(q_5) * sin(q_1) * sin(q_2) * sin(q_3) - \\
&\quad a_5 * sin(q_1) * sin(q_2) * sin(q_3) * sin(q_4) * sin(q_5)
\end{aligned}
$$

$$
\begin{aligned}
J_{21} &= a_5 * cos(q_1) * sin(q_3) * sin(q_4) * sin(q_5) - a_4 * cos(q_1) * cos(q_3) * sin(q_4) - \\
&\quad a_4 * cos(q_1) * cos(q_4) * sin(q_3) - a_3 * cos(q_3) * sin(q_1) * sin(q_2) - \\
&\quad a_5 * cos(q_1) * cos(q_3) * cos(q_4) * sin(q_5) - a_5 * cos(q_1) * cos(q_3) * cos(q_5) * sin(q_4) - \\
&\quad a_5 * cos(q_1) * cos(q_4) * cos(q_5) * sin(q_3) - a_4 * cos(q_3) * cos(q_4) * sin(q_1) * sin(q_2) - \\
&\quad a_3 * cos(q_1) * sin(q_3) + a_4 * sin(q_1) * sin(q_2) * sin(q_3) * sin(q_4) - \\
&\quad a_5 * cos(q_3) * cos(q_4) * cos(q_5) * sin(q_1) * sin(q_2) + \\
&\quad a_5 * cos(q_3) * sin(q_1) * sin(q_2) * sin(q_4) * sin(q_5) + \\
&\quad a_5 * cos(q_4) * sin(q_1) * sin(q_2) * sin(q_3) * sin(q_5) + \\
&\quad a_5 * cos(q_5) * sin(q_1) * sin(q_2) * sin(q_3) * sin(q_4) \\
J_{22} &= cos(q_1) * cos(q_2) * (a_4 * cos(q_3 + q_4) + a_3 * cos(q_3) + a_5 * cos(q_3 + q_4 + q_5)) \\
J_{23} &= a_4 * sin(q_1) * sin(q_3) * sin(q_4) - a_4 * cos(q_3) * cos(q_4) * sin(q_1) - \\
&\quad a_3 * cos(q_1) * sin(q_2) * sin(q_3) - a_3 * cos(q_3) * sin(q_1) - \\
&\quad a_5 * cos(q_3) * cos(q_4) * cos(q_5) * sin(q_1) - a_4 * cos(q_1) * cos(q_3) * sin(q_2) * sin(q_4) - \\
&\quad a_4 * cos(q_1) * cos(q_4) * sin(q_2) * sin(q_3) + a_5 * cos(q_3) * sin(q_1) * sin(q_4) * sin(q_5) + \\
&\quad a_5 * cos(q_4) * sin(q_1) * sin(q_3) * sin(q_5) + a_5 * cos(q_5) * sin(q_1) * sin(q_3) * sin(q_4) - \\
&\quad a_5 * cos(q_1) * cos(q_3) * cos(q_4) * sin(q_2) * sin(q_5) - \\
&\quad a_5 * cos(q_1) * cos(q_3) * cos(q_5) * sin(q_2) * sin(q_4) - \\
&\quad a_5 * cos(q_1) * cos(q_4) * cos(q_5) * sin(q_2) * sin(q_3) + \\
&\quad a_5 * cos(q_1) * sin(q_2) * sin(q_3) * sin(q_4) * sin(q_5) \\
J_{24} &= a_4 * sin(q_1) * sin(q_3) * sin(q_4) - a_4 * cos(q_3) * cos(q_4) * sin(q_1) - \\
&\quad a_5 * cos(q_3) * cos(q_4) * cos(q_5) * sin(q_1) - a_4 * cos(q_1) * cos(q_3) * sin(q_2) * sin(q_4) - \\
&\quad a_4 * cos(q_1) * cos(q_4) * sin(q_2) * sin(q_3) + a_5 * cos(q_3) * sin(q_1) * sin(q_4) * sin(q_5) + \\
&\quad a_5 * cos(q_4) * sin(q_1) * sin(q_3) * sin(q_5) + a_5 * cos(q_5) * sin(q_1) * sin(q_3) * sin(q_4) - \\
&\quad a_5 * cos(q_1) * cos(q_3) * cos(q_4) * sin(q_2) * sin(q_5) - \\
&\quad a_5 * cos(q_1) * cos(q_3) * cos(q_5) * sin(q_2) * sin(q_4) - \\
&\quad a_5 * cos(q_1) * cos(q_4) * cos(q_5) * sin(q_2) * sin(q_3) + \\
&\quad a_5 * cos(q_1) * sin(q_2) * sin(q_3) * sin(q_4) * sin(q_5) \\
J_{25} &= a_5 * cos(q_3) * sin(q_1) * sin(q_4) * sin(q_5) - a_5 * cos(q_3) * cos(q_4) * cos(q_5) * sin(q_1) + \\
&\quad a_5 * cos(q_4) * sin(q_1) * sin(q_3) * sin(q_5) + a_5 * cos(q_5) * sin(q_1) * sin(q_3) * sin(q_4) - \\
&\quad a_5 * cos(q_1) * cos(q_3) * cos(q_4) * sin(q_2) * sin(q_5) - \\
&\quad a_5 * cos(q_1) * cos(q_3) * cos(q_5) * sin(q_2) * sin(q_4) - \\
&\quad a_5 * cos(q_1) * cos(q_4) * cos(q_5) * sin(q_2) * sin(q_3) + \\
&\quad a_5 * cos(q_1) * sin(q_2) * sin(q_3) * sin(q_4) * sin(q_5)
\end{aligned}
$$

$$
\begin{aligned}
J_{31} &= 0 \\
J_{32} &= sin(q_2) * (a_4 * cos(q_3 + q_4) + a_3 * cos(q_3) + a_5 * cos(q_3 + q_4 + q_5)) \\
J_{33} &= cos(q_2) * (a_4 * sin(q_3 + q_4) + a_3 * sin(q_3) + a_5 * sin(q_3 + q_4 + q_5)) \\
J_{34} &= \frac{(a_4 * sin(q_3 - q_2 + q_4))}{2} + \frac{(a_5 * sin(q_2 + q_3 + q_4 + q_5))}{2} + \frac{(a_5 * sin(q_3 - q_2 + q_4 + q_5))}{2} + \\
&\quad \frac{(a_4 * sin(q_2 + q_3 + q_4))}{2} \\
J_{35} &= \frac{(a_5 * (sin(q_3 - q_2 + q_4 + q_5) + sin(q_2 + q_3 + q_4 + q_5)))}{2}
\end{aligned}
$$

$$
\begin{aligned}
J_{41} &= 0 \\
J_{42} &= cos(q_1) \\
J_{43} &= -cos(q_2) * sin(q_1) \\
J_{44} &= -cos(q_2) * sin(q_1) \\
J_{45} &= -cos(q_2) * sin(q_1) \\
J_{51} &= 0 \\
J_{52} &= sin(q_1) \\
J_{53} &= cos(q_1) * cos(q_2) \\
J_{54} &= cos(q_1) * cos(q_2) \\
J_{55} &= cos(q_1) * cos(q_2) \\
J_{61} &= 1 \\
J_{62} &= 0 \\
J_{63} &= sin(q_2) \\
J_{64} &= sin(q_2) \\
J_{65} &= sin(q_2)
\end{aligned}
$$

The numerical value of the Jacobian matrix depends on the instantaneous joint coordinates, so it varies at each of these points.

.3 Annex 3: Dynamic model

The dynamic model of the optimized exoskeleton was obtained using the Robotics Toolbox of Matlab®. This software takes as input parameters the D-H parameters (Table 5.1) and the mechanical properties of each of the links (Tables 1-6). The data in these tables were derived from the virtual prototype in SolidWorks®, considering the maximum lengths for the arm and forearm, the actuators in each joint, and the material of the parts in the optimized prototype (excluding the screws).

Table 1: Mechanical properties: Base.

Parameter	Value
Mass[kg]	4.74
Center of mass [m]	[172.44 -117.46 -77.23]*(1/1000)
Ixx $[kg/m^2]$	$795719893.45 * (1/1000)^3$
Iyy $[kg/m^2]$	$858520130.69 * (1/1000)^3$
Izz $[kg/m^2]$	$290960644.74 * (1/1000)^3$
Izy $[kg/m^2]$	$82134634.40 * (1/1000)^3$
Ixz $[kg/m^2]$	$-74705336.03 * (1/1000)^3$
Iyx $[kg/m^2]$	$-115396427.67 * (1/1000)^3$

Table 2: Mechanical properties: Link 1

Parameter	Value
Mass [kg]	1.41
Center of mass [m]	[112.91 0 73.64]*(1/1000)
Ixx $[kg/m^2]$	$19811014.72 * (1/1000)^3$
Iyy $[kg/m^2]$	$40488592.93 * (1/1000)^3$
Izz $[kg/m^2]$	$22076051.34 * (1/1000)^3$
Izy $[kg/m^2]$	$-9.56 * (1/1000)^3$
Ixz $[kg/m^2]$	$7169943.91 * (1/1000)^3$
Iyx $[kg/m^2]$	$0.07 * (1/1000)^3$

Table 3: Mechanical properties: Link 2.

Parameter	Value
Mass [kg]	1.23
Center of mass [m]	[122.36 3.06 33.56]*(1/1000)
Ixx $[kg/m^2]$	$4625763.44 * (1/1000)^3$
Iyy $[kg/m^2]$	$25501036.87 * (1/1000)^3$
Izz $[kg/m^2]$	$22002481.59 * (1/1000)^3$
Izy $[kg/m^2]$	$333634.10 * (1/1000)^3$
Ixz $[kg/m^2]$	$3339726.02 * (1/1000)^3$
Iyx $[kg/m^2]$	$368774.97 * (1/1000)^3$

Table 4: Mechanical properties: Link 3.

Parameter	Value
Mass [kg]	1.57
Center of mass [m]	[304.56 -0.17 107.08]*(1/1000)
Ixx $[kg/m^2]$	$21263120.94 * (1/1000)^3$
Iyy $[kg/m^2]$	$208040567.14 * (1/1000)^3$
Izz $[kg/m^2]$	$187868147.40 * (1/1000)^3$

Parameter	Value
Izy $[kg/m^2]$	$-17824.34 * (1/1000)^3$
Ixz $[kg/m^2]$	$58062720.10 * (1/1000)^3$
Iyx $[kg/m^2]$	$-43688.30 * (1/1000)^3$

Table 5: Mechanical properties: Link 4.

Parameter	Value
Mass[kg]	0.93
Center of mass [m]	[213.52 -6.66 75.71]*(1/1000)
Ixx $[kg/m^2]$	$6531278.76 * (1/1000)^3$
Iyy $[kg/m^2]$	$68701944.68 * (1/1000)^3$
Izz $[kg/m^2]$	$63082867.58 * (1/1000)^3$
Izy $[kg/m^2]$	$-628123.11 * (1/1000)^3$
Ixz $[kg/m^2]$	$15943791.47 * (1/1000)^3$
Iyx $[kg/m^2]$	$-2439419.34 * (1/1000)^3$

Table 6: Mechanical properties: Link 5.

Parameter	Value
Mass [kg]	0.07
Center of mass [m]	[24.29 27.21 20.94]*(1/1000)
Ixx $[kg/m^2]$	$137868.02 * (1/1000)^3$
Iyy $[kg/m^2]$	$112612.99 * (1/1000)^3$
Izz $[kg/m^2]$	$124745.09 * (1/1000)^3$
Izy $[kg/m^2]$	$26755.56 * (1/1000)^3$
Ixz $[kg/m^2]$	$33946.04 * (1/1000)^3$
Iyx $[kg/m^2]$	$49400.96 * (1/1000)^3$

where: $[Ixx, Iyy, Izz]$ They correspond to the moments of inertia of each of the links, and $[Izy, Ixz, Iyx]$ They correspond to the products of inertia of each of the links.

Considering the mechanical properties shown in the previous tables, the resulting matrix I is:

$$I = \begin{bmatrix} I_{xx} & I_{xy} & I_{xz} \\ I_{xy} & I_{yy} & I_{yz} \\ I_{xz} & I_{yz} & I_{zz} \end{bmatrix}$$

The resulting matrices $M(n \times n)$, $C(n \times n)$, and $G(n \times 1)$ can be found at the URL: https://1drv.ms/f/c/6c2dea0e8477a325/EjFyPYvFxkhEkg54u1g0IzEBv7c2JhWUy7BttfaRsanjkA?e=cpyUtT

.4 Annex 4: Questionnaire for Evaluating Interface Usability (based on ISO 25010:2001 and ISO 9241-11:2018 Standards)

Designed and administered questionnaire is presented in Table 7.

Table 7: Usability test for the user interface

Num	Statement	Strongly disagree	Disagree	Neither disagree nor agree	Agree	Strongly agree
Ease of learning						
1	Did you find it easy to learn how to use the interface?					
2	Do you consider the interface to offer a gradual learning curve?					
Ease of use						
3	Did you find the interface easy to use?					
4	Could you perform the tasks efficiently and without difficulty?					
Comprehension capacity						
5	Did the interface present information clearly and comprehensibly?					
6	Could you easily understand how to interact with the system?					
Visual appeal						
7	Did you find the visual design of the interface attractive?					
8	Did you find the interface visually pleasing?					
Responsiveness						
9	Did the interface respond quickly to your actions?					
10	Did you experience any lag or lack of response when interacting with the interface?					
Ease of navigation						
11	Could you move easily between the different sections or functionalities of the interface?					

Num	Statement	Strongly disagree	Disagree	Neither disagree nor agree	Agree	Strongly agree
12	Did you find the navigation structure of the interface intuitive?					
	Flexibility and adaptability					
13	Did the interface allow you to adapt to your individual preferences or needs?					
14	Did you find customization options that were useful to you?					
	System feedback					
15	Did you receive clear feedback from the system about your actions?					
16	Did you find the feedback provided by the interface useful?					
	System errors					
17	Did you experience any errors or failures while using the interface?					
18	Do you consider the interface to be reliable in terms of error prevention?					
	Error recovery capability					
19	Did the interface provide you with options to correct errors or unexpected situations?					
20	Could you easily recover from errors without losing your progress or work done?					
	User satisfaction					
21	Overall, how would you rate your satisfaction with the human-robot interface?					
22	Would you recommend the interface to other users?					